Anna Trauth

CHARACTERISATION AND MODELLING OF CONTINUOUS-DISCONTINUOUS SHEET MOULDING COMPOUND COMPOSITES FOR STRUCTURAL APPLICATIONS

SCHRIFTENREIHE DES INSTITUTS
FÜR ANGEWANDTE MATERIALIEN BAND 83

KIT Scientific Publishing

Anna Trauth

Characterisation and Modelling of Continuous-Discontinuous Sheet Moulding Compound Composites for Structural Applications

Schriftenreihe
des Instituts für Angewandte Materialien
Band 83

Karlsruher Institut für Technologie (KIT)
Institut für Angewandte Materialien (IAM)

Eine Übersicht aller bisher in dieser Schriftenreihe erschienenen Bände finden Sie am Ende des Buches.

Characterisation and Modelling of Continuous-Discontinuous Sheet Moulding Compound Composites for Structural Applications

by
Anna Trauth

KIT Scientific Publishing

Karlsruher Institut für Technologie
Institut für Angewandte Materialien

Characterisation and Modelling of Continuous-Discontinuous Sheet Moulding Compound Composites for Structural Applications

Zur Erlangung des akademischen Grades eines Doktors der Ingenieurwissenschaften von der KIT-Fakultät für Maschinenbau des Karlsruher Instituts für Technologie (KIT) genehmigte Dissertation

von M.Sc. Anna Trauth

Tag der mündlichen Prüfung: 1. Oktober 2018
Hauptreferent: Prof. (apl.) Dr.-Ing. Kay André Weidenmann
Korreferenten: William Altenhof, Ph.D., P.Eng.
Prof. Dr.-Ing. Peter Elsner

Impressum

KIT Scientific Publishing

Karlsruher Institut für Technologie (KIT)
KIT Scientific Publishing
Straße am Forum 2
D-76131 Karlsruhe

KIT Scientific Publishing is a registered trademark of Karlsruhe Institute of Technology.
Reprint using the book cover is not allowed.

www.ksp.kit.edu

This document – excluding the cover, pictures and graphs – is licensed under a Creative Commons Attribution-Share Alike 4.0 International License (CC BY-SA 4.0): https://creativecommons.org/licenses/by-sa/4.0/deed.en

The cover page is licensed under a Creative Commons Attribution-No Derivatives 4.0 International License (CC BY-ND 4.0): https://creativecommons.org/licenses/by-nd/4.0/deed.en

Print on Demand 2020 – Gedruckt auf FSC-zertifiziertem Papier

ISSN 2192-9963
ISBN 978-3-7315-0950-9
DOI 10.5445/KSP/1000097160

Für meine Großeltern

"Damit das Mögliche entsteht, muss immer wieder das Unmögliche versucht werden."

Hermann Hesse

Acknowledgements

The research within this doctoral dissertation was performed at the Institute of Applied Materials at the Karlsruhe Institute of Technology, during the period of April 2015 through August 2018. It was part of the International Research Training Group (IRTG), which focusses on the integrated engineering of continuous-discontinuous long fibre reinforced polymer structures (GRK 2078).

I would like to thank a number of people for their support and valuable help, throughout the last few years, in completing this doctoral dissertation. The supervisor of this work, Prof. Kay André Weidenmann, deserves my gratitude for his continuous and always encouraging support, helpful advice and hours of conversations and discussions.

I would like to express my sincere appreciation to Prof. William Altenhof for his support during my time conducting research at the University of Windsor, for this doctoral dissertation. Thank you the opportunity to be part of your research group and to conduct experimental testing. This opportunity enriched my research significantly.

I would also like to thank Prof. Peter Elsner for his valuable input in finalising this manuscript and for being a member of my committee. Much gratitude goes as well to Prof. Thomas Böhlke for chairing the committee.

Many thanks to all my colleagues at the Institute of Applied Materials, especially to the group of Hybrid and Lightweight Materials. Thank you for every discussion and critique of my work, but most importantly, thank you for making the work environment so enjoyable. My grateful thanks go to Pascal Pinter for providing the μ-CT scans and valuable input for data and image processing, as well as to Miriam Bartkowiak, who supported me particularly within the last few weeks of this dissertation. Further, thanks to the technicians at the Institute of Applied Materials. In particular, Ralf Rößler, Arndt Hermeneit and Marc Brecht, for their irreplaceable support in technical problems and questions.

David Bücheler's support and endless endurance while manufacturing the materials investigated within this dissertation was crucial in this research: thank you. To Loredana Kehrer of the Institute of Engineering Mechanics (ITM) at Karlsruhe Institute of Technology (KIT), my warm thanks for support in modelling and manufacturing the pure resin sheets required for this work.

Valuable assistance was furthermore provided by all technicians at the University of Windsor, especially Matt St.Louis and Andrew Jenner during my time in Canada, which is greatly appreciated. In addition, I would like to thank Matthias Merzkirch and Tim Foecke of the National Institute of Standards and Technology in Washington, DC, for offering to me a research visit at their institute, which offered me valuable insights for my dissertation.

Let me extend my thanks also to all students who contributed importantly to the success of this work, especially Kai Kirchenbauer, Patrick Blinzer, Sascha Zeizinger, Robin Kopp, Moritz Seidler, André Schubert and Leopold Giersch.

My gratitude is owed, too, to my friends, who succeeded in taking my mind off this work when necessary, and didn't take it amiss when I was occupied working so often. I wish to express my sincere thanks to Stefan for being there as important support, when I began to doubt everything. Your words strongly encouraged me to keep believing in my ability to reach my goal.

Lastly, I would like to thank my family. Words cannot express how grateful I am for your endless support and encouragement throughout my studies. Thank you Michael for always believing in me, more than I ever did. I am really fortunate that I had you on my side during the completion of this dissertation. Thank you especially for being worried about my eating habits when I forgot to worry about them myself. This dissertation would not have been possible without your endless support and words of encouragement.

Karlsruhe, October 2018
Anna Trauth

Abstract

A novel approach in hybridisation of composites focusses on the combination of a discontinuous (Dico) glass fibre reinforced sheet moulding compound (SMC) with continuous (Co) carbon fibre SMC, manufactured in an adapted SMC process. The hybrid continuous-discontinuous (CoDico) SMC aims to enhance load-bearing capacities due to a possible local reinforcement of components. The main objective of this work is to significantly deepen the understanding of the material and structural behaviour of CoDico SMC composites, following a holistic approach to investigate microscopic aspects and macroscopic mechanical behaviour at the coupon, structure and component level. For this purpose, the mechanical properties of the hybrid SMC and modelling approaches are presented and discussed. Criteria to evaluate the effect of hybridisation are also introduced. In general, a hybrid CoDico SMC composite is an interesting hybrid material that allows tailorable material properties in structural components through local reinforcements; it thereby achieves a property profile superior to the sum of the properties of the individual materials.

In comparison to a discontinuous glass fibre SMC, hybrid CoDico SMC composites stood out due to their superior mechanical performance at coupon, structure and component level. However, the effect of hybridisation strongly depended on loading case. The continuous component determined elastic material properties. At the coupon level, tensile and compressive moduli of elasticity were more than

doubled by a continuous reinforcement. A rule of hybrid mixtures based on the volume-averaged elastic material properties of the two individual materials was suitable to predict the tensile and compressive moduli of elasticity. The laminate layup, with two continuous carbon fibre SMC surface layers, most importantly increased the flexural modulus of elasticity, to more than four times higher than that of the discontinuous glass fibre SMC. An adaption of the classical laminate theory (CLT), which enabled consideration of the specific layup of the hybrid laminate as well as the tension-compression anisotropy of the continuous carbon fibre SMC, precisely predicted the flexural modulus of elasticity.

Evolving damage, hence the strength of the hybrid CoDico SMC composite, was strongly linked to the continuous reinforcement. Interfibre failure and (inter- as well as intralaminar) delamination were the most important failure mechanisms. Tensile and flexural strength could be tripled and doubled, respectively, due to hybridisation. Hybridisation significantly enhanced performance at the structure level in terms of maximum force and puncture energy, if exposed to quasi-static puncture. In addition, an optimised local continuous reinforcement of a discontinuous glass fibre SMC component significantly increased stiffness and load at failure.

Kurzfassung

Ein innovativer Ansatz verfolgt das Konzept diskontinuierliche glasfaserbasierte Sheet Moulding Compound (SMC) Verbunde lokal mit kontinuierlichem kohlenstofffaserbasiertem SMC zu verstärken, um die mechanischen Eigenschaften von strukturellen Komponenten gezielt an ein Anforderungsprofil anpassen zu können. Die vorliegende Arbeit basiert auf einem ganzheitlichen Ansatz, der darauf abzielt Material-, Struktur- und Bauteileigenschaften eines hybriden kontinuierlich-diskontinuierlichen SMC Verbundes zu untersuchen. Innerhalb jeder Stufe werden dabei die Eigenschaften der individuellen sowie des hybriden Materials betrachtet, um über geeignete Kriterien den Hybridisierungseffekt zu bewerten. Analytische Modellierungsstrategien werden vorgestellt, um das Materialverhalten abzubilden.

Der untersuchte kontinuierlich-diskontinuierliche SMC Verbund zeichnete sich durch ein verbessertes mechanisches Eigenschaftsspektrum, sowohl auf Proben-, Struktur- als auch auf Bauteilebene aus. Allgemein betrachtet ermöglicht die lokale Verstärkung einen vielversprechenden Ansatz, um Material-, Struktur- sowie Bauteileigenschaften gezielt auf einen vorherrschenden Lastfall abstimmen zu können und im Optimalfall ein Eigenschaftsprofil zu generieren, welches besser als die Summe der Eigenschaften der beiden individuellen Komponenten ist. Der Effekt der Hybridisierung hing

jedoch stark vom Belastungsfall ab. Die kontinuierliche Komponente bestimmte die elastischen Materialeigenschaften. Auf Probenebene wurden durch die Hybridisierung der Zug- und Druckelastizitätsmodul mehr als verdoppelt. Eine hybride Mischungsregel, basierend auf den volumengemittelten elastischen Materialeigenschaften der beiden Einzelmaterialien, war geeignet, um den Elastizitätsmodul für Zug- und Druckbelastungen vorherzusagen. Das Laminat mit zwei kontinuierlichen kohlenstofffaserverstärkten Deckschichten wies einen viermal so hohen Biegeelastizitätsmodul, verglichen mit dem diskontinuierlichen glasfaserverstärkten SMC, auf. Eine Adaption der klassischen Laminattheorie, die es ermöglicht, den spezifischen Aufbau des Hybridlaminats sowie die Zug-Druck-Anisotropie des kontinuierlichen kohlenstofffaserverstärkten SMC zu berücksichtigen, bildete den Biegeelastizitätsmodul des hybriden CoDico SMC Verbundes sehr präzise ab.

Die Schädigungsentwicklung und somit auch die Festigkeit des hybriden SMC Verbundes basierte auf dem Versagen der kontinuierlichen Verstärkung. Dieses war vor allem durch Zwischenfaserbrüche und (inter- sowie intralaminare) Delamination charakterisiert. Die Zugfestigkeit und Biegefestigkeit konnten durch die Hybridisierung verdreifacht bzw. verdoppelt werden. Die quasistatischen Durchstoßeigenschaften, abgebildet durch die maximale Kraft und die Durchstoßenergie, welche die mechanischen Eigenschaften auf Strukturebene darstellen, waren für das hybride CoDico SMC signifikant höher im Vergleich zum nicht verstärkten diskontinuierlichen SMC. Weiterhin erhöhte eine optimierte lokale kontinuierliche Verstärkung die Steifigkeit und ertragbare Last beim Versagen im Komponententest signifikant.

Contents

List of Figures ..... **xv**

List of Tables ..... **xxiii**

List of Abbreviations and Symbols ..... **xxv**

1 Introduction **1**
1.1 Motivation 1
1.2 Scope and objective 5
1.3 Contribution to the current state of research 6
1.4 Outline of this dissertation 8

2 Current state of research **9**
2.1 Definition of hybrid materials 9
2.2 Composite materials 14
2.2.1 Definition and fundamentals 14
2.2.2 Basic mechanisms of fibrous reinforcement 16
2.3 Sheet moulding compound composites 21
2.3.1 Definition and terminology delimitation 21
2.3.2 Discontinuous SMC composites 21
2.3.3 Continuous SMC composites 57
2.4 Hybrid composites 61
2.4.1 Definition, motivation and development of hybrid composites 62
2.4.2 Evaluation of hybridisation effects 65
2.4.3 Existing concepts of hybrid SMC 68
2.5 Research questions 82

3 Materials and specimen geometries **85**
3.1 Manufacturing of SMC composites 85
3.1.1 Composition of resin systems 85
3.1.2 Manufacturing of semi-finished sheets 87
3.1.3 Manufacturing of compression moulded sheets ... 89
3.1.4 Manufacturing of pure resin sheets 92
3.1.5 Manufacturing of demonstrator part 93
3.2 Specimen preparation and geometry 94
3.2.1 Water-jet cutting and milling 94
3.2.2 End tabs 95
3.2.3 Specimen geometries 95

4 Experimental setups, procedures and data evaluation **103**
4.1 Characterisation strategy 103
4.2 Characterisation at the coupon level 105
4.2.1 Microstructural characterisation 105
4.2.2 Macrostructural characterisation 106
4.3 Characterisation at the structure level 114
4.3.1 Quasi-static puncture testing 114
4.3.2 Dynamic puncture testing 116
4.4 Characterisation at the component level 118
4.5 Data evaluation 121

5 Analytical modelling **123**
5.1 Description of modelling approach 123
5.2 Micromechanics and homogenisation methods 124
5.2.1 Fundamentals of homogenisation 124
5.2.2 Analytical modelling of fibre reinforced polymers 128
5.3 Classical laminate theory 133
5.3.1 Macromechanical characterisation of a lamina 134
5.3.2 Macromechanical characterisation of a laminate ... 134

5.4 Analytical modelling of hybrid composites 138
5.4.1 Rule of hybrid mixtures 139
5.4.2 Tensile and flexural modulus based on classical laminate theory 140

6 Results 143
6.1 Evaluation of testing methods and preliminary studies . 143
6.1.1 Tensile properties of discontinuous SMC composites 144
6.1.2 Tensile properties of continuous SMC composites 150
6.1.3 Flexural properties of SMC composites 152
6.2 Microstructural analysis 158
6.2.1 Fibre volume content 158
6.2.2 Fibre orientation distribution..... 164
6.2.3 Interface of continuous-discontinuous SMC..... 173
6.3 Mechanical properties and failure at the coupon level... 176
6.3.1 Tensile and compressive properties of polyester-polyurethane hybrid resin 176
6.3.2 Process-induced material properties of discontinuous glass fibre SMC 179
6.3.3 In-plane loading of SMC composites 190
6.3.4 Out-of-plane loading of SMC composites..... 229
6.4 Mechanical properties and failure at the structure level . 237
6.4.1 Puncture properties of discontinuous glass fibre SMC 238
6.4.2 Puncture properties of continuous carbon fibre SMC 248
6.4.3 Puncture properties of continuous-discontinuous glass/carbon fibre SMC 256
6.5 Mechanical properties and failure at the component level..... 268

6.6 Analytical stiffness prediction 271
6.6.1 Analytical stiffness prediction of discontinuous glass fibre SMC 272
6.6.2 Analytical stiffness prediction of continuous carbon fibre SMC 277
6.6.3 Analytical stiffness prediction of continuous-discontinuous glass/carbon fibre SMC 279

7 Discussion 283
7.1 Testing methodology and preliminary studies 283
7.2 Material behaviour of unsaturated polyester-polyurethane two-step curing hybrid resin system 285
7.3 Discontinuous glass fibre SMC 287
7.3.1 Microstructural aspects of discontinuous glass fibre SMC 287
7.3.2 Mechanical behaviour and damage evolution of discontinuous glass fibre SMC 291
7.4 Continuous carbon fibre SMC 301
7.4.1 Microstructural aspects of continuous carbon fibre SMC 301
7.4.2 Mechanical behaviour and damage evolution of continuous carbon fibre SMC 302
7.5 Continuous-discontinuous glass/carbon fibre SMC 308
7.5.1 Microstructural aspects of continuous-discontinuous glass/carbon fibre SMC 308
7.5.2 Mechanical properties, damage evolution and hybridisation effect 310

8 Final remarks **347**
8.1 Summary 347
8.2 Conclusion 356

Bibliography **361**

A Appendix **403**
A.1 Influence of subset size and step size 403
A.2 Influence of edge preparation 405
A.3 Tensile properties of discontinuous glass fibre SMC (2D) 406
A.4 Tensile properties of discontinuous glass fibre SMC (1D) 407
A.5 Compressive properties of discontinuous glass fibre SMC 408
A.6 Tensile and compressive properties of continuous carbon fibre SMC 409
A.7 Flexural properties of continuous carbon fibre SMC 410
A.8 Flexural properties of continuous-discontinuous glass/carbon fibre SMC 411
A.9 Classical laminate theory: calculations 412

List of Figures

1.1 Drawbacks and advantages of fibrous reinforcement 3
1.2 Advantages of hybrid SMC materials 4
1.3 Subfloor structure made of CoDico SMC 4

2.1 Families of engineering materials 10
2.2 Configurations of hybrids 11
2.3 Achievable properties of a hybrid material 13
2.4 Performance and processability of FRP 16
2.5 Failure of fibre reinforced composites 19
2.6 SMC conveyor belt 24
2.7 Cutting and compression moulding of semi-finished SMC . 25
2.8 Temperature-time evolution during SMC moulding step 26
2.9 Manufacturing of SMC: evolution of viscosity 27
2.10 Fibre orientation resulting from compression moulding 28
2.11 Tensile properties of vinlyester-based SMC composites 39
2.12 Typical tensile load-elongation curves of SMC composites .. 55
2.13 Chemistry and curing process of the UPPH resin system ... 58
2.14 Modified SMC conveyor belt 59
2.15 Compression moulded Co SMC sheet 60
2.16 Main configurations of hybrid composites 62
2.17 Hybridisation effect 1 66
2.18 Hybridisation effect 2 68
2.19 Schematic SMC line to manufacture hybrid SMC 70
2.20 Tensile modulus of elasticity and strength of hybrid SMC .. 70
2.21 Stacking sequences of hybrid SMC 72
2.22 Hybrid SMC based on chopped glass and carbon fibres 73

2.23 Process cycle to combine chopped fibre SMC with fabrics .. 74
2.24 Tensile and flexural properties of hybrid SMC 74
2.25 Hybrid CoDico SMC laminates 78

3.1 SMC manufacturing line at Fraunhofer ICT 87
3.2 Feeding of fibrous reinforcement to the conveyor belt 88
3.3 Rectangular-shaped mould 89
3.4 Square-shaped mould..... 90
3.5 Schematic illustration of compression moulding step..... 91
3.6 Co, Dico and CoDico SMC..... 91
3.7 Pre-thickened UPPH resin 92
3.8 Steps to manufacture the demonstrator part..... 94
3.9 Tensile test specimens (preliminary tests) 97
3.10 Tensile specimen..... 98
3.11 Compression specimen 98
3.12 Bending specimen 99
3.13 Puncture specimen 100
3.14 Demonstrator part..... 100
3.15 Geometry of demonstrator part 101

4.1 Vertical characterisation strategy..... 104
4.2 Horizontal characterisation strategy..... 105
4.3 Tensile test setup..... 108
4.4 Compression test setup 111
4.5 Three-point bending test setup 114
4.6 Test setup of quasi-static puncture test 115
4.7 Drop tower at the University of Windsor..... 116
4.8 Test setup of component tests 118
4.9 Test procedure of component tests..... 120

5.1 Drawing of a continuously fibre reinforced lamina..... 130
5.2 Schematic drawing of a lamina..... 134
5.3 Resultant forces and moments acting on a laminate..... 136

5.4 Section through a laminate and nomenclature 137
5.5 Schematic drawing of continuous-discontinuous laminate . 139

6.1 Influence of specimen geometry and gauge section on E_t .. 146
6.2 Influence of specimen geometry on R_t 147
6.3 Influence of edge quality on tensile properties 151
6.4 Tensile properties of Co SMC: campaign 1 and 2 152
6.5 Relative flexural modulus of elasticity 154
6.6 Flexural properties of Co SMC 155
6.7 Flexural properties of CoDico SMC 156
6.8 Flexural modulus of elasticity of Dico SMC..... 157
6.9 Fibre volume content of Dico SMC sheets (1D)..... 160
6.10 Fibre volume content of Dico SMC sheets (2D)..... 161
6.11 Local fibre volume content of Dico SMC sheets 162
6.12 Fibre volume content of Co SMC sheets 163
6.13 Orientation and convention of coordinate system 165
6.14 Fibre orientation over thickness, Dico SMC (0°)..... 166
6.15 Fibre orientation over thickness, Dico SMC (90°) 167
6.16 Fibre orientation over thickness, CoDico SMC (0°) 169
6.17 μ-CT observation of a Dico SMC specimen (0°) 170
6.18 μ-CT observation of a Dico SMC specimen (90°)..... 171
6.19 μ-CT observation of a CoDico SMC specimen (0°) (1/2).... 172
6.20 μ-CT observation of a CoDico SMC specimen (0°) (2/2).... 174
6.21 SEM observations of CoDico SMC (interface) 175
6.22 CoDico SMC sheet, top 176
6.23 $\sigma - \varepsilon$ curves: uniaxial tension, UPPH resin 177
6.24 $\sigma - \varepsilon$ curves: uniaxial compression, UPPH resin 178
6.25 Tensile properties of Dico SMC (2D) 181
6.26 Tensile properties of Dico SMC (1D) 182
6.27 $\sigma - \varepsilon$ curves: uniaxial tension, Dico SMC..... 184
6.28 Compressive properties of Dico SMC (1D)..... 185
6.29 $\sigma - \varepsilon$ curves: uniaxial compression, Dico SMC 186

6.30 Flexural properties of Dico SMC 188
6.31 $\sigma - \varepsilon$ curves: three-point bending, Dico SMC..... 189
6.32 Repr. $\sigma - \varepsilon$ curves: tension/compression, Dico SMC (0°) .. 191
6.33 Repr. $\sigma - \varepsilon$ curve: uniaxial tension, Dico SMC (0°) 192
6.34 Strain field: uniaxial tension, Dico SMC (1/2)..... 193
6.35 Strain field: uniaxial tension, Dico SMC (2/2)..... 194
6.36 Dico SMC: post-mortem, uniaxial tension, side 195
6.37 SEM of fractured Dico SMC specimen (uniaxial tension)... 196
6.38 Dico SMC: post-mortem, uniaxial compression, side..... 197
6.39 Tensile and compressive properties of Co SMC (0°) 198
6.40 $\sigma - \varepsilon$ curves: tension/compression, Co SMC (0°) 199
6.41 Damage evolution: uniaxial tension of Co SMC (1/2) 200
6.42 Repr. $\sigma - \varepsilon$ curve: uniaxial tension, Co SMC (1/2) 201
6.43 Damage evolution: uniaxial tension of Co SMC (2/2) 202
6.44 Repr. $\sigma - \varepsilon$ curve: uniaxial tension, Co SMC (2/2) 203
6.45 Strain field: uniaxial tension, Co SMC 204
6.46 Fractured Co SMC specimens, uniaxial tension, top..... 205
6.47 Fractured Co SMC specimens, uniaxial compression, side . 206
6.48 $\sigma - \varepsilon$ curves: tension/compression, Co SMC/UPPH resin . 207
6.49 Tensile and compressive properties of CoDico SMC (0°) ... 210
6.50 Tensile and compressive properties of CoDico SMC (90°) .. 211
6.51 $\sigma - \varepsilon$ curves: uniaxial tension, CoDico SMC (0°, 90°)..... 214
6.52 Comparison of $\sigma - \varepsilon$ curves, uniaxial tension (90°) 215
6.53 Repr. $\sigma - \varepsilon$ curve: uniaxial tension, CoDico SMC (0°)..... 216
6.54 Strain fields: uniaxial tension, CoDico SMC (0°) 217
6.55 Tensile specimen CoDico SMC 218
6.56 Superposition: strain field-stitching yarns (tension) 219
6.57 Damage evolution: uniaxial tension of CoDico SMC 220
6.58 Damaged CoDico SMC, uniaxial tension, side..... 221
6.59 Damaged CoDico SMC, uniaxial tension, top (1/2) 221
6.60 Damaged CoDico SMC, uniaxial tension, top (2/2) 222
6.61 SEM investigation of CoDico SMC (1/2) 223

6.62 SEM investigation of CoDico SMC (2/2) 224
6.63 Repr. $\sigma - \varepsilon$ curve: uniaxial compression, CoDico SMC 225
6.64 Strain field, uniaxial compression, CoDico SMC 226
6.65 Superposition: strain field-stitching yarns (compression) .. 227
6.66 Damaged CoDico specimen, uniaxial compression, top 228
6.67 Damaged CoDico specimen, uniaxial compression, side ... 229
6.68 $\sigma - \varepsilon$ curve: three-point bending, Dico SMC 230
6.69 Failure evolution of Dico SMC (three-point bending) 231
6.70 $\sigma - \varepsilon$ curves: three-point bending, Co SMC 234
6.71 Failure evolution of Co SMC (three-point bending) 234
6.72 $\sigma - \varepsilon$ curves: three-point bending, CoDico SMC 236
6.73 Failure evolution of CoDico SMC (three-point bending).... 237
6.74 Puncture properties of Dico SMC 240
6.75 Force- and energy-deflection responses of Dico SMC 242
6.76 Repr. $F - d$ response, Dico SMC (qs) 244
6.77 Evolution of crack volume: Dico SMC 244
6.78 Damage evolution: quasi-static puncture of DiCo SMC 245
6.79 Repr. $F - d$ response, Dico SMC (dyn) 247
6.80 Damage evolution: dynamic puncture of Dico SMC 247
6.81 Puncture properties of Co SMC. 249
6.82 Force- and energy-deflection responses, Co SMC 251
6.83 Damage evolution: quasi-static puncture of Co SMC 252
6.84 Repr. $F - d$ response, Co SMC (qs) 253
6.85 Repr. $F - d$ response, Co SMC (dyn) 254
6.86 Damage evolution: dynamic puncture of Co SMC..... 255
6.87 Puncture properties of CoDico SMC 258
6.88 Force- and energy-deflection responses, CoDico SMC 259
6.89 Repr. $F - d$ response, CoDico SMC (qs) 261
6.90 Evolution of crack volume: CoDico SMC..... 261
6.91 Damage evolution: quasi-static puncture of CoDico SMC.. 262
6.92 Damaged CoDico SMC specimen, puncture (qs)..... 264
6.93 Repr. $F - d$ response, CoDico SMC (dyn) 265

6.94 Damage evolution: dynamic puncture of CoDico 266
6.95 Damaged CoDico SMC specimen, puncture (dyn) 267
6.96 Evolution of F_{max}: Dico and CoDico demonstrator part 269
6.97 Stiffness evolution: Dico and CoDico demonstrator part ... 270
6.98 Damage evolution: Dico and CoDico demonstrator part ... 271
6.99 Halpin–Tsai approach: tensile modulus of elasticity 273
6.100 Halpin–Tsai approach: shear modulus 273
6.101 Orientation and convention of coordinate system 274
6.102 Mori–Tanaka approach: modulus of elasticity (0°) 275
6.103 Mori–Tanaka approach: modulus of elasticity (90°) 275
6.104 Prediction of $E_{t,L}$ of Co SMC (RoM) 278
6.105 Tensile modulus of elasticity (RohM) 280
6.106 Flexural modulus of elasticity of CoDico SMC (CLT) 282

7.1 Damaged UPPH specimens 286
7.2 Dry spots on Co SMC sheet 302
7.3 Fibre misalignment of Co SMC composite 305
7.4 Ondulation and fibre waviness in Co SMC composite 306
7.5 Section through moulded CoDico SMC sheet 311
7.6 Tensile properties of Co, Dico and CoDico SMC 313
7.7 Prediction of tensile strength of hybrid CoDico SMC 319
7.8 Tensile stress-strain curves: Dico, Co, CoDico SMC 320
7.9 Comparison of strain fields: uniaxial tension 323
7.10 Compressive properties of Dico, Co and CoDico SMC..... 325
7.11 Prediction of compressive strength of CoDico SMC 327
7.12 Compressive stress-strain curves: Dico, Co, CoDico SMC .. 329
7.13 Flexural properties of Dico, Co and CoDico SMC 331
7.14 Prediction of flexural strength of hybrid CoDico SMC..... 334
7.15 Flexural stress-strain curves: Dico, Co and CoDico SMC ... 335
7.16 Quasi-static puncture properties: Dico, Co, CoDico SMC .. 338
7.17 Comparison of $F-d$ and $E-d$ curves (qs) 340
7.18 Dynamic puncture properties: Dico, Co, CoDico SMC..... 342

7.19 Comparison of $F - d$ and $E - d$ curves (dyn) 343
7.20 Macroscopic observation of damaged demonstrator parts . 345

8.1 Effect of hybridisation 352
8.2 Analytical stiffness prediction 354

A.1 Influence of subset size and step size (1/2) 403
A.2 Influence of subset size and step size (2/2) 404
A.3 Surface quality before edge preparation 405
A.4 Surface quality after edge preparation 405
A.5 Tensile and compressive properties of Co SMC (90°)..... 409
A.6 Stress-strain curves: three-point bending, Co SMC 410
A.7 Stress-strain curves: three-point bending, CoDico SMC 411

List of Tables

2.1 Properties of standard thermoset materials 22
2.2 Typical properties of a standard SMC composite 34
2.3 Overview of mechanical properties of SMC composites 45
2.4 Tensile properties of continuous CFRP 61
2.5 Mechanical properties of polyester-based SMC composites .. 69
2.6 Summary of concepts to hybridise SMC composites 80

3.1 Resin components and fibre type of Dico SMC 86
3.2 Resin components and fibre type of Co SMC 86
3.3 Dimensions of tensile specimens 96

4.1 Three-point bending test parameters 112
4.2 Cycle number and corresponding maximum deflection..... 119

6.1 Tensile test parameters of preliminary tests 145
6.2 Dimensions of gauge sections for preliminary tensile tests .. 145
6.3 Tensile properties: variation of subset and step sizes 148
6.4 Tensile and compressive properties of UPPH resin 179
6.5 Flexural properties of Dico SMC (1D) 187
6.6 Tensile and compressive properties of Co SMC..... 208
6.7 Tensile and compressive properties of CoDico SMC (0°)..... 212
6.8 Tensile and compressive properties of CoDico SMC (90°) ... 213
6.9 Flexural properties of Co SMC in fibre direction (0°) 233
6.10 Flexural properties of CoDico SMC 236
6.11 Puncture properties of Dico SMC 239
6.12 Puncture properties of Co SMC 250

6.13 Puncture properties of CoDico SMC 257
6.14 Input parameters of Dico SMC 272
6.15 Mori–Tanaka approach: tensile modulus of elasticity 276
6.16 Mori–Tanaka approach: flexural modulus of elasticity 277
6.17 Input parameters of Co SMC 278
6.18 Input parameters considered for CLT 281

A.1 Tensile properties of Dico SMC (2D) 406
A.2 Tensile properties of Dico SMC (1D) 407
A.3 Compressive properties of Dico SMC (1D) 408
A.4 Flexural properties of Co SMC (0°) 410
A.5 Flexural properties of CoDico SMC (0°) 411

List of Abbreviations and Symbols

Abbreviations

BMC	Bulk moulding compound
BPA	Bisphenol A
$CaCO_3$	Calcium carbonate
CF	Carbon fibre
CLT	Classical laminate theory
CMS	Computational material science
CO_2	Carbon dioxide
Co	Continuous
CV	Coefficient of variation
CoDico	Continuous-discontinuous
DIC	Digital image correlation
Dico	Discontinuous
dyn	Dynamic
EoH_1,EoH_2	Effect of hybridisation
FOT	Fibre orientation tensor
FRP	Fibre reinforced polymer/plastic
FVC	Fibre volume content
FWC	Fibre weight content
GF	Glass fibre

GFRP	Glass fibre reinforced polymer/plastic
GRK	Graduate school
IAM	Institute for Applied Materials
ICT	Institute for Chemical Technology
IRTG	International Research Training Group
ITM	Institute of Engineering Mechanics
IWM	Institute for Mechanics of Materials
KIT	Karlsruhe Institute of Technology
nom.	Nominal
qs	Quasi-static
RohM	Rule of hybrid mixtures
RoM	Rule of mixtures
SEM	Scanning electron microscopy
SMC	Sheet moulding compound
TGA	Thermogravimetric analysis
P	Polyester
UP	Unsaturated polyester
UPPH	Unsaturated polyester-polyurethane hybrid resin
VE	Vinylester
vol.%	Volume percent
wt.%	Weight percent
1D	One-dimensional
2D	Two-dimensional
3D	Three-dimensional
μ-CT	Micro-computed tomography

Indices

$(\cdot)_A$	Anisotropy
$(\cdot)_C$	Composite
$(\cdot)_{C1}$	Component 1
$(\cdot)_{C2}$	Component 2
$(\cdot)_c$	Compressive
$(\cdot)_{crit}$	Critical
$(\cdot)_{exp}$	Experimental
$(\cdot)_F$	Fibre
$(\cdot)_f$	Flexural
$(\cdot)_{hyb}$	Hybrid
$(\cdot)_i$	Summation index
$(\cdot)_{int}$	Interfacial
$(\cdot)^k, (\cdot)_k$	kth layer
$(\cdot)_L$	Longitudinal
$(\cdot)_M$	Matrix
$(\cdot)_{m1}$	Material 1
$(\cdot)_{m2}$	Material 2
$(\cdot)_{max}$	Maximum
$(\cdot)_{min}$	Minimum
$(\cdot)_n$	Number
$(\cdot)^0$	Mid-plane
$(\cdot)_p$	Puncture
$(\cdot)_{RoM}$	Rule of mixtures
$(\cdot)_r$	Reference
$(\cdot)_T$	Transverse
$(\cdot)_t$	Tensile

$(\cdot)_u$	Ultimate
$(\bar{\cdot})$	Averaged (effective) value
$(\cdot)_{1,2,3}$	Axes of coordinate system (continuous lamina)
$(\cdot)_0$	Origin
$\langle\cdot\rangle$	Volume-averaged arithmetic mean value
$(\cdot)_{x,y,z}$	Axes of coordinate system

Scalars

A	Section
b	Width
b_f	Bending factor
D	Damage variable
d	Deflection (puncture)
E	Energy
$E_{(\cdot)}$	Modulus of elasticity
F	Force
f	Factor
h	Thickness
h_f	Thickness of face layer
I	Moment of inertia
L	Span
l	Length
m	Mass
N	Total number of layers
n	Number
$R_{(\cdot)}$	Strength (macroscopic scale)
r	Radius

r^2	Regression coefficient
S	Stiffness (macroscopic scale)
s	Deflection (bending)
V	Volume (macroscopic scale)
N_v	Number of fibre voxels
z	Vertical distance from midplane
α	Number of phases
γ_1, γ_2	Correction factor
$\varepsilon^0_{xx}, \varepsilon^0_{yy}, \gamma^0_{xy}$	Mid-plane strains of laminate
$\varepsilon_{xx}, \varepsilon_{yy}$ and γ_{xy}	Deformation of laminate
η_N, η_T	Parameter of Halpin-Tsai approach
$\kappa^0_{xx}, \kappa^0_{yy}$, κ^0_{xy}	Mid-plane curvatures of laminate
μ	Standard deviation
ν	Poisson's ratio
ρ	Density
ϕ	Volume content
ψ	Weight content

Tensors

A	Extensional stiffness
B	Coupling stiffness
C	Stiffness
D	Bending stiffness
M	Resultant moments
N	Resultant forces
n	Direction of fibre axis
O	Fibre orientation tensor

$\mathbf{Q}$	Reduced stiffness matrix
ε	Strain
σ	Stress
$\mathbb{C}$	Stiffness
$\mathbb{I}^S$	Identity
$\mathbb{L}_A$, $\mathbb{L}_B$,$\mathbb{L}_{MT}$	Localisation tensor
$\mathbb{O}$	Fibre orientation tensor
$\mathbb{S}$	Compliance

Operators

$\otimes$	Dyadic product

1 Introduction

This section presents the framework and motivation of this dissertation in the broader scientific context. The objectives are stated, and the contribution of this work to the state of research is specified. Finally, the structure of the document is outlined, and the relationship between the chapters is explained.

1.1 Motivation

Today, cars are major emitters of greenhouse gasses, responsible for 12 % of total carbon dioxide (CO_2) emissions in the European Union (European Union, 2009). The transport sector as a whole represents almost a quarter of Europe's greenhouse gas emissions and is the main cause of air pollution in cities (European Commission, 2016). The European Union enforces car manufacturers to reduce the fleet average of CO_2 emission to be achieved by all new cars to 95 g of CO_2 per kilometre (European Union, 2009). For this purpose, car and truck manufacturers will also have to reduce the average weight of their vehicles. In addition, given the stated goal of replacing conventional engines with electrical drives as part of the German energy turnaround and given the significant weight of vehicle batteries, manufacturers of electric vehicles must also develop new material concepts and manufacturing techniques.

Lightweight design in the transportation sector, whose significance has continued to grow in recent decades, will thus remain an increasingly important field of research for the foreseeable future.

Substituting both non-structural and semi-structural components with fibre reinforced polymers has been a vital method of reducing vehicle weight. However, this approach seems to have already been quite thoroughly exploited. The logical step forward to address vehicle weight is therefore to make structural components of vehicles from lightweight fibre reinforced polymers. Naturally, this step places the mechanical properties of lightweight materials directly in focus. Depending on the type and architecture of fibrous reinforcement, fibre reinforced polymers have different advantages and drawbacks regarding their mechanical properties and their manufacturing.

Sheet moulding compound composites (SMC), which are characterised by a discontinuous reinforcement, comprise an attractive material class for many technical applications and have long been successfully used for non-structural components. In Europe, truck manufacturing was the first industry to fully recognise the commercial potential of SMC to be considered in body panels. Pioneering independent truck builders used an all-SMC truck cab as far back as the early 1970s (The European Alliance for SMC/BMC, 2016). Since then, the use of SMC materials has intensified tremendously, especially in the transportation sector. Mass transit is an important market for SMC composites, which are used for the interior parts of trains, for example. The SMC technology attracts attention due to its low material and tooling costs, the prospect of fully automated manufacturing as well as short manufacturing times. It also allows for manufacturing of complex geometries due to its high formability during the compression moulding step.

Its significant disadvantages, however, include its low strength and stiffness, caused by the discontinuous fibres used in conventional chopped, fibre reinforced SMC composites.

Continuous fibre reinforced polymers, in contrast, stand out due to their high stiffness and strength in fibre direction, which make them very attractive for load-bearing components. Nevertheless, the excellent mechanical properties of this material class come at the expense of higher material and manufacturing costs and limited formability (Figure 1.1).

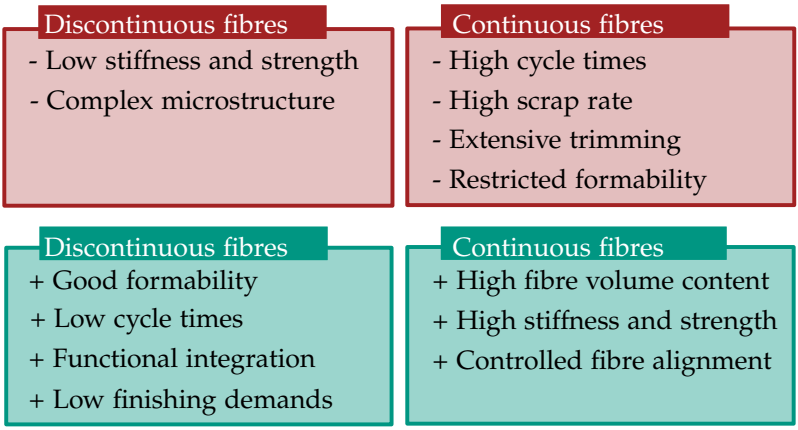


Figure 1.1: Drawbacks (red) and advantages (green) of discontinuous (Dico) and continuous (Co) fibrous reinforcement.

Hybridising composites would theoretically enable the creation of a material that combines the benefits of the individual composite materials. An innovative approach followed by the International Research Training Group (IRTG) on the integrated engineering of continuous-discontinuous long fibre reinforced polymer structures (GRK 2078)

aims to accomplish exactly this goal (Böhlke et al., 2016). In this project, continuous and discontinuous SMC composites are combined in a one-shot process to attain both the flowability of discontinuous SMC and the superior mechanical properties of continuous SMC (Figure 1.2), ultimately obtaining locally reinforced parts made from SMC composites (Figure 1.3).

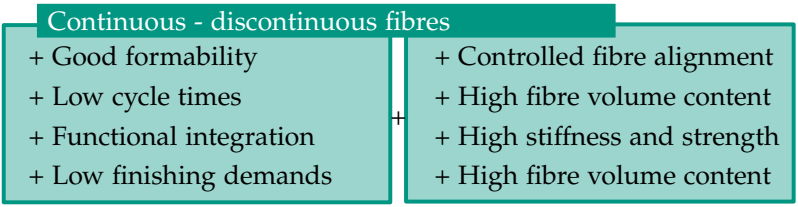


Figure 1.2: Advantages of hybrid continuous-discontinuous SMC materials.

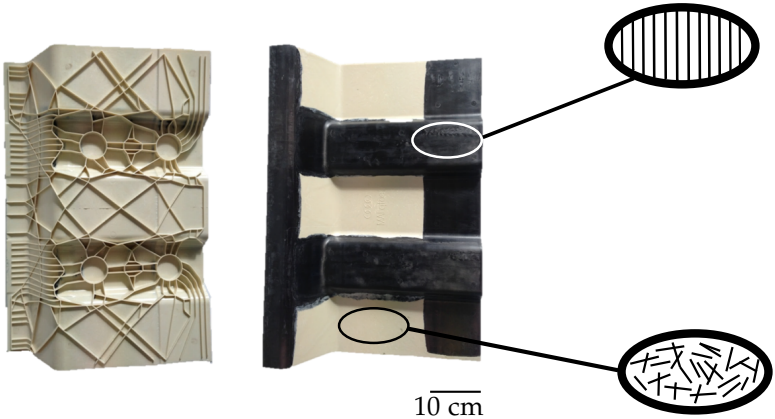


Figure 1.3: Subfloor structure made of discontinuous glass fibre (GF) SMC with continuous carbon fibre (CF) SMC reinforcements (image provided by Fraunhofer ICT).

1.2 Scope and objective

Hybrid materials, which are based on a combination of different composites, offer interesting mechanical and structural property profiles. Depending on the architecture of the reinforcing fibres and the macroscopic structure, a hybrid composite with properties tailored to the specific requirements of a certain component can be designed. However, the resulting material and structural properties become arbitrarily complicated and represent an important challenge for material characterisation and modelling. Generally, hybrid composites are heterogeneous both on the macroscopic scale (e.g. stacking sequence of different layers) and on the microscopic scale (e.g. fibre orientation and length distribution). Hence, the resulting material properties depend not only on stacking sequence and the macroscopic architecture of the hybrid composite but also on the process-induced microstructure and the interaction between the individual components. Numerous test methods and standards, considering different fibre architectures have been established to characterise the mechanical properties of fibre reinforced polymers. However, as soon as different reinforcing architectures are combined, these standards are no longer necessarily valid. Robust experimental and analytical tools are required to explain and describe the resulting properties and characteristics of the hybrid composites, in order to successfully combine continuous and discontinuous SMC for structural applications. Thus, this dissertation aims primarily to characterise the structure-property-relationships of continuous, discontinuous and hybrid continuous-discontinuous SMC composites. For this purpose, reliable characterisation methods must be defined, including adapting testing methods and investigating novel and improved experimental techniques to gain insight into SMC's material behaviour. In addition, characterisation of discontinuous, continuous and hybrid continuous-discontinuous SMC has

to be carried at the coupon, structure and component levels to deduce material, structural and component properties. A second objective is the investigation and evaluation of the hybridisation effect. For this purpose, criteria to characterise an effect of hybridisation are presented and chosen according to their suitability. Apart from mechanical material properties, the damage evolution and failure mechanisms resulting from different loading cases are thoroughly considered. The hybrid material and its individual components have therefore been described at micro-, meso- and macroscopic levels. Furthermore, this dissertation aims to analytically predict and model the stiffness and strength of hybrid SMC composites exposed to uniaxial loads. The aforementioned objectives strongly focus on an interaction with simulation tools and mechanics to clearly identify which data and parameters are necessary to define to obtain a robust and reliable material model. With respect to the implementation of continuous-discontinuous SMC composites in technical applications, a profound understanding of material properties and damage evolution enables one to accommodate safety factors, creating more potential for lightweight applications.

1.3 Contribution to the current state of research

This dissertation investigates the mechanical material, structural and component properties, and damage evolution and failure mechanisms of a hybrid continuous-discontinuous (CoDico) SMC composite. In particular, it contributes insight into mechanical performance of a novel hybrid composite based on advanced experimental approaches:

- Both components, the discontinuous glass and the continuous carbon fibre SMC composite, are based on a novel unsaturated

polyester-polyurethane *two-step curing hybrid resin* system. The *continuous (Co) SMC* considered for local reinforcement is manufactured by an *adapted SMC process* on a conventional SMC conveyor belt. The discontinuous (Dico) *structural SMC* within this contribution aims to present better mechanical properties than standard SMC composites. To meet this requirement, the resin system features *no fillers*. This absence leads to a SMC composite featuring a high fibre volume content combined with a low density. A method is presented to successfully *manufacture hybrid CoDico SMC laminates*.

- *Mechanical testing methods are adapted* to meet the difficulties of testing continuous (Co), discontinuous (Dico) and continuous-discontinuous (CoDico) materials.
- *Digital image correlation (DIC)* enabled the capturing of three-dimensional (3D) strain fields to get a deeper understanding of evolving damage on a macroscale.
- The mechanical characterisation also focusses on *structural properties* and rate dependence, as well as *component testing*.
- *An analytical approach* is presented to predict mechanical properties of hybrid CoDico SMC composites exposed to different loading cases.
- *The damage evolution and failure mechanisms* of hybrid CoDico SMC composites are investigated on a macroscopic scale (in-situ and ex-situ) and on a microscopic scale (ex-situ and post-mortem).
- Methods and criteria to *evaluate the effect of hybridisation* are introduced, evaluated and applied.

In summary, this dissertation concerns manufacturing, characterising and analytically modelling of sheet moulding compound composites considering a new hybrid material, based on different fibrous reinforcement architectures and a novel resin system.

1.4 Outline of this dissertation

Chapter 2 begins with a summary of the current state of research of discontinuous sheet moulding compound composites, which focusses on processing technology and mechanical material properties. It then reviews conceptions of structural SMC and hybridisation. Chapter 3 introduces the material system considered for characterisation and modelling. Experimental methods to determine mechanical material, structural and component properties of hybrid SMC composites are described in chapter 4. Chapter 5 introduces the basics of analytical modelling with respect to existing approaches for continuous and discontinuous (long) fibre reinforced polymers. Chapter 6 and chapter 7 present and discuss the results of the experimental characterisation and analytical modelling of the hybrid SMC. In chapter 8 this dissertation closes with a summary of the study's main conclusions.

2 Current state of research

This chapter starts with a definition and description of hybrid materials and composites in general before turning to sheet moulding compounds (SMC). Besides the material's composition and manufacturing process, the advantages and disadvantages of this material class are discussed, and recent trends in the field of (structural) SMC are presented. A focus lies on the description of macromechanical material properties and the interaction of the material's microstructure with resulting mechanical and structural behaviour as well as failure mechanisms. In the second part, hybrid composites, their definition and development within the last few years are introduced. Closing the chapter, hybridisation concepts of SMC are presented to bridge existing approaches and novel insights of this dissertation.

2.1 Definition of hybrid materials

Engineering materials can be classified into metals, ceramics, glasses, elastomers and polymers (Figure 2.1). Every family of material is characterised by common features, including properties, processing routes and similar applications. A distinct profile of properties relating to a specific technical application, is the main criterion by which to choose materials for a component (Ashby, 2006). Due to recent technological developments and expanded requirements on material properties, standard materials belonging to one of the aforementioned families can not entirely meet all requirements. Thus, hybrids

unite two or more materials, aiming to combine the advantageous properties of different families while avoiding their shortcomings.

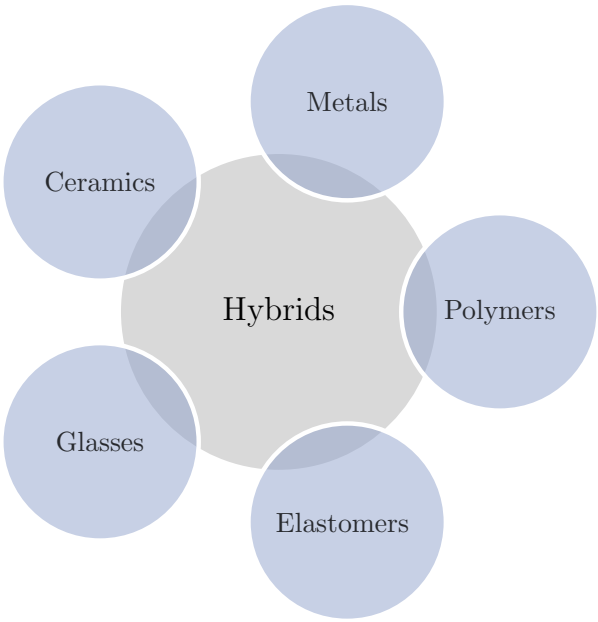


Figure 2.1: Basic families of engineering materials: metals, ceramics, glasses, polymers and elastomers, which can be combined into hybrids, according to Ashby (2006).

According to Ashby (2006) hybrids can be defined as a combination of two (or more) materials in a predetermined configuration, relative volume and scale. Hybrids occupy areas of property space previously unoccupied by bulk materials, and they are to serve a specific engineering purpose in an optimal manner. On the macroscopic scale, a hybrid behaves like a homogeneous solid, described by its own set of thermomechanical properties. The resulting properties of the hybrid material cannot always be described or calculated easily. Hence, it is

favourable to define bounds or limits of a mechanical property. The main representative classes of hybrids are composites, sandwiches, segmented structures, lattices and foams (Figure 2.2).

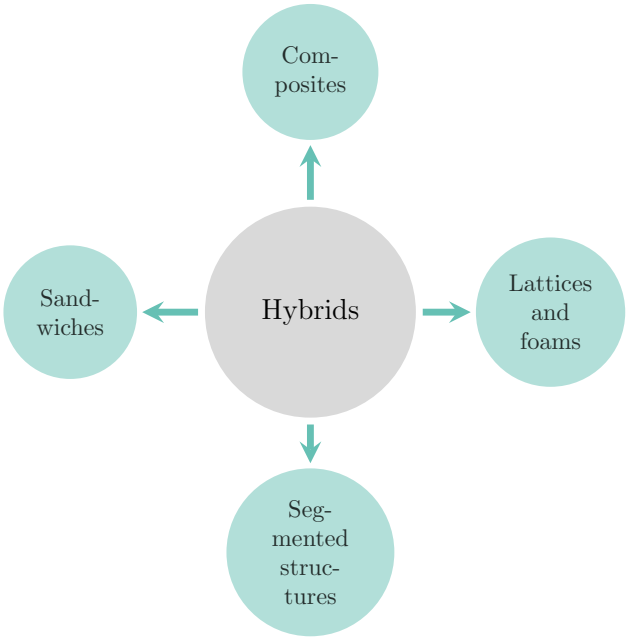


Figure 2.2: Configuration of hybrids: composites, sandwiches, segmented structures and lattices, according to Ashby (2006).

Nestler (2012) has presented a slightly different definition, describing a composite as a macroscopically homogeneous material, in contrast to a hybrid, which is heterogeneous on the macroscopic scale. A distinction is made between mixed materials design and hybrid materials (compounds). Mixed materials design is characterised by combining different materials considering joining technologies. A joining zone exists. Each material exists in an autarkic manner and

offers a distinct profile of properties. One of the materials may be dominant. On the other hand, hybrid materials (compounds) are based on at least two different subsystems (materials). In general, the different subsystems work equivalently as a functional and structural unit, and the property profile results from the combination of the properties of the individual constituents. The materials are combined without joining elements or additives and the transition between the subsystems is marked by an interface.

Nestler (2012) has defined five main groups of materials - metals, polymers, ceramics, composites and natural materials - as well as three levels of mixed materials design and the creation of hybrid materials (compounds). Mixed materials design and hybrid materials can, first of all, be formulated by combining materials belonging to different material main groups. A second possibility arises in the combination of materials belonging to the same material main group or even in the combination of the same type of material but with different compositions.

Depending on the shape of materials and the way they are combined, different possibilities arise for the properties that be achieved with hybridisation. The possible resulting properties of a hybrid material, which reflect those of its individual components combined in a distinct way, are depicted in Figure 2.3. In the "best of both" scenario (point A), the hybrid, which is based on a combination of material 1 (M1) and material 2 (M2), exhibits the best properties of both components. In point B (the "rule of mixtures" [RoM] scenario) the resulting property of the hybrid is described by the arithmetic average of the individual component properties, weighted by their volume fractions. If "the weaker link dominates" (point C) the hybrid properties are described by the harmonic rather than the arithmetic

mean value. Point D describes "the least of both" scenario, for which a component of the hybrid might be designed to fail early to fulfil a special function.

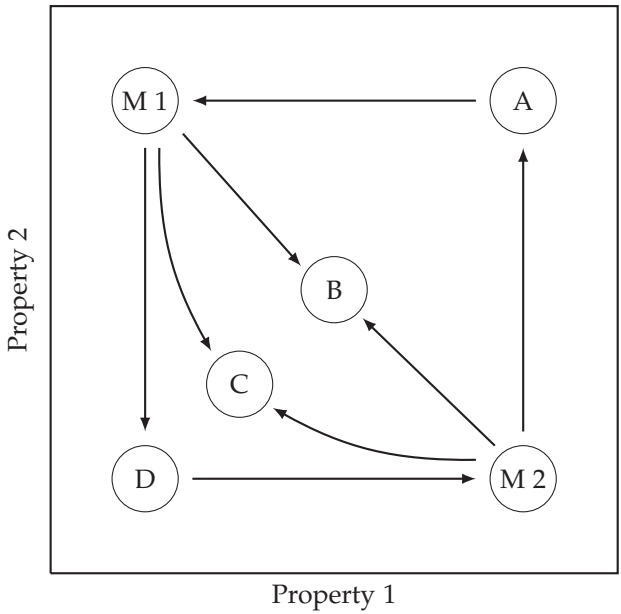


Figure 2.3: Achievable properties of a hybrid material consisting of material 1 (M1) and material 2 (M2). A: "the best of both", B: "rule of mixtures (RoM)", C: "the weaker link dominates", D: "the least of both" (Ashby, 2006).

Within this dissertation, the term hybrid composite refers to a combination of different polymer-based composites (macroscopically homogeneous) combined into a hybrid material (macroscopically heterogeneous). In the following, a more detailed description of composites and hybrid composites is presented.

2.2 Composite materials

2.2.1 Definition and fundamentals

In contrast to hybrids, which consist of two or more materials with individual components that can clearly be distinguished on the macroscopic scale, composite materials are macroscopically homogeneous multiphase materials. In principle, and according to Ashby (2006), any two material families depicted in Figure 2.1 can be combined to form a composite. Each component, which is different in terms of composition or form, remains together and retains its identity and properties (Lee, 1995). A well-designed combination of the different materials leads to a material with desirable properties, not obtainable with only one of the constituents. The application of composite materials enables one to optimise the mechanical properties of a structure, which can be tailored to fulfil specific requirements (Ashby, 2006; Rösler et al., 2012).
In general, a composite consists of a matrix and a reinforcing phase. The reinforcing element holds the load-bearing function, while the surrounding matrix aims to protect the reinforcing component, transfers loads to the reinforcement and defines the shape of the composite (Henning et al., 2011). A first classification of composite materials is based on the type of the matrix phase (Cardarelli, 2008; Rösler et al., 2012). Considering polymer matrix composites, the polymer-based matrix system, which can be either a thermoset, thermoplastic or elastomer, is reinforced by particles, whiskers or fibres. Thus, the second level of classification refers to the type of reinforcement characterised by the aspect ratio (Henning et al., 2011). In contrast to whiskers and particles, fibres have one dominating dimension that is significantly larger, by orders of magnitudes, than the other two dimensions. The structure and properties of the reinforcing

component of a composite have the most pronounced effect on resulting material properties. The advantage of considering fibres as a form of reinforcement arises from the fact that the load transfer from the matrix is particularly efficient when the dimensions of the reinforcing material extend as far as possible in the load direction. In addition, fibres feature a typical diameter between 5 µm to 25 µm, and their defects are therefore also very small size. The third level classifies fibre reinforced polymers by the length and geometry of the reinforcing fibres and distinguishes between short (length < 1 mm), long and continuous fibre composites (Rösler et al., 2012).

Short and long fibre composites might be defined either by a random or by a partially aligned fibre orientation and are also named discontinuous or chopped fibre composites. Continuous fibre composites are reinforced by oriented, unidirectionally aligned, fibres. Finally, hybrid composites, consisting of either a mix of discontinuous and continuous fibrous reinforcement or of different fibre types, can be distinguished (Gibson, 2007). Since this chapter aims to generally introduce composite materials, hybrid composites are described in more detail in section 2.4.

A significant characteristic of a fibre reinforced polymer is its anisotropy and the heterogeneous microstructure that strongly affects the macroscopic material properties. Continuous fibre reinforced polymers stand out due to their high stiffness and strength in the fibre direction, and they are very attractive for load-bearing structures and components. However, the high load-bearing capacity of continuous fibre reinforced polymers is accompanied by higher material and manufacturing costs. Another drawback is the material's very limited formability. Consequently, unidirectionally reinforced composites are considered only for structures manufactured with a

small-to-average number of pieces and low geometrical complexity. In contrast, discontinuous, long fibre reinforced polymers offer much design freedom and lower material and manufacturing costs. However, a decisive disadvantage of discontinuous, long fibre reinforced polymers is significantly reduced mechanical properties, as compared to unidirectional fibre reinforced composites, due to the finite fibre length (Figure 2.4).

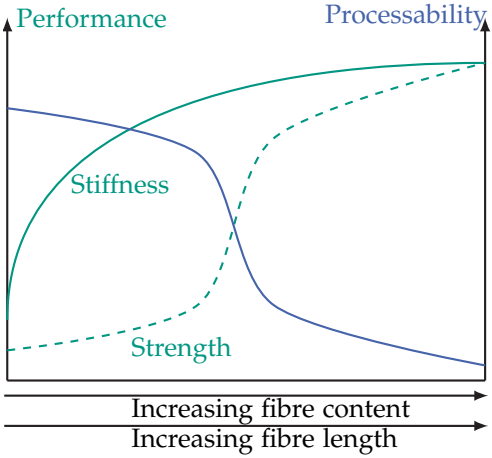


Figure 2.4: Schematic and qualitative drawing of performance of fibre reinforced polymers in terms of stiffness, strength and processability depending on fibre content and fibre length.

2.2.2 Basic mechanisms of fibrous reinforcement

Fibre reinforced polymers are based on the principle of load sharing and load transfer between different material phases. One phase, the fibres, are the reinforcing component, and the second phase, the matrix, transfers loads between the reinforcing elements. Characterised

by high specific stiffness and strength, fibres improve the mechanical performance of a polymer, whereas the improvement strongly depends on fibre content, fibre orientation and length distribution, as well as the fibre-matrix interface.

In composites, reinforced with unidirectionally aligned fibres, stress applied in the fibre direction results in the same strain in the fibres and the matrix, if one assumes that both components behave elastically and are perfectly bonded. Sustained stresses, however, occur in the same ratio as their tensile moduli of elasticity. Generally, failure mechanisms and damage evolution result from the behaviour of the matrix, the fibres and the fibre-matrix interface (Friedrich, 1989), and important failure mechanisms for continuous fibre reinforced polymers are fibre and matrix fracture (Hull and Clyne, 1996). Since continuous fibre reinforced polymers often build up as laminates consisting of individual plies, featuring an equal or different fibre orientation, fibre breakage (translaminar) may be accompanied by fractures along the fibres (inter-fibre or intralaminar) and interlaminar fractures between different plies (Friedrich, 1989), commonly termed delamination (Marom, 1989).

If exposed to uniaxial tension, a continuous fibre reinforced composite deforms as the load increases in the following stages (Jones, 1999):

1. Fibres and matrix deform elastically.
2. Fibres continue to deform elastically, and the matrix deforms plastically.
3. Fibres and matrix may deform plastically.
4. Fibres fracture, followed by failure of the composite material.

Depending on the ultimate (u) or failure strain of matrix (M) ($\varepsilon_{M,u}$) and fibre (F) (ε_{Fu}), two cases of failure evolution can be identified (Figure 2.5a and 2.5b).

In case (a), the fibres break before matrix failure strain ($\varepsilon_{M,u}$) is reached. Below the critical fibre content ($\phi_{F,crit}$), failure is matrix-dominated. In case (b), the strength of the composite follows a rule of mixtures with elastic behaviour of the matrix and fibres up to a deformation equal to the failure strain of the matrix ($\varepsilon_{M,u}$). At this point, matrix cracking is initiated, and the load is progressively transferred to the fibres, which gradually break. Final fracture occurs when strain is equal to fibre failure strain ($\varepsilon_{F,u}$).

If a composite is subjected to mechanical loads, independent from velocity, energy absorption is based on material deformation and the creation of new surfaces. The properties of the reinforcing component, loading case and loading rate generally define which mechanisms appear where at what time and in what amount (Schoßig, 2011).

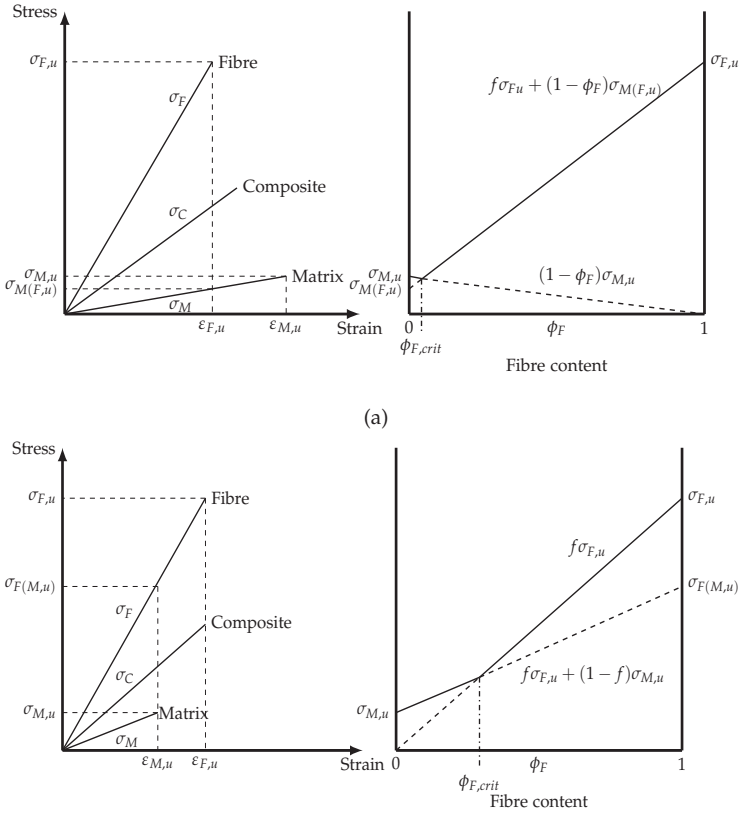


Figure 2.5: Schematic plot for idealised failure of fibre reinforced composites with fibre and matrix failing in a brittle manner. Stress-strain curves of fibre, matrix and composite as well as dependence of composite failure stress on fibre (volume) fraction are depicted. $\sigma_{F,u}$ and $\sigma_{M,u}$ refer to the failure stress of fibre and matrix. $\sigma_{F(M,u)}$ is the stress in the fibre when matrix strength is reached. $\sigma_{M(F,u)}$ refers to the stress in the matrix at fibre failure stress (strength), respectively. In case (a) failure strain of the matrix is higher than failure strain of the fibre and in case (b) failure strain of the fibre is higher than failure strain of the matrix, adapted from Hull and Clyne (1996).

Stress transfer from matrix to the fibres leads to a tensile stress distribution of zero at the ends of the fibre and maximum in the centre. In contrast, interfacial shear stresses show a maximum at the fibre ends and are equal to zero in the centre (Hull and Clyne, 1996). The length of the reinforcing component, hence the fibres, plays a significant role in the mechanical performance of fibre reinforced composites. A decrease in fibre length decreases the reinforcing effect, since the proportion of the total fibre length, which is not fully loaded increases. Below the critical fibre length, l_{crit}, with

$$l_{crit} = \frac{d_F \cdot \sigma_{F,u}}{2\tau_{int}}, \tag{2.1}$$

considering the diameter and strength of the fibre (d_F and $\sigma_{F,u}$) and the interfacial shear strength (τ_{int}), the fibre cannot undergo any further fracture, and damage is characterised by pull-out of the fibres. If the fibre length l exceeds l_{crit} the orientation of the fibre with respect to direction of crack extension determines whether fibre fracture or pull-out is more likely to happen (Hull and Clyne, 1996; Piggott, 1980).

In discontinuous fibre reinforced composites, one can no longer assume that strains in the fibre and the matrix are the same. Pulling on a composites results in a smaller extension of the fibre than the matrix, and shear strains develop at the surfaces of the fibre, which transfer the stress between the fibre and the matrix (Piggott, 1980). Failure in discontinuous fibre reinforced composites may favourably start at microvoids or microcracks, which might be a result of the manufacturing process.
The growth of cracks and final failure are a result of different separation mechanisms on the microscale, and in particular, matrix

deformation and fracture, fibre-matrix debonding, fibre pull-out and fibre fracture are of special importance (Lauke et al., 1990). The fracture energy of a composite is finally given by a summation of the energy contributions of the different failure mechanisms and their involvement with the damage evolution (Friedrich, 1989).

2.3 Sheet moulding compound composites

2.3.1 Definition and terminology delimitation

Sheet moulding compound composites (SMC) belong to the material class of fibre reinforced thermosets. In combination with bulk moulding compounds (BMC), SMC have recently had the highest economic importance in terms of production volume in Europe (Witten et al., 2016). The term SMC describes the flowable pre-impregnated semi-finished material, generally consisting of the resin, reinforcing fibres and inorganic fillers and additives (AVK - Industrievereinigung Verstärkte Kunststoffe e.V., 2013; Neitzel et al., 2014). Depending on application and special requirements, ingredients may vary widely (Kia, 1993; Wang et al., 2011). In addition, SMC also refers to the process of converting the semi-finished material into a composite part, usually achieved through compression moulding (Orgéas et al., 2011).

2.3.2 Discontinuous SMC composites

2.3.2.1 Composition

In general SMC consist of a matrix, a fibrous reinforcement, and additives and fillers. The individual constituents are described in the following.

The matrix

The matrix aims to bind the fibrous reinforcement together, protecting the fibres from the environment and shielding them from damage due to handling, for example. In addition, the matrix distributes the load to the fibres. Although it has relatively low mechanical properties compared to the fibres, matrix properties play a significant role in the resulting mechanical performance, especially due to resulting interface properties with a specific fibre type. Sheet moulding compounds are based on thermosets. Table 2.1 details the characteristics of different resin systems, considered for SMC composites.

Table 2.1: Characteristic mechanical and thermal properties of standard thermoset materials, according to Berreur et al. (2002) and Orgéas et al. (2011).

Polymer	Density in $g\,cm^{-3}$	Tensile modulus of elasticity in GPa	Tensile strength in MPa	Tensile elongation in %	Flexural modulus of elasticity in GPa	Heat resistance in °C
Polyester (UP)	1.2	3.0 – 3.5	50 – 65	1.5	3.0	120
Vinylester	1.1 – 1.3	3.5 – 4.0	70 – 90	3.0	3.5	140
Phenolic resin	1.2	3.0 – 3.5	40 – 55	1.5	3.0	120 – 150
Epoxy	1.1 – 1.4	3.5 – 4.0	50 – 90	3.0	3.0	120 – 200
Polyurethane	1.1 – 1.5		20 – 50		1.0	100 – 120
Polyimide	1.3 – 1.4		30 – 40		4.0	250 – 300

Unsaturated-polyester (UP) resins are most commonly used as matrix material of standard SMC, due to their good physical and mechanical performance in solid state, low cost and short curing times (Malik et al., 2000). Furthermore, vinylester, phenolic or epoxy resins are also widely considered depending on specific demands (Abrams, 2001; Orgéas et al., 2011).

Fillers and additives

Possible additional ingredients include low-profile additives, cure initiators, thickeners, process additives and mould release agents, which aim to enhance the processability of the material and the end-performance of the part (The European Alliance for SMC/BMC, 2016). Thickening agents, especially, are important to increase the viscosity of the paste since a sufficiently high viscosity is needed for the handling of the semi-finished sheets. Magnesium oxide, magnesium hydroxide and calcium oxide are typical thickening agents (Abrams, 2001; Bücheler, 2018). Fillers, most commonly calcium carbonate ($CaCO_3$), are generally added to the paste to reduce costs and to improve specific properties, for example chemical or heat resistance, dimensional stability, surface quality or shrinkage (Abrams, 2001).

Fibrous reinforcement

A standard SMC is reinforced by discontinuous glass fibres, with a typical length of 25 mm to 50 mm (Mallick, 2007; Wang et al., 2011); the individual filaments feature a diameter between 9.5 µm to 16 µm (Orgéas et al., 2011). Fibre mass fraction in standard SMC formulations vary between 10 wt.% to 65 wt.% (Mallick, 2007; Orgéas et al., 2011). Fibres are present as bundles of individual filaments, (randomly) oriented in the plane of the sheet. The cross section of the fibre bundles is commonly described as an ellipse with a minor axis ranging between 60 µm to 200 µm and a major axis between 500 µm to 1000 µm (Le et al., 2008). The glass fibre volume fraction in a bundle is 65 % on average and the remaining volume is either occupied by sizing, entrapped air or resin (Orgéas et al., 2011). The sizing occupies in general 1.4 wt.% to 1.8 wt.% (Feuillade et al., 2006).

2.3.2.2 Manufacturing

Manufacturing of discontinuous fibre reinforced SMC is based on a conventional two-step process. Firstly, all ingredients of the paste, except the reinforcing fibres, are mixed together, and the paste is then doctored onto a moving carrier foil on a flat conveyor belt (Figure 2.6).

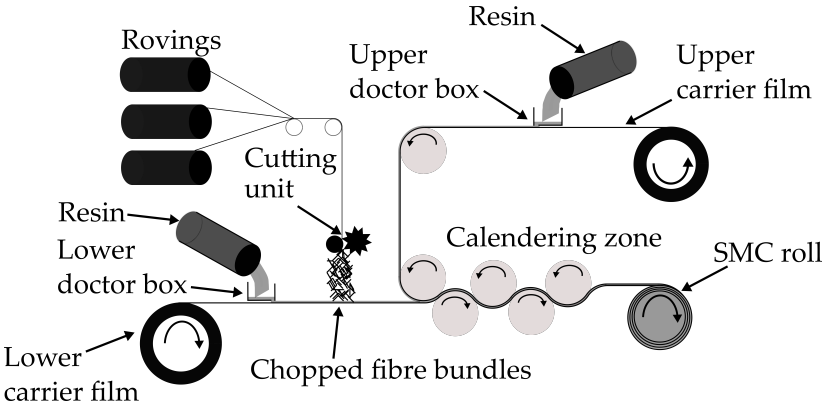
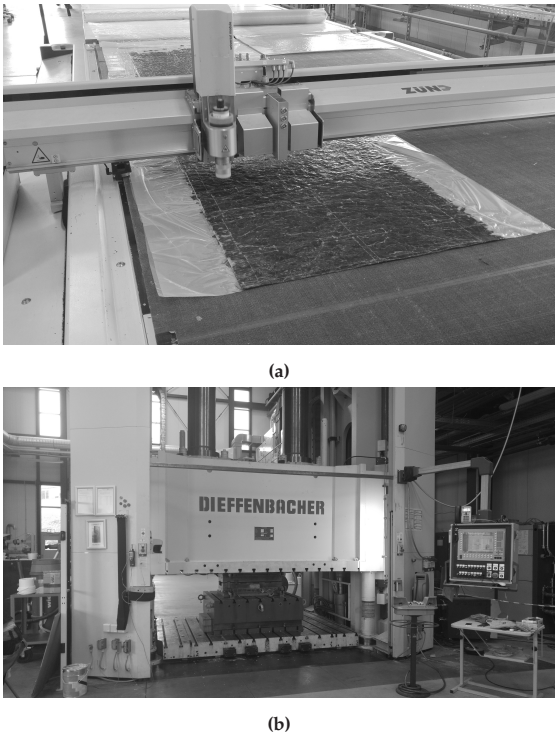


Figure 2.6: SMC conveyor belt to manufacture discontinuous fibre reinforced semi-finished SMC sheets.

The glass fibre rovings are cut and fall onto the paste layer to form an SMC mat. With control of the speed of the conveyor belt and the rotation of the cutting unit, the fibre length and volume content of the SMC material can be adjusted. The SMC mat is sandwiched between another layer of carrier foil and paste. The following calendering aims to impregnate the fibres at a relatively low viscosity of the matrix material. In addition, this step may dispel the entrapped air within the sandwich. Finally, the semi-finished sheet is rolled up and stored for maturation, which is necessary to allow the resin to chemically thicken to facilitate handling and cutting as well as to enable the following compression moulding step. After maturation,

the semi-finished sheets are cut into plies (Figure 2.7a), the carrier film is withdrawn, multiple sheets are stacked and placed inside the preheated mould, usually with a coverage of 30 % to 70 % (Orgéas et al., 2011) (Figure 2.7b).



(a)

(b)

Figure 2.7: Cutting (a) and compression moulding (b) of semi-finished SMC sheets.

The stacking of the charge is crucial step in manufacturing as it may entrap air into the material. During closure of the mould, the charge is continuously heated and forced to flow to fill the cavity of the mould. As soon as the material touches the surface of the heated mould, the temperature of the semi-finished material rapidly

increases. Figure 2.8 shows the temperature-time evolution in the surface and subsurface layers, as well as in the centreline, during compression moulding of SMC. It shows that the charge surface quickly attains the mould temperature, which, in contrast to the temperature-time evolution on the centreline, remains relatively uniform during the process.

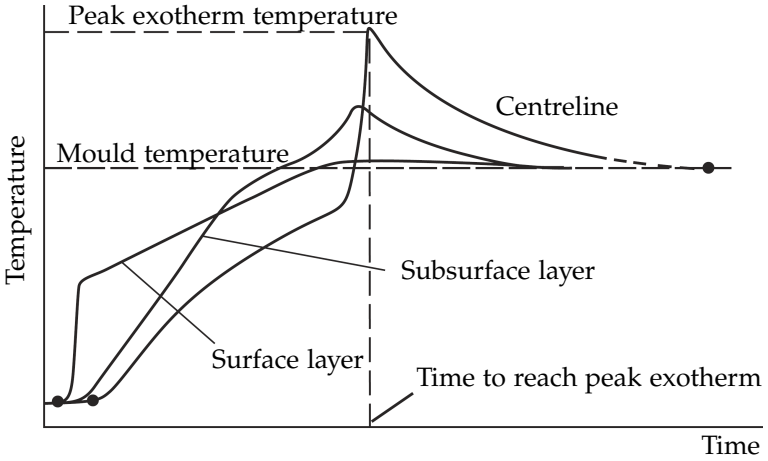


Figure 2.8: Temperature-time evolution during compression moulding process in surface layer, subsurface layer and centreline, adapted from Mallick and Raghupathi (1979).

Temperature increases slowly in the centreline until a curing reaction starts, but due to low thermal conductivity, the generated exothermic heat cannot be efficiently transferred to the surface layers, and the temperature at the centreline peaks. At the end of the curing reaction, centreline temperature is decreased, and equals the mould surface temperature (Mallick, 2007). The fast increase in temperature in the surface layers leads to a significant decrease of the material's viscosity

due to a breakdown of the network structure created by a thickening reaction with MgO (Newman and Fesko, 1984) (Figure 2.9).

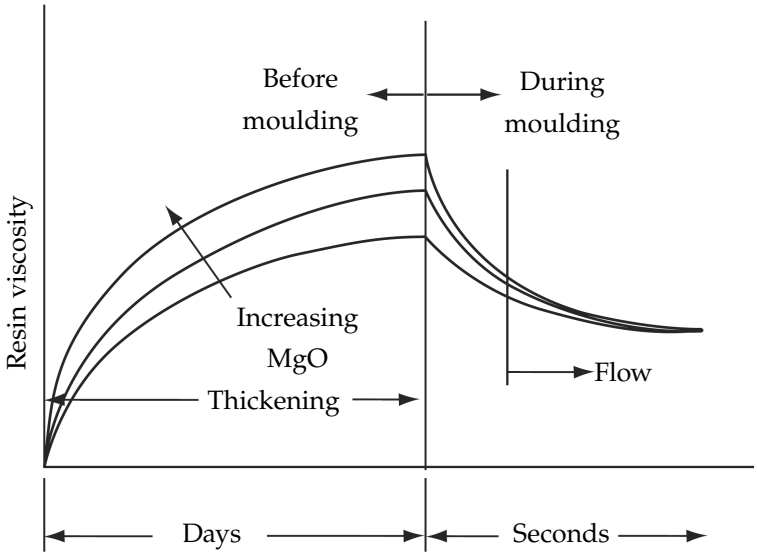


Figure 2.9: Evolution of viscosity before and during compression moulding of SMC, adapted from Mallick (2007).

These layers act as lubrication layers and exhibit significant shear deformation (Lee and Tucker, 1987) with preferential flow of hot material from the surface to the periphery (Newman and Fesko, 1984). For thick charges, the viscosity significantly decreases due to the high moulding temperature in the surface layers but viscosity remains high in the interior layers. Hence, the semi-finished material in the outer layers begins to flow prior to the interior layers and the surface layers may squirt into the uncovered areas of the mould undergoing greater extensional deformation than the interior layers. As a result, slip at the surface of the mould may occur (Barone and Caulk, 1985). In contrast, the core layers deform uniformly in (extensional) plug

flow (Lee et al., 1981). Resulting from the described flow conditions, fibre bundles in the core tend to align along the in-plane flow direction, and fibres in the shell layers may disaggregate and bend (shell-core effect) (Figure 2.10).

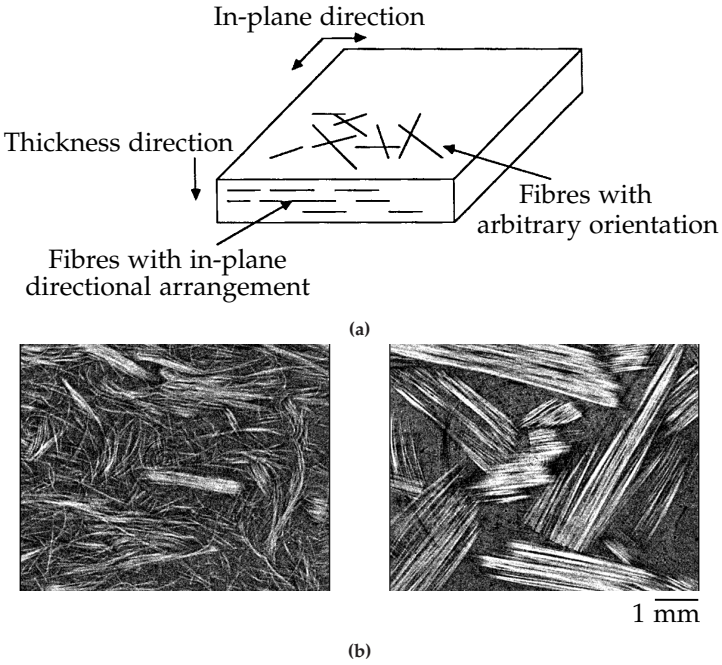


Figure 2.10: Fibre orientation (a) and shell-core effect (b) resulting from compression moulding of semi-finished SMC sheets (Kim et al., 1992; Le et al., 2008).

The important degree of shear flow also results in a spreading of fibre bundles (Mei and Piggott, 2004). Characteristic flow phenomena favour anisotropic fibre orientation and fibre distribution of the SMC composite (Lin and Weng, 1999) affecting material performance (Watanabe and Yasuda, 1982). The degree of orientation of the fibres increases if initial mould coverage is reduced (Advani and Tucker,

1990). However, a significant advantage of a compression moulding process is the low fibre attrition during processing, and fibre damage is less severe than with other moulding techniques, such as injection moulding (Osswald and Menges, 2012).

2.3.2.3 Development and application

Driven by an invention of Fisk (1953) to increase the viscosity of an uncured alkyd copolymer resinous mixture, glass fibre reinforced polyester composites originated in the early 1950s. Sheet moulding compounds (SMC), as they are known today, date back to the end of the 1960s. With regard to specific properties, commercial SMC formulations are an interesting alternative to steels and aluminium alloys (Orgéas et al., 2011).

The advantages of SMC composites are manifold (McConnell, 2007; Stachel, 2012; The European Alliance for SMC/BMC, 2013, 2016), and one must highlight the following, in particular:

- **Economy and automation of manufacturing process**
  The sheet moulding compound technology stands out due to low material and tooling costs, the opportunity for a fully automated process, and short manufacturing times.

- **Formability and functional integration**
  Sheet moulding compounds allow for the manufacturing of complex 3D structures due to their high formability during the compression moulding step, with excellent dimensional accuracy. Co-moulding of screws and inserts can replace the requirement of sub-assembly of different parts.

- **Outstanding physical and chemical properties**
  Specific sheet moulding compound formulations stand out due to their high chemical and temperature resistance, low thermal expansion, flame retardancy and paintability.

- **Time to market**
  The timeframe from design to production is very short for SMC composites.

- **Customisation**
  A sheet moulding compound and its resin formulation can be tailored to meet special requirements in terms of mechanical, chemical or physical material properties.

- **Lightweight potential**
  Sheet moulding compounds offer low densities, thus low-weight final parts, resulting in greater fuel efficiency and reduced CO_2 emissions throughout the life of a vehicle, for example.

- **Favourable life cycle**
  In terms of greenhouse warming potential in kilogram-CO_2-equivalent per functional unit, light composites outperform steel and aluminium.

Modern industries demand structural materials that are lightweight, but strong and versatile at the same time (The European Alliance for SMC/BMC, 2016). Sheet moulding compounds can largely fulfil

these requirements. Beyond the transportation sector, SMC composites are applied in the electrical and electronics industry as well as in fuses and switchgears, for example. Its mechanical integrity and electrical insulation also allows for an implementation in motor and armature insulations. The construction industry takes advantages of the durability and design freedom that comes with SMC. Furthermore, domestic applications, sporting equipment and medical devices made from SMC underline the variety of possible applications (The European Alliance for SMC/BMC, 2016).

Technical applications of SMC are manifold, but the most important sector is the automotive industry. With an annual production of 120 000, Volvo Cars recently introduced a tailgate mainly made of SMC and considered for a mass-production car. Following this approach, the upper part of the divided tailgate of the Volvo XC90 was also made of SMC (Oldenbo, 2004). This application of SMC was only the beginning of a very successful story concerning the implementation of SMC components into vehicle designs. Such designs have continuously been improved to enhance material performance for the needs of the automotive industry. In 2007, 227 SMC parts manufactured and implemented in 78 different car and truck models worldwide were officially listed (McConnell, 2008). Presently, a quarter of the overall volume of glass fibre reinforced plastics (GFRP) in Europe comprise the production of SMC and BMC, for a total of 274 000 tonnes (with 198 000 tonnes of SMC). It is the biggest segment in Europe's GFRP production. The most important market in the automotive industry, for both SMC and BMC, is France, followed by Germany and Italy (Witten et al., 2016).

One may think that after more than four decades in use, SMC represents a well-established technique with few new perspectives but

the SMC segment remains a hive of activity, and recently, an important effort was made to improve the SMC manufacturing process (Castro and Griffith, 1989; Castro and Lee, 1987) and the mechanical performance of SMC in general. In particular, the improvement and development of novel resin formulations led to structural and advanced SMC composites. The historical SMC, presented in the preceding sections and in the following referred to as standard SMC, is based on resin formulations with a significant amount of fillers. These fillers may decrease material costs and improve surface quality, but they also increase the material's density and limit the fibre volume content of the composites. Different approaches have been presented to decrease the material's density to values in the range of $1.2\,\mathrm{g\,cm^{-3}}$ to $1.3\,\mathrm{g\,cm^{-3}}$, for example by adding hollow glass spheres (Oldenbo, 2004; Shirinbayan et al., 2017) or cellulose nanocrystals (Asadi et al., 2016) to produce high-volume lightweight SMC. Recently, the SMC industry has focussed on enhancing mechanical material properties by developing advanced SMC formulations especially for the automotive industry (Lamanna and Ceprano, 2014). Replacement of the glass by carbon fibres further enhanced the mechanical performance of SMC composites (Boylan and Castro, 2003; Cabrera-Ríos and Castro, 2006). The importance of recycling also advanced the material's development, and the approach of replacing glass with recycled carbon fibres came more and more to the fore (Palmer et al., 2010). Carbon fibre sheet moulding compound composites were successfully considered in the windshield surround, inner door panels at the hinge and the front fender support on the 2003 Dodge Viper Convertible, for instance, which marked one of the first production uses of this material (Bruderick et al., 2003). In 2004, Menzolit Compounds International GmbH, Heidelberg, Germany, also introduced a carbon fibre SMC recipe for automotive applications. Its advanced SMC formulation debuted on the Mercedes SLR

Silver Arrow sports car in a three-piece scuttle panel (McConnell, 2008). With the BMW 7 series, structural carbon fibre SMC was again successfully implemented in a production vehicle in the form of the cross member or trunk cover, moulded from an epoxy sheet moulding compound (Gardiner, 2016).

In today's context, *"SMC is now a much more robust material and tailorable to customer needs"* (citation by Tom Hilburn, vice president of Continental Structural Plastics, Detroit, Michigan, USA [McConnell, 2007]). Recent approaches to simulate flow-induced fibre orientation (Hohberg et al., 2017; Song et al., 2017) and the consideration of microstructural parameters to predict material behaviour and damage (Chen et al., 2018) highlight that SMC composites continue to enjoy great popularity in material research.

Contrary to the aforementioned advantages and despite all developments in terms of processing, composition, reinforcing fibre type and architectures, the comparatively limited mechanical performance of SMC, due to the finite length of the fibrous reinforcement, hindering SMC materials' application in highly loaded structural components.

2.3.2.4 Mechanical material properties

The following section refers to the mechanical material and structural properties of sheet moulding compounds, focussing on monotonic loads at ambient temperatures. The overview starts with a description of tensile and compressive properties, followed by flexural properties. For discontinuous fibre reinforced composites in general, of significant importance are not only the properties of the individual components and the fibre-matrix interface, but also the microstructure in terms of fibre volume fraction as well as the fibre

orientation and length distribution (Fu et al., 2009). Table 2.2 lists typical properties of a standard SMC composite considered in the automotive industry (Orgéas et al., 2011), offering a general overview of mechanical and thermal performance.

Table 2.2: Typical properties of a standard SMC composite for automotive applications consisting of polyester resin, calcium carbonate ($CaCO_3$) and 25 wt.% of glass fibres (Orgéas et al., 2011).

Property	Value
Specific mass	$1.85\,\mathrm{g\,cm^{-3}}$
Tensile modulus of elasticity	10 GPa
Flexural modulus of elasticity	10 GPa
Tensile strength	75 MPa
Flexural strength	170 MPa
Izod impact strength	$800\,\mathrm{J\,m^{-1}}$
Elongation at rupture	1.2 %
Thermal expansion coefficient	$15 \times 10^{-6}\,\mathrm{K^{-1}}$

Based on the heterogeneous microstructure, the principal factor influencing mechanical material properties of SMC composites is fibrous reinforcement, more precisely fibre orientation, length distribution and fibre volume content (Orgéas et al., 2011). Moulding parameters like mould temperature, moulding pressure and time have a fundamental impact on the material's microstructure and thus, resulting mechanical material properties. Garmendia et al. (1995) showed that an increase in moulding temperature from 125 °C to 135 °C with constant moulding pressure (14.7 MPa) elevated flexural modulus of elasticity of a standard (low-shrink) SMC featuring a fibre content of 25 wt.% from approximately 9.8 GPa (12 GPa) to approximately 11 GPa (13.5 GPa) and flexural strength from approximately 140 MPa

(170 MPa) to approximately 145 MPa (190 MPa). A further increase in moulding temperature resulted in a decrease in flexural performance and for a mould temperature of 145 °C resulting stiffness was approximately 10 GPa (9.5 GPa), with a corresponding flexural strength of approximately 125 MPa (145 MPa). Although the influence of the moulding pressure on flexural properties was less significant, a slight variation of flexural modulus and flexural strength appeared when the pressure was varied (Garmendia et al., 1995). Mould closing speed also affects material performance of SMC, and Kim and Im (1996) reported an influence on the surface quality and mechanical performance of SMC composites.

As generally true for fibre reinforced polymers, fibre orientation, fibre volume content and fibre length generally influence tensile and flexural stiffness. Glass fibre reinforced polypropylene with sheets prepared in a wet deposition process, for example, showed a linear increase in tensile and flexural modulus of elasticity resulting from an increase of fibre content. From pure polymer to a fibre reinforced laminate featuring 40 wt.% of glass fibres, moduli increased from 2 GPa to 6 GPa, independent of fibre length (Thomason and Vlug, 1996). In the same manner, tensile strength increased from approximately 32 MPa to 70 MPa. The same trend was observed for flexural strength with an increase from approximately 50 MPa to 130 MPa. The investigated materials were characterised by an opposite trend for failure strain (Thomason et al., 1996).

Additionally, placement of the charge has an important effect on resulting material properties and although the fibres may be randomly distributed at the beginning of moulding, fibres align in flow direction leading to anisotropic material properties depending on flow conditions (Boylan and Castro, 2003; Kim and Im, 1996).

The following presents representative results that depict the influence of fibre content as well as fibre orientation on the material properties of SMC composites focussing only on glass fibre reinforced SMC composites.

Tensile and compressive properties
Standard polyester or vinylester-based SMC composites reinforced with glass fibres showed a significant positive correlation between fibre volume content and tensile modulus of elasticity and tensile strength.

Orgéas et al. (2011) showed that the specific tensile strength increased from $2 \times 10^4\,\mathrm{N\,m\,kg^{-1}}$ to $18 \times 10^4\,\mathrm{N\,m\,kg^{-1}}$ when fibre content was raised from 10 wt.% to 60 wt.%. The investigations also pointed out that the increase in specific modulus of elasticity from $5 \times 10^6\,\mathrm{N\,m\,kg^{-1}}$ to $1.5 \times 10^7\,\mathrm{N\,m\,kg^{-1}}$ was less significant.

Taggart et al. (1979) also reported that an increase in fibre volume content had a significant effect on the tensile strength of a polyester-based SMC reinforced with chopped glass fibres. The resulting stiffness was more than twice as high (215 MPa) for a material with 65 wt.% of glass fibres, as compared to an SMC featuring only 25 wt.% of glass fibres (90 MPa). The tensile modulus of elasticity increased only slightly from lowest to highest fibre weight content (FWC) (14.3 %). The same tendencies were observed for compressive loads of the considered SMC materials. With an increase from 12.4 GPa to 23.4 GPa, compressive modulus of elasticity was almost doubled due to an increase in FWC from 25 wt.% to 65 wt.%. Compressive strength, which was significantly higher than tensile strength, showed an increase from 204 MPa to 284 MPa. For both loading cases, increased FWC resulted in reduced failure strain (-20 %) for tensile

and (−60 %) for compressive loads, from lowest to highest considered FWC. In addition to the influence of fibre content, material properties were characterised by significant anisotropy. Specimens extracted perpendicular to flow featured lower stiffness and strength for both considered loading cases (i.e. the average tensile modulus of elasticity [tensile strength] decreased ≈ 17 % [≈ 30 %] for SMC featuring 25 wt.% of glass fibres and ≈ 12 % [≈ 30 %] with a reinforcement equal to 65 wt.% of glass fibres). Compressive testing resulted in a modulus of elasticity (strength) perpendicular to flow of 11 GPa (162 MPa) for SMC featuring 25 wt.% and 12.4 GPa (233 MPa) for SMC featuring 65 wt.%.

Chaturvedi et al. (1983) investigated the material behaviour of glass fibre reinforced SMC materials featuring different fibre contents ranging from 30 wt.% to 65 wt.%. Their observations indicated that no significant fabrication-induced anisotropy was present for the lowest FWC (longitudinal modulus of elasticity and tensile strength were equal to 14.6 GPa and 80 MPa, transverse modulus of elasticity and tensile strength were equal to 14.5 GPa and 83 MPa). However, from lowest to highest FWC, tensile modulus increased significantly (≈ 22 %). In addition, tensile strength was nearly tripled, increasing from 81 MPa to 228 MPa. In contrast to the findings presented in Taggart et al. (1979), failure strain increased from lowest to highest fibre content (≈ 44 %).

Riegner and Sanders (1979) also reported an increase in tensile modulus of elasticity (≈ 12 %), tensile strength (≈ 175 %) and compressive strength (≈ 32 %) corresponding to a fibre content increasing from 25 wt.% to 65 wt.%.

The influence of fibre content on tensile and compressive properties has also been reported by Trauth et al. (2017a) in preliminary investigations characterising the mechanical material properties of a vinylester-based SMC composites featuring no fillers and a fibre weight content in the range of 41 wt.% to 61 wt.% ($\approx$ 17 vol.% to 31 vol.%, respectively) of 25.4 mm long fibres. In addition, SMC materials featuring a mixture of 1 in. long (25.4 mm) and 2 in. long (50.8 mm) fibres (ratio $\approx$ 6:5) were characterised. A 100 % mould coverage was realised to manufacture the SMC sheets. Specimens were extracted with different orientations relative to the manufacturing direction (movement of the conveyor belt equals 0°) to investigate anisotropy resulting only from manufacturing of the semi-finished material. SMC sheets were not exposed to flow during moulding. Figure 2.11 depicts experimentally determined tensile properties in terms of modulus of elasticity and strength. As clearly shown in Figure 2.11 and described in Table 2.3, an increase in fibre content enhanced mechanical material performance if the SMC material was exposed to uniaxial tension and compression. Fibre length distribution did hardly affected material behaviour.
Although the semi-finished sheets did not flow during moulding, the orientation of the fibrous reinforcement due to a movement of the conveyor belt led to anisotropic mechanical material properties in the aforementioned study.

In contrast, Chen and Tucker (1984) showed that SMC sheets manufactured with a 100 % mould coverage exhibited nearly planar isotropic mechanical properties.

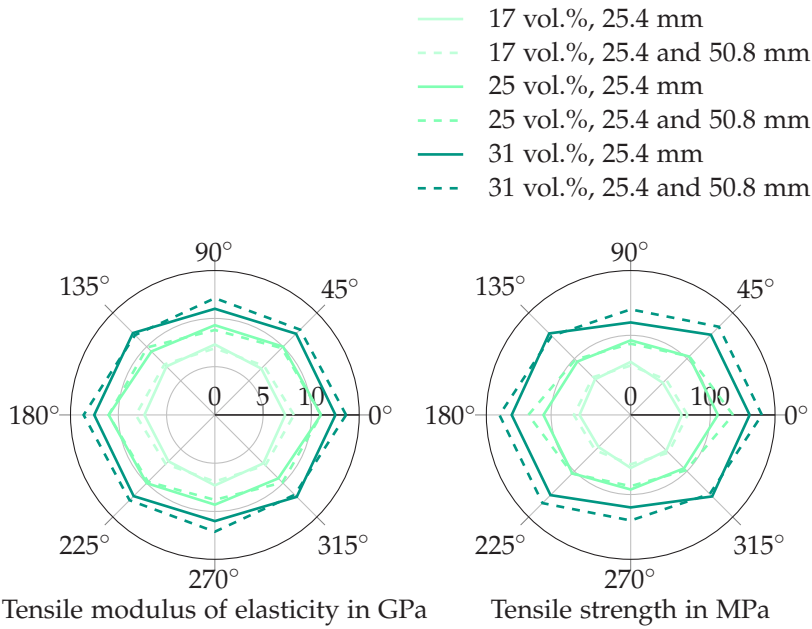


Figure 2.11: Tensile modulus of elasticity and tensile strength of vinylester-based glass fibre reinforced SMC composites resulting from uniaxial tension of specimens extracted with different orientations with respect to the movement of the conveyor belt, which equals 0° (Trauth et al., 2017a).

Contrary to the findings presented by Trauth et al. (2017a), an influence of fibre length distribution on resulting material properties was reported by Boylan and Castro (2003). In this extensive study, 12 different SMC formulations (unsaturated polyester-based with a significant amount of calcium carbonate) with different fibre types and length distributions were characterised in order to define the effect of reinforcement type and length on the physical properties of SMC composites. Hard and soft glass fibres (28 wt.%) with a length of 0.5 in., 1 in. and 2 in. in were considered as reinforcement. In addition, SMC composites featuring a mix of either 0.5 in. and 1 in. or 1 in.

and 2 in. long fibres of the individual fibre type were considered for testing. By placing the charge in the middle or at one side of the mould a one-dimensional (1D) or two-dimensional (2D) flow was realised. The most important results of this study pointed out that the tensile strength increased with increasing fibre length from 0.5 in. to 2 in. and the performed analysis of variance showed an increase from 65 MPa to 91 MPa. Hard glass fibres featured the highest tensile strength ($\approx$ 96 MPa), followed by soft glass ($\approx$ 81 MPa). The modulus of elasticity did not significantly differ for the two glass fibre types, but an increase from 0.5 in. to 2 in. long fibres resulted in an increase of 15 %.

In the following, orthotropic behaviour is described by the ratio of a property in flow direction divided by the equivalent value determined perpendicular to flow. No anisotropy was observed for material properties of SMC moulded with 2D flow in a square shaped mould. In contrast, the tensile modulus of SMC materials forced to flow 1D during moulding differed with respect to the orientation of the specimen. However, no significant difference was observed for the two considered types of glass fibres with a ratio of anisotropy equal to 1.55 for hard and 1.6 for soft glass fibres. An increase in fibre length from 1 in. to 2 in. led to a more significant anisotropy in terms of tensile modulus (1.85 for 1 in. and 1.55 for 2 in. long fibres). Tensile strength was defined by a ratio of anisotropy of 1.9 if specimens extracted in two orthogonal directions were considered for testing.

The anisotropic material properties of SMC composites were also stated by Kim and Im (1996). Depending on moulding parameters (moulding temperature and mould closing speed) the tensile strength of a bisphenol type resin-based SMC featuring 28 wt.% of glass fibres showed a ratio of tensile strength (measured in 0° and 90° at yield

or break) of 1.5 – 2.2. The effect was less severe for tensile modulus of elasticity (1 – 1.2). Investigated SMC sheets featured a nominal thickness of 3 mm and were manufactured in a flat and cross-sectional T-shaped mould. No detailed information on charge placement and mould coverage was given.

Taggart et al. (1979) reported, that tensile properties of SMC materials based on polyester resin with 25 wt.%, 30 wt.% or 65 wt.% of chopped glass fibre exhibit anisotropic tensile properties in terms of stiffness and strength resulting from flow during moulding. A ratio of anisotropy of 1.17 and 1.2 could be determined for SMC materials with 25 wt.% or 65 wt.% of glass fibres, respectively. The effect of fibre orientation due to material flow was slightly more severe for the resulting tensile strength, with a ratio of anisotropy of 1.3 for both materials. For compressive loads, a ratio of anisotropy of 1.13 and 1.26 (SMC material featuring a fibre content of 25 wt.%) could be determined considering materials' stiffness and strength. For an equivalent material featuring a higher fibre content (65 wt.%) the ratio of anisotropy of stiffness and strength was equal to 1.89 and 1.27, respectively. In general, the compressive strength of the investigated SMC composites was greater than the tensile strength.

The material properties of SMC composites are generally characterised by an important variation and scatter resulting from the heterogeneous microstructure. Lamanna and Ceprano (2014) observed a significant scatter of material properties of a polyester-based SMC composite featuring 30 wt.% of glass fibres. The coefficient of variation (CV) in terms of tensile modulus of elasticity and tensile strength was CV = 25 % and CV = 39 %. However, a positive correlation of tensile modulus of elasticity and tensile strength was observed, indicating a preferred fibre orientation aligned with flow direction.

In the aforementioned study, no distinction was made in terms of orientation of the specimen during variations calculation. Considering longitudinal and transverse properties with respect to flow, a comparable material system (polyester-based SMC with 30 wt.% of glass fibres) featured variations of CV = 15 % and CV = 12 %, respectively. Scatter in material properties may also be favoured due to an extraction of the specimens considered for testing near the edges of the sheets (Mrkonjic et al., 2015).

Recent developments in low-density SMC composites have focussed on formulations considering hollow-glass spheres as presented by Oldenbo et al. (2003), for example. Adding hollow glass spheres ($\approx$ 5 wt.%) to a standard unsaturated polyester-based SMC composite ($\approx$ 30 wt.% of glass fibres, 44 wt.% of $CaCO_3$) by a simultaneous reduction of filler content (≈ -10 %) decreased tensile modulus of elasticity of the composites (-25 % to -30 %). Whereas tensile strength remained unchanged, compressive strength also decreased (-19 %). With an average value of 1.6 g cm^{-3}, the density was significantly lower compared to that of the standard SMC material, considered as reference by Oldenbo et al. (2003) (ρ = 1.95 g cm^{-3}), and the presented SMC composites offered a high lightweight potential.

Following the same approach, Shirinbayan et al. (2017) have recently presented investigations of an SMC composite considering hollow glass spheres to reduce material density to 1.3 g cm^{-3} which equals a decrease of 30 % compared to the considered reference material in the their study (ρ = 1.85 g cm^{-3}).

SMC formulations dispensing with fillers have recently been investigated by Trauth et al. (2018) to enhance mechanical performance and

to increase the suitability of SMC composites for structural applications. The SMC composites were based on an unsaturated polyester-polyurethane two-step curing hybrid resin system, featuring a fibre weight content of 41 wt.% ($\approx$ 23 vol.%) and a density of 1.48 g cm^{-3}. An initial mould coverage of $\approx$ 33 % and a two dimensional flow led to planar isotropic material properties.

Flexural properties

Flexural properties of different SMC materials have frequently been investigated by means of three- and four-point bending tests in recent decades. The results of these investigations indicated that similar tendencies have been observed for flexural loads as they were already described in terms of tensile or compressive properties. In general, flexural strength was observed to be higher than tensile strength, and Orgéas et al. (2011), for example, reported a difference of 127 %.

Chaturvedi et al. (1983) also reported an increase in flexural strength for SMC composites featuring 50 wt.% or 65 wt.% of glass fibres of 38 % and 20 %. For a lower fibre content (30 wt.%), flexural strength was twice as high as tensile strength. In terms of flexural modulus of elasticity, no significant variations were observed, except for the highest FWC (65 wt.%). This material became slightly stiffer (12 %) when exposed to flexural loads.

In Riegner and Sanders (1979) and Walrath et al. (1982), tensile strength increased from 220 MPa to 403 MPa with an increasing fibre content from 25 wt.% to 65 wt.%. In terms of flexural modulus of elasticity, scatter in mechanical performance was more important than the observed variations. No significant difference was examined with respect to tensile modulus of elasticity. The investigations revealed in a higher flexural than tensile strength. The increase

tended to be more significant for lower fibre contents (25 wt.%: 167 %, 50 wt.%: 100 %, 65 wt.%: 78 %).

Flexural properties were less sensitive to anisotropy induced by the movement of the conveyor belt, and anisotropy became only slightly visible for a vinylester-based SMC composites featuring a combination of 1 in. and 2 in. long fibres. Ratios of anisotropy ranged between 0.9 – 1.3 for flexural modulus of elasticity, strength and failure strain (Trauth et al., 2017a).

Generally, the mechanical material properties of an SMC depend strongly on the materials' microstructure, especially fibre orientation and fibre content, which evolves from the manufacturing of the semi-finished sheets and moulding. In this matter, the process-related microstructure of an investigated SMC composite must be considered in the characterisation of mechanical material properties, generally defined by a significant scatter due to the heterogeneity of the material. SMC composites commonly exhibit a tension-compression anisotropy in terms of strength. Flexural modulus of elasticity and flexural strength were shown to be higher than stiffness and strength resulting from uniaxial tension or compression. Table 2.3 lists tensile, compressive and flexural properties of different SMC composites to provide an overview of mechanical performance and to summarise the aforementioned studies and findings.

Table 2.3: Overview of tensile, compressive and flexural properties of SMC materials (FWC = fibre weight content; E_t,E_c and E_f = tensile, compressive and flexural modulus of elasticity; R_t, R_c and R_f = tensile, compressive and flexural strength, $\varepsilon_{max,t}$, $\varepsilon_{max,c}$ and $\varepsilon_{max,f}$ = tensile, compressive and flexural failure strain). If specimens were extracted in different orientations, the dominating property in terms of stiffness, strength and failure strain is presented, and the ratio of anisotropy of longitudinal to transverse property is indicated in brackets. The following abbreviations have been considered: nom. = nominal; VE = vinylester; UP = Unsaturated polyester; P = polyester; UPPH = unsaturated polyester-polyurethane two-step curing hybrid resin system; BPA = bisphenol A; - = not specified. SMC composites were generally based on 25.4 mm long glass fibres, unless otherwise stated. * = combination of 25.4 mm and 50.8 mm long fibres, ratio 6:5, ** = average value.

Reference	Resin	FWC in %	ρ in g cm^{-3}	E_t in GPa	R_t in MPa	$\varepsilon_{max,t}$ in %	E_c in GPa	R_c in MPa	$\varepsilon_{max,c}$ in %	E_f in GPa	R_f in MPa	$\varepsilon_{max,f}$ in %
Orgéas et al., 2011	P	25	1.85	10	75	1.2	-	-	10	17.0	-	
Riegner and Sanders, 1979; Walrath et al., 1982	P	25	1.83	13.2	82.4	1.34	-	183	-	14.8	220	-
Riegner and Sanders, 1979; Walrath et al., 1982	P	50	1.87	15.8	164	1.73	-	225	-	14.0	314	-
Riegner and Sanders, 1979; Walrath et al., 1982	P	65	1.82	14.8	227	1.67	-	241	-	15.7	403	-
Chaturvedi et al., 1983	-	30	-	14.6 (1.0)	80.1 (0.97)	1.14 (1.1)	-	-	-	13.2	156.7	-
Chaturvedi et al., 1983	-	45	-	14.7	-	-	-	-	-	16.1	228.7	-
Chaturvedi et al., 1983	-	50	-	14.0	157.3	1.56	-	-	-	14.1	206.0	-
Chaturvedi et al., 1983	-	55	-	16.3	-	-	-	-	-	16.1	282.7	-
Chaturvedi et al., 1983	-	65	-	17.8	227.6	1.59	-	-	-	20.0	303.3	-
Trauth et al., 2017a	VE	31	1.36	7.3 (1.0)	64.3 (1.0)	1.40 (0.9)	6.9 (1.3)	178.6 (1.1)	4.5 (1.0)	7.7 (1.1)	157.0 (1.0)	3.4 (1.0)
Trauth et al., 2017a	VE	41	1.45	11.0 (1.2)	109.6 (1.2)	1.41 (0.9)	6.8 (1.1)	148.8 (1.1)	4.0 (1.1)	9.2 (1.1)	205.5 (0.9)	3.3 (0.9)
Trauth et al., 2017a	VE	51	1.57	12.5 (1.1)	149.5 (1.3)	1.70 (1.1)	10.0 (1.2)	156.7 (1.1)	3.0 (0.8)	12.2 (1.1)	277.1 (0.9)	3.0 (0.9)
Trauth et al., 2017a	VE	31*	1.36	8.2 (1.2)	71.5 (1.2)	1.26 (0.8)	8.0 (1.3)	156.7 (1.1)	3.0 (0.8)	7.5 (1.1)	163.6 (1.2)	3.2 (1.0)
Trauth et al., 2017a	VE	41*	1.45	11.0 (1.3)	128.6 (1.4)	1.63 (1.0)	8.0 (1.2)	171.8 (1.1)	5.5 (1.4)	9.8 (1.3)	244.8 (1.3)	3.5 (1.0)
Trauth et al., 2017a	VE	51*	1.57	13.6 (1.1)	164.9 (1.2)	1.62 (0.9)	8.0 (1.0)	194.5 (0.9)	4.0 (0.8)	13.4 (1.2)	303.2 (1.2)	3.0 (0.9)
Trauth et al., 2018	UPPH	41	1.48				-	-	-	-	-	-
CES EduPack, 2017**	UP	40	1.80	11.6	98.6	1.5	11.6	246.5	-	11.6	167.5	-
Taggart et al., 1979	P	25	-	14.5 (1.2)	90(1.3)		12.4 (1.3)	204 (1.3)	-	-	-	-
Taggart et al., 1979	P	65	-	16.6 (1.2)	215 (1.3)		23.4 (1.9)	284 (1.3)	-	-	-	-
Oldenbo et al., 2003	UP	30	1.95	11.7	84 (1.2)	1.4 (1.3)	-	155	-			

2.3.2.5 Structural properties

Several attempts have been made to define the influence of testing parameters on the resulting impact properties of SMC composites; specifically, the geometry of the striker (Chaturvedi and Sierakowski, 1985) was highlighted to have a significant influence. In addition, the clamping situation and the impacting energy (Chaturvedi and Sierakowski, 1983; Khetan and Chang, 1983; Lee et al., 1999) significantly affected the impact response of SMC materials. The geometry of the specimen, for example thickness (Kau, 1990; Lee et al., 1999), the composition of the material, for example fibre length (Kau, 1990), and fibre content (Chaturvedi and Sierakowski, 1983; Dear and Brown, 2003) were also important to consider.

Comparable to quasi-static material properties, studies on random in-plane glass fibre reinforced polypropylene indicated that Charpy impact strength increased with increasing fibre content (10 wt.% to 40 wt.%) from 8 kJm^{-2} to 28 kJm^{-2}. An increase in fibre length from 3 mm to 12 mm also affected impact properties, and Charpy impact strength was between 1.3 and 1.7 times higher for composites based on 12 mm long fibres compared to a reinforcement with only 3 mm long glass fibres (Thomason and Vlug, 1997). However, a standard Charpy impact test does not capture the force-deflection evolution but only measures the impact energy absorbed by the specimen (e.g. DIN EN ISO 179, 2010). Further information of damage evolution and energy absorption capability of a material may be gained with instrumented puncture tests, an appropriate test setup to provide information on the structural properties of a material at different loading rates.

Puncture testing of SMC composites has aroused great interest in recent decades. Considering SMC materials as front-end panels or structural reinforcement in the automotive industry underlines the need for a profound understanding of the puncture properties of this material class (Knakal and Ireland, 1986).

A first attempt to investigate the impact properties of SMC was made in the investigations of Khetan and Chang (1983). Polyester-based SMC composites, featuring 31 wt.% of 25.4 mm long glass fibres and 31 wt.% of $CaCO_3$, were impacted with a steel ball, which featured a diameter of 22.2 mm and a mass of 45.5 g, at speeds ranging from 12.5 m s^{-1} to 28 m s^{-1}. The specimen was clamped on the edges to provide an exposure area of 102×102 mm^2. Absorbed energy significantly increased with impacting velocity, from approximately 2 J to 11 J.

Chaturvedi and Sierakowski (1983) carried out puncture tests on polyester-based SMC, featuring a significant amount of fillers (20 wt.% $CaCO_3$) and reinforced by 25.4 mm long chopped glass fibres with a fibre content of either 50 wt.% or 65 wt.%, respectively. Rectangular specimens (150×150 mm^2) were mechanically clamped at all four sides, resulting in an exact test specimen size of 140×140 mm^2. In a first study, the blunt-ended cylindrical steel impactor with a diameter of 9.7 mm and a length of 25.4 mm was accelerated and hit the centre of the specimen with a nominal velocity ranging from 30 m s^{-1} to 95 m s^{-1}. Residual tensile stiffness and strength were evaluated. Polyester-based SMC featuring 50 wt.% of glass fibres, exhibited a significant decrease in residual stiffness (12.9 GPa to 9.7 GPa) and strength (137.6 MPa to 94.3 MPa) with increasing impact velocity (from $\approx$ 31 m s^{-1} to $\approx$ 68 m s^{-1}). For the same range of impact velocity, residual stiffness decreased from 16.5 GPa to 12.4 GPa for

an SMC composite featuring 65 wt.% of glass fibres, accompanied by a drop in strength from 209 MPa to 124 MPa. The results of mechanical performance were characterised by a definite scatter with a coefficient of variation (CV) of between 10 % and 23 % evaluating residual stiffness and between 2 % and 20 % evaluating residual strength, clearly indicating a heterogeneity of the material and the effects of a very localized loading. It has to be considered that the thickness of the considered specimens slightly varied (50 wt.%: average thickness = 2.44 mm, CV = 2.8 %; 65 wt.%: average thickness = 2.74 mm, CV = 2.0 %). The thickness variation might marginally falsify quantitative results, since the thickness of the specimen is of major importance in resulting impact properties, as mentioned in EN ISO 6603-2 (2000), for example.

In a subsequent study by Chaturvedi and Sierakowski (1985), the same setup and material (SMC composite featuring 50 wt.% of glass fibres) was considered. A plane-ended cylindrical steel impactor (diameter = 9.7 mm) with different lengths and thus masses, impacted the specimen with a nominal energy ranging of 15 J to 52 J. The impact velocity was set to realise the same impact energy with different impactor shapes. Considering residual tensile properties, the results suggested, that independent from impactor size, residual properties always decreased with increasing impact energy. With a 38.1 mm long striker, residual tensile stiffness and strength decreased from 11.4 GPa to 7.2 GPa (13 % < CV < 23 %) and from 130 MPa to 88 MPa (10 % < CV < 16 %), respectively. If the specimens were punctured with a 29.5 mm long striker, stiffness and strength declined from 11.8 GPa to 2.6 GPa and 146 MPa to 39 MPa.

An investigation by Kau (1990) tied in with the described findings. Instrumented puncture tests were carried out on rectangular SMC

specimens ($100 \times 100\,\mathrm{mm}^2$), based on an unsaturated polyester resin, featuring a significant amount of fillers (calcium carbonate). Fibre weight content was 25 wt.%, and fibre length was 25 mm for most of the specimens; however, specimens with a mixture of 13 mm and 38 mm long fibres were also considered in this investigation. The specimens were fully clamped over a diameter of 73 mm and punctured by a hemispherical striker with a diameter of 12.7 mm. Puncture velocity was $2.5\,\mathrm{m\,s}^{-1}$. Kau's study suggested that an increase in specimen thickness (2 mm to 3.1 mm) led to an exponential rise of absorbed energy (power of 2.7), which rose most extremely if the specimen's thickness was greater than 2.5 mm. Apart from geometry, the composition of the SMC material itself was another important influencing factor. A specific fast-curing SMC composite showed a slightly higher load (47 %) and energy (170 %) compared to a standard formulation, although characterised by a large scatter of 11 % < CV < 20 % for measured load and 22 % < CV < 59 % for measured energy.

Lee et al. (1999) also concluded that the thickness of the specimen was the most important factor influencing the puncture properties of SMC. Their investigations centred on drop weight tests on a polyester-based SMC with a fibre content of 30 wt.%, a fibre length of 25.4 mm and a thickness between 2.4 and 4.9 mm. Dissipated impact energy increased from $\approx$ 12.5 J to $\approx$ 43 J from smallest to thickest simply supported specimen, impacted by a semi-cylindrical striker, 10 mm in diameter, and an initial impact velocity of $4.75\,\mathrm{m\,s}^{-1}$, resulting in an initial impact energy of 102 J. Specimens, featuring a nominal thickness of 2.4 mm, were impacted at $3.9\,\mathrm{m\,s}^{-1}$ with a semi-cylindrical striker featuring a mass in the range of 2.7 kg to 4.3 kg, and the increase in impactor mass slightly decreased dissipated impact energy from 14 J to 12 J. A variation in impacting velocity had only a

marginal influence on dissipated impact energy, considering a semi-cylindrical striker and specimens featuring a thickness of 2.4 mm (increase from $\approx$ 11.5 J to $\approx$ 13.5 J for an increase from 3.4 m s^{-1} to 3.9 m s^{-1}, with a further increase in velocity leading again to a slight decrease $\approx$ 13 J at 4.4 m s^{-1}). In addition, four different impacting tube types (cone, flat, hemispherical and semi-cylinder) were considered, and the individual shapes of the impactor led to different failure mechanisms with increasing dissipated impact energy ($\approx$ 11.5 J to $\approx$ 14 J) from conical to semi-cylindrical to hemispherical to flat impactor. For all considered experiments, specimens were simply supported at two ends.

Sadasivam and Mallick (2002) investigated the puncture properties of a vinylester-based SMC, featuring a fibre content of 50 wt.% and a fibre length of 25 mm. Square shaped specimens (100×100 mm^2) were simply supported on a fixture containing a central opening (diameter = 70 mm) and impacted with a hemispherical striker of 12 mm diameter. Different impact energies were realised by a variation of the mass of the impactor and the impacting height, leading to impact velocities from 1.35 m s^{-1} to 2.92 m s^{-1}. The impact energy varied between 1.14 J and 20.2 J. Up to 5 J, no variation in residual tensile strength was observed compared to strength values of virgin (non-impacted) SMC specimens. At 10 J, the residual tensile strength of polypropylene, polyethylene terephthalate and a polyisocyanurate-based continuous random reinforced composites with fibre contents of 30 wt.%, 35 wt.% and 40 wt.%, respectively, decreased 60 %, 62.5 % and 65 %. With a decline of 52 % the decrease in mechanical performance was less severe for the investigated SMC composites. In addition, maximum impact load increased from 2.3 kN to 3.7 kN if input impact energy was increased from 3.5 J to 9.5 J .

An investigation by Dear and Brown (2003) considered the impact properties of two different SMC materials, based on polyester resin, which featured 30 wt.% or 62 wt.% of 25.4 mm long glass fibres. The results were compared to the impact properties of a polypropylene-based glass mat thermoplastic with continuous fibre reinforcement and a fibre weight content of 30 wt.%. Servo-hydraulic and drop weight tests were carried out on plates ($60 \times 60 \times 3$ mm^3), which were simply supported on a ring (diameter = 40 mm) with a round-nosed (hemispherical) striker (diameter = 10 mm). The drop-weight impact tests were performed in accordance with EN ISO 6603-2 (2000) with an impacting velocity of 4.4 m s^{-1}. Absorbed energy was $\approx$ 17 J (30 wt.%) and $\approx$ 22 J (62 wt.%) with the same property $\approx$ 12 J for the glass-mat. With $\approx$ 4 kN (30 wt.%) and $\approx$ 6 kN (62 wt.%) peak load was also higher compared to the glass-mat with $\approx$ 2 kN (Dear and Brown, 2003).

The aforementioned studies dealt with puncture properties of SMC composites impacted at elevated loading rates. Few efforts have been realised to characterise the rate dependent properties of glass fibre reinforced SMC composites.

A first attempt to characterise the rate dependence of SMC materials was realised by Trauth et al. (2018). Quasi-static and dynamic puncture tests were carried out on square SMC specimens (140×140 mm^2), with a nominal thickness of 3 mm. The specimens have been extracted either from flow or charge region of the compression moulded sheets to investigate the influence of material flow during compression moulding (initial mould coverage of approx. 35 % and 2D flow). The specimens were fully clamped to provide a circular exposure area with a diameter of 100 mm. Low-velocity puncture testing was carried out according to EN ISO 6603-2, 2000 in the form

of instrumented drop weight-impact tests with an impact velocity of $4.4 \pm 0.2\ \mathrm{m\,s^{-1}}$ and a hemispherical striker (diameter = 20 mm). The study considered a glass fibre reinforced SMC (41 wt.% and 25.4 mm long fibres) based on an unsaturated polyester-polyurethane two-step curing hybrid resin system, the same considered for the SMC materials characterised within this dissertation. Quasi-static puncture tests at a velocity of $2.6\ \mathrm{mm\,min^{-1}}$ were carried out with a test setup comparable to the dynamic puncture tests to investigate rate dependence of the material. The results suggest, that the glass fibre SMC exhibited a positive rate dependence and for elevated loading rates, maximum force and puncture energy increased significantly for charge (65 % and 67 %) and flow region specimens (73 % and 64 %).

2.3.2.6 Damage mechanisms

From a general point of view, SMC composites behave as anisotropic, viscoelastic, brittle solids that undergo damage that alters mechanical performance until final failure (rupture). The formation of new surfaces is the dominating energy absorbing mechanism. Common experimental methods to determine damage mechanisms and the failure evolution of SMC materials are based, for example, on the determination of the evolution of the material's stiffness due to cyclic loading (Oldenbo, 2004; Wang et al., 1983). Non-destructive test methods, such as acoustic emission (Meraghni and Benzeggagh, 1995; Meraghni et al., 1996; Mildred et al., 2004; Trauth et al., 2017a; Watanabe and Yasuda, 1982) or ultrasound (Derrien et al., 2000) successfully determined damage mechanisms and the failure evolution of SMC materials. Due to the inhomogeneous distribution and random orientation of fibres in SMC materials, which are thus characterised by matrix-rich and matrix-poor areas within the composite

(Bert and Kline, 1985), three important (microscopic) failure mechanisms generally result for SMC composites. If SMC materials are mechanically loaded, damage is initiated by the formation of matrix cracks, normal to loading direction, in matrix-rich regions, which only contain sparsely dispersed fibres. Generally, the fibres represent an effective barrier to the propagation and opening of individual cracks (Aveston and Kelly, 1973). The amount of energy necessary for a crack to propagate around the obstacle is very high, so the formation of new cracks is favoured (Bernstorff and Ehrenstein, 1990). Redistribution of forces, based on a transmission of shear stresses in the fibre-matrix interface, gives rise to the formation of cracks. Hence, the shear strength of the interface predominantly influences the spacing between cracks in the matrix (Aveston and Kelly, 1973). If the fibres bundles are oriented in an angle to the loading direction, microcracks tend to grow along the interface between fibre and matrix (debonding). As stated by Bert and Kline (1985), Wang and Chim (1983) and Wang et al. (1983), for example, fibre-bundle or filament fracture is rarely detected in sheet moulding compounds. On a macroscopic scale, damage leads to a decrease in stiffness, since each fibre contributes to the macroscopic stiffness of the composite, but as soon as interfacial damage occurs, its contribution to global material properties decreases (Fitoussi et al., 1998; Larbi et al., 2006). Taking the principal failure mechanism into account, the importance of fibre-sizing and the strength of the fibre-matrix interface in an SMC material is clearly underlined.

Based on preceded observations, Meraghni and Benzeggagh (1995) introduced a micromechanical model of matrix degradation and the failure behaviour of randomly oriented discontinuous fibre composites. Failure mechanisms were classified into two distinct groups. The first group includes damage mechanisms related to the degradation

of the matrix, in detail initiation, coalescence and propagation of cracks. Shirinbayan et al. (2015) have stated that propagation of cracks into the matrix occur, but, favoured by a high fibre content, bifurcation of existing cracks around surrounding, more disoriented fibre-bundles and pseudo-delamination between different bundles are favoured. The second group defined by Meraghni and Benzeggagh (1995) considers mechanisms linked to interfacial decohesion (fibre-matrix debonding) and fibre pull-out, which, combined with pseudo-delamination, lead to final failure by coalescence of the microcracks.

The stress-strain response resulting from uniaxial tension of SMC composite is, in general, defined by a linear stress-strain evolution in the beginning of loading, which reflects the initially linear behaviour of the material (Watanabe and Yasuda, 1982). No significant damage occurs within this first state (Jendli et al., 2005). The second state, characterised by a distinct 'knee-point' in the stress-strain curve (Chaturvedi et al., 1983), is related to the first interfacial cracks localised on fibres, which feature an orientation of 90° to 60° with respect to loading direction, indicating a transition from an elastic to a plastic region of deformation (Figure 2.12). The macroscopic non-linearity is caused by damage mechanisms occurring inside the material (Derrien et al., 2000). Microcracks in the matrix may also occur in matrix-rich regions, which quickly stabilise and play only a minor role in the macroscopic damage evolution of SMC composites. In the second stage, behind the 'knee-point', already existing interfacial cracks propagate around fibres, cracks open and grow and new interfacial cracks are formed on less disorientated fibres and crazes (Watanabe and Yasuda, 1982).

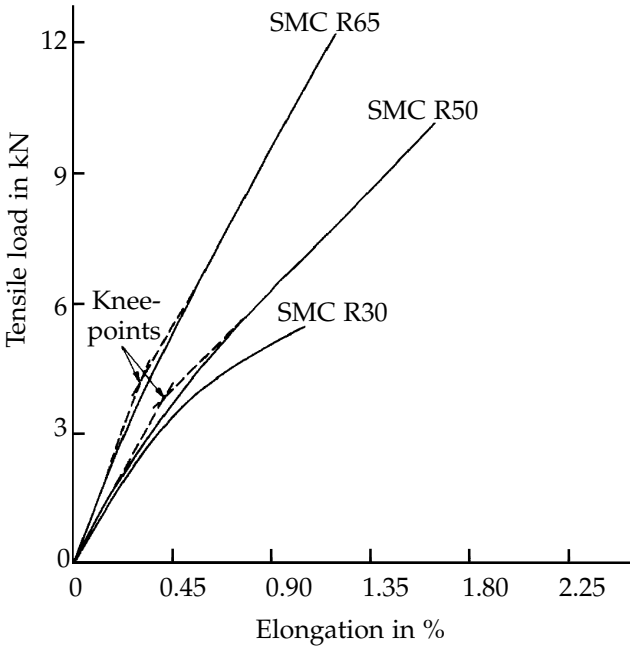


Figure 2.12: Typical tensile load-elongation curves of SMC composites featuring different fibre contents, adapted from Chaturvedi et al. (1983).

The important contribution of matrix failure to the overall damage evolution of sheet moulding compounds has also been stated by Hour and Sehitoglu (1993). Their experimental observations record, that the damage volumetric strain resulting from a monotonic load was initially zero and evolved with increasing stress due to the formation of microcracks and fibre-matrix debonding. They concluded that the strains in thickness direction correlated with the damage state inside the material.

SMC featured different damage evolutions if exposed to tensile or compressive loads. The volumetric strain due to damage induced

in the specimen was ≈ 0 for stresses below 30 MPa in tension and 65 MPa in compression. This finding correlated with the generally higher compressive strength of SMC composites. The magnitude of volumetric strain was larger for compression loads (>0.01) than for tensile loads (0.008) shortly prior to fracture. The gradual damage evolution, resulting from uniaxial tension of SMC composites did not exist for uniaxial compression, and the damage growth occurred shortly before failure. Examination of fractured specimens, exposed to compressive loads, showed that failure was mainly based on matrix shear failure (Dano et al., 2006).

In impact situations, toughness, rather than strength, is the key factor determining whether a material is suitable for a distinct application or not (Hull and Clyne, 1996). Due to their brittle nature, sheet moulding compounds are susceptible to internal damage caused by a transverse impact or puncture load. Depending on impact energy, damage might be barely visible at the surface (Agrawal et al., 2014).

As shown by Kau (1990), the evolving failure mechanisms resulting from puncture loads were strongly affected by the constituents of the material, thus fibre and matrix type and a combination of fibre pull-out and fibre breakage has been present. With a uniform distribution of fibre length (all fibres featuring a length of 25.4 mm) damage consisted of an even mixture of fibre breakage and fibre pull-out. If the mixture of fibres contained an equal number of longer (38 mm) and shorter (13 mm) fibres, the predominant failure mechanism was fibre breakage of the longer fibres. Resulting from the heterogeneous microstructure the damage zone was furthermore generally irregular with respect to the thickness of the specimen. Not only fibre length distribution but also fibre content may affect damage, since a higher

fibre content may lead to a larger damage zone, due to weak fibre-matrix interfaces (Chaturvedi and Sierakowski, 1983).

An increase in impact energy increased the size of damaged zone (Chaturvedi and Sierakowski, 1983), with damage on the rear side being more significant (Khetan and Chang, 1983). In addition, SMC composites exhibited hidden through-thickness damage before damage became visible on the outer surface (Dear and Brown, 2003). The greatest damage-growth and extent of damage were caused by the smallest impactor, which featured the highest impact velocity compared to the other impactors, at a constant impact energy level (Chaturvedi and Sierakowski, 1985).

2.3.3 Continuous SMC composites

2.3.3.1 Manufacturing and composition

Continuous fibre reinforced polymers benefit from high fibre contents and outstanding material properties. Major drawbacks include the time- and cost-consuming manufacturing processes, which offer only limited potential for automation (Lengsfeld et al., 2014). Although prepreg compression moulding has gained importance recently (Akiyama, 2011; Malanti, 2015), commercially available products are not suitable for the realisation of a local continuous reinforcement.

The integration of unidirectional carbon fibre fabrics in the sheet moulding compound (SMC) technology offers a novel approach to manufacture unidirectional and continuous carbon fibre reinforced polymers cost-effectively (Karcher, 2016). The adapted process is

based on an unsaturated polyester-polyurethane two-step curing hybrid resin system. It enables precise control of the curing of the continuously reinforced material, which can be used to locally reinforce structures (Bücheler and Henning, 2016). The particular characteristic of this resin system is a two-step curing process (Figure 2.13), which provides a chemically stable and highly viscous B-stage ideal for cutting, preforming and handling of the prepregs prior to moulding. First, the paste is thickened with the help of di-isocyanate, which leads to a chemically stable and highly viscous B-stage due to chain extension. In a second curing step, during moulding at elevated temperatures, a radical polymerisation is performed, which allows for fast curing and chemical bonding (Bücheler, 2018).

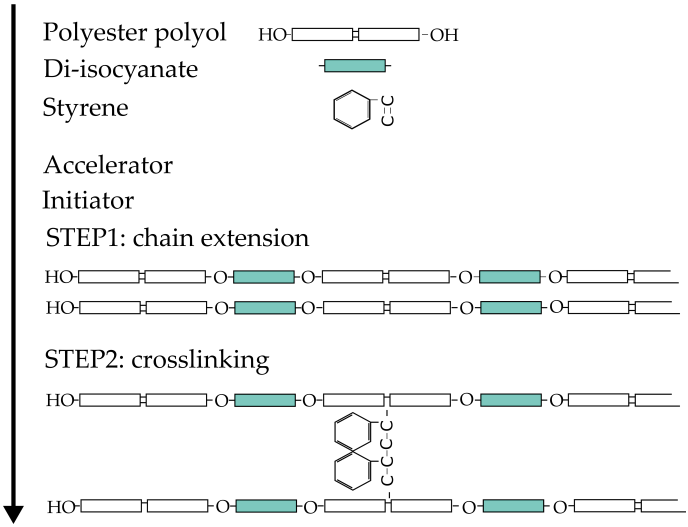


Figure 2.13: Chemistry and two-step curing process of the unsaturated polyester-polyurethane hybrid resin system, according to Bücheler (2018).

A unidirectional prepreg is fed to a slightly modified conveyor belt to manufacture the continuous carbon fibre SMC (Figure 2.14). The viscosity has to be increased during manufacturing of the semi-finished continuous carbon fibre SMC sheets to allow for handling and cutting of the semi-finished material. This increase is realised with an additional heating and cooling unit at the end of the conveyor belt to achieve a defined B-stage of the semi-finished material. The heatable tables allow for increasing the temperature of the impregnated fabric, accelerating chemical reaction and the reduction of the viscosity. The semi-finished sheets are then subsequently cooled down to room temperature to stop this chemical reaction. At the end of the conveyor belt, the B-staged continuously reinforced sheet is wound onto a roll before the material may be directly compression moulded. A compression moulded sheet of continuous carbon fibre SMC is shown in Figure 2.15.

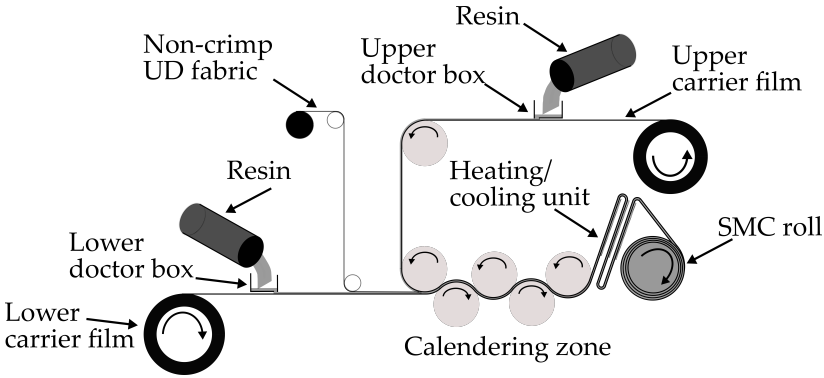


Figure 2.14: Modified SMC conveyor belt to manufacture continuous carbon fibre reinforced semi-finished sheets.



Figure 2.15: Compression moulded continuous carbon fibre SMC sheet.

2.3.3.2 Mechanical material properties

The considered unsaturated polyester-polyurethane two-step curing hybrid resin system (UPPH) enables the manufacturing of continuous carbon fibre reinforced SMC with mechanical properties comparable to unidirectional carbon fibre reinforced polymers, manufactured in a conventional (e.g. autoclave) process (Trauth et al., 2016). Table 2.4 lists mechanical properties of different continuous carbon fibre reinforced polymers (unidirectional configuration), manufactured by either a conventional autoclave or a compression moulding process. For materials 2 – 6, the same carbon fibre (Panex35 by Zoltek) in the form of a unidirectional prepreg tape (material 2), or a (non-crimp) fabric in unidirectional configuration (material 3 – 6) was considered as fibrous reinforcement. Material 6 is based on the same fibre type,

resin system and manufacturing process as the continuous carbon fibre SMC composite considered within the present dissertation. The tensile modulus of elasticity and tensile strength were normalised to a fibre volume content of 50 vol.%.

Table 2.4: Tensile properties of continuous carbon fibre reinforced polymers based on conventional manufacturing routes (e.g. autoclave) or on compression moulding. Depicted values of tensile modulus of elasticity (E_t) and tensile strength (R_t) were normalised to a FVC of 50 vol.%.

Material	Reference	Fibre prepreg	Resin system	Manufacturing process	Average norm. E_t in GPa	Average norm. R_t in MPa
1	SGL Group, 2011	UD prepreg	Epoxy	Autoclave	112.3	1648
2	Zoltek, 2018b	UD prepreg	Not specified	Not specified	108.1	1535
3	Zoltek, 2018d	UD fabric	Epoxy	Not specified	108.2	1273
4	Karcher, 2016	Non-crimp fabric	Epoxy	Compression moulding	103.5	1436
5	Karcher, 2016	Non-crimp fabric	Epoxy	Compression moulding	115.5	1413
6	Trauth and Weidenmann, 2016	Non-crimp fabric	UPPH	Compression moulding	109.6	1658

2.4 Hybrid composites

This section starts with a definition of hybrid composites. It highlights the motivation to develop and apply hybrid composites and presents methods to evaluate a hybridisation effect. The description of the state of research focusses only on hybrid polymer-based composites. Different kinds, for example fibre-metal-laminates, are not considered. It ends with an overview of concepts of hybrid SMC composites.

2.4.1 Definition, motivation and development of hybrid composites

According to Summerscales and Short (1978), a hybrid composite is defined as a macroscopically heterogeneous material consisting of a matrix and at least two different reinforcing fibre types. Hybrid composites are most frequently realised in the form of a laminate (Kaw, 2005). For this purpose, as depicted in Figure 2.16, three different types of hybrid (polymer) composites can be classified (Swolfs et al., 2014). For an interlayer configuration (Figure 2.16a), individual layers reinforced by different fibre types are stacked (Summerscales and Short, 1978; Yu et al., 2018). An intralayer hybrid (Figure 2.16b) is based on a combination of different fibres within one layer, and if mixing is realised on fibre level, an intrayarn hybrid can be created (Figure 2.16c) (Yu et al., 2015, 2018).

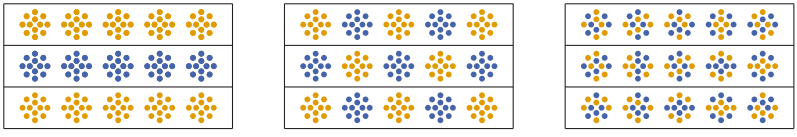


Figure 2.16: Main configurations of hybrid composites: interlayer (a), intralayer (b) and intrayarn (c) (Swolfs et al., 2014).

A recent description of hybrid composites differentiates three groups. In addition to the aforementioned combination of at least two different fibre types, a second group involves a hybridised matrix. The third way to form a hybrid composite can be realised by hybridising the matrix and the reinforcing material (Mészáros, 2018).

Hybridisation of polymer-based composite materials was an important field of research until the late 1980s, driven especially by the

high material and manufacturing costs of carbon fibre composites and the objective of replacing expensive carbon fibres with cheaper fibres while maintaining the material properties as well as possible (Hardaker and Richardson, 1980; Kretsis, 1987). Furthermore, as pointed out by Manders and Bader (1981), hybrid composites were a promising approach to increase failure strain by combining low- (brittle) and high-elongation (ductile) fibres within one composites. Hybridisation, hence, aimed to shift the brittle failure of low elongation (brittle) fibres, such as carbon or graphite, to a more ductile and gradual failure by combining them with a fibre type featuring a higher elongation in the same matrix.

The interest in hybrid composites faded slightly due to a price reduction of carbon fibres and the development of more precise analytical methods to predict the mechanical behaviour of composites, but this interest has been renewed by today's wider range of materials and processing technologies. Nowadays, the motivation to create and apply hybrid composites in different technical applications is not only cost reduction but also the ability to tailor the properties of a composite in terms of stiffness, strength, fatigue life or impact resistance, for example. In addition, to counteract the brittleness of especially unidirectionally carbon fibre reinforced polymers, damage tolerance may be increased due to pseudo-ductility realised by adding ductile fibres. Czél et al. (2015) and Czél and Wisnom (2013), for example, developed an advantageous composite, based on glass and carbon fibres, and have presented an approach and material architecture to overcome the inherent brittleness and unstable failure characteristic of conventional high-performance unidirectional composites. It exhibited a more ductile failure characteristic. Pseudo-ductility has also been obtained in intermingled hybrid composites (Yu et al., 2015).

Recently, different approaches to hybridise composites have been presented. However most work considered combinations of different fibre types in a continuous configuration within the same matrix. The most important recent work was summarised by Swolfs et al. (2014) and Sathishkumar et al. (2014). Only a few studies exist that focus on the combination of continuous and discontinuous fibres to realise a hybrid composite. Selmy et al. (2011), for example, investigated the mechanical properties of hybrid composites consisting of differently stacked unidirectional or random glass fibre reinforced layers, and they have pointed out that hybrid composites show enhanced tensile properties compared to the pure discontinuous glass fibre reinforced reference. Tensile modulus of elasticity increased by approximately 54 % to 85 %, depending on the volume fraction of the randomly reinforced component. The stacking sequence had a significant influence on tensile strength, with only slight influence on elastic properties. When the randomly oriented plies formed the outer layers of the composite and unidirectionally reinforced layers were considered within the core, tensile strength was improved (20 %) in comparison to a hybrid composites with the opposite arrangement. Selmy et al. (2011) attributed this behaviour to a better load transfer from the weak exterior layers, resulting in improved crack arrest mechanisms by the interior layers reinforced with stronger fibres. In addition, flexural modulus of elasticity and flexural strength increased as the relative volume fraction of unidirectional fibres increased. By placing the unidirectionally reinforced layers at the surface of the composite and the randomly oriented plies in the core, flexural strength increased (25 %) in comparison to composites with the opposite arrangement. Additionally, hybrid composites with unidirectionally reinforced surface layers featured a higher flexural modulus of elasticity. In a subsequent study, Selmy et al. (2012) have showed that in-plane shear properties in terms of shear strength and shear modulus

of a unidirectional fibre reinforced composite could be considerably improved by incorporating of randomly glass fibre reinforced layers, forming hybrid composites. Stacking sequence also influenced shear properties. With randomly glass fibre reinforced layers placed in the core of the laminate and unidirectionally fibre reinforced layers at the surface, shear strength was improved by about 22 % in comparison to a hybrid composite laminate with the opposite arrangement. Selmy et al. attributed this increase to improved crack-arrest mechanisms resulting from the interior layers. A combination of random, chopped glass fibre reinforced layers with layers featuring a unidirectional continuous fibrous reinforcement (based on polyamide fibres) also enabled the achievement of high ductility due to the polyamide fibres combined with high stiffness and strength resulting from the glass fibres. However, depending on layup, negative hybridisation effects were also observed (Selmy, 2018).

2.4.2 Evaluation of hybridisation effects

Different approaches have been presented in literature to evaluate a hybridisation effect. Basically, the possible resulting properties of a hybrid material, which reflects those of the individual components, have already been presented in section 2.1 and are depicted in Figure 2.3. The following section sums up the suitable ways to evaluate a hybridisation effect considering an interlayer, intralayer or intrayarn hybridisation of different fibre types to create a hybrid composite.

A first definition, by Hayashi (1972), was based on the enhancement of the failure strain of a hybrid composites. However, the introduced method has been controversially discussed (Summerscales and Short, 1978). Another possibility to evaluate a hybridisation effect is to

determine whether properties show a positive or negative deviation from a (linear) rule of mixtures considering a distinct property (Figure 2.17) (Marom et al., 1978; Summerscales and Short, 1978).

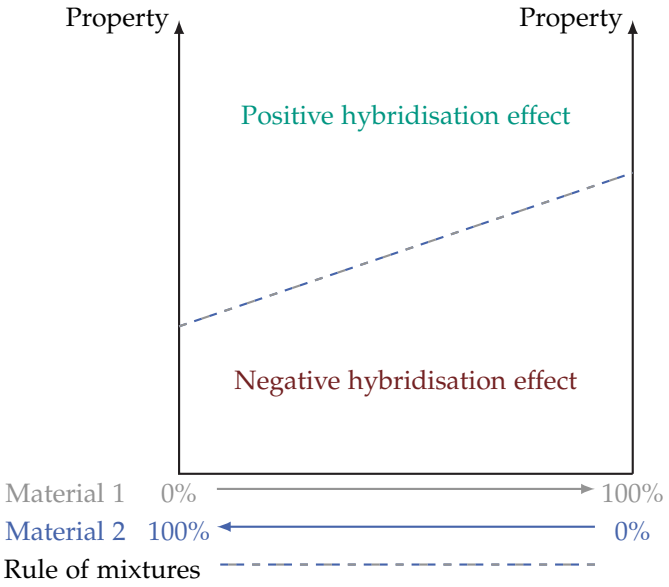


Figure 2.17: Hybridisation effect evaluated due to a deviation from the rule of mixtures, adapted from Swolfs et al. (2014).

This approach has several distinct disadvantages. Firstly, every rule of mixtures is based on a certain parameter to define the ratio of each individual component in a hybrid composite. As pointed out by Phillips (1976), it is extremely important to choose the right parameter for successful predictions. Secondly, the rule of mixtures is not linear for all mechanical properties, and the strength of hybrid composites rather follows a bilinear rule of mixtures, for example (Manders and Bader, 1981). Considering flexural stiffness, for instance, the stacking of differently reinforced layers significantly influences the

resulting mechanical properties and has therefore been considered for an analytical approach. More advanced theories, such as the classical laminate theory (CLT), are more suitable in this case.

For the sake of easy applicability, the evaluation of an effect of hybridisation (EoH_1) in terms of a deviation from the rule of mixtures is nevertheless frequently considered (Selmy, 2018; Swolfs et al., 2014) and is

$$EoH_1 = \frac{P_{hyb}}{P_{RoM}}, \tag{2.2}$$

with P_{RoM} being the analytically predicted value of a distinct property P by applying a rule of mixtures (Figure 2.17) and P_{hyb} being the property of the hybrid composite. However, as mentioned in the preceding section, a rule of mixtures approach is not suitable for every property of a composite and the application of the EoH_1 must be implemented conscientiously.

In general, and as described by Yahaya et al. (2014), an effect of hybridisation (EoH_2) can also be defined by an increase of distinct property of the hybrid material (P_{hyb}) with respect to an individual component (material 1 or material 2) of the hybrid as reference (P_{ref}) with

$$EoH_2 = \frac{P_{hyb}}{P_{ref}}, \tag{2.3}$$

with P_{hyb} and P_{ref} being the property of the hybrid and reference material, respectively (Figure 2.18).

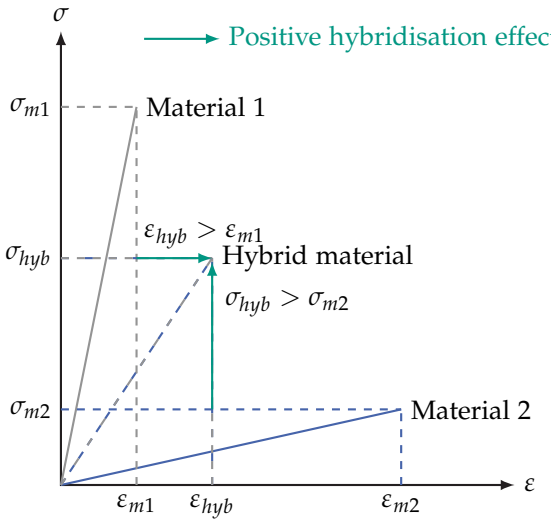


Figure 2.18: Hybridisation effect evaluated due to an increase of elongation at failure and strength, adapted from Swolfs et al. (2014).

2.4.3 Existing concepts of hybrid SMC

Early attempts to realise a hybrid SMC with unidirectionally continuous fibre reinforced surface layers and randomly oriented chopped fibres in the core date back to Taggart et al. (1979). Glass fibres were considered for the fibrous reinforcement, and the weight content of the continuously and randomly reinforced components were 20 wt.% and 30 wt.%, respectively. The unidirectional reinforcement in the surface plies led to a significant increase of the material's stiffness and strength in the surface fibre direction. The transverse tensile modulus of elasticity and strength were not significantly affected. The same trends have been observed for compressive loads (Table 2.5).

Table 2.5: Tensile and compressive properties of three different polyester-based SMC materials reinforced with glass fibres, SMC-25: 25 wt.% of randomly oriented glass fibres, SMC-65: 65 wt.% of randomly oriented glass fibres, SMC-C20/R30: 20 wt.% continuously oriented glass fibres in the surface and 30 wt.% of randomly oriented glass fibres in the core (Taggart et al., 1979).

Property	SMC-25	SMC-65	SMC-C20/R30
Longitudinal tensile modulus of elasticity in GPa	14.5	16.6	32.5
Transverse tensile modulus of elasticity in GPa	21.4	13.8	14.9
Longitudinal tensile strength in MPa	90	215	375
Transverse tensile strength in MPa	68	163	96
Longitudinal compressive modulus of elasticity in GPa	12.4	23.4	20.3
Transverse compressive modulus of elasticity in GPa	11.0	12.4	11.9
Longitudinal compressive strength in MPa	204	284	407
Transverse compressive strength in MPa	162	223	171

Following the same approach and manufacturing process, hybrid SMC containing continuous as well as chopped glass fibres based on vinylester and filled with calcium carbonate have been investigated by Sridharan (1982). A modified conveyor belt enabled the addition of a layer of continuous (C) fibre rovings on the top of a layer of randomly (R) oriented chopped fibres (intralayer hybridisation) to manufacture the hybrid SMC (Figure 2.19).

A combination of numerous semi-finished sheets allowed for the realisation of different combinations in terms of the nominal weight content of the continuous and discontinuous components. The results of experimental characterisation, depicted in Figure 2.20, indicate that the continuous fibres contributed significantly to an increase in the stiffness and strength of the hybrid SMC composite if loaded in fibre direction of the continuous component.

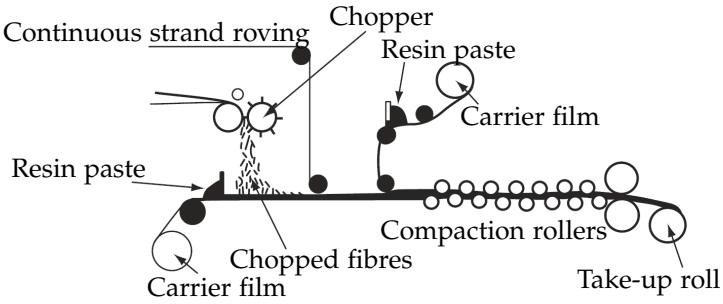


Figure 2.19: Schematic SMC line to manufacture hybrid SMC in Sridharan (1982), adapted from Mallick (2007).

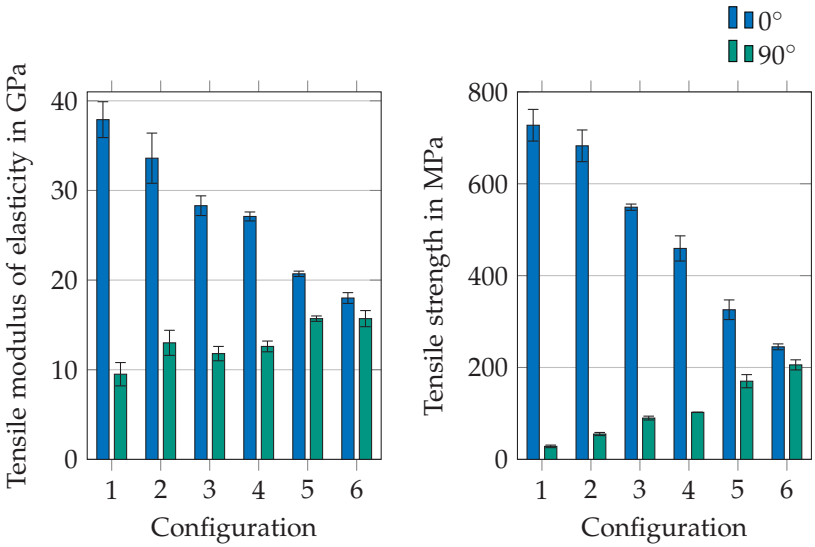


Figure 2.20: Tensile modulus of elasticity and tensile strength of hybrid continuous-discontinuous SMC composites with 0° parallel to fibre direction of the continuous component. 'C' and 'R' indicate the fibre weight content of the continuous (C) and discontinuous (R) component, respectively: configuration 1: SMC-C60R5; configuration 2: SMC-C45R20; configuration 3: SMC-C40R25; configuration 4: SMC-C30R35; configuration 5: SMC-C15R50; configuration 6: SMC-R65. Materials 1,2,4 and 6 were manufactured according to the process described in Figure 2.19, while materials 3 and 5 were commercially available (Sridharan, 1982).

Although the aforementioned investigations successfully demonstrated the positive effect of hybridisation of SMC composites by means of combining discontinuous and continuous fibres, further studies related to hybrid SMC materials date back no more than a few years.

A slightly different hybridisation approach was presented by Cabrera-Ríos and Castro (2006), based on a combination of layers of chopped glass and carbon fibres reinforced semi-finished SMC sheets on a ply-per-ply basis prior to moulding (interlayer hybridisation). The objective of this study was to characterise the effect of improvement of mechanical material performance based on a (partial) substitution of the glass by carbon fibres. The semi-finished chopped glass or carbon fibre SMC materials were based on a vinylester resin system and contained 25.4 mm long fibres with a fibre weight content of 50 %, respectively. The charge, consisting of differently stacked glass and carbon fibre reinforced semi-finished sheets (Figure 2.21), was placed in the centre of the mould, leading to randomly oriented fibrous reinforcement. From all glass (configuration d) to all carbon (configuration h) relative tensile modulus and relative tensile strength increased significantly (100 %, 150 %). For the same number of carbon and glass fibre reinforced plies, the stacking sequence significantly affected the relative tensile strength, and the best results were obtained if the two carbon fibre plies were placed in the middle of the stack. Considering two carbon and two glass fibre plies (configuration a, b and c), the best performance in terms of relative tensile strength was obtained while placing the two carbon fibre plies in the middle of the stack (a $\approx$ 10 MPa g^{-1}, b and c $\approx$ 8 MPa g^{-1}). In terms of relative tensile modulus of elasticity, no influence was observed, and configurations a – c ranged within $\approx$ 14 GPa g^{-1} to $\approx$ 16 GPa g^{-1}. For configurations e – g no significant variations were observed in terms of relative tensile modulus of elasticity, which showed a slight, but not

significant increase from $\approx 15\,\mathrm{GPa\,g^{-1}}$ (e) to $\approx 20\,\mathrm{GPa\,g^{-1}}$ (g). Relative tensile strength was highest for configuration f ($\approx 11\,\mathrm{MPa\,g^{-1}}$) followed by g ($\approx 10\,\mathrm{MPa\,g^{-1}}$) and e ($\approx 7\,\mathrm{MPa\,g^{-1}}$). As the number of carbon fibre plies increased (configuration e, f and g), relative flexural strength increased from $\approx 2\,\mathrm{MPa\,g^{-1}}$ to $\approx 52\,\mathrm{MPa\,g^{-1}}$. Flexural strength was equal to $\approx 25\,\mathrm{MPa\,g^{-1}}$, $30\,\mathrm{MPa\,g^{-1}}$ and $\approx 38\,\mathrm{MPa\,g^{-1}}$.

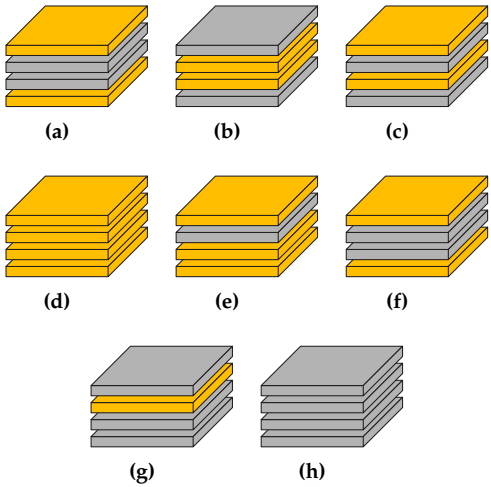


Figure 2.21: Stacking sequences to realise a hybrid SMC considered by Cabrera-Ríos and Castro (2006), a – c: 2 plies carbon and 2 plies glass fibre SMC; d: all plies glass fibre SMC; e: 3 plies glass and 1 ply carbon fibre SMC; f: 2 plies carbon and 2 plies glass fibre SMC; g: 1 ply glass and 3 plies carbon fibre SMC; h: all plies carbon fibre SMC.

Figure 2.22 depicts a hybrid SMC sheet compression moulded with alternating discontinuous glass and carbon fibres plies manufactured within the framework of the International Research Training Group (IRTG, GRK 2078), following the same manufacturing approach as reported by Cabrera-Ríos and Castro (2006).

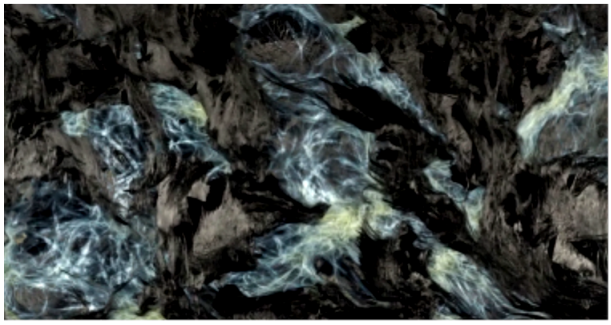


Figure 2.22: Hybrid glass/carbon fibre reinforced SMC sheet in interlayer configuration based on stacking of chopped glass and carbon fibres reinforced semi-finished sheets prior to moulding and manufactured within the framework of the IRTG (GRK 2078).

Following a continuous-discontinuous hybridisation approach, a recent publication by Wulfsberg et al. (2014) dealt with the combination of chopped glass fibre SMC, reinforced with a pre-impregnated carbon fibre woven or unidirectional fabric as core layer in a single-stage compression moulding process (Figure 2.23). The continuous as well as the discontinuous material were based on an unsaturated polyester resin featuring a significant amount of fillers to meet the requirements of fire safety and flame retardancy of the aerospace industry. Considering the pure discontinuous glass fibre reinforced SMC composite, which featured a fibre content of either 25 wt.% or 50 wt.%, as reference, the unidirectional or woven carbon fibre fabric generally increased tensile and flexural modulus of elasticity as well as tensile and flexural strength, as depicted in Figure 2.24. Due to the positioning of the continuous reinforcement in the core of the laminate, the increase of flexural properties was less distinct.

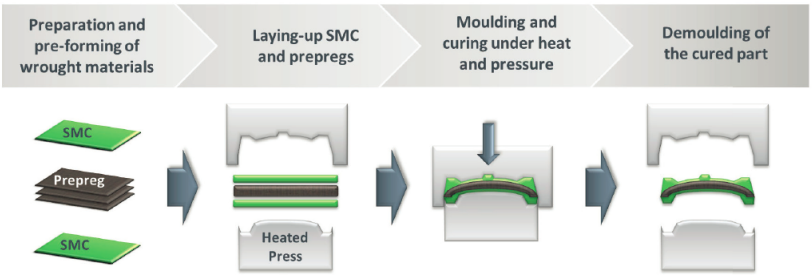


Figure 2.23: Process cycle to combine discontinuous chopped glass fibre SMC with a pre-impregnated carbon fibre fabric (Wulfsberg et al., 2014).

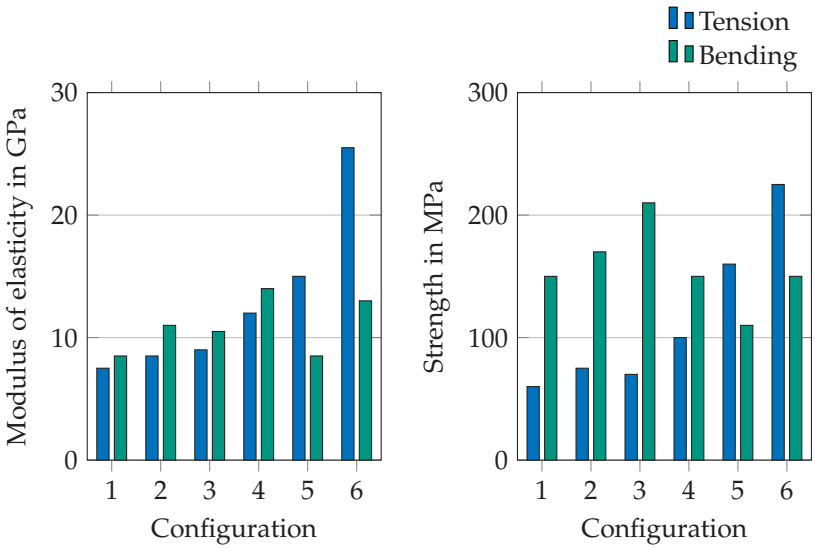


Figure 2.24: Tensile and flexural modulus as well as tensile and flexural strength of hybrid SMC investigated in Wulfsberg et al. (2014) considering different configurations: 1: discontinuous glass fibre SMC (25 wt.%); 2: discontinuous glass fibre SMC (50 wt.%); 3: discontinuous glass fibre SMC (25 wt.%) combined with woven carbon fibre fabric; 4: discontinuous glass fibre SMC (50 wt.%) combined with woven carbon fibre fabric; 5: discontinuous glass fibre SMC (25 wt.%) combined with unidirectional carbon fibre fabric; 6: discontinuous glass fibre SMC (50 wt.%) combined with unidirectional carbon fibre fabric, only average values were published.

Charpy impact strength was also influenced by the additional woven or unidirectional fabric, increasing up to $\approx 37\,\%$ if glass fibres were considered in the surface plies (25 wt.%). A higher fibre content in the surface plies decreased the reinforcing effect to $\approx 10\,\%$ with a woven carbon fibre fabric and was also negative, if unidirectional carbon fibre fabrics were considered as reinforcing component ($\approx -20\,\%$). Taking up the results on promising material behaviour, further studies on automated and cost-efficient production (Fette et al., 2016) as well as methods for computing (Fette et al., 2017) have recently been presented by the same research group. However, major drawbacks of the considered hybridisation approach include the high material and manufacturing costs of the pre-impregnated unidirectional or woven carbon fibre fabric.

In 2015, Gortner et al. analysed the combination of a standard SMC composite based on an unsaturated polyester resin reinforced by glass fibres (chopped, 30 wt.%) and dry textile preforms in a $\pm 45°$ non-crimp fabric configuration, made from either glass or carbon fibres, considered as surface plies. The discontinuous material featured fillers and the density was $1.73\,\mathrm{g\,cm^{-3}}$. The discontinuously reinforced semi-finished material and the dry textile preforms were stacked outside the mould, to realise either a one or two-sided continuous reinforcement. The initial mould coverage was between 40 % and 60 %. Impregnation of the textile preform took place within the mould during compression moulding. Quasi-static mechanical properties of the hybrid material in terms of tensile stiffness and strength were significantly influenced by the reinforcement. A single-sided glass fibre textile reinforcement led to an increase of tensile modulus and strength of $\approx 45\,\%$ and $\approx 300\,\%$, respectively. With an increase of $\approx 65\,\%$ and $\approx 400\,\%$ of tensile modulus of elasticity and tensile strength, a double-sided reinforcement was slightly more

effective. A double-sided reinforcement with carbon fibre fabrics most importantly influenced tensile properties and tensile stiffness and strength increased 125 % and 420 %, respectively. Flexural stiffness and strength were also significantly improved by a single-sided glass fibre reinforcement. A glass fibre fabric in the lower surface (tensile loading) led to an increase of flexural modulus (125 %) and flexural strength (140 %). A double-sided reinforcement did not further enhance flexural strength. However, a double-sided carbon fibre based reinforcement had an important influence on flexural modulus, which increased 190 % with respect to the reference. Gortner et al. also conducted puncture tests according to EN ISO 6603-2 (2000) with a drop tower. The increase in maximum force and maximum absorbed energy was 114 % and 106 % for a double-sided reinforcement. Charpy impact properties could only be increased by a double-sided reinforcement based on glass fibres ($\approx$ 50 %). Although the presented results were promising in terms of hybrid SMC, the quality of the impregnation of the dry textile, which strongly depended on the filler content and thus density of the SMC semi-finished sheets, was a crucial factor while evaluating the resulting mechanical material properties (Gortner et al., 2015a,b).

The International Research Training Group on the integrated engineering of continuous-discontinuous long fibre reinforced polymer structures aims to contribute significantly to a fundamental understanding of combined continuous-discontinuous SMC composites (CoDico SMC). Within this framework, a first study by the author of this dissertation investigated the mechanical properties of laminates based on a combination of continuous (Co) carbon fibre as well as discontinuous (Dico) glass fibre SMC with different ply arrangements. The discontinuous glass fibre SMC was based on a vinylester resin system (type Atlac XP810X by Aliancys). No fillers

were added to optimise structural properties. The nominal weight content of the reinforcing glass fibres (type Multistar 272 by Johns Manville) was set to 41 wt.%. The unidirectional carbon fibre SMC sheets were manufactured on a laboratory-size impregnation line, built at the Fraunhofer Institute for Chemical Technology (process described in Karcher et al., 2015, and Karcher, 2016) and based on a carbon fibre fabric (type Panex35 by Zoltek) and an unsaturated polyester-polyurethane hybrid resin system (type Daron 41 by Aliancys). The unidirectional carbon fibre SMC semi-finished sheets featured a nominal fibre weight content of 62 wt.%. After maturation, the Dico and Co sheets were cut into plies, stacked and compression moulded. Two different laminates architectures with a nominal thickness of 3 mm were realised, which differed in the stacking sequence of the continuously and discontinuously reinforced plies (type A: glass-carbon-glass; type B: carbon-glass-carbon, Figure 2.25). A mould coverage of 100% was realised. Tensile, compressive, flexural and impact properties (determined with non-clamped rectangular specimens in a drop tower) were investigated for the specimens, which were extracted in 0° and 90° with regard to the orientation of the unidirectional carbon fibres. Trauth and Weidenmann (2016) investigated the mechanical performance of the two different hybrid SMC laminates. For both types, a significant increase in tensile (pure discontinuous reinforced SMC: 11±0.2 GPa, laminate A: 43±3.2 GPa, laminate B: 83±3.5 GPa) and compressive modulus (pure discontinuous reinforced SMC: 9±0.9 GPa, laminate A: 29±8.4 GPa, laminate B: 67±12.5 GPa) as well as compressive strength (pure discontinuous reinforced SMC: 149±19.3 MPa, laminate A: 290±81 MPa, laminate B:420±29 MPa) was observed. For each property, the increase was proportional to the fraction of continuous carbon fibre SMC. Flexural modulus of elasticity was only significantly increased for laminate B

with continuously carbon fibre reinforced outer layers (pure discontinuous reinforced SMC: 7±0.8 GPa, laminate A: 10±0.7 GPa, laminate B: 71±2.9 GPa). Flexural strength increased for both hybrid SMC configurations (pure discontinuous reinforced SMC: 199±38 MPa, laminate A: 384±22 MPa, laminate B: 1042±65 MPa). Considering impact properties, no significant difference was observed for the two investigated laminate types with respect to the reference (pure discontinuous reinforced SMC: 53±10.3 J m^{-2}, laminate A: 95±8.3 J m^{-2}, laminate B: 123±21.6 J m^{-2}).

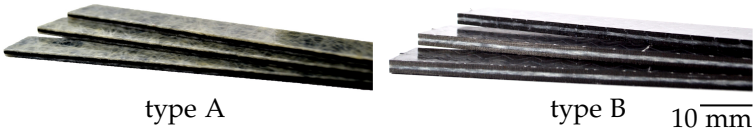


Figure 2.25: Hybrid continuous-discontinuous glass/carbon fibre SMC laminates, featuring different stacking sequences. Type A: continuous carbon fibre reinforced face sheets and discontinuous glass fibre reinforced core, type B: discontinuous glass fibre reinforced face sheets and continuous carbon fibre reinforced core (Trauth and Weidenmann, 2016).

The aforementioned studies highlighted a positive effect of hybridisation of SMC on resulting mechanical material properties. Nevertheless, little information was given on challenges of manufacturing. As demonstrated by Mallick (1986), flow of the semi-finished material during compression moulding, which is important to fill the mould and to reduce the amount of entrapped air, led to severe misorientation of the continuous fibres in hybrid SMC. For his investigations, SMC sheets, based on vinylester resin, were manufactured on a modified conveyor belt, as depicted in Figure 2.19. The fibre content of the continuous and the chopped, 25.4 mm long glass fibres were 40 and 30 wt.%, respectively. Rectangular-shaped semi-finished sheets were stacked to realise a (C-R)/(C-R)(R-C)/(R-C) layup. The initial

mould coverage was decreased from the reference value of 88 % to characterise the influence of material crossflow during moulding on resulting fibre orientation of the continuous material. In the reference sheet little evidence of fibre misorientation was present. Severe misorientation of the continuous fibre (as large as 15° to 20°) resulted from more important crossflow due to a lower mould coverage. The tensile strength of the resulting hybrid material was severely affected by the fibre misorientation of the moulded sheets. A deviation in fibre orientation of 5° with respect to loading direction decreased the average tensile strength from 524 MPa (reference sheet) to 333 MPa. In addition, failure modes of the hybrid SMC changed from tensile failure of the fibres for misorientation angles less than 5° to inter-fibre shear for larger angles. For a fibre orientation close to 90°, matrix failure was the predominating failure mechanism.

Corbridge et al. (2017) have reported comparable results. Epoxy-based advanced SMC composites (reinforced by chopped carbon fibres 57 vol.%) and epoxy-based unidirectional prepregs (53 vol.%) were combined in a one-shot compression moulding process, and distortion of the continuous component resulting from co-moulding was analysed. Results pointed out, that fibre misalignment could be reduced by increasing the degree of cure of the continuous reinforcement prior to moulding. Flexural stiffness, determined by four-point bending tests, could be increased from 47 GPa of the pure discontinuously reinforced sheet to 74 GPa of the hybrid SMC sheets, both of which manufactured with a mould coverage of 60 %. A rule of mixtures approach could successfully predict the resulting stiffness of the hybrid material, which was proportional to the amount of unidirectionally reinforced plies considered to mould the hybrid sheets. Flow during moulding led to shearing of the unidirectional plies, if the fibres were oriented transversely to flow direction. This

shearing caused variations in local fibre content and fibre waviness. Ply migration occurred for continuous fibres aligned in flow direction. It was shown, that staging the resin to 50 % cure decreased ply distortion during moulding (Corbridge et al., 2017).

Summary of hybridisation concepts

To summarise the findings described within this section and to deduce research questions, Table 2.6 lists the aforementioned approaches to hybridise SMC composites and focusses on the shortcomings of each concept.

Table 2.6: Summary of concepts to hybridise SMC composites - hybridisation approach and shortcomings. The following abbreviations have been considered: GF = glass fibre; CF = carbon fibre; Dico = discontinuous; Co = continuous; UD = unidirectional.

Reference	Hybridisation approach	Shortcomings
Taggart et al., 1979	Intralayer hybridisation: UD GF reinforced surface layers (20 wt.%, polyester-based) and randomly oriented short GF in the core (30 wt.%, polyester-based).	No CF were considered. Variability of stacking limited. Local Co reinforcement not possible.
Sridharan, 1982	Intralayer hybridisation: Placing of parallel lines of Co GF strand rovings on top of a chopped GF reinforced layer to obtain a hybrid CoDico semi-finished sheet (both components based on vinylester).	No CF were considered. Variability of stacking limited. Local Co reinforcement not possible.

Reference	Hybridisation approach	Shortcomings
Cabrera-Ríos and Castro, 2006	Intralayer hybridisation: Combining layers of chopped GF and CF reinforced semi-finished SMC sheets (25.4 mm long fibres, 50 wt.%, vinylester-based) in a ply-per-ply basis to realise different stacking sequences.	Neither Co nor local reinforcement realised.
Wulfsberg et al., 2014	Interlayer hybridisation: Combining layers of epoxy-based Dico CF SMC and epoxy-based UD CF prepregs in a one-shot moulding of the hybrid stack with variable mould coverage.	CF considered for the Dico material. No local reinforcement realised.
Wulfsberg et al., 2014	Interlayer hybridisation: Combination of chopped GF and CF reinforced semi-finished sheets with pre-impregnated CF woven or unidirectional reinforcements as core layers, semi-finished material was based on unsaturated polyester resin.	High material costs of pre-impregnated unidirectional or woven fabric. Co (or woven) reinforcement considered only as core layer.
Gortner et al., 2015a,b	Interlayer hybridisation: Combining layers of unsaturated-polyester-based chopped GF reinforced semi-finished SMC sheets with dry textile preforms (±45° non-crimp fabric) made from GF or CF.	Unsatisfactory impregnation of dry textile. No local reinforcement realised. No unidirectional reinforcement realised.
Trauth and Weidenmann, 2016	Interlayer hybridisation: Combining layers of unsaturated polyester-polyurethane-based Co CF SMC and vinylester-based chopped GF reinforced SMC (featuring no fillers) in a one-shot moulding to realise two different hybrid laminates.	Different resin systems for the Co and Dico material considered. Dico chopped GF SMC did not flow during moulding. No local reinforcement realised.

2.5 Research questions

Standard SMC materials have been widely used for numerous technical applications in recent decades. Manufacturing of continuous carbon fibre SMC composites, presented in section 2.3.3.1 and based on the work of Bücheler (2018), is a novel approach. The work of Bücheler has identified that the presented manufacturing method can overcome the shortcomings of existing concepts of hybrid SMC composites (Table 2.6) so as to consider cost-efficient continuous carbon fibre reinforced SMC materials to hybridise chopped glass fibre SMC composites. In addition, locally reinforced and complex multidimensional structures have been manufactured successfully. Based on the aforementioned work, the following research questions arise:

Microstructure and process-induced anisotropy
As described in section 2.3.2.2, the manufacturing and especially the compression moulding step strongly influence the fibre orientation and fibre distribution of SMC composites. With regard to mechanical performance, it is important to understand the influence of material flow on resulting mechanical properties and to consider anisotropic material behaviour depending on material composition, but more importantly on mould design and mould coverage (section 2.3.2.4).
In this regard, open questions remain:

- How can the characteristic microstructure of the unfilled unsaturated polyester-polyurethane two-step curing hybrid resin-based SMC composite be described? Does it resemble to the microstructure of conventional SMC material and exhibits a shell-core effect and to what extent do the chosen processing parameters influence the anisotropy of mechanical properties?

- Which geometry of the specimens is appropriate to account for the highly heterogeneous microstructure of SMC composites if the same geometry has to be considered to also evaluate the mechanical performance of continuous and hybrid continuous-discontinuous SMC composites?
- What microstructure results due to co-moulding of CoDico hybrid SMC materials, and what is the quality of the hybrid CoDico SMC sheets in terms of fibre misalignment of the continuous material resulting from flow of the discontinuous component during compression moulding?

Definition of appropriate measurement techniques

Conventional methods to measure strains in tensile or compression tests, for example those based on extensometers or strain gauges, are not appropriate to define a stress-strain response of highly heterogeneous or hybrid materials, and digital image correlation (DIC) must be considered. Hence, this dissertation inquires the following:

- What is the best way to evaluate resulting displacement fields accounting for a highly heterogeneous microstructure by means of digital image correlation?
- Which techniques are most suitable to capture damage evolution of hybrid CoDico SMC composites?

Characterising hybridisation effects and evaluation of failure mechanisms of hybrid continuous-discontinuous glass/carbon fibre SMC composites

As described in section 2.4.2, evaluation of hybridisation effects is not always straight forward. Although a rule of mixtures approach is often considered, this strategy might not be the best solution for every loading case (e.g. for flexural loadings). In this regard the following questions arise:

- What is the best way to define an effect of hybridisation of the presented continuous-discontinuous glass/carbon fibre SMC material?
- What effect does the presented hybridisation approach have on coupon, structural and component properties of hybrid SMC composites?
- Which component, either the discontinuous or continuous SMC, dominates mechanical performance in a distinct loading case?

Although hybrid composites do not stand out due to their general novelty, few approaches have focussed on failure and damage evolution resulting from a mechanical loading of hybrid fibre reinforced polymer-based materials. The failure of composites is a complex phenomenon, based on the interaction of several different failure mechanisms, characteristic of a special fibrous reinforcement architecture (section 2.2.2). In-situ observation techniques may enable one to capture damage evolution to understand effects of hybridisation on failure and to answer the following questions:

- What are the predominating failure mechanisms of the individual components exposed to uniaxial and multiaxial loads?
- How does damage evolution change, when SMC composites are hybridised?
- Which component, either the discontinuous or continuous SMC, dominates the damage evolution and failure of a distinct loading case?

3 Materials and specimen geometries

The investigated materials within this dissertation are sheet moulding compound composites featuring either a discontinuous (Dico), continuous (Co) or hybrid continuous-discontinuous (CoDico) fibrous reinforcement. The following chapter details the manufacturing of the semi-finished materials and the compression moulding of the SMC sheets. Preparation and geometry of specimens considered for mechanical testing are also presented.

3.1 Manufacturing of sheet moulding compound composites

3.1.1 Composition of resin systems

The composition of the resin systems, considered to manufacture the discontinuous glass and continuous carbon fibre SMC semi-finished sheets, were developed at the Fraunhofer Institute for Chemical Technology (ICT) (Bücheler, 2018). Both components were based on an unsaturated polyester-polyurethane two-step curing hybrid resin system (UPPH) by Aliancys, reinforced with either chopped glass fibres or a non-crimp fabric made from carbon fibres in a unidirectional configuration. No fillers were added to the resin system, and the detailed compositions are listed in Tables 3.1 and 3.2.

Table 3.1: Resin components and fibre type of discontinuous glass fibre SMC.

Component	Product name	Supplier	Parts
UPPH resin	Daron ZW 14141	Aliancys	100
Release agent	BYK 9085	BYK	2.0
De-airing	BYK-A-530	BYK	0.5
Inhibitor	pBQ	Fraunhofer ICT	0.3
Peroxide	Trigonox 117	Akzonobel	1.0
Thickener (Isocyanate)	Lupranat M20R	BASF	19.5
Fibre	Multistar 272	Johns Manville	41 wt.% (nom.)

Table 3.2: Resin components and fibre type of continuous carbon fibre SMC.

Component	Product name	Supplier	Parts
Resin	Daron AQR 9001	Aliancys	100
Release agent	BYK 9085	BYK	2.0
Impregnation additive	BYK 9076	BYK	3.0
Inhibitor	pBQ	Fraunhofer ICT	0.3
Styrene	Mono Styrol	BASF	2.9
Peroxide	Trigonox 117	Akzonobel	1.0
Thickener (Isocyanate)	Lupranat M20R	BASF	25.0
Accelerator	BorchiKat 0243	Borchers	0.17
Fibre	PX3505015W-13	Zoltek	60 wt.% (nom.)

3.1.2 Manufacturing of semi-finished sheets

Manufacturing of the discontinuous glass fibre reinforced SMC started with mixing of the resin components listed in Table 3.1 (except the fibres) in a vacuum. The semi-finished materials were manufactured on a flat conveyor plant, type HM-LB-800 by Schmidt and Heinzmann, at the Fraunhofer ICT in Pfinztal, Germany (Figure 3.1). In the first part of the conveyor belt, the resin was deposited onto a polymeric carrier film. Continuous glass fibres, type Multistar 272 by Johns Manville, were cut to a length of 25.4 mm in a cutting unit, and the fibre bundles were dropped onto the paste layer (Figure 3.2a). Covered with a second polymeric film and resin, the sandwich or SMC mat was calendered, rolled up, and matured for at least 3 days at 18 °C. Maturation aimed to increase the viscosity of the compound to facilitate cutting and handling.



Figure 3.1: SMC manufacturing line at Fraunhofer Institute for Chemical Technology, ICT (image provided by Fraunhofer ICT).

In order to manufacture the continuous carbon fibre SMC, the resin components listed in Table 3.2 were mixed into two separate components, which were first combined by pouring them into the doctor box. This special manufacturing step was necessary because the two components react as soon as combined. A continuous reinforcement was achieved by feeding a unidirectional non-crimp fabric, type PX3505015 by Zoltek, to the conveyor belt (Figure 3.2b). Heatable tables at the end of the conveyor belt allowed for increasing the temperature of the impregnated fabric, to improve impregnation and to start curing. The semi-finished sheets were then again subsequently cooled down to room temperature to stop this chemical reaction (Bücheler, 2018). In a final step, the semi-finished sheet was wound onto a roll before being cut and prepared for moulding.

Within this dissertation, the non-moulded sheets are referred to as semi-finished material or semi-finished sheets.



(a) (b)

Figure 3.2: Feeding of fibrous reinforcement to the conveyor belt: chopped glass fibres (a) or unidirectional non-crimp carbon fibre fabric (b) (images provided by Fraunhofer ICT).

3.1.3 Manufacturing of compression moulded sheets

After maturation, the semi-finished SMC sheets were cut into plies, stacked and compression moulded at approximately 150 °C, 2500 kN, and 112 s mould closing time on a press by Dieffenbacher (type COMPRESS PLUS DCP-G 3600/3200 AS).

One-dimensional (1D) flow sheets, made from discontinuous glass fibre SMC or continuous-discontinuous glass/carbon fibre SMC, were manufactured by placing the discontinuous charge in the middle of the rectangular-shaped mould (Figure 3.3) with a mould coverage of approximately 35 %, forcing the discontinuous component to flow in one direction (Figure 3.5a).

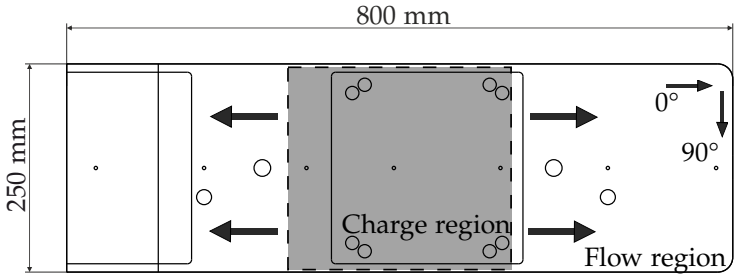


Figure 3.3: Rectangular-shaped mould to compression mould 1D flow SMC sheets; grey section indicates charge region.

A two-dimensional (2D) flow was implemented by placing the charge of discontinuous glass fibre SMC in the middle of a square-shaped mould, with a mould coverage of approximately 35 % (Figure 3.4). The discontinuous glass fibre SMC sheets featured a nominal thickness of 3 mm.

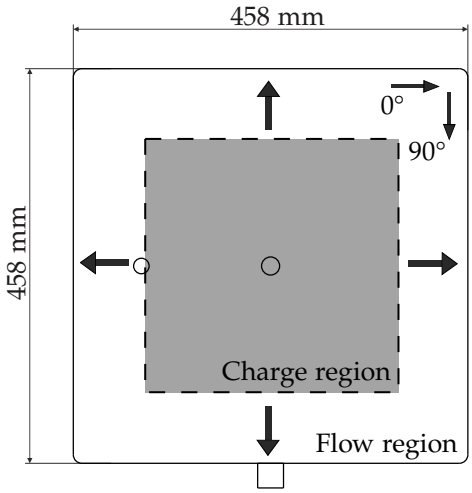


Figure 3.4: Square-shaped mould to compression mould 2D flow SMC sheets; grey section indicates charge region.

Hybrid continuous-discontinuous glass/carbon fibre SMC sheets were manufactured by placing the stack, which consisted of one layer of the continuously reinforced semi-finished material on bottom and top, combined with either 6 or 7 core layers of discontinuous glass fibre SMC in the middle of the mould. This enabled the realisation of a symmetric hybrid CoDico SMC laminate with a total nominal thickness of 3 mm. The face layers featured a thickness of approximately 0.33 mm each. The discontinuous component flew during moulding between the continuous carbon fibre reinforced sheets to fill the mould (Figure 3.5b).

Continuous carbon fibre SMC sheets were also compression moulded within the rectangular-shaped mould; however, the mould coverage was 100 % and the semi-finished material did not flow. The nominal thickness of the continuous carbon fibre sheets was 1 mm, 2 mm or

3 mm to account for the various specimen geometries considered for mechanical testing.

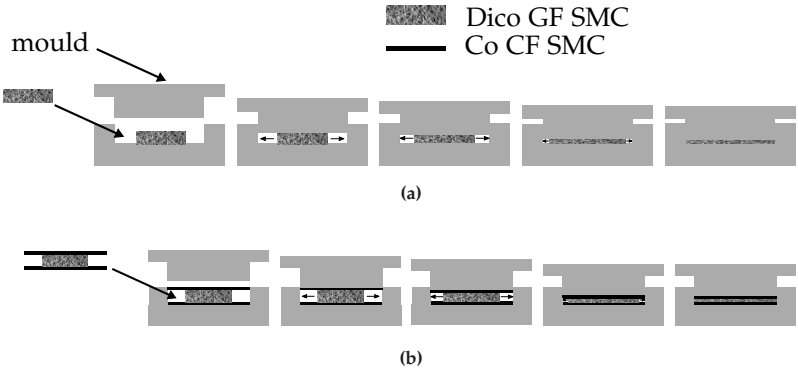


Figure 3.5: Schematic illustration of compression moulding of discontinuous glass fibre SMC sheets (a) and hybrid continuous-discontinuous glass/carbon fibre SMC sheets (b).

In the following, the term sheet, plaque, SMC material or composite refers to the compression moulded final part. Figure 3.6 shows the three different materials investigated within this dissertation.



Figure 3.6: From bottom to top: continuous carbon fibre SMC, discontinuous glass fibre SMC and hybrid continuous-discontinuous glass/carbon fibre SMC.

3.1.4 Manufacturing of pure resin sheets

Manufacturing of pure unsaturated polyester-polyurethane two-step curing hybrid resin sheets was carried out in collaboration with the Institute of Production Science at Karlsruhe Institute of Technology (KIT), the Fraunhofer ICT in Pfinztal Germany, Loredana Kehrer (Institute of Engineering Mechanics [ITM], KIT) and Michael Schober (Institute for Applied Materials [IAM] - Computational Material Science [CMS], KIT and Fraunhofer Institute for Mechanics of Materials [IWM], Freiburg, Germany) within the framework of the IRTG. The pre-thickened resin (Figure 3.7), consisting of the components listed in Table 3.1, which were mixed under vacuum, was compression moulded at the Institute of Production Science at KIT, with a moulding temperature of 145 °C at 2000 kN and 90 s mould closing time (press: Lauffer type RP 400).

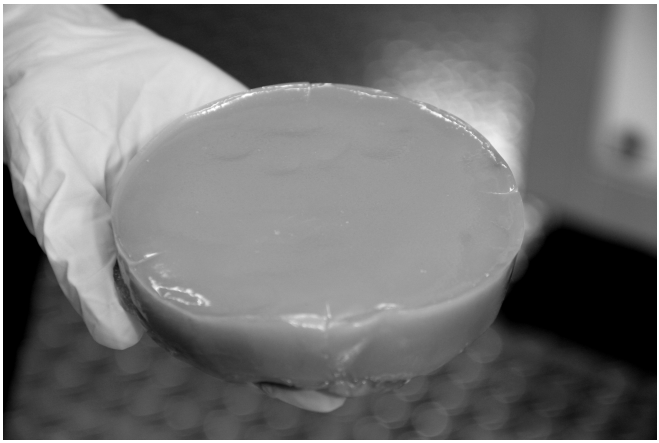


Figure 3.7: Pre-thickened unsaturated polyester-polyurethane hybrid resin prepared for moulding of a pure resin sheet (image provided by Michael Schober, IAM CMS and Fraunhofer IWM).

3.1.5 Manufacturing of demonstrator part

Within the framework of the International Research Training Group on the integrated engineering of continuous-discontinuous long fibre reinforced polymer structures, a special reference structure as demonstrator part was designed. It was optimised to maintain bending loadings. For this purpose, position and geometry of local reinforcement were defined by optimisation methods (Fengler et al., 2018). The local reinforcement of the demonstrator part was implemented by continuous carbon fibre SMC tapes in a 0°-90°-0° layup, which were cut to a special shape and placed inside the mould. Next, three layers of discontinuous glass fibre SMC, also cut to a particular shape and featuring a mould coverage of $\approx 35\,\%$, were placed on top of the continuous carbon fibre SMC. Three additional discontinuous glass fibre SMC sheets (rectangular-shaped, mould coverage $\approx 35\,\%$) were placed on top. The demonstrator part was then compression moulded using a special insert placed inside the rectangular-shaped mould (Figure 3.3) with a mould temperature of approximately 150 °C with 2500 kN and a mould closing time of 112 s. As a last step, the demonstrator part was extracted from the moulded plaque by milling at the Institute of Production Science, KIT. Demonstrator parts, made from only discontinuous glass fibre SMC, were manufactured in the same way, without considering step one and two. Geometric details of the demonstrator part can be found in Figure 3.14.

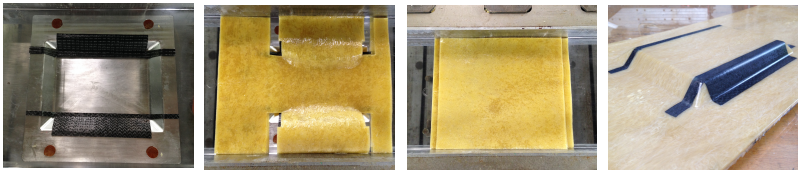


Figure 3.8: Steps to manufacture the demonstrator part. Step 1: Insertion of preformed and specially cut continuous carbon fibre SMC into mould. Step 2: Insertion of specially cut first stack of discontinuous glass fibre SMC into mould. Step 3: Insertion of second stack of discontinuous glass fibre SMC into mould. Step 4: Compression moulded rectangular sheet with demonstrator part (images 1–4 provided by Fraunhofer ICT).

3.2 Specimen preparation and geometry

Specimen preparation is an important topic in accurately determining the mechanical properties of composite materials. Specimens considered in this dissertation were extracted using water-jet or milling technologies. However, these techniques may lead to a certain quality of edges of the specimens. The influence of specimen preparation and the resulting condition of the edges must be considered when mechanical material properties are sought.

3.2.1 Water-jet cutting and milling

Specimens for experimental investigations were extracted by water jet cutting by SNZ Schneidbetrieb GmbH, Mühlacker, Germany. The water-jet beam featured a width between 1 and 1.2 mm. The feed was 800 mm min^{-1}. For sheets thicker than 3 mm the feed was reduced to 600 mm min^{-1}. Cutting pressure was 3400 bar, and Garnet Mesh 80 (nominal diameter of abrasive medium: 0.18 mm to

0.36 mm, throughput: 450 g min^{-1}) was used as the abrasive medium. Specimens were stored at room temperature ($\approx$ 23 °C) for several days before testing. No special drying treatment was carried out. The thickness and width of each specimen was determined by three different measurements of the two lengths in the gauge section and by calculating the average mean value. Pure resin specimens were extracted by milling at the Institute for Applied Materials, KIT.

3.2.2 End tabs

End tabs to protect specimens during mechanical loading were designed, taking into account guidelines presented in Adams and Adams (2002). For this purpose, the ends of both sides of the specimens were abraded using sand paper (180-grit) to roughen the surface. The abraded surfaces were wiped with isopropyl alcohol to get them ready for adhesive bonding. End tabs (cut from PREGNIT GMBE glass fibre reinforced epoxy plastic laminates by Krempel, Vaihingen an der Enz, Germany with a nominal thickness of 1.3 mm) were glued on the specimens. The choice of adhesive was 3M Scotch-Weld™ Low Odor Acrylic Adhesive DP810. The acrylic was generously dispensed on the tab and SMC specimens before the tabs were bonded on the ends of each side of the specimen and left to cure at room temperature for at least 24 hours.

3.2.3 Specimen geometries

3.2.3.1 Tensile specimens

In order to characterise anisotropic, heterogeneous materials, such as discontinuous SMC composites, a preliminary study was carried out to define an appropriate specimen geometry. For this

purpose, rectangular and dog-bone-shaped specimens were designed according to DIN EN ISO 527-4 (1997) and DIN EN ISO 527-5 (2009) and ASTM D3039/D3039M (2017) to evaluate and compare mechanical properties.

The geometry of the specimens, considered for this preliminary test – as well as the tensile testing of pure UPPH resin – are depicted and described in Figure 3.9 and Table 3.3. All specimens made from discontinuous glass fibre SMC featured a nominal thickness of 3 mm. Pure resin specimens featured a nominal thickness of 2 mm.

Table 3.3: Dimensions of rectangular-shaped (R) and dog-bone-shaped (B) specimens depicted in Figure 3.9.

Type	l in mm	b in mm	l_1 in mm	l_2 in mm	l_3 in mm	b_1 in mm	b_2 in mm	r in mm
R 1	200	15						
R 2	200	30						
B 1			80	128	229	15	25	60
B 2			80	146	246	30	50	60
Pure resin			80	110	150	10	20	60

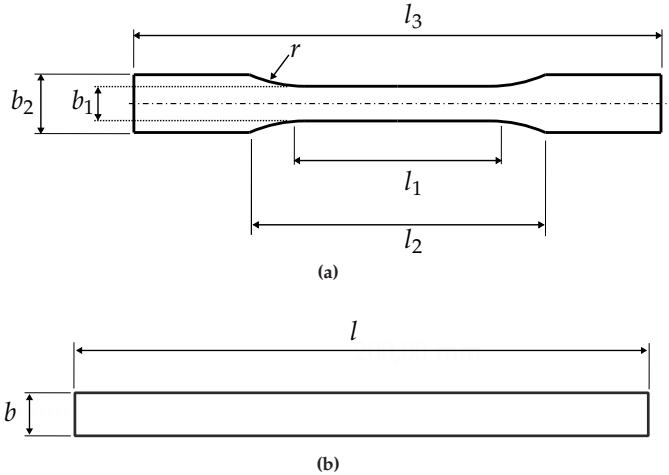


Figure 3.9: Specimen geometries for preliminary tensile tests and characterisation of pure resin: (a) dog-bone-shaped specimen (B_1 and B_2) and (b) rectangular-shaped specimen (R_1 and R_2).

Tensile tests, aiming to define hybridisation effects and properties of the discontinuous glass fibre, continuous carbon fibre and continuous-discontinuous glass/carbon fibre SMC were carried out with rectangular-shaped specimens, which featured a length of 200 mm and a width of 15 mm. The nominal thickness of specimen, h, was 1 mm (continuous carbon fibre SMC loaded in fibre direction), 2 mm (continuous carbon fibre SMC loaded perpendicular to fibre direction) or 3 mm (discontinuous and continuous-discontinuous SMC). End tabs, considered for all material types, had a length of 50 mm and were tapered with a tapered section of 5 mm (Figure 3.10).

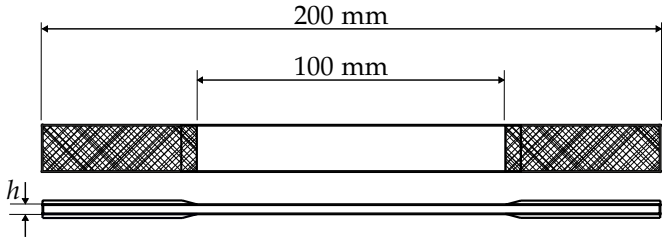


Figure 3.10: Geometry of tensile specimen made of discontinuous, continuous and continuous-discontinuous SMC with end tabs.

3.2.3.2 Compression specimens

Rectangular specimens were considered for compression testing (Figure 3.11), which featured a length of 100 mm and a width of 15 mm, and they were designed according to DIN EN ISO 14126 (1999). The nominal thickness of the specimen, h, was either 3 mm (discontinuous and continuous-discontinuous SMC) or 2 mm (continuous carbon fibre SMC in fibre direction). End tabs, considered for continuous carbon fibre SMC and continuous-discontinuous glass/carbon fibre SMC specimens loaded in fibre direction, were 44×15 mm^2 and were not tapered.

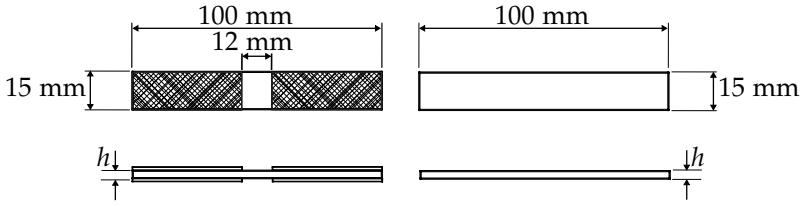


Figure 3.11: Geometry of compression specimen of discontinuous, continuous and continuous-discontinuous SMC with and without end tabs.

3.2.3.3 Bending specimens

According to DIN EN ISO 14125, 1998, rectangular specimens were considered for bending testing (Figure 3.12), which featured a width of 15 mm. The nominal thickness was 3 mm. Specimens for flexural testing featured different lengths (l) to realise variable span (L) to thickness (h) ratios (L/h) with a constant overlap of $\approx$ 20 %. For this purpose, continuous carbon fibre SMC specimens were also extracted from 2 mm thick sheets to enlarge the testing matrix in terms of the L/h ratio.

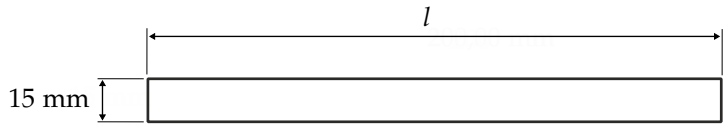


Figure 3.12: Geometry of bending specimen of discontinuous, continuous and continuous-discontinuous SMC.

3.2.3.4 Puncture specimens

Quasi-static and dynamic puncture tests were carried out on rectangular specimens with a side length of 140 mm, according to EN ISO 6603-2 (2000) (Figure 3.13). Specimens featured a nominal thickness of 3 mm.

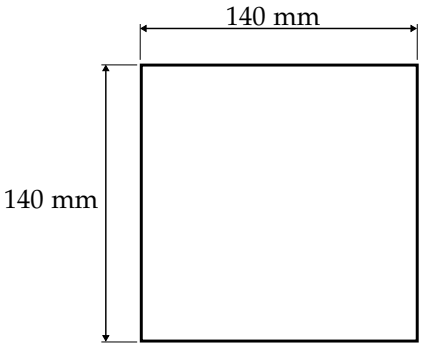


Figure 3.13: Geometry of puncture specimen of discontinuous, continuous and continuous-discontinuous SMC.

3.2.3.5 Demonstrator part

The demonstrator part designed within the framework of the IRTG (GRK 2078) and considered to investigate component properties, is shown in Figure 3.14. A detailed description of the geometry, designed and optimised to maintain bending loads, can be found in Figure 3.15.

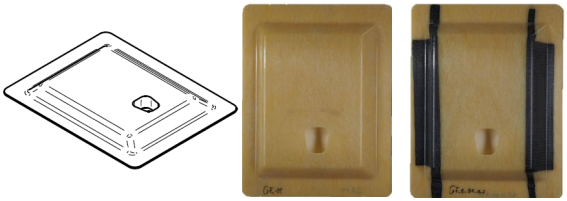


Figure 3.14: Schematic drawing of demonstrator part (a), demonstrator part of discontinuous glass fibre SMC (b) and locally reinforced demonstrator part (c).

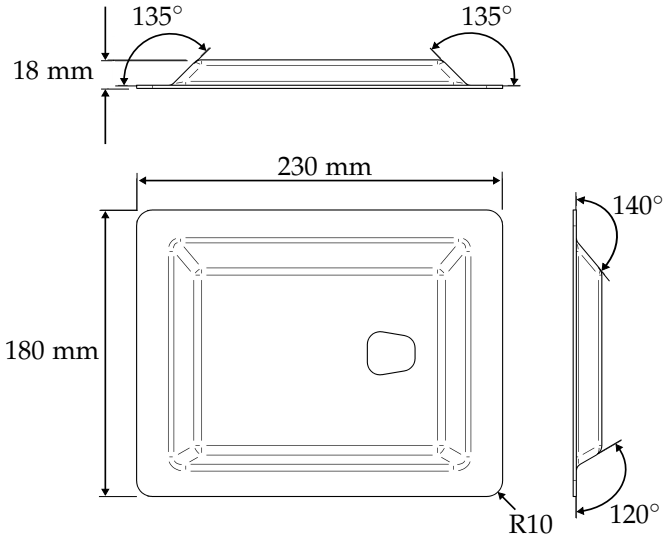


Figure 3.15: Geometry of the demonstrator part designed within the framework of the IRTG (GRK 2078).

4 Experimental setups, procedures and data evaluation

The following chapter describes micro- and macroscopic characterisation methods to investigate mechanical properties and structure-property relationships of discontinuous, continuous and hybrid continuous-discontinuous sheet moulding compound composites. Starting with the investigation of the micro- and macromechanical material properties of the individual and hybrid materials, macromechanical testing is continued on structure level at different loading rates. Finally, component tests are considered.

4.1 Characterisation strategy

Characterisation on the macroscopic scale was based on a vertical and horizontal strategy, as depicted in Figure 4.1 and 4.2. Starting on a coupon level, characterisation of SMC materials is carried out to deduce micro- and macrostructural material properties. Micromechanical observations aim to describe the material's microstructure in terms of fibre length and fibre orientation distribution. In addition, a qualitative investigation of the influence of co-moulding on the resulting microstructure is carried out. Optical observation of a (post-mortem) specimen enables the identification of failure mechanisms due to different loading cases and the architecture of fibrous reinforcement. Characterisation at the structure level was carried

out to deduce structural properties resulting from a specific loading case, as well as to consider the rate effects of the investigated SMC composites. Finally, component testing, realised on a more complex geometry, was aimed to evaluate the effect of a local reinforcement if CoDico SMC structures are exposed to a specific bending loading case. Every level of characterisation is itself based on a horizontal approach which starts by defining the material, structural and component properties of the individual components. In a subsequent step and by characterising the hybrid coupon, structure or component, mechanical properties and damage mechanisms can be compared. Suitable tools to define an effect of hybridisation are introduced to quantify the differences in mechanical performance.

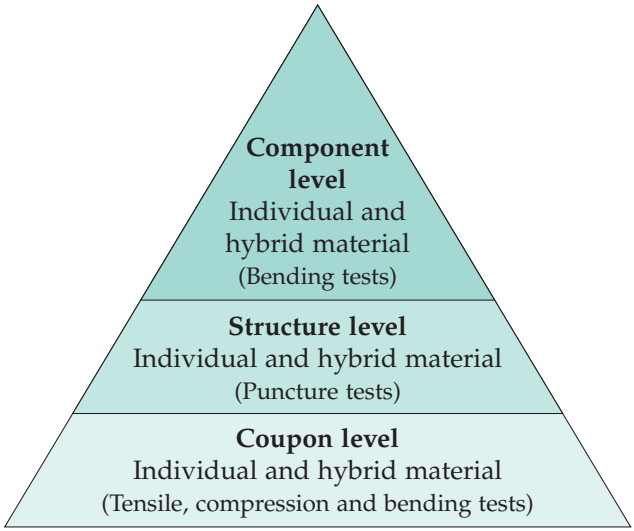


Figure 4.1: Vertical characterisation strategy to investigate material, structural and component properties of discontinuous glass, continuous carbon and hybrid continuous-discontinuous glass/carbon fibre SMC composites.

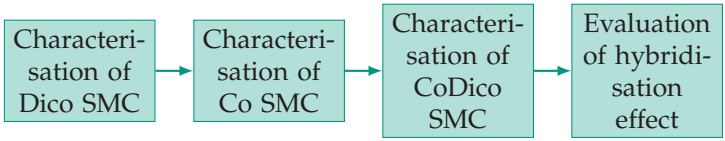


Figure 4.2: Horizontal characterisation strategy to investigate discontinuous glass, continuous carbon and hybrid continuous-discontinuous glass/carbon fibre SMC composites in order to evaluate the effects of hybridisation.

4.2 Characterisation at the coupon level

4.2.1 Microstructural characterisation

4.2.1.1 Thermogravimetric analysis

To determine the (real) fibre volume content (FVC) of the discontinuous and continuous SMC sheets, circular specimens with a diameter of 20 mm were extracted from different locations of the sheets, and a thermogravimetric analysis (TGA) was performed with a Leco TGA701 (LECO Corporation, St. Joseph, MI, USA) at the Fraunhofer ICT in Pfinztal, Germany. Thermogravimetric analyses generally enable one to determine the fibre weight content by burning off the matrix of a specimen (Equation 5.17); moreover, with the density of the matrix material (ρ_M) and the fibres (ρ_F), the fibre volume content of the specimen can be determined (Equation 5.18).

For the investigation of the discontinuous glass fibre SMC, the chamber was heated to 550 °C at a heating rate of 37 °C min^{-1}. This temperature stayed constant for 2 h. For the investigation of the continuous carbon fibre SMC, the TGA was carried out according to the method proposed by Bücheler et al. (2016).

4.2.1.2 X-ray micro-computed tomography

The microstructure of the SMC composites has been investigated by means of micro-computed tomography (μ-CT). For this purpose, some specimens were scanned in a high-resolution cone-beam industrial CT System (Yxlon-CT Precision, Yxlon International CT GmbH, Hattingen, Germany) containing an open micro-focus X-ray transmission tube with a tungsten target and a 2048 x 2048 pixel^2 flat panel detector from Perkin Elmer (Waltham, MA, USA). The acceleration voltage was 100 kV and the tube current 0.05 mA. The scans were acquired with a focus object distance of 31.3 mm and a focus detector distance of 750 mm, leading to a voxel size of 8.04 µm.

4.2.1.3 Scanning electron microscopy

Selected post-mortem specimens have been investigated by means of scanning electron microscopy (SEM) to characterise the important damage mechanisms of SMC materials. Examinations were carried out using a SUPRA 55 VP SEM by Zeiss, located at the Fraunhofer ICT in Pfinztal Germany, with an angle-selective backscatter detector. Some images were captured in low pressure mode (23 Pa) to counteract charging effects. However, the standard working condition was a vacuum.

4.2.2 Macrostructural characterisation

Macrostructural characterisation at the coupon level aimed to define tensile, compressive and flexural properties of the discontinuous glass fibre, continuous carbon fibre and continuous-discontinuous glass/carbon fibre SMC composites. The highly heterogeneous microstructure of discontinuous SMC composites, combined with a

macroscopically important heterogeneity of the hybrid material, generally complicated the prediction of mechanical properties in terms of an appropriate displacement measurement technique. It is not recommended to measure the modulus with strain gauges or an extensometer, since these techniques do not account for the variability of material properties resulting from the anisotropic and heterogeneous microstructure (Feraboli et al., 2009). Digital image correlation (DIC) has been used extensively to define material properties and damage evolution of composite materials (e.g. by Hild and Roux, 2006; Laurin et al., 2012; Roux et al., 2008 or Johanson et al., 2015) and is considered to measure displacements to define mechanical properties of the SMC composites investigated in this dissertation. Another challenge in characterising long fibre reinforced composites, such as SMC, is the important scatter of material properties, especially considering strength that arises from the heterogeneous microstructure (Shirrell, 1985). Hence, specimens with different orientation with respect to manufacturing and flow direction are considered for mechanical material characterisation.

4.2.2.1 Tensile tests

Tensile tests were carried out in a conditioned laboratory at 23 °C on a ZMART.PRO universal testing machine by ZwickRoell, with a load cell capacity of 200 kN according to DIN EN ISO 527-4, 1997 and DIN EN ISO 527-5 (2009). The specimens for tensile testing are described in section 3.2.3.1. Before testing, specimens were hydraulically clamped at a clamping distance of 100 mm (unless otherwise noted) and preloaded to level out any compressive loads resulting due to clamping. The preload was defined according to the recommendation in DIN EN ISO 527-1 (2012) and adjusted for the different materials (Dico GF SMC, Co CF SMC and CoDico GF/CF SMC). It

featured a load corresponding to 10 MPa for the continuous carbon fibre SMC tested in the fibre direction and 2 MPa for all other specimen types. Digital image correlation was used to measure the displacement field resulting from uniaxial tension (Figure 4.3).

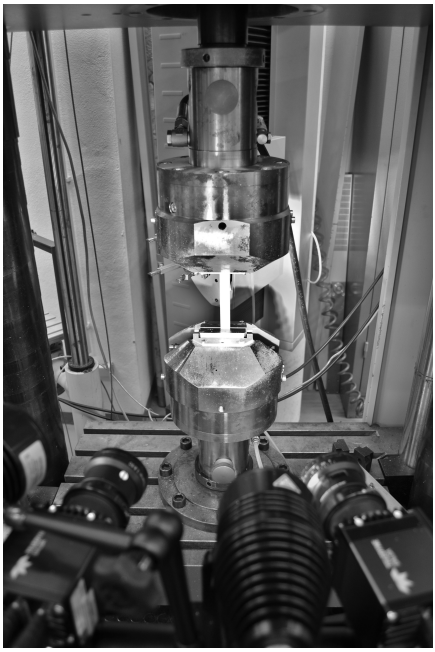


Figure 4.3: Tensile test setup with stereo digital image correlation (DIC).

A 4M GOM ARAMIS three-dimensional (3D) DIC system featured an adjustable base with two 4MP Teledyne Dalsa cameras with 50 mm Schneider Kreuznach objectives. Lighting was realised by two light-emitting diodes (LED) lights (16 W each) with a polarisation filter, and thermal changes to the specimen were negligible. A gauge section of approximately 70×10 mm^2 was considered, and technical strains were calculated. Uniaxial tensile tests were conducted with a nominal

loading rate of 1.8 mm min^{-1} ($\dot{\varepsilon} \approx 2 \times 10^{-4}$) until fracture. The frame rate of image acquisition was 5 Hz. Tensile modulus of elasticity (E_t) and Poisson's ratio (ν_t) were determined with a least squares method according to ASTM E111 (2010) (Equation 4.10 in section 4.5) in a strain range of 0.05 % to 0.25 %. The arithmetic mean value of the technical strains was taken into account. Tensile modulus of elasticity and Poisson's ratio of continuous carbon fibre SMC specimens loaded perpendicular to fibre direction were determined in the strain range of 0.05 % to 0.15 %, due to low failure strains. For all specimen types, tensile modulus of elasticity and Poisson's ratio were evaluated for all specimens which did not fail in the clamping region and if the regression coefficient r^2 was higher than 0.9. Tensile strength was evaluated for all specimens which did not fail in the clamping region. Tensile strength was defined as the maximum load sustained by the specimen before failure (R_t). Strain at tensile strength ($\varepsilon_{R,t}$) and failure strain ($\varepsilon_{max,t}$) were evaluated for all specimens which failed within the gauge section. Failure corresponded to a load drop to $0.8 \cdot F_{max}$ with F_{max} describing the preceded maximum load.

4.2.2.2 Compression tests

Compression tests were performed in a conditioned laboratory at 23 °C on a ZMART.PRO universal testing machine by ZwickRoell with a load cell capacity of 100 kN according to DIN EN ISO 14126 (1999). The machine was equipped with a hydraulic composite compression fixture (Figure 4.4a). The preload was defined according to the recommendation in DIN EN ISO 527-1 (2012) and adjusted for the different specimen types. It featured a load corresponding to 45 MPa for the continuous carbon fibre SMC loaded in fibre direction (0°) and 2 MPa for all other specimen types. The specimens for compression testing were described in section 3.2.3.2. Clamping distance was

set to 15 mm and uniaxial compression tests were carried out with a nominal crosshead displacement of 0.8 mm min^{-1} ($\dot{\varepsilon} \approx 2 \times 10^{-4}$) until fracture. Displacement of the specimen was measured with a clip-on extensometer (type MINI MFA2 Hand clamped extensometer by Mess-& Feinwerktechnik GmbH, accuracy class 0.2 according to EN ISO 9513) on both sides of the specimen (Figure 4.4a). This tool enabled control of the bending of the specimen through calculation of a bending factor (b_f) according to DIN EN ISO 14126, 1999. The compressive modulus of elasticity (E_c) was determined with a least squares method according to ASTM E111 (2010) (Equation 4.10 in section 4.5) in the strain range of 0.05 % to 0.25 % with averaged strains resulting from displacement measurement of two sides of the specimen. It was evaluated for all specimens which did not fail in the clamping region, if the regression coefficient r^2 was higher than 0.9 and the bending factor, b_f, did not exceed 0.1. Compressive strength (R_c) was evaluated, if the specimen did not fail in the clamping region and if the bending factor (b_f) was below 0.1 until fracture. Strain at compressive strength ($\varepsilon_{R,c}$) and failure strain ($\varepsilon_{max,c}$) corresponding to a force value equal to $0.8 \cdot F_{max}$ were evaluated for all discontinuous glass and continuous carbon fibre SMC specimens which failed within the gauge section. A slightly modified test setup (Figure 4.4b) enabled the capture of damage evolution and resulting strain fields. For this purpose, selected tests were run in combination with a 4M GOM ARAMIS 3D digital image correlation system featuring an adjustable base with two 4MP Teledyne Dalsa cameras with 50 mm Schneider Kreuznach objectives. Lighting was realised by two LED lights (16 W each) with polarisation filter, and thermal changes to the specimen were negligible. The digital image correlation system captured displacement fields of the front or side face of the specimen, and an OLYMPUS E-M5 Mark II 16MP digital camera with a

50 mm objective additionally captured the damage evolution of some specimens (Figure 4.4b).



(a) (b)

Figure 4.4: Compression test setup with HCCF clamping system and (a) two sided clip-on extensometer, (b) digital image correlation system and digital camera.

4.2.2.3 Bending tests

Flexural properties were determined by three-point bending tests. The methodology for bending testing of fibre reinforced polymers is detailed, for example, in ASTM D7264/D7264M (2015) and DIN EN ISO 14125 (1998). However, depending on type of reinforcement, slightly different test setups, most importantly in terms of the distance of lower supports, are recommended. Difficulties arise mainly due to possible shear effects in the material leading to a falsified flexural modulus. To accommodate these effects, preliminary tests aimed to define an appropriate test setup in terms of the distance of lower supports. In this matter, three-point bending tests were performed in a conditioned laboratory at 23 °C on a ZMART.PRO universal testing machine by ZwickRoell with a load cell capacity of 20 kN with rectangular specimens featuring a width of 15 mm. The length of the specimens varied from 15 mm to 150 mm, realising different length to thickness ratios. The distance of the lower support

was set to a nominal distance of 12 mm, 18 mm, 24 mm or 48 mm (Figure 4.5). Specimens were loaded with a constant crosshead displacement of 1 mm min^{-1} according to ASTM D7264/D7264M (2015). Three-point bending tests with a nominal distance of 96 mm and 120 mm (span-to-thickness ratio of 32:1 and 40:1) were carried out with a loading speed to achieve a nominal strain rate $\dot{\varepsilon} = 0.01\,min^{-1}$ at the lower surface of the specimen according to DIN EN ISO 14125 (1998). Table 4.1 lists the different test setups and testing parameters considered for three-point bending tests. Every specimen was preloaded with 2 MPa. Deflection was measured with a laser measurement system type opto NCDT 2300 by MICRO-EPSILON.

Table 4.1: Three-point bending test parameters.

Nom. distance of lower supports	Diameter of lower supports	Diameter of loading nose	Loading speed
12 mm	4 mm	7.5 mm	1 mm min^{-1}
16 mm	4 mm	7.5 mm	1 mm min^{-1}
24 mm	4 mm	7.5 mm	1 mm min^{-1}
48 mm	4 mm	7.5 mm	1 mm min^{-1}
96 mm	10 mm	7.5 mm	5.12 mm min^{-1}
120 mm	10 mm	7.5 mm	8 mm min^{-1}

Maximum strain at the outer surface (ε_f) and stress at the outer surface (σ_f) were determined according to ASTM D7264/D7264M (2015) and DIN EN ISO 14125, 1998.

Stress (σ_f) and strain (ε_f) are equal to

$$\sigma_f = \frac{3FL}{2bh^2} \tag{4.1}$$

and

$$\varepsilon_f = \frac{6sh}{L^2} \tag{4.2}$$

with the applied force F, support span L, mid-span deflection s, thickness h and width b of the specimen. However, Equation 4.1 and Equation 4.2 are valid only for small deflections. If maximum deflection exceeds $0.1 \cdot L$, DIN EN ISO 14125, 1998 recommends to calculate flexural stresses and strains according to

$$\sigma_f = \frac{3FL}{2bh^2} \left\{ 1 + 6 \left(\frac{s}{L} \right)^2 - 3 \left(\frac{sh}{L^2} \right) \right\} \tag{4.3}$$

and

$$\varepsilon_f = \frac{h}{L} \left\{ 6 \left(\frac{s}{L} \right) - 24.37 \left(\frac{s}{L} \right)^3 + 62.17 \left(\frac{s}{L} \right)^5 \right\}. \tag{4.4}$$

Flexural modulus of elasticity (E_f) was determined with a least squares method according to ASTM E111 (2010) in the strain range of 0.05 % to 0.25 % (according to Equation 4.10). Strain at flexural strength ($\varepsilon_{R,f}$) and flexural failure strain ($\varepsilon_{max,f}$), defined as the resulting strain corresponding to the point in stress-strain evolution at which load has dropped to a $0.8 \cdot F_{max}$ were also evaluated.

Additionally, damage evolution was captured for a number of selected specimens with an OLYMPUS E-M5 Mark II 16MP digital camera with a 50 mm objective. All specimens were mechanically loaded with the same side up with respect to placement of the semi-finished sheet in the mould.



Figure 4.5: Three-point bending test setup combined with DIC (a) or OLYMPUS-M5 Mark E (b).

4.3 Characterisation at the structure level

4.3.1 Quasi-static puncture testing

Quasi-static puncture tests were performed in the deformable bodies laboratory at the University of Windsor, Canada, on an MTS Criterion Model 45 electromechanical load frame. A lubricated (PC Waylube 68) hemispherical striker, having a diameter of 20 mm, punctured the rectangular test specimen perpendicular to its surface with a nominally uniform velocity of 2.6 mm min^{-1} (approx. 4.4×10^{-5} m s^{-1}) up to a defined maximum deflection of 16 mm. A custom-made fixture allowed for mechanical clamping of the flat, square specimen under a metallic plate to provide a circular puncture area with a diameter of 100 mm (Figure 4.6). The resulting force was recorded by a load cell with a capacity of 150 kN. Displacement between the striker and the specimen support, starting from first contact between the striker and the test specimen, was measured by the crosshead displacement of the MTS load frame. The test rig was designed such that a front-surface mirror allowed for video capturing during the

test to track damage evolution. For this purpose, a Point Grey Research Grasshopper GRAS-50S5M 5.0 MP monochrome camera with 35 mm CM120 Schneider-Kreuznach lens was placed at one side of the fixture underneath the specimen. One frame per second was captured throughout the quasi-static loading up to the maximum displacement. An external light source and an inclined mirror beneath the specimen ensured sufficient illumination (LED light, type Source 4 WRD by Electronic Theatre Controls, Inc. with 155 W). Synchronisation between the load frame and camera was established with the Correlated Solutions VIC-Snap transistor-to-transistor logic interface and a signal from the load frame at a user defined digital output connected to a National Instruments USB 6221 BNC data acquisition device.

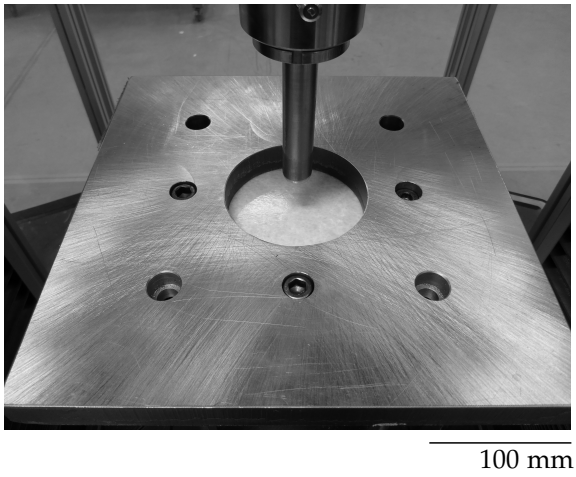


Figure 4.6: Test setup of quasi-static puncture testing.

4.3.2 Dynamic puncture testing

Low-velocity impact tests, in the following named dynamic puncture tests, were conducted at the University of Windsor, Canada. Tests were carried out with a custom drop tower modified to carry out instrumented impact tests according to EN ISO 6603-2 (2000) (Figure 4.7).



Figure 4.7: Drop tower to carry out dynamic puncture tests at the University of Windsor, Canada.

The impacting unit featured a weight of 61 kg and consisted of three different parts, namely the crosshead, a shaft including the load cell and a hemispherical tip with a diameter of 20 mm. During the test, the drop weight was released at a defined height and traversed down guide rails to impact the specimen at its centre, perpendicular to the surface, at a nominal uniform velocity of 4.4 ± 0.2 m s^{-1}. The flat, square specimens were mechanically clamped under a metal plate to provide a circular impact area with a diameter of 100 mm, consistent

to the quasi-static puncture testing and shown on Figure 4.6. The test rig was designed such that an inclined front-surface mirror allowed for high-speed photography with a Photron SA4 camera placed on the floor in front of the drop tower. The lighting system used was a series of two ARRI halogen lights (1000 W). To avoid heating of the specimen, lights were turned on only during the impacting event. The displacement of the crosshead and force were measured with an Acuity laser displacement transducer with a sensitivity of 30 mm V^{-1} and a Dytran Model 1050 Integrated Electronic Piezoelectric load cell, respectively. The load cell featured a sensitivity of 1.04 mV/lbf (0.234 mV N^{-1}) and was integrated in the shaft of the striker to ensure a measurement of the impact load very close to the location of contact between the nose and SMC specimen. A custom LabVIEW program was developed to acquire force and displacement data, appropriately trigger the high-speed camera and synchronise transducer data acquisition with the high-speed photograph acquisition. Force data was acquired at 50 kHz with a 24 bit resolution National Instrument 9233 Integrated Electronic Piezoelectric load cell data acquisition module in a National Instrument CompactDAQ chassis. Displacement data was acquired at 50 kHz with a 16 bit NI 9205 analogue input module. A transistor-to-transistor logic signal from a NI 9401 digital input-output module allowed for triggering and synchronisation of the captured high-speed images for a total duration of 10 ms. A four pole Butterworth filter (two pole filter with forward and reverse passes) was applied to the load-time data with a channel frequency class of 600 (approximately 1000 Hz cutoff) consistent with Society of Automotive Engineers (SAE) standard SAE J211-1 (1995). For the discontinuous glass and hybrid continuous-discontinuous glass/carbon fibre SMC specimens, images were captured with a frame rate of 50 000 frames per second, a shutter speed of 1/70 000 s and a resolution of 320×192 pixels^2. For the continuous carbon fibre SMC

parameters of image acquisition were 20 000 frames per second with a shutter speed of 1/50 000 s and a resolution of 256×256 pixels^2.

4.4 Characterisation at the component level

Component testing was performed on a ZwickRoell Universal testing machine with 500 kN load capacity. As shown in Figure 4.8, the demonstrator part was placed on two lower supports, aligned at a distance of 120 mm. The supports themselves were mounted on a cage to be able to measure the deflection directly below the sample with a tactile transducer.

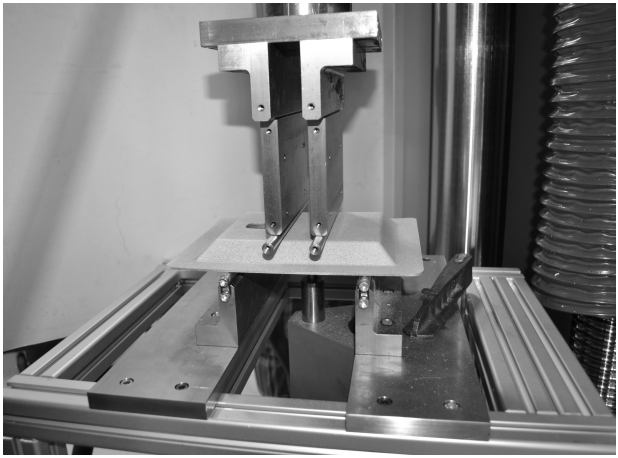


Figure 4.8: Test setup of four-point bending component tests.

The specimens were loaded by two upper supports, having a distance of 40 mm. As a first step, a preload of 100 N was realised to ensure contact between the specimen and the upper supports. Subsequently, the four-point bending test was carried out with numerous loading-unloading cycles with a constant nominal crosshead speed of

$2\,\mathrm{mm\,m^{-1}}$. Each cycle consisted of a maximum deflection (Table 4.2) and four subsequent sub-cycles with a deflection equal to 30 % to 70 % of the preceded maximum value.

Table 4.2: Cycle number and corresponding maximum deflection of four-point bending component tests.

Cycle	1	2	3	4	5	6	7	8
Max. deflection in mm	0.5	1	1.5	2	2.5	3	4	5

Between different loading sequences, a load of 100 N was maintained for 90 s. After eight loading sequences, the deflection was increased until the specimen fractured (Figure 4.9).

The global stiffness S of the specimen was calculated from the load F and the deflection s. It reads

$$S = \frac{F_{max,i} - F_{min,i}}{s_{max,i} - s_{min,i}} \quad \text{with} \quad i \in \{1,2,3\} \tag{4.5}$$

with s_{min} and s_{max} referring to the maximum and minimum deflection reached within the 30 % to 70 % cycle after the preceded maximum deflection of the cycle. F_{min} and F_{max} were the corresponding forces at these points. The stiffness was calculated over the unloading phases and the arithmetic mean value of the three calculated stiffness values considered for one cycle was evaluated.

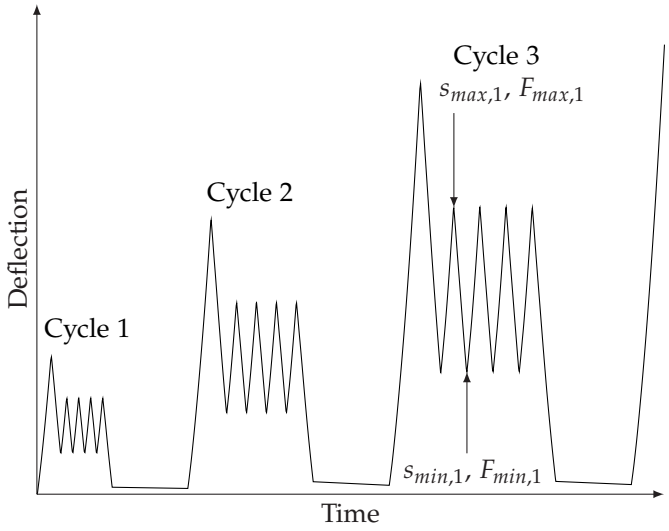


Figure 4.9: Test procedure of cyclic four-point bending component tests, adapted from Rösner, 2015.

A damage variable, D, is a suitable tool to describe the degradation of mechanical performance and evolution of damage (Gross and Seelig, 2011; Krajcinovic, 1998; Krajcinovic and Mastilovic, 1995), with D equal to

$$D = 1 - \frac{S}{S_0} \quad \text{with} \quad D \in [0, 1]\,. \tag{4.6}$$

The stiffness of the first cycle was defined as S_0. For a value of D equal to zero, the structure shows no damage ($S = S_0$). If D is equal to 1, the structure would be fully damaged with a resulting stiffness of $S = 0$.

4.5 Data evaluation

Raw data of experimental characterisation was processed with Matlab, Version 2017b and 2018a. To compare and characterise mechanical and structural properties, the average value, standard deviation and coefficient of variation have been taken into account.

The arithmetic average ($\bar{x}$) of a property (x) equals

$$\bar{x} = \frac{1}{n}\left(\sum_{i=1}^{n} x_i\right) \tag{4.7}$$

with n individual values. In addition, standard deviation μ reads

$$\mu = \sqrt{\left(\sum_{i=1}^{n} x_i^2 - n\bar{x}^2\right) \cdot (n-1)^{-1}}. \tag{4.8}$$

A third statistical value, the coefficient of variation (CV) enables the determination of a variation in percentage of a distinct property.

$$\mathrm{CV} = 100 \cdot \frac{\mu}{\bar{x}}. \tag{4.9}$$

Moduli of elasticity, stiffness, respectively, were defined by fitting according to the method of least squares with n σ - ε data pairs, following

$$E = \left(\sum_{i=1}^{n} (\sigma_i \varepsilon_i) - n\bar{\sigma}\bar{\varepsilon}\right) \cdot \left(\sum_{i=1}^{n} \sigma_i^2 - n\bar{\sigma}^2\right). \tag{4.10}$$

The same fitting method, based on $F - d$ data pairs, was considered to evaluate puncture stiffness.

5 Analytical modelling

This chapter introduces a modelling approach to analytically describe mechanical properties of hybrid SMC composites. It starts with a short summary to derive mechanical properties of a discontinuously or continuously reinforced lamina based on homogenisation. A next step considers the macromechanical properties of the laminae which may finally be combined to a laminate. The mechanical properties of the laminate can be deduced by the classical laminate theory (CLT) which is briefly introduced. Lastly, methods to estimate the resulting stiffness of hybrid laminates are presented.

5.1 Description of modelling approach

The interest in hybrid composites increases demand to define modelling strategies for these complex composite materials. The most important property to consider for structural applications is the stiffness of a material. In the following section, methods to analytically predict the tensile and flexural modulus of elasticity of hybrid materials are presented, applicable to hybrid SMC composites.

Composite materials are in general neither isotropic nor homogeneous, so analysis and design of such materials differ from that of conventional, bulk materials. Different modelling strategies applied to brittle composites, such as SMC, were introduced, based on micromechanics (Chen and Tucker, 1984; Jendli et al., 2009) or finite

element approaches (Chen et al., 2017). Most composite materials are multiscale in nature (Kanouté et al., 2009) and in material science, micromechanical approaches are powerful tools to predict the different macroscopic properties of a composite material (Desrumaux et al., 2001; Tucker and Liang, 1999). Micromechanical approaches and homogenisation methods, which consider the properties of the individual constituents and thus fibre and matrix, enable prediction of the properties of a composite, which can then be described as a homogenised material.

5.2 Micromechanics and homogenisation methods

5.2.1 Fundamentals of homogenisation

Although a composite may consist of homogeneous isotropic fibres and an isotropic homogeneous matrix material, the resulting mechanical properties are not necessarily homogeneous or isotropic. For this reason, the description of macromechanical properties is normally founded on homogenisation methods that derive macroscopic material properties of a fibre reinforced polymer with microstructural information. Homogenisation methods approximate effective properties of a multiphase material to represent a heterogeneous material through an equivalent homogeneous continuum.

In the following, the fibres are assumed to be homogeneous, linear-elastic and isotropic with a circular cross section. In addition, the matrix is considered to be isotropic, ideal-elastic or ideal-plastic, and the interface between fibres and matrix is infinitely thin. A separation of scales is important to apply homogenisation schemes (Gross and

Seelig, 2011; Ju and Chen, 1994; Zaoui, 2002). The effective stresses $\bar{\sigma}$ and strains $\bar{\varepsilon}$, which act on a continuum, are described as the volume-averaged $\langle\cdot\rangle$ arithmetic mean values of the (local) microscopic stress $\sigma(x)$ and strain $\varepsilon(x)$ to deduce homogenised properties (Hill, 1963, 1965; Walpole, 1969)

$$\bar{\sigma} = \langle\sigma(x)\rangle = \frac{1}{V}\int_V \sigma(x)dV \tag{5.1}$$

and

$$\bar{\varepsilon} = \langle\varepsilon(x)\rangle = \frac{1}{V}\int_V \varepsilon(x)dV. \tag{5.2}$$

Considering a microstructure with piecewise constant properties, the total volume V can be divided in α partial volumes. Subsequently, V_α is the partial volume for phase α. Accounting for the phase volume fraction ϕ of a phase α with $\phi_\alpha = V_\alpha/V$, the effective stresses and strains equal

$$\bar{\sigma} = \langle\sigma(x)\rangle = \frac{1}{V}\sum_{\alpha=1}^{n}\int_{V\alpha}\sigma(x)dV = \sum_{\alpha=1}^{n}\phi_\alpha\langle\sigma\rangle_\alpha \tag{5.3}$$

and

$$\bar{\varepsilon} = \langle\varepsilon(x)\rangle = \frac{1}{V}\sum_{\alpha=1}^{n}\int_{V\alpha}\varepsilon(x)dV = \sum_{\alpha=1}^{n}\phi_\alpha\langle\varepsilon\rangle_\alpha. \tag{5.4}$$

Assuming that the material is a continuum without gaps or voids and that the local and effective material properties can be described as hyperelastic, the generalised Hooke's law of a composite material reads

$$\bar{\sigma} = \bar{\mathbb{C}}[\bar{\varepsilon}] = \langle\mathbb{C}(x)[\varepsilon(x)]\rangle \tag{5.5}$$

and

$$\bar{\varepsilon} = \bar{\mathbb{S}}[\bar{\sigma}] = \langle\mathbb{S}(x)[\sigma(x)]\rangle, \tag{5.6}$$

with $\mathbb{C}$ the stiffness tensor and $\mathbb{S}$ the compliance tensor ($\mathbb{C}^{-1} = \mathbb{S}$ and $\bar{\mathbb{C}}^{-1} = \bar{\mathbb{S}}$). The local stresses and strains can furthermore be defined with localisation tensors of strain, $\mathbb{L}_A$, and stress, $\mathbb{L}_B$, such that

$$\boldsymbol{\varepsilon}(\boldsymbol{x}) = \mathbb{L}_A(\boldsymbol{x})[\bar{\boldsymbol{\varepsilon}}] \tag{5.7}$$

and

$$\boldsymbol{\sigma}(\boldsymbol{x}) = \mathbb{L}_B(\boldsymbol{x})[\bar{\boldsymbol{\sigma}}]. \tag{5.8}$$

For $\mathbb{L}_A$ and $\mathbb{L}_B$ holds

$$\langle \mathbb{L}_A(\boldsymbol{x}) \rangle = \sum_{\alpha=1}^{n} \phi_\alpha \mathbb{L}_{A_\alpha}(\boldsymbol{x}) = \mathbb{I}^S \tag{5.9}$$

and

$$\langle \mathbb{L}_B(\boldsymbol{x}) \rangle = \sum_{\alpha=1}^{n} \phi_\alpha \mathbb{L}_{B_\alpha}(\boldsymbol{x}) = \mathbb{I}^S, \tag{5.10}$$

with $\mathbb{I}^S$ denoting the symmetric identity of the fourth order. Considering the definition of effective stresses

$$\bar{\boldsymbol{\sigma}} = \bar{\mathbb{C}}[\bar{\boldsymbol{\varepsilon}}] = \langle \mathbb{C}(\boldsymbol{x}) \mathbb{L}_A(\boldsymbol{x}) \rangle [\bar{\boldsymbol{\varepsilon}}] \tag{5.11}$$

and strains

$$\bar{\boldsymbol{\varepsilon}} = \bar{\mathbb{S}}[\bar{\boldsymbol{\sigma}}] = \langle \mathbb{S}(\boldsymbol{x}) \mathbb{L}_B(\boldsymbol{x}) \rangle [\bar{\boldsymbol{\sigma}}], \tag{5.12}$$

the effective stiffness and compliance tensors ($\bar{\mathbb{C}}$ and $\bar{\mathbb{S}}$) read

$$\bar{\mathbb{C}} = \langle \mathbb{C}(\boldsymbol{x}) \mathbb{L}_A(\boldsymbol{x}) \rangle \tag{5.13}$$

and

$$\bar{\mathbb{S}} = \langle \mathbb{S}(\mathbf{x}) \mathbb{L}_B(\mathbf{x}) \rangle. \tag{5.14}$$

Estimates for $\bar{\mathbb{C}}$ and $\bar{\mathbb{S}}$ can be obtained with appropriate localisation tensors $\mathbb{L}_A$ and $\mathbb{L}_B$ (Zaoui, 2002). For a composite material, which

consists of n fibres embedded in a (polymer) matrix, the effective stiffness is determined, assuming that the material properties are isotropic and piecewise constant, by

$$\bar{\mathbb{C}} = \mathbb{C}_M + \sum_{\alpha=1}^{n} \phi_\alpha (\mathbb{C}_\alpha - \mathbb{C}_M) \mathbb{L}_{A_\alpha}, \tag{5.15}$$

with M referring to matrix properties, and $\alpha = 1, ..., n$ representing the fibres. If one assumes equal material properties for all fibres ($\mathbb{C}_\alpha = \mathbb{C}_F$), Equation 5.15 reads

$$\bar{\mathbb{C}} = \mathbb{C}_M + (\mathbb{C}_F - \mathbb{C}_M) \langle \mathbb{L}_A \rangle_F \tag{5.16}$$

with $\langle \cdot \rangle_F$ as the sum over all fibres. By substitution of the localisation tensors $\mathbb{L}_A$ and $\mathbb{L}_B$ with the identity tensor $\mathbb{I}^S$, one obtains the rule of mixtures (RoM). It assumes that strains are equal in all phases of the material for a load in fibre direction (Voigt, 1887). For a loading perpendicular to fibres, equal stresses in all phases are assumed (Reuss, 1929). These two basic assumptions form an upper and lower bound to estimate effective properties of a multiphase material. A method to define closer bonds was proposed by Hashin and Shtrikman (1962).

Eshelby proposed the solution of a single inclusion problem to consider the morphology of the material's microstructure in a more detailed way (Eshelby, 1957, 1959). This approach considers reinforcing fibres as ellipsoid inclusions, with the Eshelby tensor describing the uniform stress and strain field within the inclusion. An extension of the Eshelby approach was presented by Mori and Tanaka (1973) and Benveniste and Dvorak (1990), commonly used due to its simple and explicit formulation. For a more detailed review of homogenisation methods, see Zaoui (2002) or Kanouté et al. (2009).

5.2.2 Analytical modelling of fibre reinforced polymers

5.2.2.1 Tensile modulus of a continuous fibre reinforced polymer loaded in fibre direction

The effective properties of a continuous (unidirectional) composite base on the properties of the fibres (E_F, ν_F) and the matrix (E_M, ν_M) as well as on the volume fractions of the different individual phases. For any number of different constituents in a composite material, the sum of the constituent volume fraction must be equal to 1 (Gibson, 2007). By means of thermogravimetric analysis, the fibre weight content (ψ_F) of a specimen, can be determined by burning off the matrix of a specimen and by measuring the mass of the fibres, m_F, remaining in the crucible, divided by the initial mass of the specimen (composite), m_C and

$$\psi_F = \frac{m_F}{m_C}. \tag{5.17}$$

The resulting fibre volume content, ϕ_F, is then equal to

$$\phi_F = \frac{1}{(1 + \frac{1-\psi_F}{\psi_F}) \cdot \frac{\rho_F}{\rho_M}}, \tag{5.18}$$

with ρ_F and ρ_M as the density of the fibre and the matrix, respectively (Schürmann, 2007).

A continuous (unidirectional) fibre reinforced lamina, with length l, width b and thickness h, as shown in Figure 5.1, is characterised by two symmetry planes parallel and transverse to the fibre direction (transverse isotropy). In the following description, coordinate axis 1 is parallel to the fibrous reinforcement. A micromechanics approach may determine the engineering constants of a continuous fibre

reinforced lamina (Reddy, 2003; Soni and Pagano, 1983) if the fibres are

- homogeneous,
- linear elastic and obey the Hooke's law,
- isotropic (e.g. glass fibre, with $E_{F,L} = E_{F,T} = E_F$) or orthotropic (e.g. carbon fibre $E_{F,L} \neq E_{F,T} \neq E_F$),
- homogeneously distributed,
- perfectly aligned and parallel, and
- perfectly bonded to the matrix;

if the matrix is

- homogeneous,
- linear elastic and obeys the Hooke's law,
- isotropic, and
- free of voids and microcracks; and

if the lamina is

- initially stress-free,
- linear elastic, and
- macroscopically homogeneous and transverse isotropic.

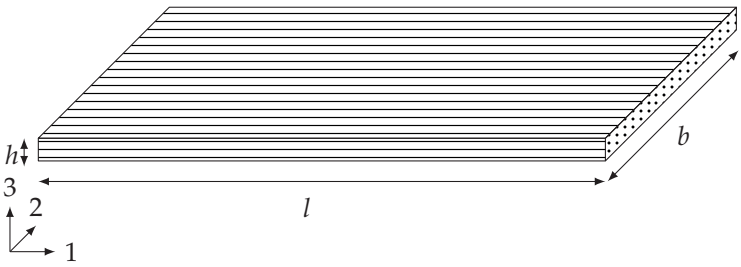


Figure 5.1: Schematic drawing of a continuously fibre reinforced lamina.

Considering a strain in fibre direction (ε_1) with both phases behaving elastically, and assuming that equal strains apply in fibres and matrix, the corresponding stresses in the matrix σ_M and the fibres σ_F are

$$\sigma_F = E_F \cdot \varepsilon_1 \qquad \text{and} \qquad \sigma_M = E_M \cdot \varepsilon_1. \tag{5.19}$$

Following this, the resultant force (F) on the surface of the representative volume element is equal to

$$F = \sigma_1 \cdot A = \sigma_F \cdot A_F + \sigma_M \cdot A_M = E_1 \cdot \varepsilon_1 \cdot A. \tag{5.20}$$

With the volume fractions of fibres ϕ_F and matrix ϕ_M equal to

$$\phi_F = \frac{A_F}{A} \qquad \text{and} \qquad \phi_M = \frac{A_M}{A}, \tag{5.21}$$

the longitudinal elastic modulus of the composite in fibre direction (E_1) is

$$E_1 = \phi_F \cdot E_{F,L} + (1 - \phi_F) \cdot E_M, \tag{5.22}$$

with the longitudinal modulus of the fibres $E_{F,L}$. Equation 5.22 is known as the rule of mixtures (RoM) and describes the Voigt bound.

5.2.2.2 Tensile and shear modulus of a discontinuous fibre reinforced polymer

Elastic properties of a discontinuous fibre reinforced polymer can also be derived by homogenisation methods (Tucker and Liang, 1999), considering the geometry of the fibrous reinforcement and fibre orientation. First of all, a generalised rule of mixtures (RoM) with the tensile modulus of elasticity E equal to

$$E = \gamma_1 \cdot \gamma_2 \cdot \phi_F \cdot E_F + (1 - \phi_F) \cdot E_M \tag{5.23}$$

enables one to predict the tensile modulus of elasticity of a discontinuous fibre reinforced composite. In Equation 5.23, γ_1 is a correction factor to account for the fibre length, and $\gamma_1 = 1$ for fibres with a minimum length of 10 mm. The second correction factor, γ_2, takes fibre orientation into account and equals 0.375 in the case of a random (in-plane) fibre orientation (Piggott, 1980; Watanabe and Yasuda, 1982).

A semi-empirical approach that is based on the Halpin–Tsai equations (Halpin, 1969), also enables one to estimate the elastic constants of a discontinuous fibre reinforced composite. The modulus of elasticity and the shear modulus of a discontinuous fibre reinforced polymer (E_C and G_C) with a two-dimensional (2D) random fibre orientation read (Lavengood and Goettler, 1971)

$$E_C = \frac{3}{8}E_1 + \frac{5}{8}E_2 \tag{5.24}$$

and

$$G_C = \frac{1}{8}E_1 + \frac{1}{4}E_2. \tag{5.25}$$

According to Affdl and Kardos (1976) and Hahn and Tsai (1980), E_1 and E_2 in Equation 5.24 and 5.25 are equal to

$$\frac{E_1}{E_M} = \frac{(1 + 2 \cdot (l/d)\eta_L \phi_f)}{(1 - \eta_L \phi_F)} \tag{5.26}$$

and

$$\frac{E_2}{E_M} = \frac{(1 + 2\eta_T \phi_F)}{(1 - \eta_T \phi_F)}, \tag{5.27}$$

with l/d the fibre aspect ratio,

$$\eta_L = \frac{E_F/E_M - 1}{(E_F/E_M + 2 \cdot (l/d))} \tag{5.28}$$

and

$$\eta_T = \frac{E_F/(E_M - 1)}{(E_F/E_M + 2)}. \tag{5.29}$$

Although semi-empirical approaches are easy to solve analytically, the fibre orientation of a discontinuous fibre reinforced polymer is important to consider to more precisely determine elastic material properties (Fu et al., 2002; Halpin and Pagano, 1969). Generally, the Mori–Tanaka approach is a suitable tool to predict the material properties of discontinuous fibre reinforced polymers considering fibre orientation (Brylka, 2017; Desrumaux et al., 2001).

Information about fibre orientation distribution can be stored efficiently in the form of fibre orientation tensors (FOTs) (Advani and Tucker, 1978; Kanatani, 1984), and the Mori–Tanaka homogenisation method determines the effective stiffness $\bar{\mathbb{C}}^{MT}$ of a composite with a localisation tensor $\mathbb{L}_{\alpha}^{MT}$ (Benveniste, 1987; Castañeda and Suquet, 1997; Mori and Tanaka, 1973) premised on orientation averages.

Fibre orientation tensors of second- and fourth-order ($\mathbf{O}$ and $\mathbb{O}$) equal

$$O_{ij} = \oint_S n_i n_j \phi(\mathbf{n}) dS \tag{5.30}$$

and

$$O_{ijkl} = \oint_S n_i n_j n_k n_l \phi(\mathbf{n}) dS. \tag{5.31}$$

Computed tomography offers discrete local fibre orientation in every fibre voxel. Thus, the empirical second- and fourth-order FOTs read

$$\mathbf{O} = \frac{1}{N_v} \sum_{\alpha=1}^{N_v} \mathbf{n}_\alpha \otimes \mathbf{n}_\alpha \tag{5.32}$$

and

$$\mathbb{O} = \frac{1}{N_v} \sum_{\alpha=1}^{N_v} \mathbf{n}_\alpha \otimes \mathbf{n}_\alpha \otimes \mathbf{n}_\alpha \otimes \mathbf{n}_\alpha, \tag{5.33}$$

with N_v fibre voxels and $\mathbf{n}$ representing the direction of the fibre axis. Based on the orientation tensors of second- and fourth-order, the Mori–Tanaka homogenisation method with orientation averages provides precise results of the anisotropic stiffness of SMC components (Oldenbo et al., 2004).

5.3 Classical laminate theory

Classical laminate theory (CLT) enables one to virtually combine different laminae with homogenised properties into a laminate (Reddy, 2003) and to define the resulting macromechanical properties. The hybrid SMC material considered within this study can be defined as an interply hybrid laminate, and the CLT is a suitable method to predict the resulting mechanical properties.

5.3.1 Macromechanical characterisation of a lamina

In the following, a lamina (Figure 5.2) is a sheet of a composite, which contains continuous or discontinuous fibres embedded in a polymer matrix.

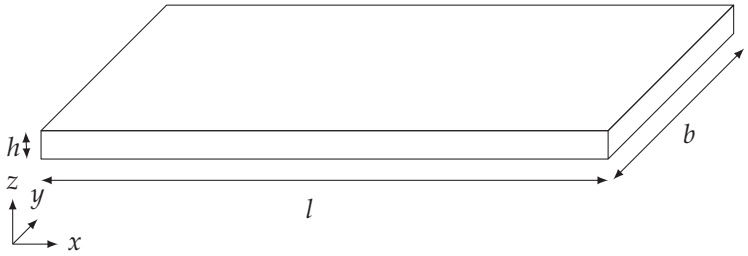


Figure 5.2: Schematic drawing of a lamina.

Assuming a linear elastic behaviour of the lamina, the generalised Hooke's law is valid to relate applied stresses (σ_i) to resulting strains (ε_j). Considering an anisotropic material under isothermal conditions with respect to an orthogonal Cartesian coordinate system, the stress (σ_i) equals

$$\sigma_i = C_{ij}\varepsilon_j \qquad i, j = 1, ..., 6, \tag{5.34}$$

with the stress components σ_i and the strain components ε_j. The stiffness tensor, C_{ij}, is a fourth-rank tensor, which represents the material constants. The number of independent constants depends on material symmetry.

5.3.2 Macromechanical characterisation of a laminate

The classical laminate theory (CLT) can be applied to predict the properties of a laminate considering normal, bending or torsional

stresses in a plane-state loading condition (Jones, 1999), if the following assumptions hold true (Mittelstedt and Becker, 2017):

- the thickness (h) of the laminate is significantly smaller than the length (l) and width (b) of the laminate ($h << l, b$) and remains constant during loading,
- the different laminae are perfectly bonded,
- the laminate is initially undamaged (no voids, delamination, etc. are present),
- the laminate is loaded in plane-stress condition ($\sigma_z = \tau_{xz} = \tau_{yz} = \gamma_{xz} = \gamma_{yz} = 0$), and
- the laminate deforms according to the Kirchhoff assumptions for bending of thin plates and a normal to the mid-plane remains straight and normal to the mid-plane.

Deformation of a laminate (in terms of $\varepsilon_{xx}, \varepsilon_{yy}$ and γ_{xy}) is described by the the mid-plane strains $\varepsilon^0_{xx}, \varepsilon^0_{yy}$ and γ^0_{xy} (elongation and distortion) as well as the mid-plane curvatures $\kappa^0_{xx}, \kappa^0_{yy}$ and κ^0_{xy} (bending curvature and torsion) with

$$\begin{pmatrix} \varepsilon_{xx}(x,y,z) \\ \varepsilon_{yy}(x,y,z) \\ \gamma_{xy}(x,y,z) \end{pmatrix} = \begin{pmatrix} \varepsilon^0_{xx}(x,y) \\ \varepsilon^0_{yy}(x,y) \\ \gamma^0_{xy}(x,y) \end{pmatrix} + z \begin{pmatrix} \kappa^0_{xx}(x,y) \\ \kappa^0_{yy}(x,y) \\ \kappa^0_{xy}(x,y) \end{pmatrix}. \tag{5.35}$$

With the reduced stiffness matrix Q_{ij}, the stresses σ_{xx}, σ_{yy} and τ_{xy} within the k^{th}-layer can be expressed as

$$\begin{pmatrix} \sigma_{xx} \\ \sigma_{yy} \\ \tau_{xy} \end{pmatrix}_k = \begin{bmatrix} Q_{11} & Q_{12} & Q_{16} \\ Q_{12} & Q_{22} & Q_{26} \\ Q_{16} & Q_{26} & Q_{66} \end{bmatrix}_k \left[\begin{pmatrix} \varepsilon^0_{xx} \\ \varepsilon^0_{yy} \\ \gamma^0_{xy} \end{pmatrix} + z \begin{pmatrix} \kappa^0_{xx} \\ \kappa^0_{yy} \\ \kappa^0_{xy} \end{pmatrix} \right]. \tag{5.36}$$

Resultant forces, **N**, and moments, **M**, in the mid-plane of the laminate (Figure 5.3) are equal to

$$\begin{pmatrix} N^0_{xx} \\ N^0_{yy} \\ N^0_{zz} \end{pmatrix} = \int_{-\frac{h}{2}}^{\frac{h}{2}} \begin{pmatrix} \sigma_{xx} \\ \sigma_{yy} \\ \tau_{xy} \end{pmatrix} dz \tag{5.37}$$

and

$$\begin{pmatrix} M^0_{xx} \\ M^0_{yy} \\ M^0_{xy} \end{pmatrix} = \int_{-\frac{h}{2}}^{\frac{h}{2}} \begin{pmatrix} \sigma_{xx} \\ \sigma_{yy} \\ \tau_{xy} \end{pmatrix} z dz. \tag{5.38}$$

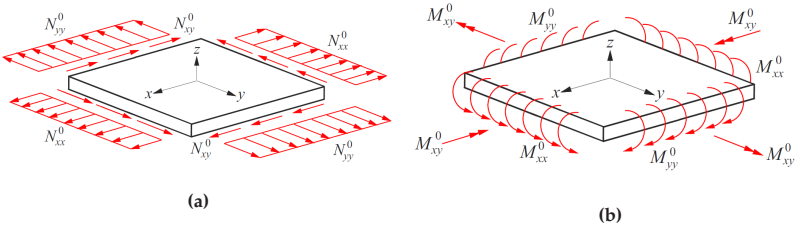


Figure 5.3: Resultant forces (a) and moments (b) acting on a laminate (Mittelstedt and Becker, 2017).

In a subsequent step, the extensional stiffness (A_{ij}), the bending-extension coupling stiffness (B_{ij}) and the bending stiffness (D_{ij}), assuming constant properties within one layer, can be determined for a layer k. N defines the total number of layers (Figure 5.4), z_k represents the vertical distance of layer k from the mid-plane, and A_{ij}, B_{ij} and D_{ij} equal

$$A_{ij} = \sum_{k=1}^{N} Q_{ij}^{k}(z_k - z_{k-1}) \tag{5.39}$$

$$B_{ij} = \frac{1}{2}\sum_{k=1}^{N} Q_{ij}^{k}(z_k^2 - z_{k-1}^2) \tag{5.40}$$

$$D_{ij} = \frac{1}{3}\sum_{k=1}^{N} Q_{ij}^{k}(z_k^3 - z_{k-1}^3). \tag{5.41}$$

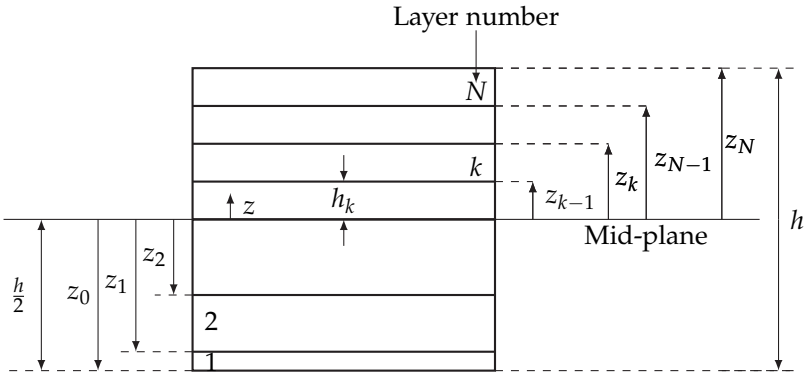


Figure 5.4: Section through a laminate and nomenclature.

The [ABD] matrix (stiffness matrix) of the laminate leads to the constitutive equation in symbolic form considering forces ($\underline{N}$) and moments ($\underline{M}$) acting on the laminate and

$$\begin{pmatrix} \underline{N}^0 \\ \underline{M}^0 \end{pmatrix} = \begin{bmatrix} \underline{\underline{A}} & \underline{\underline{B}} \\ \underline{\underline{B}} & \underline{\underline{D}} \end{bmatrix} \begin{pmatrix} \underline{\varepsilon}^0 \\ \underline{\kappa}^0 \end{pmatrix}. \tag{5.42}$$

Taking the flexibility matrix [abd] (with $[abd]^{-1} = [ABD]$) into consideration, the constitutive equation equals

$$\begin{pmatrix} \underline{\varepsilon}^0 \\ \underline{\kappa}^0 \end{pmatrix} = \begin{bmatrix} \underline{\underline{a}} & \underline{\underline{b}} \\ \underline{\underline{b}} & \underline{\underline{d}} \end{bmatrix} \begin{pmatrix} \underline{N}^0 \\ \underline{M}^0 \end{pmatrix}, \tag{5.43}$$

and forces as well as moments acting on a laminate can be related to deformation.

5.4 Analytical modelling of hybrid composites

In the following, approaches to predict the mechanical properties of an interlayer hybrid composite, based on two different composite materials (further referred to as components) are presented. The laminate consists of continuously (unidirectional) fibre reinforced face sheets and a discontinuously reinforced core, and it is schematically depicted in Figure 5.5.

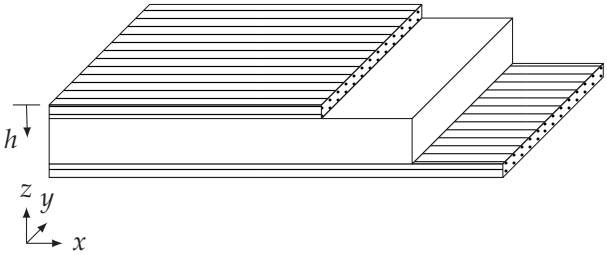


Figure 5.5: Schematic drawing of continuous-discontinuous glass/carbon fibre SMC laminate, with $x-, y-$ and $z-$axes referring to the global coordinate system of the laminate.

5.4.1 Rule of hybrid mixtures

In general, the stiffness of a hybrid material can be described by a rule of hybrid mixtures (RohM) which reads

$$P_{hyb} = P_{C1}\phi_{C1} + P_{C2}\phi_{C2}, \tag{5.44}$$

with the property of the hybrid material (P_{hyb}), the property of the first and the second component (P_{C1} and P_{C2}), and the corresponding volume fractions (ϕ_{C1} and ϕ_{C2}) (Trauth and Weidenmann, 2018). Equation 5.44 was successfully implemented to predict the tensile modulus of elasticity of hybrid composites based on randomly oriented (Fu et al., 2001; Mansor et al., 2013) or aligned short fibre composites (Henry and Pimenta, 2017a,b) as well as hybrid particle/short fibre polymer composites (Fu et al., 2002). In addition, this approach was already successfully applied for a combination of chopped carbon fibres SMC materials with unidirectional prepregs (Corbridge et al., 2017) and is hence a promising analytical tool to estimate the elastic properties of hybrid SMC laminates.

5.4.2 Tensile and flexural modulus based on classical laminate theory

Another possible approach relies upon the classical laminate theory (CLT). Combining Equations 5.34 and 5.42, with consideration of a uniform width of the laminate, the tensile moduli of elasticity in x- and y-direction of a laminate equal

$$E_{xx} = \frac{1}{a_{11} \cdot h} \tag{5.45}$$

and

$$E_{yy} = \frac{1}{a_{22} \cdot h} \tag{5.46}$$

with a_{11} and a_{22} components of the $[abd]$ matrix and h the thickness of the laminate.

Furthermore, the constitutive relation to describe the bending of a laminate reads

$$\begin{pmatrix} M_{xx} \\ M_{yy} \\ M_{xy} \end{pmatrix} = \begin{bmatrix} D_{11} & D_{12} & D_{16} \\ D_{12} & D_{22} & D_{26} \\ D_{16} & D_{26} & D_{66} \end{bmatrix} \cdot \begin{pmatrix} \kappa_{xx} \\ \kappa_{yy} \\ \kappa_{xy} \end{pmatrix}, \tag{5.47}$$

with the bending and twisting moments (M_{xx}, M_{yy}, M_{xy}) per unit width and the bending and twisting curvatures $(\kappa_{xx}, \kappa_{yy}, \kappa_{xy})$. Inverting Equation 5.47 leads to

$$\begin{pmatrix} \kappa_{xx} \\ \kappa_{yy} \\ \kappa_{xy]} \end{pmatrix} = \begin{bmatrix} d_{11} & d_{12} & d_{16} \\ d_{12} & d_{22} & d_{26} \\ d_{16} & d_{26} & d_{66} \end{bmatrix} \cdot \begin{pmatrix} M_{xx} \\ M_{yy} \\ M_{xy} \end{pmatrix}, \tag{5.48}$$

with the flexural compliance d_{ij}. Considering pure bending by a moment M_1, Equation 5.47 becomes

$$\kappa_{xx} = d_{11} \cdot M_{xx} = d_{11} \cdot \frac{M_{xx}}{b}, \tag{5.49}$$

with the width of the laminate (b). Hence, the flexural modulus (E_f) is equal to

$$E_f = \frac{M_{xx}}{\kappa_{xx}} = \frac{b}{d_{11}}. \tag{5.50}$$

Taking into account the moment of inertia, $I = \frac{bh^3}{12}$, E_f finally reads

$$E_f = \frac{12}{h^3 d_{11}}. \tag{5.51}$$

6 Results

The results of characterisation and modelling are presented in this chapter. It follows the vertical characterisation strategy described in section 4.1 and describes micro- and macroscopic material properties of the materials introduced in chapter 3, hence of the continuous carbon fibre SMC (Co CF SMC), discontinuous glass fibre SMC (Dico GF SMC) and hybrid continuous-discontinuous glass/carbon fibre SMC (CoDico GF/CF SMC). Structure-property relationships are highlighted and this chapter includes the results of the investigations at the structure level and component testing. In addition to material, structural and component properties, the failure mechanisms and damage evolution of the individual components (Dico GF SMC and Co CF SMC) – but more importantly of the hybrid (CoDico GF/CF SMC) composite – are presented. Analytical estimation of material properties based on the approaches presented in chapter 5 are depicted at the end of the chapter.

6.1 Evaluation of testing methods and preliminary studies

This section deals with results of preliminary studies aimed to define appropriate specimen geometries and testing methods as well as the conditions to evaluate the mechanical material properties of the discontinuous glass fibre SMC (Dico GF SMC), the continuous carbon

fibre SMC (Co CF SMC) and the hybrid continuous-discontinuous glass/carbon fibre SMC (CoDico GF/CF SMC).

6.1.1 Tensile properties of discontinuous SMC composites

Due to the heterogeneous microstructure of (discontinuous) SMC composites and the significant length of the fibrous reinforcement (in general 25.4 mm), determination of mechanical material properties is difficult. Fibre orientation distribution resulting from manufacturing additionally complicates the mechanical characterisation of discontinuous fibre reinforced polymers. The heterogeneous microstructure justifies the need to define an appropriate specimen geometry. In addition, the defect size in SMC is rather large compared to the size of a specimen considered for experimental characterisation (Shirrell and Onachuk, 1986), and the dimensions of the specimen may also affect the material's failure mechanisms and damage evolution (Wisnom, 1991). Hence, the design of specimens to define mechanical material properties is of significant importance.

A preliminary study was conducted to investigate the influence of specimen design on the resulting tensile properties of Dico GF SMC. For this purpose, tensile tests on two different rectangular and two different dog-bone shaped specimens were carried out (a detailed description of the specimens' geometry can be found in section 3.2.3.1). In addition, different clamping blocks (fine and coarse profiling) were used to determine a possible influence of clamping (Table 6.1).

A variation of the size of the gauge section enabled deeper understanding of the influence of a representative section of the specimen

on evaluated strains and tensile properties (Table 6.2). In general, evaluations considered eight specimens of each type. For geometry B 2, the results are based on seven specimens. Relative tensile moduli of elasticity were considered to account for a process–induced variation of fibre volume content.

Table 6.1: Tensile test parameters considering different geometries of discontinuous glass fibre SMC. *Geometries of specimens are described in section 3.2 (Table 3.3 and Figure 3.9).

Name	Type*	Clamping distance	Clamping blocks	End tabs
R 1.1	R_1	100 mm	Fine	Yes
R 1.2	R_1	100 mm	Fine	No
R 1.3	R_1	100 mm	Coarse	No
R 2.1	R_2	100 mm	Fine	No
R 2.2	R_2	130 mm	Fine	No
B 1	B_1	128 mm	Fine	No
B 2	B_2	146 mm	Coarse	No

Table 6.2: Dimensions of gauge sections for different specimen geometries considered for preliminary tensile tests of discontinuous glass fibre SMC.

Specimen Type	R 1	R 2	B 1	B 2
Gauge section 1 in mm^2	70×10	70×10	70×10	70×10
Gauge section 2 in mm^2	80×13	80×28	80×13	80×28
Gauge section 3 in mm^2	70×13	70×28	70×13	70×28

An increase of the width of the specimen led to a marginal decrease of stiffness for both considered geometries (R 2.1 and B 2). Rectangular specimens with a width of 15 mm showed slightly increased stiffness if no end tabs were used (R 1.1). Moreover, for a rectangular

specimen with a width of 30 mm, clamping distance affected the stiffness of the material (R 2.1 and R 2.2). However, for all considered specimen types, no significant variations could be observed in terms of tensile modulus of elasticity (Figure 6.1). In addition, a variation of the gauge section had no influence on the calculated tensile modulus of elasticity.

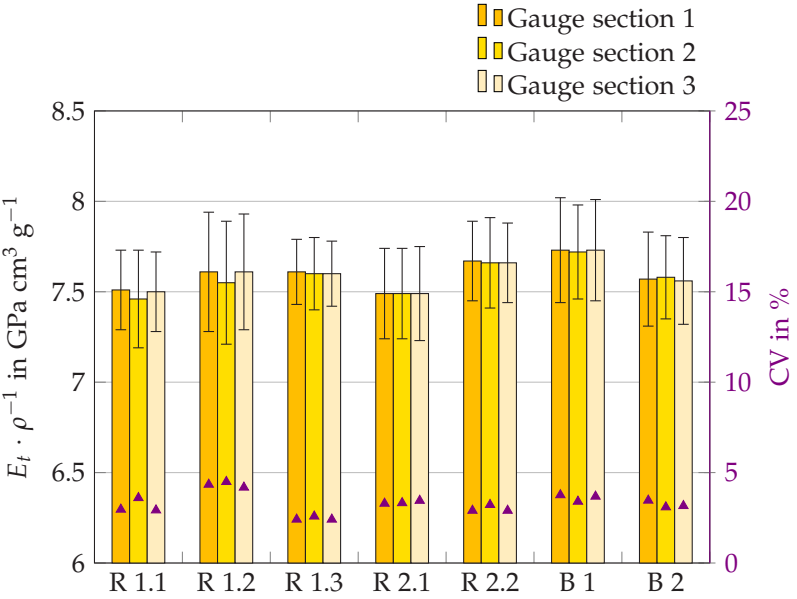


Figure 6.1: Specific tensile modulus of elasticity of discontinuous glass fibre SMC (two-dimensional [2D] flow with approximately 35 % initial mould coverage) determined for different rectangular (R) and dog-bone (B) shaped specimens with different gauge sections. A detailed overview of specimen geometries can be found in section 3.2 (Table 3.3 and Figure 3.9). Bar represents arithmetic mean value, whiskers represent standard deviation, ▲ = coefficient of variation (CV).

Specimens which failed within the clamping were not considered to evaluate tensile strength. With regard to tensile strength, variation

of specimens' geometry did not significantly influence the material behaviour (Figure 6.2). Rectangular specimens with a width of 15 mm and clamped without end tabs showed slightly lower tensile strength. In addition, scatter was more distinct. An increase in width and a change from rectangular to dog-bone specimen slightly decreased measured tensile strength (R 2.2, B 1, B 2) and led to a more significant scatter in tensile strength. For specimen types R 1 and B 1 no specimen failed within the clamping. In contrast, for wider specimens, failure within the clamping was more likely (R 2.1 50 %, R 2.2 25 %, B 2 37.5 %).

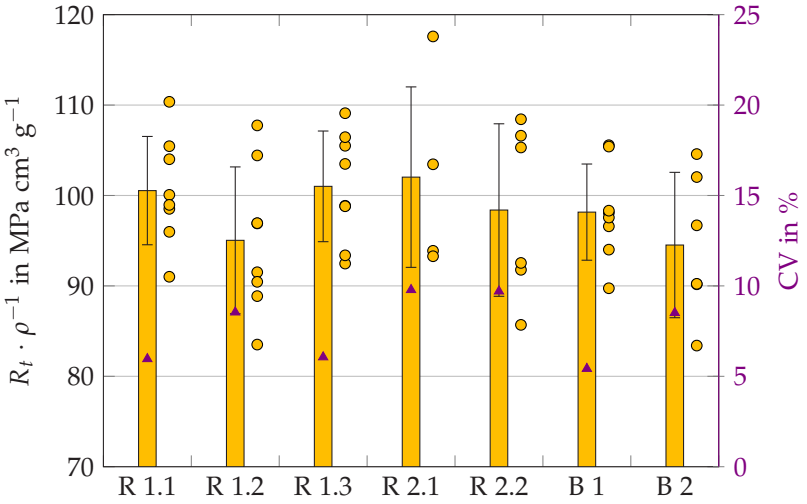


Figure 6.2: Specific tensile strength of discontinuous glass fibre SMC (2D flow with approximately 35 % initial mould coverage) determined for different rectangular (R) and dog-bone (B) shaped specimens. A detailed overview of specimen geometries can be found in section 3.2 (Table 3.3 and Figure 3.9). Bar represents arithmetic mean value, whiskers represent standard deviation; ● = individual specimen; ▲ = coefficient of variation (CV).

A second preliminary study aimed to define the influence of subset size and step size on resulting strains evaluated by means of digital image correlation. In a first step, image processing enabled analysis of the speckle pattern of the specimens to define the average speckle size. According to Byrne (2018), a subset may contain at least three speckles, consisting of not less than five pixels each. In addition, an appropriate step size leads to an overlap of two different subsets of 50 % to 80 % (GOM, 2018). To meet these recommendations, different combinations of subset size and step size have been considered to evaluate the arithmetic mean value of technical strains based on measured displacements in the gauge section. The results are summarised in Table 6.3.

Table 6.3: Tensile modulus of elasticity and failure strain evaluated for a gauge section of 70×100 mm^2 with different subset and step sizes.

Subset size in pixel^2	Step size in pixel	E_t in GPa	$\varepsilon_{max,t}$ in %
10×10	8	10.884	1.659
15×15	10	10.892	1.657
15×15	12	10.880	1.657
15×15	8	10.878	1.658
19×19	10	10.892	1.660
19×19	15	10.893	1.661
25×25	12	10.885	1.659
25×25	20	10.886	1.660
30×30	15	10.877	1.660
30×30	20	10.905	1.655

Although Dico GF SMC exhibits a heterogeneous microstructure leading to heterogeneous strain fields resulting from uniaxial tension, no difference was observed in terms of specimen stiffness and

failure strain for the considered combinations of subset size and step size. Hence, it can be concluded that for evaluating average technical strains, the size of subset and step do not influence the results, if the two parameters were chosen with respect of a common understanding of digital image correlation. With respect to the aforementioned findings, the following guidelines were considered to investigate tensile properties of continuous, discontinuous and continuous-discontinuous SMC materials:

- Rectangular specimens with a width of 15 mm were considered to account for the recommendations of DIN EN ISO 527-5, 2009. In addition, this allowed more efficient use of the manufactured sheets to obtain a higher number of specimens with the same amount of material. Preliminary tests showed that dog-bone shaped specimens were not suitable to determine material properties of continuous and continuous-discontinuous fibre reinforced materials.

- End tab were used to decrease the possibly harmful interaction between clamping blocks and SMC specimen. This is especially important to mechanically load continuous carbon fibre SMC specimens. For the sake of comparability, end tabs were used for all material types.

- A gauge section of 70×100 mm^2 was considered for further testing to avoid possible edge effects. A clamping distance of 100 mm was chosen, equalling the length of the gauge section (70 mm) plus two times the specimen's width, to take Saint-Venant's principle into account (Saint-Venant, 1855).

6.1.2 Tensile properties of continuous SMC composites

The influence of the quality of the edges have been intensively discussed, especially for unidirectional fibre reinforced materials (for example in O'Brien et al., 2001 or ASTM D5687/D5687M-95, 2015), and this research's third preliminary study aimed to investigate the influence of edge preparation on resulting mechanical material properties of Co CF SMC. For this purpose, a selected number of specimens were grinded by hand (approximately 10 s seconds with 150 rotations per minute) with sand paper (600, 1000 then 2500 grit) after water-jet cutting. In a finishing step, the edges of the specimen were grinded with a graining of 4000 for approximately 30 s.

Figure 6.3 summarises mechanical performance of Co CF SMC (0°) depending on edge quality. Although there was a significant improvement of the edge quality in terms of roughness, the tensile properties of continuous carbon fibre SMC in fibre direction (0°) were hardly affected (Figure 6.3). The same held true for mechanical properties, if specimens were loaded perpendicular to fibre direction.

The unsaturated polyester-polyurethane hybrid (two-step curing) resin system is a novel resin system with special curing conditions. Due to possible variations in material properties due to storage time, specimens have been extracted from two sheets and tensile tests were carried out twice (testing campaign 1 and testing campaign 2), with an intervening time interval of one year. The determined moduli of elasticity and tensile strength, depicted in Figure 6.4, exhibited a significant decrease over time.

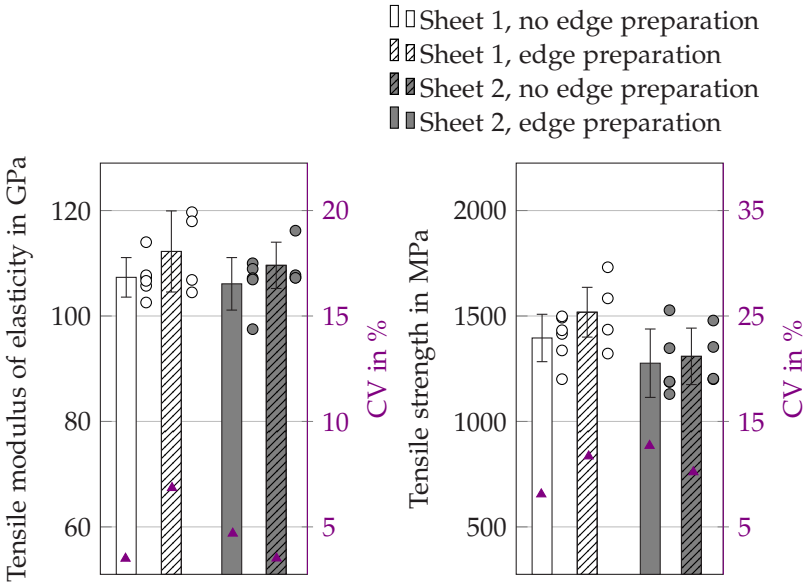


Figure 6.3: Influence of edge preparation on tensile modulus of elasticity and tensile strength of continuous carbon fibre SMC measured in fibre direction (0°) of two different sheets. Bar represents arithmetic mean value, whiskers represent standard deviation, ● = individual specimen, ▲ = coefficient of variation (CV).

With an average FVC of 55.2 vol.%, sheet 2 featured a slightly higher FVC than the reference sheet (sheet 1, FVC = 52.2 vol.%). However, tensile strength was considerably lower.

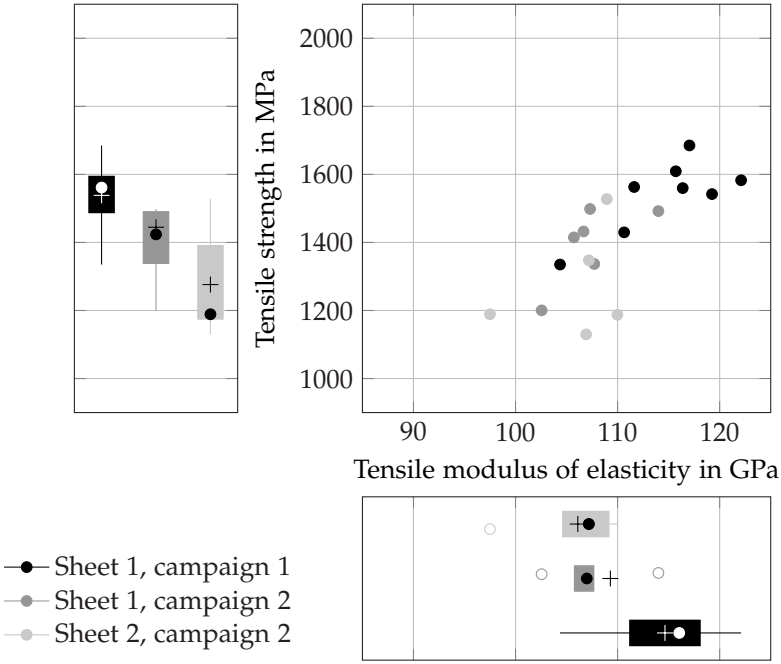


Figure 6.4: Tensile modulus of elasticity and tensile strength of continuous carbon fibre SMC resulting from uniaxial tension in fibre direction (0°), comparison of two different sheets (sheet 1 and 2) and influence of time period between manufacturing and testing (campaign 1 and 2). Experimental results of individual specimens on the right are summarised in box-plot diagrams depicting tensile modulus of elasticity on the bottom and tensile strength on the left, with • = median, + = mean, box = 25^{th} to 75^{th} percentile, lines indicate minimum and maximum or 1.5 interquartile range, respectively, ○ = outlier.

6.1.3 Flexural properties of SMC composites

Determination of flexural properties of fibre reinforced polymers requires consideration of the heterogeneous microstructure of the composite and a non-uniform stress distribution over the specimen's

thickness (Zweben et al., 1978). Depending on test setup and the distance of the lower supports, a more or less significant shear stress results due to an out-of-plane force acting on the specimen, which strongly depends on reinforcement architecture and is more pronounced for continuous fibre reinforced materials than for fibrous reinforcement based on chopped fibres. Different standards recommend different test setups in terms of minimum support span to handle the aforementioned challenges and to minimise shear effects during bending testing of fibre reinforced polymers (ASTM D7264/D7264M, 2015; DIN EN ISO 14125, 1998).

A fourth preliminary study involved three-point bending tests with different support distances to define an appropriate support distance for the different SMC composites. It aimed to characterise the evolution of the apparent flexural modulus, which theoretically reaches a value in the same range as the tensile modulus of elasticity if a sufficiently large span distance is considered (Zweben et al., 1978). Figure 6.5 depicts the evolution of the relative modulus of elasticity of Co CF SMC, Dico GF SMC and CoDico GF/CF SMC as a function of the span-to-thickness ratio. The experimentally determined tensile modulus of elasticity (arithmetic average) was considered to calculate the relative modulus. As clearly seen, the continuous carbon fibre SMC is most sensitive to evolving shear stresses if an out-of-plane load is applied. In DIN EN ISO 14125 (1998), a span-to-thickness ratio of 40:1 is recommended to evaluate flexural properties of continuous carbon fibre reinforced composites in fibre direction. The American Society for Testing and Materials (ASTM D7264/D7264M, 2015) recommends a span-to-thickness ratio of 32:1. In order to define a suitable test setup to deduce the flexural properties of continuous carbon fibre SMC and continuous-discontinuous glass/carbon fibre SMC, bending tests were carried out with a span-to-thickness ratio

of 32:1 and of 40:1. Flexural modulus of elasticity E_f and flexural strength σ_f were determined based on stress and strain calculations according to Equations 4.2 and 4.1.

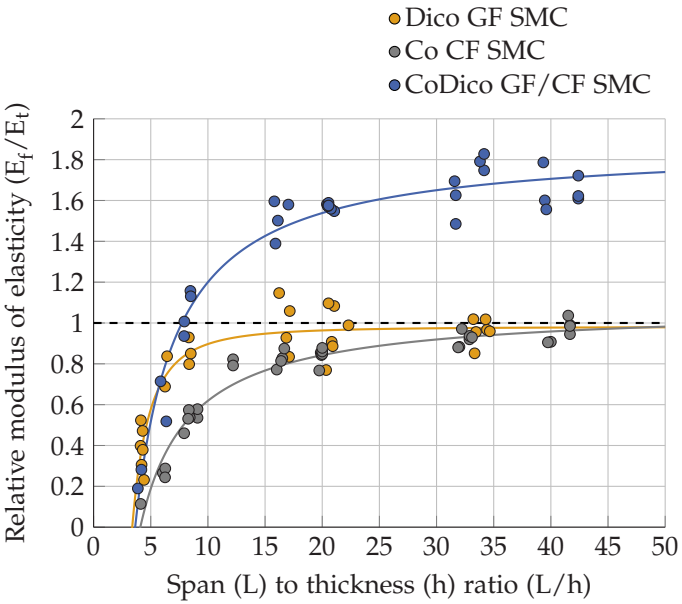


Figure 6.5: Relative flexural modulus of elasticity of continuous carbon fibre SMC, discontinuous glass fibre SMC and continuous-discontinuous glass/carbon fibre SMC as a function of span-to-thickness ratio.

Figure 6.6 depicts flexural properties of continuous carbon fibre SMC, with fibres aligned parallel the longitudinal axis of the specimen, determined for a span-to-thickness ratio of 32:1 and of 40:1. Flexural modulus of elasticity slightly increased with an increasing span-to-thickness ratio. However, considering the variations of stiffness within the testing campaign, this increase was not significant. No variation in terms of flexural strength was observed.

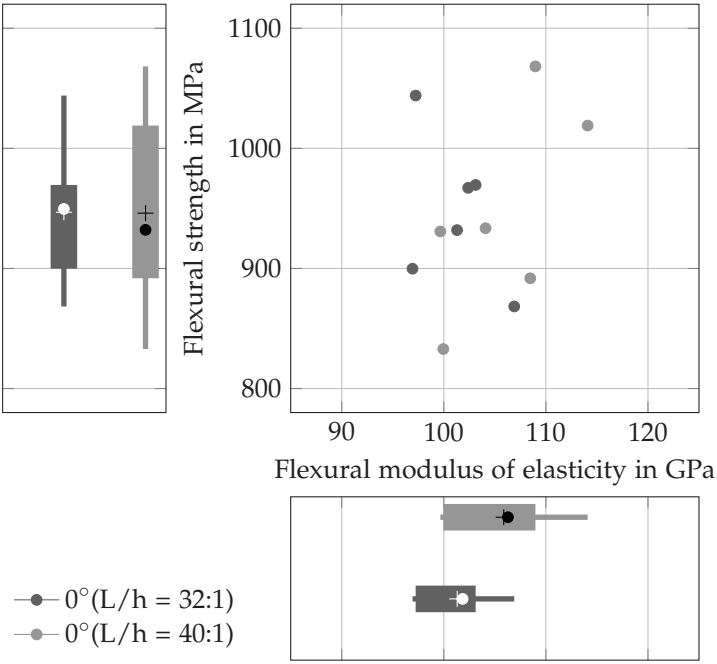


Figure 6.6: Flexural modulus of elasticity and flexural strength of continuous carbon fibre SMC for a span-to-thickness ratio of 32:1 and 40:1 (• = median, + = mean, box indicates 25^{th} to 75^{th} percentile, lines indicate minimum and maximum or 1.5 interquartile range, respectively).

In addition, flexural properties of continuous-discontinuous glass/carbon fibre SMC in terms of flexural modulus of elasticity and flexural strength did not show considerable difference if the span-to-thickness ratio was increased from 32:1 to 40:1 (Figure 6.7). Based on the aforementioned results, a span-to-thickness ratio of L/h = 32:1 was chosen to characterise flexural properties.

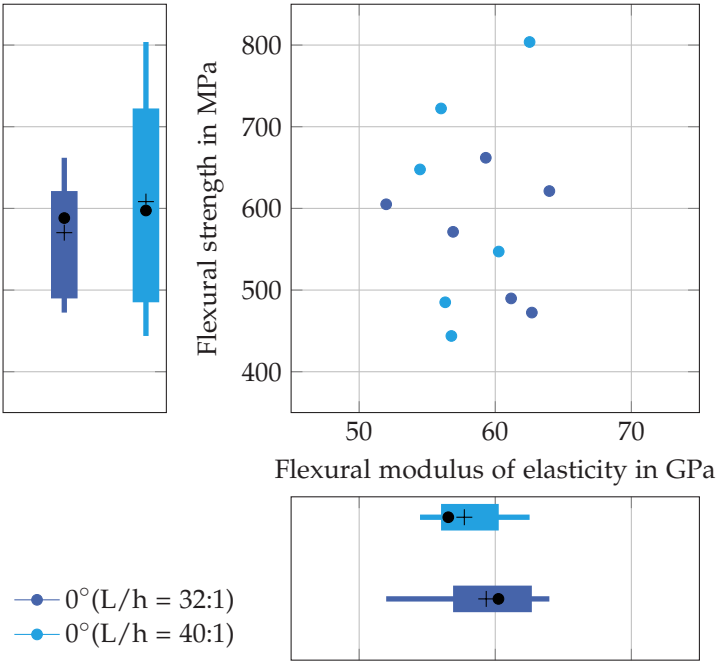


Figure 6.7: Flexural modulus of elasticity and flexural strength of continuous-discontinuous glass/carbon fibre SMC for a span-to-thickness ratio of 32:1 and 40:1 (• = median, + = mean, box indicates 25^{th} to 75^{th} percentile, lines indicate minimum and maximum or 1.5 interquartile range, respectively).

Three-point bending leads to a highly localised stress and strain field. A fifth preliminary study was conducted, aiming to define the variation of stiffness within one discontinuous glass fibre SMC specimen to account for the highly heterogeneous microstructure. For this purpose, flexural modulus of elasticity was determined three times for the same specimen. First, the specimen was placed symmetrically in the middle on the two lower supports. Two further measurements were carried out with the specimen shifted 10 mm to the left and right, respectively. This preliminary study was carried out with a

span-to-thickness ratio of 20:1 to allow a sufficient overlap of the specimen at the lower supports when shifting the specimen between the measurements. As depicted in Figure 6.5, a span-to-thickness ratio of 20:1 already enables to neglect of the influence of shear during an out-of plane loading of Dico GF SMC.

Figure 6.8 shows, that intra-specimen variations considering flexural modulus of elasticity were marginal for specimens aligned in the flow direction, with variations in the range of 1.3 % < CV < 4.5 %. Variations were slightly more important for specimens extracted perpendicular to flow (2.1 % < CV < 7.3 %).

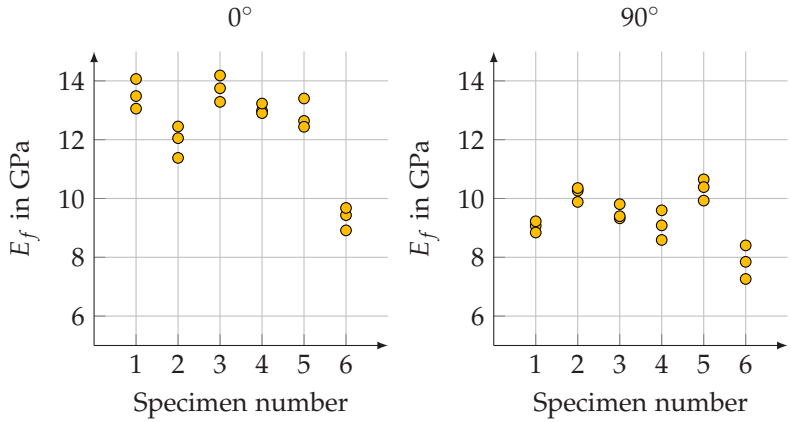


Figure 6.8: Flexural modulus of elasticity (E_f) determined for three different positions of six discontinuous glass fibre SMC specimens in 0° and 90°, with a span-to-thickness ratio (L/h) of 20:1, ● = individual stiffness value for a distinct specimen.

A sixth preliminary study aimed to determine the coefficient of friction (μ_f) between SMC material and support of the test setup. The experimentally determined value was $\mu_f \approx 0.24$. Considering

Equation 3b in DIN EN ISO 14125 (1998) and Equation 4.3, resulting frictional forces lead to an overestimation of flexural stresses of $\approx 0.1\,\mathrm{MPa}$ for a deflection of 20 mm (L/h = 32:1, nominal specimen thickness of 3 mm). This deflection equals a flexural strain $\varepsilon_f \approx 3.9\,\%$ and is hence significantly higher than that of the observed failure strains for the considered SMC materials. Hence, frictional effects have no relevance.

6.2 Microstructural analysis

As generally true for fibre reinforced polymers (e.g. demonstrated by Thomason and Vlug, 1996; Thomason et al., 1996 or Hassan et al., 2011), and presented in section 2.3.2.4, mechanical properties of SMC composites strongly depend on the material's microstructure – and inter alia, fibre length, fibre orientation and fibre volume fraction. Heterogeneous, flow-induced, fibre orientation distributions and a variation of fibre volume content may result in significant scatter of resulting stiffness and strength of the material, and a qualitative investigation of the local microstructure of the considered SMC materials was carried out by means of micro-computed tomography (μ-CT) and scanning electron microscopy (SEM). A quantitative description was built upon thermogravimetric analyses (TGA) to determine fibre volume content. A variation in fibre orientation was evaluated by calculating (local) fibre orientation tensors (FOT) based on μ-CT data.

6.2.1 Fibre volume content

Thermogravimetric analysis enabled measurement of the fibre weight content of SMC specimens, allowing determination of the fibre volume content in a following step by application of Equations 5.17

and 5.18. The calculations considered the densities of the unsaturated polyester-polyurethane two-step curing resin hybrid system ρ_{UPPH} = 1.14 g cm^{-3} (DSM Daron 41/B1, 2012), the carbon fibres ρ_{CF} = 1.82 g cm^{-3} (Zoltek, 2015) and the glass fibres ρ_{GF} = 2.6 g cm^{-3} (AZO Materials, 2018).

6.2.1.1 Fibre volume content of discontinuous glass fibre SMC

The semi-finished material of discontinuous glass fibre SMC was manufactured with a nominal fibre content of 41 wt.%; hence, the nominal fibre volume content of Dico GF SMC ($\phi_{DicoGF,nom}$) is equal to $\phi_{DicoGF,nom} \approx 23$ vol.%. Specimens for TGA have been extracted from flow and charge region to determine the resulting fibre volume content of Dico GF SMC compression moulded sheets. For one-dimensional (1D) flow Dico GF SMC plaques manufactured within one campaign, average (real) fibre volume content was 26.6 vol.% (μ = 2.25 vol.%, CV = 8.48 %) equalling an average fibre weight content of 45.3 wt.% and resulting in a density of the Dico GF SMC composite of $\rho_{Dico} = 1.53\,\mathrm{g\,cm^{-3}}$. Individual values of all 14 considered sheets are depicted in Figure 6.9. In general, the fibre volume content of moulded Dico GF SMC sheets was higher than the nominally set value when manufacturing the semi-finished SMC sheets. With an arithmetic mean value in the range of 21.5 vol.% to 28.2 vol.% process-induced real FVC showed a significant intra-campaign variation considering the results of different sheets. However, variations within one sheet were below 10 %.

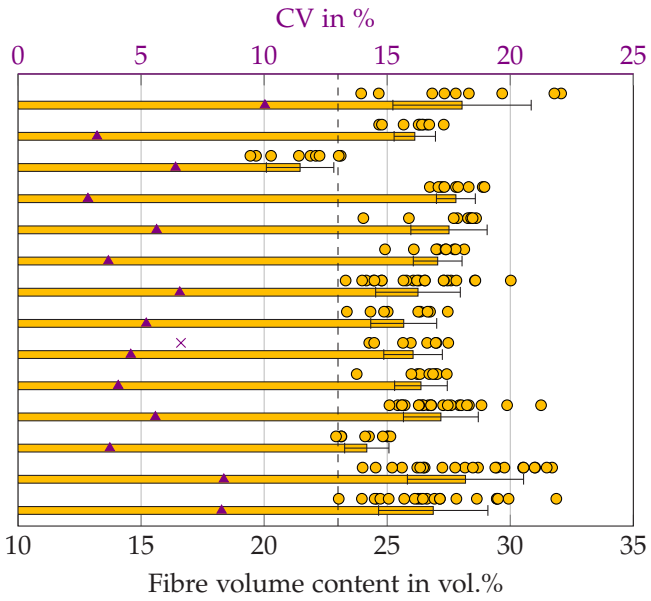


Figure 6.9: Fibre volume content of individual discontinuous glass fibre SMC sheets (manufactured within one campaign), with approximately 35 % initial mould coverage and one-dimensional (1D) flow. Dashed line indicates nominal fibre weight content, bar represents arithmetic mean value, whiskers represent standard deviation, ● = individual specimen, ▲ = coefficient of variation (CV), x = outlier.

Based on the same resin system and manufacturing parameters – with the exceptions of a slightly increased force during compression moulding from campaign 1 (1600 kN) – to campaign 2 (2500 kN) no significant inter-campaign variation of FVC could be observed (Figure 6.10). The two-dimensional (2D) Dico GF SMC sheets of campaign 1 featured an average FVC of 26.0 vol.% (μ = 0.9 vol.%, CV = 3.6 %). The average fibre content of 2D sheets of campaign 2 equalled 24.9 vol.% (μ = 1.6 vol.%, CV = 6.5 %), and the real fibre volume content was systematically higher than the nominally set value at both times.

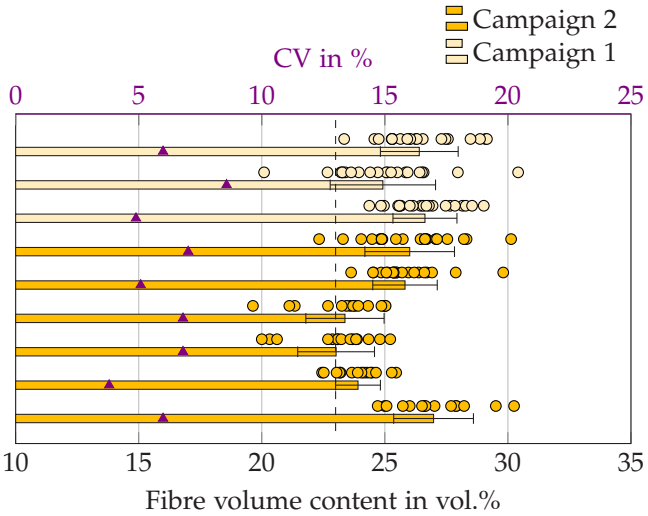


Figure 6.10: Fibre volume content of individual discontinuous glass fibre SMC sheets, with approximately 35 % initial mould coverage and two-dimensional (2D) flow, comparison of two different manufacturing campaigns. Dashed line indicates nominal fibre weight content, bar represents arithmetic mean value, whiskers represent standard deviation, ● = individual specimen, ▲ = coefficient of variation (CV).

Investigations of local fibre volume content of three different Dico GF SMC sheets showed no significant difference between the charge and flow region could be observed (Figure 6.11). However, specimens extracted at the corners tend to show a slightly higher FVC. In contrast, specimens located at the edges of the flow region featured a marginally lower FVC. These findings indicate the influence of material flow of resulting fibre distribution. In addition, the bundles at the edges of the part or sheet may additionally deform and flatten (Motaghi and Hrymak, 2017). Consequently, specimens for mechanical characterisation have not been extracted from the edges or corners of the sheets.

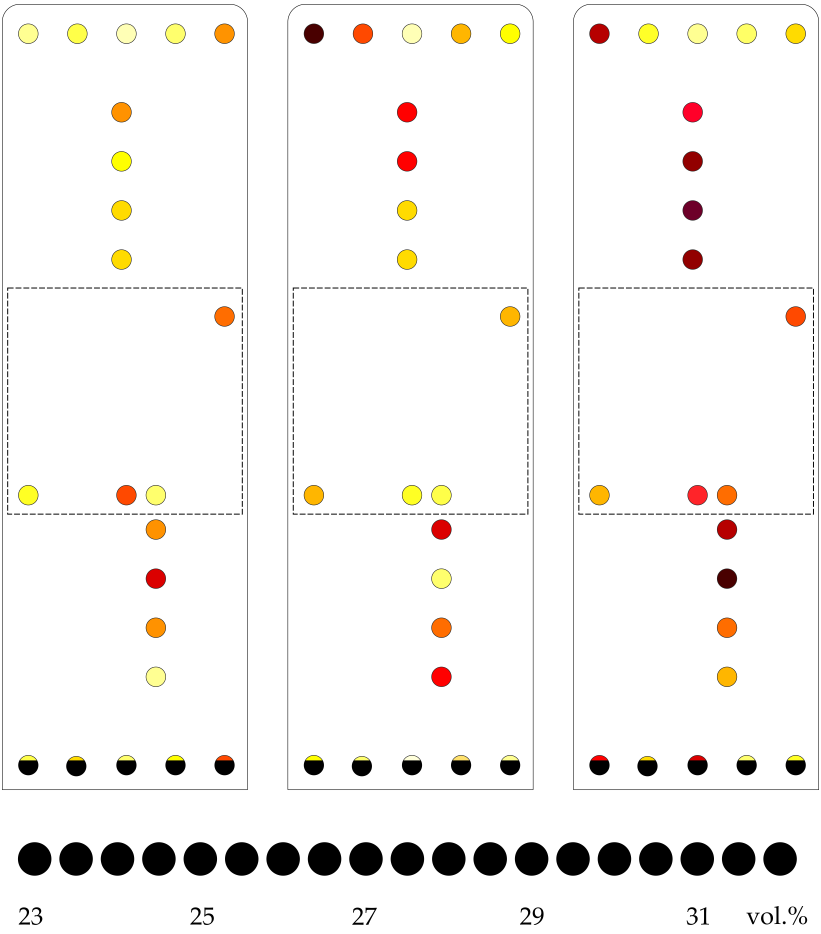


Figure 6.11: Local fibre volume content of three discontinuous glass fibre SMC sheets manufactured in rectangular shaped mould (1D flow). Circles depict location of individual specimens, considered for TGA analysis with colour-coded experimentally determined fibre volume content. Dashed line indicates initial charge region of approximately 35 %.

6.2.1.2 Fibre volume content of continuous carbon fibre SMC

Continuous carbon fibre SMC sheets were reinforced by a non-crimp unidirectional fabric and featured a nominal fibre weight content of 60 vol.% ($\phi_{CoCF,nom} \approx 48$ vol.%). Experimentally determined fibre volume content was significantly higher for all considered sheets (Figure 6.12).

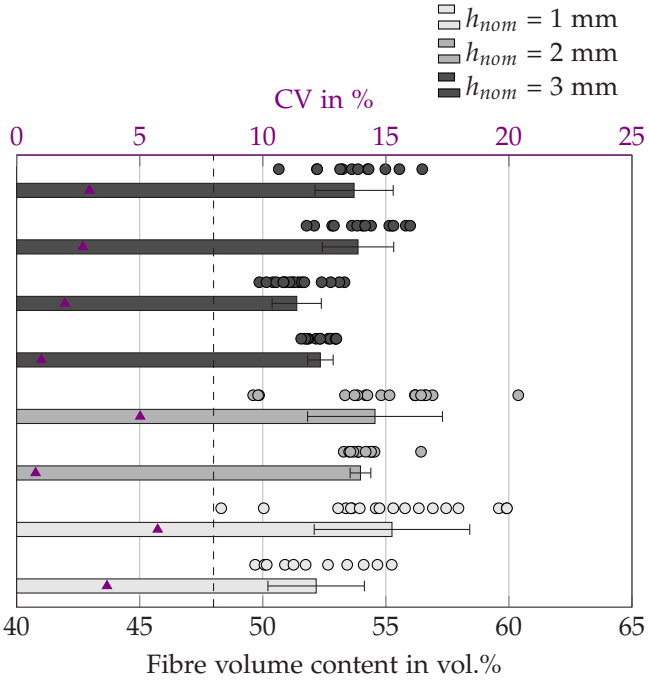


Figure 6.12: Fibre volume content of individual continuous carbon fibre SMC sheets featuring different nominal thicknesses. The dashed line indicates nominal fibre weight content, bar represents arithmetic mean value, whiskers represent standard deviation, ● = individual specimen, ▲ = coefficient of variation (CV).

The thinner the sheet, the higher the variations in terms of fibre volume content. With the exception of one 1 mm thick sheet, variations were equal to or below 5 %. Considering an average fibre volume content of 53.4 vol.%, the density of the continuous fibre reinforced SMC equals $\rho_{C0} = 1.50\,\mathrm{g\,cm^{-3}}$.

6.2.2 Fibre orientation distribution

For SMC materials – resulting from manufacturing parameters, movement of the conveyor belt but especially material flow during compression moulding – a specific process-induced microstructure with a distinct fibre orientation distribution is formed. If the fibre orientation deviates from being totally random, anisotropic rather transverse isotropic material properties result (Bert and Kline, 1985).

The following investigations of local fibre orientation distribution of Dico GF SMC were based on μ-CT data of four representative specimens and on Equation 5.32. Twice two specimens were extracted from flow region of the same one-dimensionally flown sheet either parallel or perpendicular to direction of flow. In the following, index 1 and 2 indicate the sheet of extraction, while 0° and 90° refer to the specimen's orientation. Figure 6.13 depicts the longitudinal axis of the (total) 100 mm long specimens equal to the y-axis in the coordinate system to define FOTs and the orientation of the components O_{xx}, O_{yy} and O_{zz}.

Figures 6.14 and 6.15 depict the evolution of the components O_{xx}, O_{yy} and O_{zz} with respect to specimen thickness. For this purpose, the components were defined for different slices of the specimen featuring a thickness of $\approx 8\,\mu\mathrm{m}$ each.

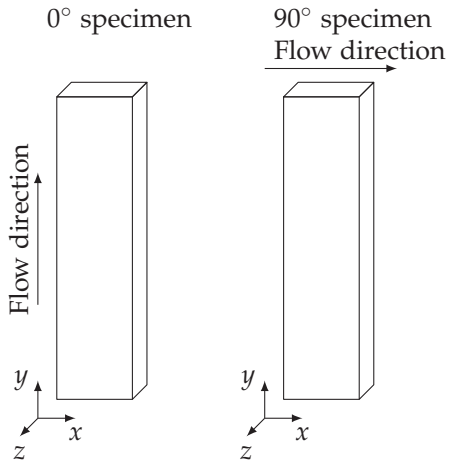


Figure 6.13: Orientation and convention of coordinate system to define fibre orientation tensors (FOTs).

Regardless of the orientation of the specimen, Dico GF SMC showed a slightly anisotropic fibre orientation in the $x-y$ plane. Due to fibre length and limited thickness of semi-finished sheets, fibre bundles did not tend to orientate perpendicular to the $x-y$ plane, and the value of O_{zz} (green line) is negligible.

The averaged second-order FOTs for the two specimens (index 1 and 2) extracted parallel to flow (0°) are equal to

$$O_{1,0^\circ} = \begin{pmatrix} 0.354 & -0.038 & -0.007 \\ -0.038 & 0.617 & 0.002 \\ -0.007 & 0.002 & 0.029 \end{pmatrix} O_{2,0^\circ} = \begin{pmatrix} 0.346 & 0.012 & -0.004 \\ 0.012 & 0.633 & -0.001 \\ -0.004 & 0.001 & 0.021 \end{pmatrix}.$$

Fibres were preferably aligned parallel to flow direction with

$$O_{yy} > O_{xx}.$$

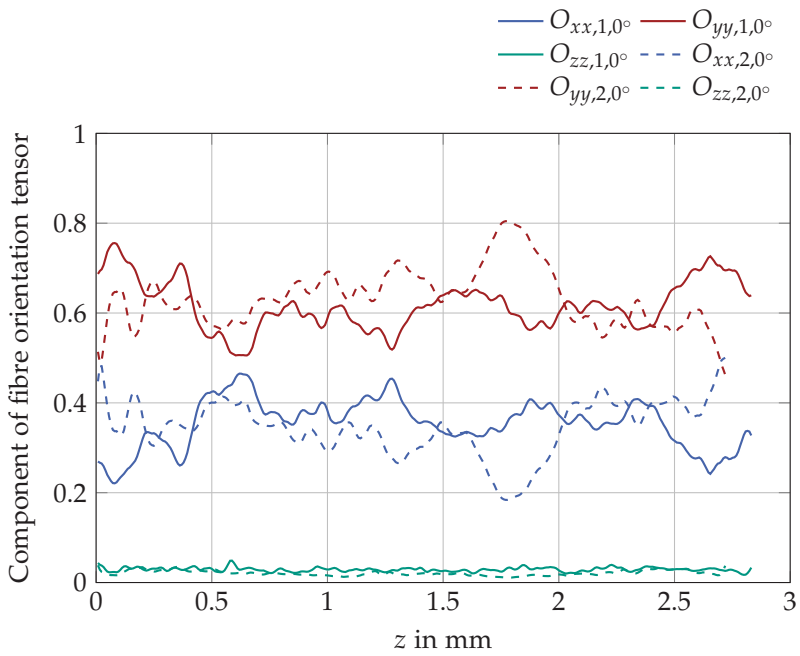


Figure 6.14: Components O_{xx}, O_{yy} and O_{zz} over thickness of two discontinuous glass fibre SMC specimens (index 1 or 2) extracted parallel to flow (0°).

The averaged second-order FOTs for the two specimens (index 1 and 2) extracted perpendicular to flow (90°) equal

$$O_{1,90°} = \begin{pmatrix} 0.577 & 0.042 & 0.007 \\ 0.042 & 0.382 & 0.000 \\ 0.007 & 0.000 & 0.040 \end{pmatrix} \quad O_{2,90°} = \begin{pmatrix} 0.524 & 0.013 & -0.011 \\ 0.013 & 0.449 & -0.008 \\ -0.011 & -0.008 & 0.027 \end{pmatrix}.$$

Hence, fibres were also preferably aligned parallel to flow direction with $O_{xx} > O_{yy}$. Global fibre orientation did not significantly differ between the four considered specimens. However, the deviation between the components O_{xx} and O_{yy} was slightly more important at

the edges, especially for the two specimens extracted perpendicular to flow (Figure 6.15). This deviation indicates that the fibre orientation was influenced by material flow during moulding and the interaction between mould, and external layers of the semi-finished sheets (as described in section 2.3.2.2) resulted in a slight shell-core effect.

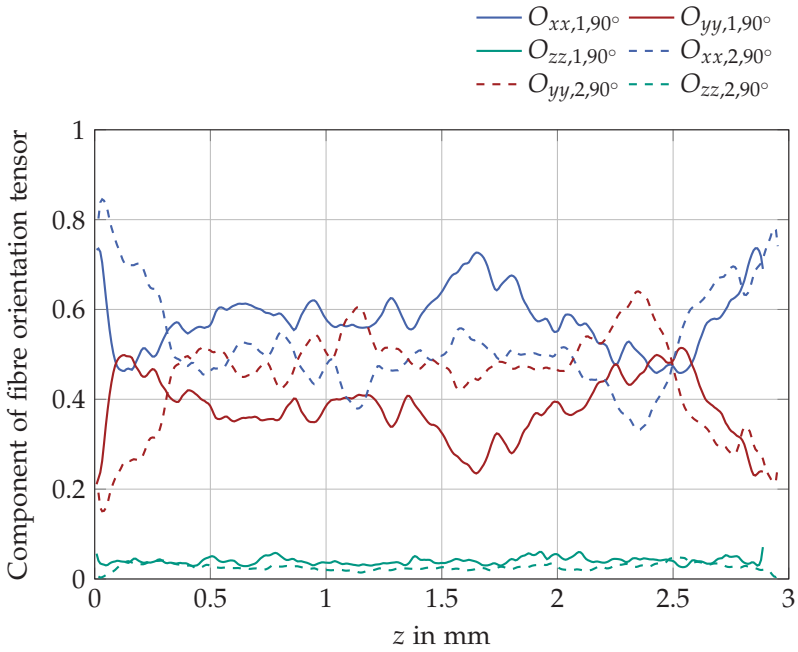


Figure 6.15: Components O_{xx}, O_{yy} and O_{zz} over thickness of two discontinuous glass fibre SMC specimens (index 1 or 2) extracted perpendicular to flow (90°).

Figures 6.17 and 6.18 depict the colour-coded fibre orientation of two representative Dico GF SMC specimens, with the coordinate z referring to the thickness direction. On the schematic drawing on the top left, the grey section indicates the selected region for μ-CT observations. It is clearly visible that material flow during

compression moulding not only caused the fibre bundles to orient in the flow direction, but also led to a spreading of the fibre bundles with individual fibres (or agglomerations of a small number of fibres) becoming visible in the shell layers ($z \approx 0.01\,\text{mm}$ and $z \approx 2.83\,\text{mm}$ for the specimen extracted in flow direction and $z \approx 0.01\,\text{mm}$ and $z \approx 2.89\,\text{mm}$ for the specimen extracted perpendicular to flow). Some fibres and fibre bundles in the shell were also characterised by a distinct curvature, which was not present in the core layers. In the core layers, microstructural observations depict individual fibre bundles, tending to align in flow direction.

The fibre orientation distribution of the discontinuous component of a hybrid CoDico glass/carbon fibre SMC specimen is depicted in Figure 6.16. The coordinate z refers to the thickness of the entire specimen. The material flow of the discontinuous component during compression moulding of the hybrid material also led to a preferable fibre bundle orientation in the flow direction ($O_{yy} > O_{xx}$), comparable to the resulting fibre orientation distribution of the pure discontinuous glass fibre SMC specimen in flow direction (Figure 6.14). The second-order FOT (considering only the discontinuous component of the hybrid CoDico SMC) reads

$$O_{hyb,0^\circ} = \begin{pmatrix} 0.388 & -0.014 & 0.005 \\ -0.014 & 0.593 & 0.003 \\ 0.005 & 0.003 & 0.019 \end{pmatrix}.$$

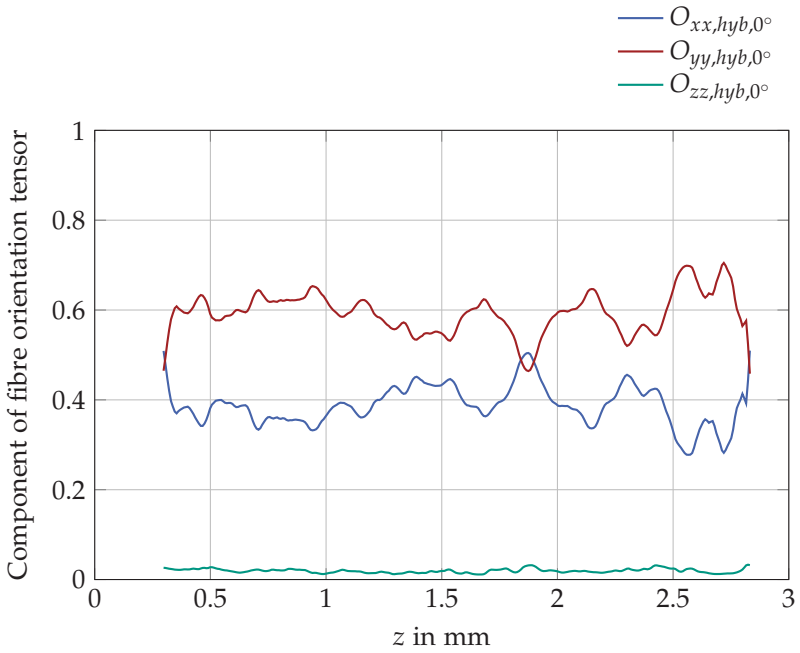


Figure 6.16: Components O_{xx}, O_{yy} and O_{zz} over thickness of a continuous-discontinuous glass/carbon fibre SMC specimen extracted parallel to flow (0°).

Figure 6.19 depicts the colour-coded fibre orientation at different positions with respect to the entire specimen's thickness, with coordinate z equal to zero at the surface. Within the core, fibre orientation distribution and appearance of fibre bundles show the same characteristics already highlighted for a pure Dico GF SMC specimen at the beginning of this section. In addition, the transition between the continuous face sheets and the discontinuously reinforced core is gradual (Figure 6.19: $z \approx 0.01$ mm and $z \approx 2.89$ mm) and the glass fibre bundles immingle with the continuous reinforcement.

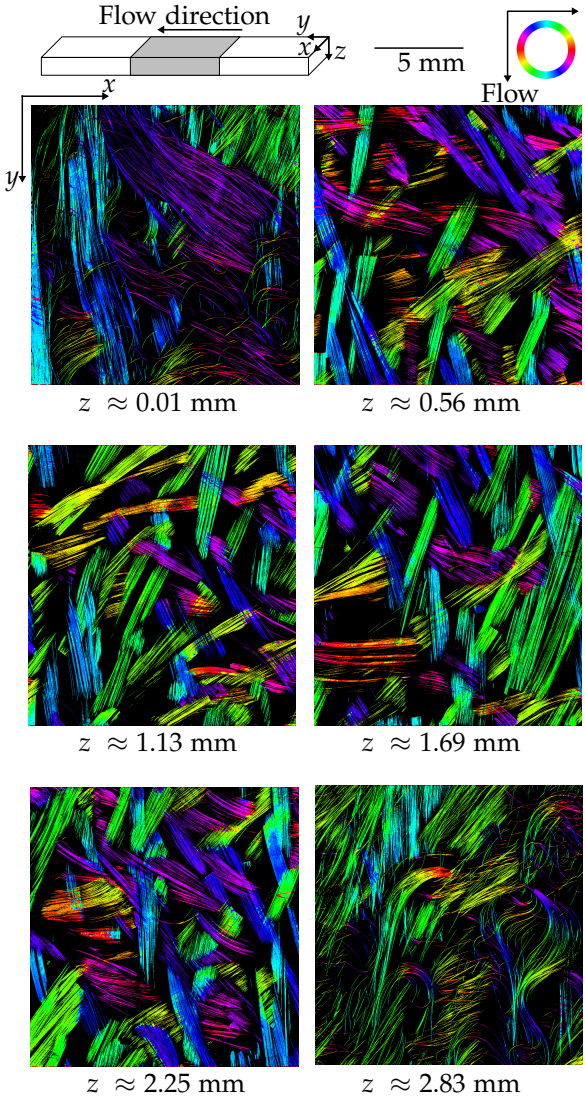


Figure 6.17: μ-CT observation of a discontinuous glass fibre SMC specimen extracted in flow direction (0°): Colour-coded fibre orientation with respect to the thickness of the specimen.

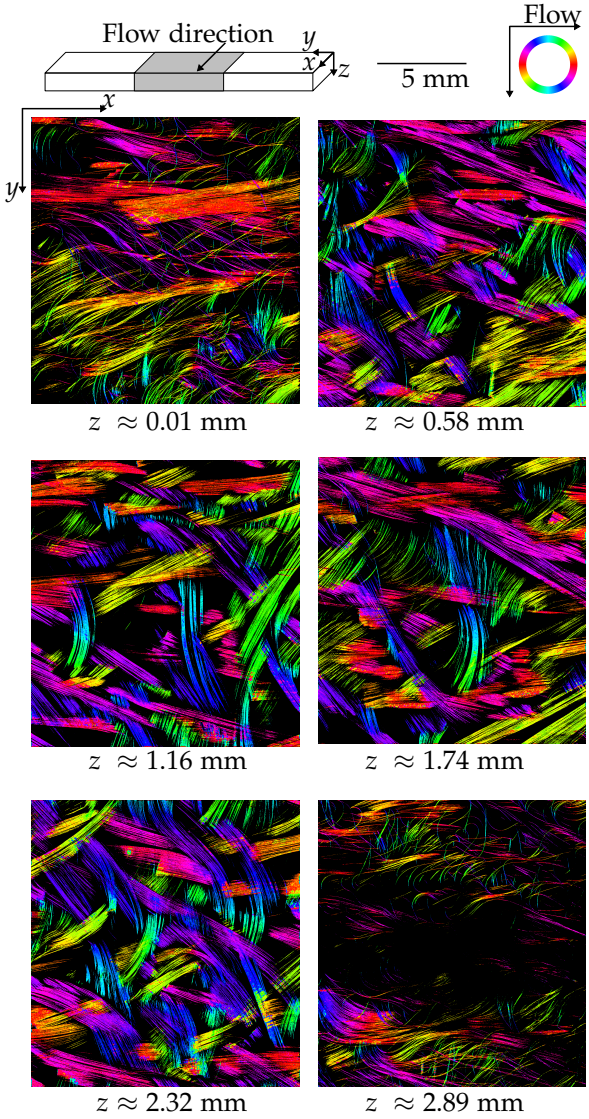


Figure 6.18: μ-CT observation of a discontinuous glass fibre SMC specimen extracted perpendicular to flow direction (90°): Colour-coded fibre orientation with respect to the thickness of the specimen.

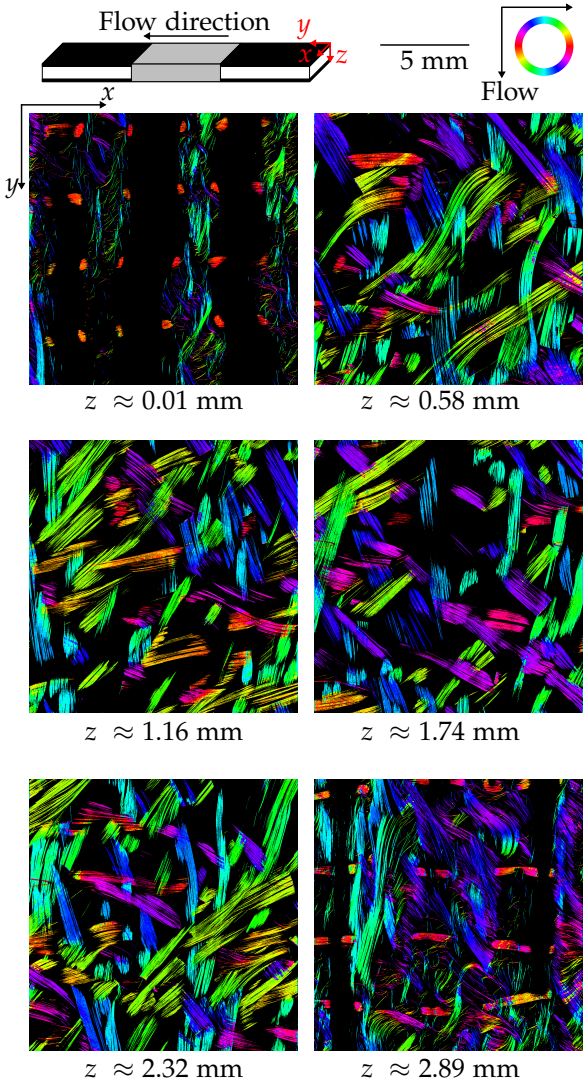


Figure 6.19: μ-CT observation of a hybrid continuous-discontinuous glass/carbon fibre SMC specimen extracted in flow direction (0°): Colour-coded fibre orientation with respect to the thickness of the specimen.

6.2.3 Interface of continuous-discontinuous SMC

The quality of the interface between different layers in a laminated composite is important to consider with respect to resulting material properties and damage evolution. Figure 6.20 clearly depicts a transition zone between the discontinuous glass fibre reinforced core and the continuous carbon fibre reinforced shell layers of the hybrid CoDico SMC. With z equal to zero at the top surface of the (entire CoDico) specimen, the transition zone between the continuous carbon fibre face sheets and the discontinuous glass fibre reinforced core is also clearly visible. At the outer surface, the representative investigated CoDico SMC specimen shows continuously reinforced face layers ($z \approx 0.05\,\text{mm}$ and $z \approx 2.96\,\text{mm}$). Towards the centre of the specimen, the continuous carbon fibre bundles were slightly pushed apart ($z \approx 0.37\,\text{mm}$ and $z \approx 0.64\,\text{mm}$) due to the flow of the discontinuous material during moulding and due to the glass fibre bundles' interaction with the continuous reinforcement. Below the continuous face sheets, featuring a thickness of $\approx 0.3\,\text{mm}$ to $0.4\,\text{mm}$, the glass fibre bundles are spread and characterised by splaying. Individual filaments or agglomerations of a small number of fibres define the fibrous reinforcement within this zone. It is also highly possible that the fibrous reinforcement within this section is defined by a distinct curvature, more important than the general SMC bundle structure observed within the core. Due to hybridisation, the spreading of the glass fibre rovings combined with the formation of a curvature was more severe with respect to the thickness of the transition zone within the hybrid material compared to the shell-core effect of the pure Dico GF SMC. The typical SMC microstructure, with fibre bundles oriented in the plane of the sheet ($x-y$-plane) not featuring a remarkable curvature, is representative of the microstructure of the core layers ($z \approx 0.85\,\text{mm}$ to $z \approx 2.16\,\text{mm}$).

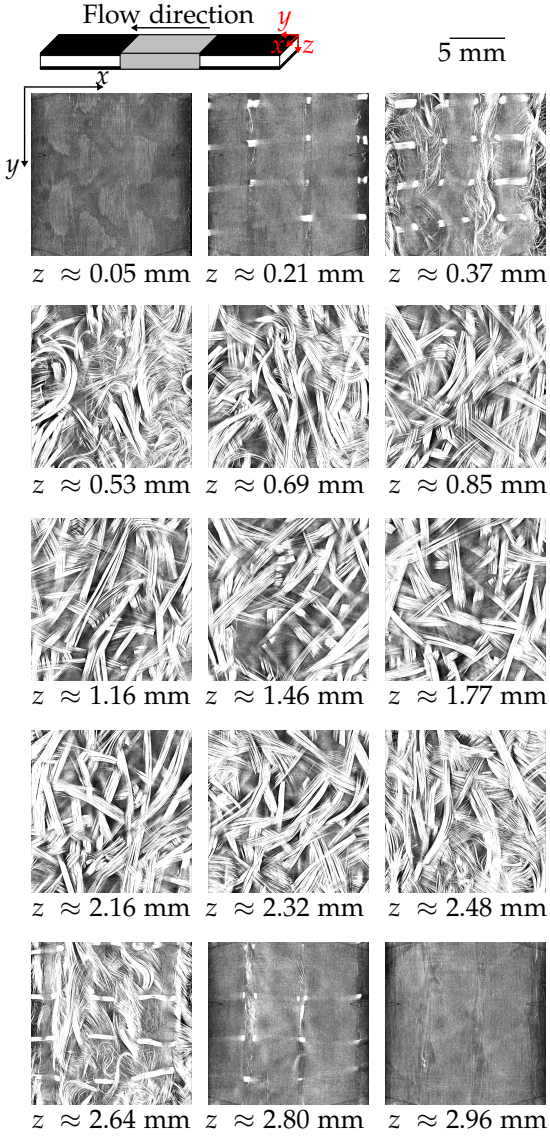


Figure 6.20: μ-CT observation of a hybrid continuous-discontinuous glass/carbon fibre SMC specimen extracted in flow direction (0°): Interface.

Investigations based on SEM allowed for deeper evaluation of the interface of CoDico SMC at the microscopic scale, and the transition zone can clearly be identified on the microscopic scale as shown in Figure 6.21. In the transition zone, few fibres of the discontinuous material were observed (Figure 6.21, marked in yellow).

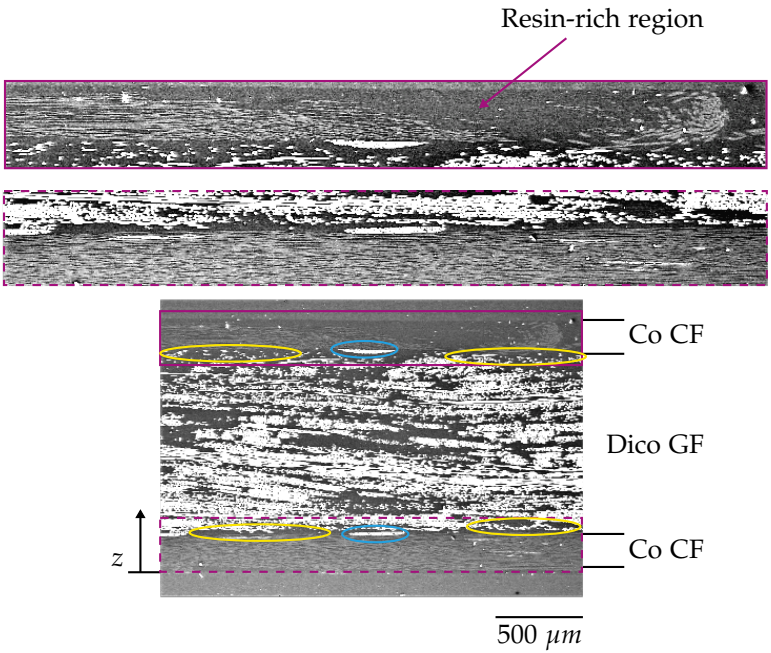


Figure 6.21: SEM observation of a hybrid continuous discontinuous glass/carbon fibre SMC specimen (microscale).

The pushing apart of the continuous fibre bundles led to resin-rich regions sporadically present at the surface, which also become macroscopically visible (Figure 6.22). For this reason, significant variations of the thickness of the continuously reinforced shell layers must be considered in predicting material properties. In addition, stitching yarns (Figure 6.21, marked in blue) pervade the transition zone.

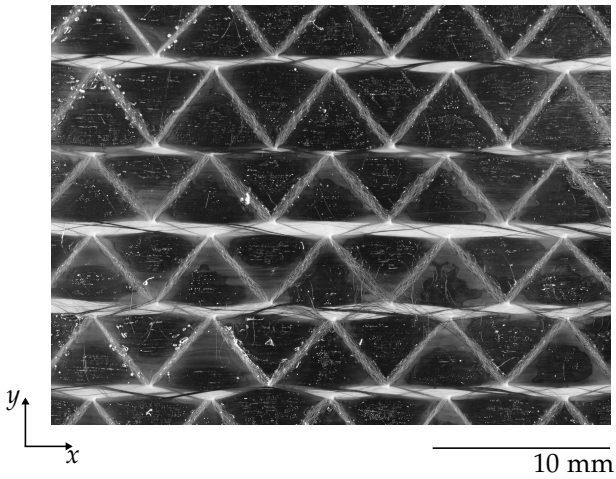


Figure 6.22: Digital photography: top view of continuous-discontinuous glass/carbon fibre SMC sheet (macroscale).

6.3 Mechanical properties and failure at the coupon level

6.3.1 Tensile and compressive properties of polyester-polyurethane hybrid resin

Elastic tensile and compressive properties (E_t, ν_t and E_c) of pure unsaturated polyester-polyurethane hybrid (UPPH) resin have been determined in order to be able to analytically model material properties of the continuous carbon and discontinuous glass fibre SMC. In addition, tensile and compressive strength (R_t and R_c) – as well as strain at tensile failure ($\varepsilon_{max,t}$) in combination with the stress-strain evolution resulting from tensile and compressive loadings – allowed

for characterisation of the failure and damage behaviour of the UPPH resin system (Figure 6.23, Figure 6.24 and Table 6.4).

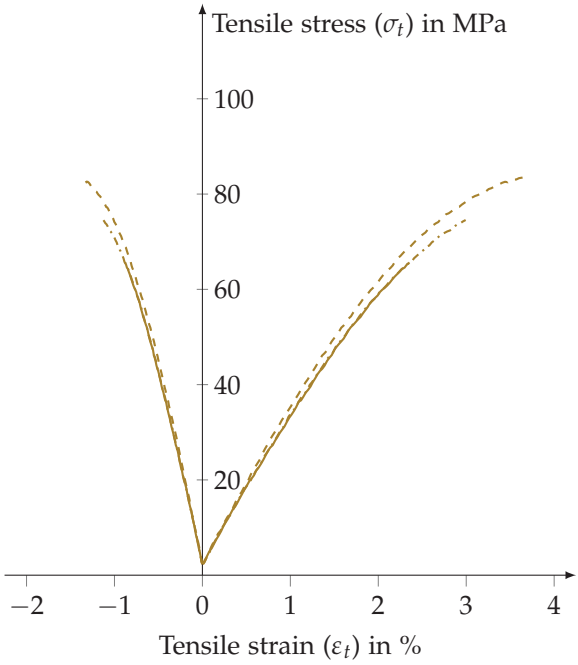


Figure 6.23: Representative stress-strain curves resulting from uniaxial tension of unsaturated polyester-polyurethane two-step curing hybrid resin system depicting transverse and longitudinal strains.

For the UPPH resin system, tensile and compressive moduli of elasticity did not significantly differ, reflecting the isotropic nature of the polymer. Considering tensile strength, the specimens' high porosity led to significant variation of the sustained maximum load. If failure was initiated at a pore, the measured strength was not considered for the presented average mean value in Table 6.4.

Exposed to uniaxial compression, pure resin specimens tend to bend easily, due to the setup of testing and did not completely fail (Figure 6.24). Hence, compressive strength was determined as the maximum sustained load before the bending factor b_f exceeded 0.1.

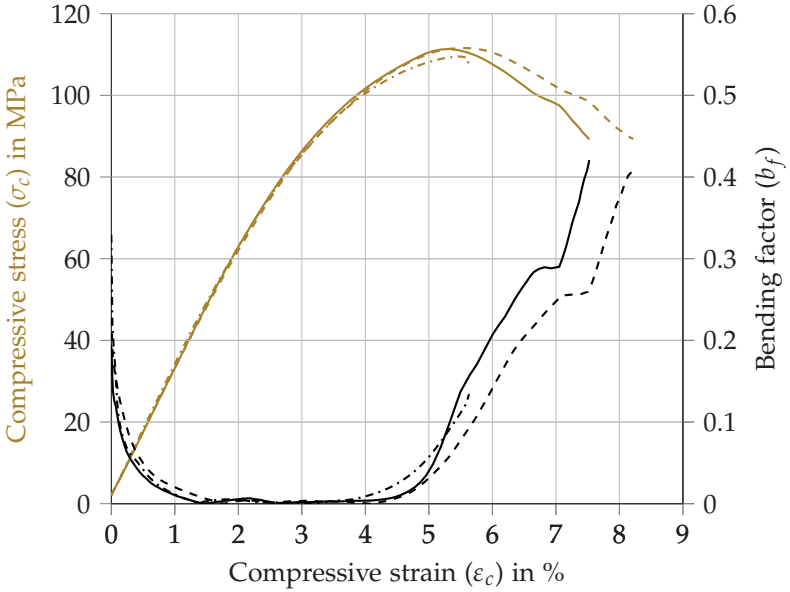


Figure 6.24: Representative stress-strain curves resulting from uniaxial compression of unsaturated polyester-polyurethane two-step curing hybrid resin system.

Stress-strain evolution of the unsaturated polyester-polyurethane two-step curing hybrid resin system resulting from uniaxial tension (Figure 6.23) or compression (Figure 6.24) was characterised by a linear elastic region in the beginning, followed by a gradual decrease in stiffness and a brittle and abrupt failure for tensile loadings.

Table 6.4: Tensile and compressive properties of unsaturated polyester-polyurethane two-step curing hybrid resin system with tensile and compressive modulus of elasticity (E_t and E_c), Poisson's ratio (ν_t), tensile and compressive strength (R_t and R_c) and tensile failure strain ($\varepsilon_{max,t}$) corresponding to the strain at a load drop to $0.8 \cdot F_{max}$. Variable n indicates number of evaluated specimens.

	E_t (n=3)	ν_t (n=3)	R_t (n=3)	$\varepsilon_{t,max}$ (n=3)	E_c (n=6)	R_c (n=3)
$\bar{x}$	3.45 GPa	0.38	75 MPa	3.0 %	3.06 GPa	111 MPa
μ	0.2 GPa	0.01	9 MPa	0.7 %	0.06 GPa	1 MPa
CV	4.4 %	1.6 %	11.9 %	21.4 %	2.0 %	1.1 %

6.3.2 Process-induced material properties of discontinuous glass fibre SMC

Generally chopped, discontinuous fibre reinforced materials, such as standard SMC, are characterised by an extremely heterogeneous microstructure, which arises due to manufacturing. The movement of the conveyor belt (Trauth et al., 2017a) – but more importantly the flow during moulding and the initial mould coverage – force the fibrous reinforcement to align in the flow direction, leading to a non-random fibre orientation (Chen and Tucker, 1984; Le et al., 2008). As a consequence, anisotropic material properties must be considered, and experimental characterisation has to be realised for specimens extracted in different directions with respect to manufacturing or flow direction (Dumont et al., 2007; Trauth et al., 2017a). The heterogeneous fibre orientation and fibre distribution may affect the measured modulus of elasticity depending on specimen geometry (Varna et al., 1992).

In addition, characterisation of long fibre reinforced composites, such as SMC, are determined by an important scatter of material properties, especially considering strength (Shirrell, 1983), which arises from the heterogeneous microstructure (Shirrell, 1985).

In the following, 0° refers to the flow direction of the semi-finished material within the rectangular mould. The coordinate system of the square mould was defined with the 0°-axis and 90°-axis parallel to the edges, equal for every sheet.

6.3.2.1 Tensile and compressive properties of discontinuous glass fibre SMC - mechanical performance

Uniaxial tensile and compression tests were carried out to define the mechanical material behaviour and process-induced anisotropy of discontinuous glass fibre SMC. Specimens have been extracted from the flow and charge region of one and two-dimensionally flown sheets in 0° and 90° with respect to material flow during compression moulding, to determine a possible influence of material flow on mechanical properties.

In the case of a two-dimensional (2D) flow, realised by placing the charge in the middle of a square mould (Figure 3.4), no significant variations in terms of tensile modulus of elasticity and tensile strength could be observed with respect to the orientation of the specimen (Figure 6.25). Flow region specimens showed slightly increased tensile moduli of elasticity and tensile strength in 0° as well as in 90°. Hence, it can be concluded that material flow marginally reoriented fibre bundles in the flow direction. With no distinction between charge and flow region specimens, tensile modulus of elasticity in 0° was equal to 11.8 GPa (μ = 1.2 GPa, CV = 10.1 %). For 90° specimens,

the average mean value was 11.3 GPa (μ = 0.8 GPa, CV = 7.1 %). Tensile strength was 158 MPa (μ = 20 MPa, CV = 12.9 %) and 151 MPa (μ = 15 MPa, CV = 10.3 %) in 0° and 90°, respectively.

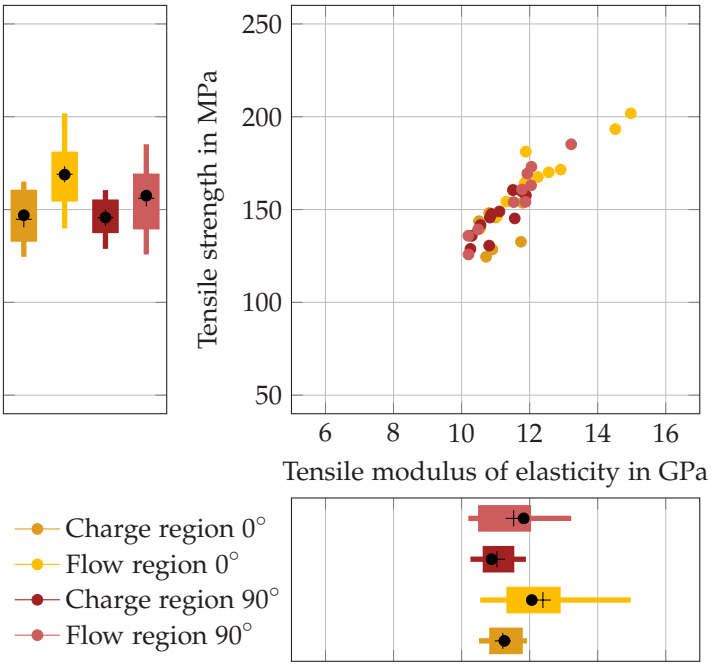


Figure 6.25: Tensile modulus of elasticity and tensile strength of discontinuous glass fibre SMC, 2D flow with approximately 35 % initial mould coverage. Longitudinal strains were measured with an extensometer, gauge length = 70 mm (• = median, + = arithmetic mean value, box = 25^{th} to 75^{th} percentile; lines indicate minimum and maximum or a 1.5 interquartile range, respectively).

In contrast to the planar isotropic material properties resulting from a two-dimensional (2D) flow of the semi-finished material during compression moulding, a one-dimensional (1D) flow in the rectangular mould (Figure 3.3) led to a considerable anisotropy of the material's

tensile stiffness and strength (Figure 6.26), with flow region specimens showing slightly better mechanical performance compared to specimens extracted from the charge region. However, the difference in mechanical performance depending on the location of the specimen was marginal and is of no technical consequence compared to the general scatter in the SMC material's properties.

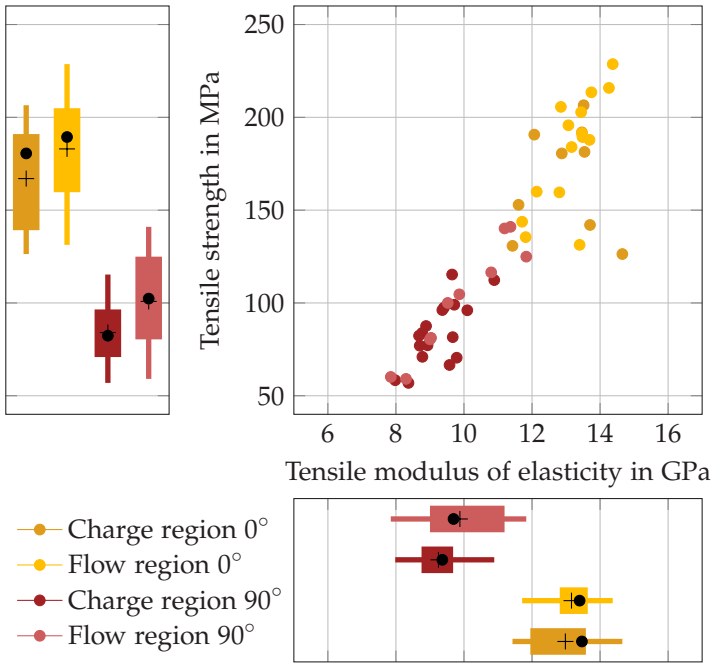


Figure 6.26: Tensile modulus of elasticity and tensile strength of discontinuous glass fibre SMC, 1D flow with approximately 35 % initial mould coverage (• = median, + = arithmetic mean, box = 25^{th} to 75^{th} percentile; coloured lines indicate minimum and maximum or 1.5 interquartile range, respectively).

To evaluate the anisotropy quantitatively, a factor of anisotropy (f_A) was introduced. It is defined by the ratio of the material's property in

the flow direction to the property perpendicular to the flow direction, and it reads, for example for the tensile modulus of elasticity,

$$f_A = \frac{E_{t,0°}}{E_{t,90°}}. \tag{6.1}$$

The resulting factor of anisotropy of 1D Dico GF SMC in terms of tensile modulus of elasticity was equal to f_A = 1.38 (0°: $\bar{x}$ = 13.1 GPa, μ = 0.9 GPa, CV = 6.8 % and 90°: $\bar{x}$ = 9.5 GPa, μ = 1.0 GPa, CV = 10.8 %). Anisotropy in terms of tensile strength could be characterised by a factor of f_A = 1.96, with an average strength of 177 MPa (μ = 30 MPa, CV = 17.2 %) in flow and 90 MPa (μ = 24 MPa, CV = 26.3 %) perpendicular to flow. Poisson's ratio of specimens extracted in the flow direction was equal to 0.37 (μ = 0.02, CV = 5.5 %), and with a value of 0.28 (μ = 0.04, CV = 13.4 %), Poisson's ratio was slightly lower if the load was applied on specimens extracted perpendicular to the flow direction.

Specimens extracted parallel to flow (0°) showed higher elongation at tensile strength ($\varepsilon_{R,t}$: $\bar{x}$ = 1.6 %, μ = 0.3 %, CV = 18.8 %) and failure strain ($\varepsilon_{max,t}$: $\bar{x}$ = 1.6 %, μ = 0.3 %, CV = 18.8 %) compared to 90° specimens ($\varepsilon_{R,t}$: $\bar{x}$ = 1.2 %, μ = 0.3 %, CV = 26.6 %, $\varepsilon_{max,t}$: $\bar{x}$ = 1.2 %, μ = 0.3 %, CV = 26.3 % Figure 6.27). Considering the influence of the specimens' location, charge region specimens showed slightly lower failure strain than did flow region specimens (−10 %). However, due to the high scatter, this difference is not significant. Regardless of flow condition during compression moulding, the considered discontinuous glass fibre SMC exhibited a significant positive correlation between tensile modulus of elasticity and tensile strength (Figure 6.25, Figure 6.26 and Figure 6.27).

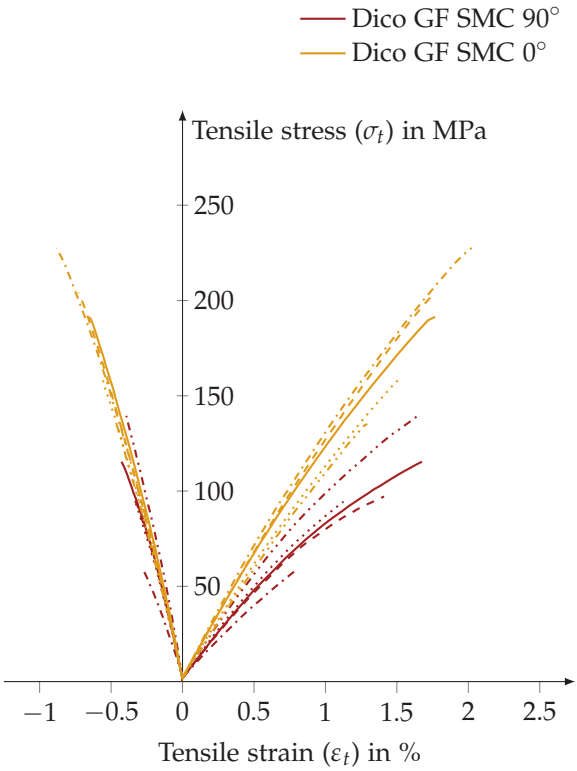


Figure 6.27: Transverse and longitudinal stress-strain curves resulting from uniaxial tension of discontinuous glass fibre SMC (Dico GF SMC) in 0° and 90°.

No significant difference was observed for compressive properties in terms of stiffness and strength between charge and flow region specimens. The average compressive modulus of elasticity of specimens extracted in the flow direction (0°) was 12.6 GPa (μ = 0.9 GPa, CV = 6.9 %). Specimens extracted perpendicular to the flow direction (90°) featured an average compressive modulus of elasticity of 9.2 GPa (μ = 1.4 GPa, CV = 14.7 %). Corresponding average strength was 298 MPa (μ = 33 MPa, CV = 11.1 %) in 0° and 224 MPa (μ = 24 MPa,

CV = 10.6 %) in 90°. Anisotropy could be defined by a ratio of 1.37 and 1.33. Compressive modulus of elasticity and compressive strength showed a positive correlation (Figure 6.28).

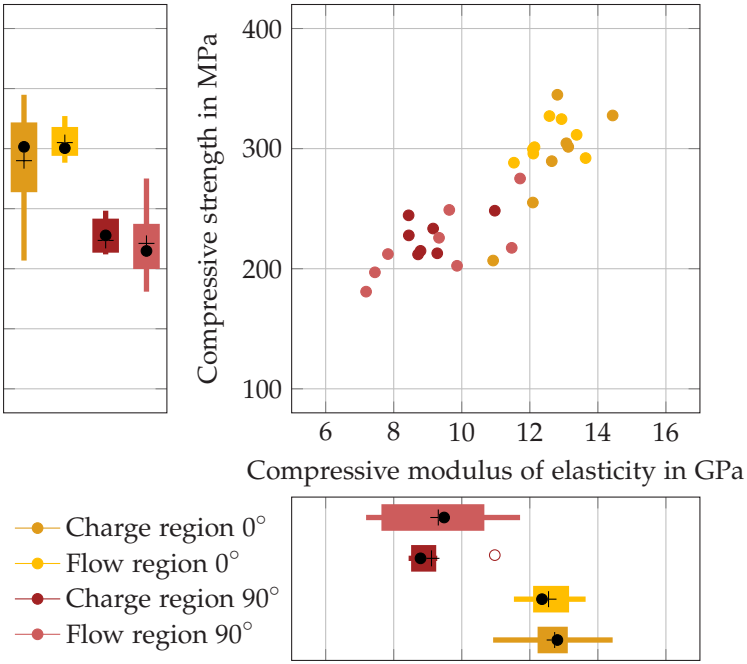


Figure 6.28: Compressive modulus of elasticity and compressive strength of discontinuous glass fibre SMC, 1D flow with approximately 35 % initial mould coverage (• = median, + = arithmetic mean, box = 25^{th} to 75^{th} percentile; lines indicate minimum and maximum or 1.5 interquartile range, respectively, ○ = outlier).

Compared to uniaxial tension, strain at compressive strength, $\varepsilon_{R,c}$, and compressive failure strain, $\varepsilon_{max,c}$, were significantly increased in 0° and 90° (Figure 6.29, 0°: $\varepsilon_{R,c}$: $\bar{x}$ = 2.8 %, μ = 0.2 % CV = 8.2 %, $\varepsilon_{max,c}$: $\bar{x}$ = 2.8 %, μ = 0.2 %, CV = 7.9 % and 90°: $\varepsilon_{c,R}$: $\bar{x}$ = 3.2 %, μ = 0.4 % CV = 12.8 %, $\varepsilon_{max,c}$: $\bar{x}$ =3.3 %, μ = 0.4 %, CV = 12.6 %).

Considering the aforementioned results, the UPPH-based Dico GF SMC composite was characterised by significant tension-compression anisotropy in terms of strength.

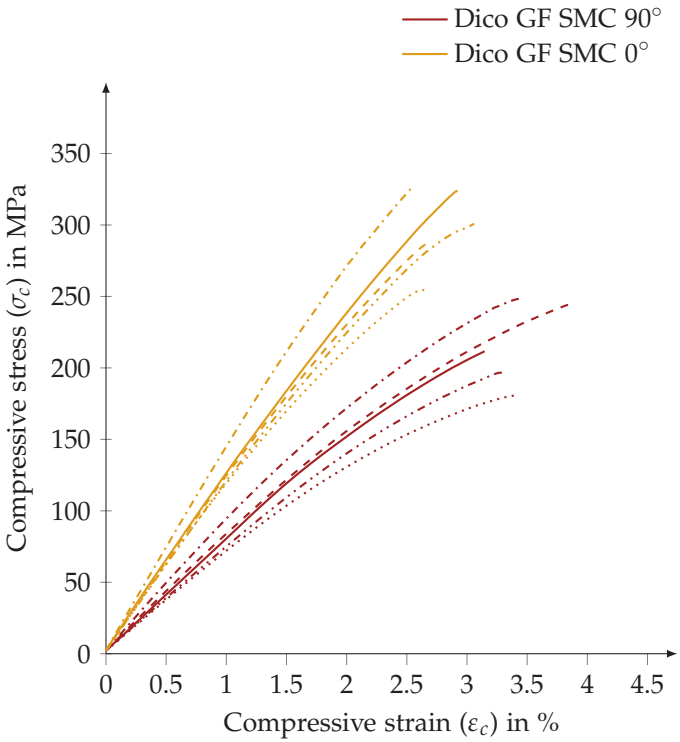


Figure 6.29: Stress-strain curves resulting from uniaxial compression of discontinuous glass fibre SMC (0° and 90°).

6.3.2.2 Flexural properties of discontinuous glass fibre SMC

Figure 6.30 depicts the flexural properties (three-point bending) of Dico GF SMC. The flexural properties were investigated for specimens extracted from flow region (0° and 90°) with a span-to-thickness

ratio of 32:1. No significant difference of flexural modulus of elasticity of discontinuous glass fibre SMC compared to tensile and compressive modulus of elasticity was observed in 0° nor in 90° (Table 6.5). Flexural strength was significantly higher than tensile strength, but lower than compressive strength. Although three-point bending leads to a very localised heterogeneous stress state within the specimen, variations in terms of flexural strength were not significantly higher compared to the variation in the experimental results of tensile and compressive strength (Table 6.5).

Table 6.5: Flexural properties of discontinuous glass fibre SMC for a span-to-thickness ratio (L/h) = 32:1 with flexural modulus of elasticity (E_f) and flexural strength (R_f). Calculations of $\varepsilon_{R,f}$ and $\varepsilon_{max,f}$ based on corrections proposed in DIN EN ISO 14125 (1998) and described in Equations 4.4 and 4.3. Variable n indicates number of evaluated specimens.

		Flow region 0°	Flow region 90°			Flow region 0°	Flow region 90°
E_f		(n=6)	(n=6)	R_f		(n=6)	(n=6)
$\bar{x}$	in GPa	12.6	9.1	$\bar{x}$	in MPa	283	170
μ	in GPa	0.8	0.3	μ	in MPa	29	19
CV	in %	6.4	3.3	CV	in %	10.2	11.0
$\varepsilon_{R,f}$		(n=6)	(n=6)	$\varepsilon_{max,f}$		(n=6)	(n=6)
$\bar{x}$	in %	2.7	2.4	$\bar{x}$	in %	2.9	2.6
μ	in %	0.3	0.3	μ	in %	0.4	0.4
CV	in %	12.3	13.8	CV	in%	14.7	15.6

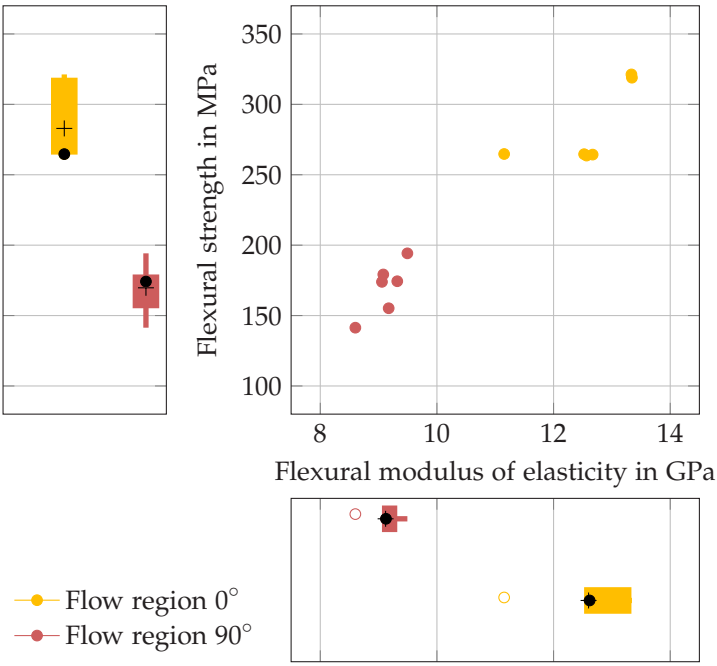


Figure 6.30: Flexural modulus of elasticity and flexural strength of discontinuous glass fibre SMC, 1D flow with approximately 35 % initial mould coverage for a span-to-thickness ratio (L/h) of 32:1 (• = median, + = mean, box indicates 25^{th} to 75^{th} percentile; lines indicate minimum and maximum or 1.5 interquartile range, respectively, ○ = outlier).

With a factor of anisotropy of f_A = 1.38 and f_A = 1.67 in terms of flexural modulus of elasticity and flexural strength, respectively, orientation dependent material properties were evident. A positive correlation could be observed for the flexural modulus of elasticity and flexural strength for specimens in 0° and 90°. Representative stress-strain responses resulting from three-point bending of discontinuous glass fibre SMC specimens extracted in flow direction as well as perpendicular to flow are depicted in Figure 6.31. The flexural

response was characterised by an initially linear increase, followed by a non-linear stress-strain evolution resulting from a stiffness decrease at the very end of loading. The transition from linear to non-linear stress-strain evolution is shifted to higher strains, compared to tensile loadings. Discontinuous glass fibre SMC exposed to three-point bending was able to maintain high deflections (Table 6.5). Deviation between strain at flexural strength ($\varepsilon_{R,f}$) and strain at failure ($\varepsilon_{max,f}$) was marginal (Table 6.5).

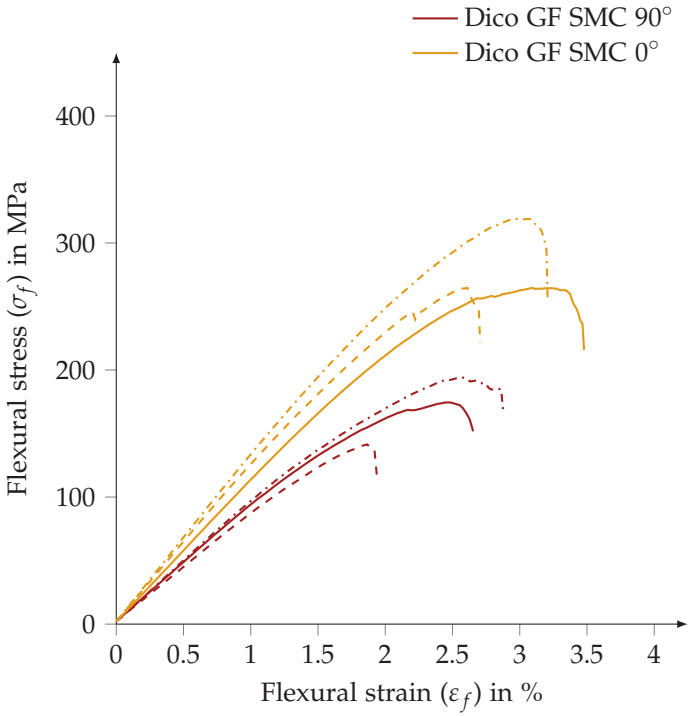


Figure 6.31: Stress-strain curves resulting from three-point bending (L/h = 32:1) of discontinuous glass fibre SMC (Dico GF SMC) in 0° and 90°.

6.3.3 In-plane loading of SMC composites

The following section deals with mechanical performance of Dico GF SMC, Co CF SMC and hybrid CoDico SMC exposed to uniaxial tension and compression. Damage mechanisms and failure evolution types are also displayed. In the following, "in fibre direction" refers to the axis parallel to the fibres of the continuous SMC composite (0°). In the same manner, and with regard to the orientation of local reinforcement of the hybrid CoDico SMC, 0° corresponds to the flow direction of the discontinuous material.

6.3.3.1 Tensile and compressive properties of discontinuous glass fibre SMC - material behaviour

Figure 6.32 shows representative stress-strain curves which resulted from uniaxial tensile or compressive loading of a discontinuous glass fibre SMC extracted parallel to flow direction. With no distinction between charge and flow region specimens, tensile modulus of elasticity was 13.1 GPa (μ = 0.9 GPa, CV = 6.8 %) for discontinuous glass fibre SMC. Generally, Dico GF SMC exhibited comparable tensile and compressive moduli of elasticity (E_c : $\bar{x}$ = 12.6 GPa, μ = 0.9 GPa, CV = 6.9 %). However, compressive strength was significantly higher than tensile strength (increase of average strength of 70 % and 140 % for 0° and 90° specimens, respectively). The aforementioned tensile-compression asymmetry manifested not only in a significantly increased compressive strength compared to maximum sustained tensile stress, but also due to a meaningful increase of strain at compressive strength ($\varepsilon_{R,c} \approx 1.8 \cdot \varepsilon_{R,t}$) and strain at compressive failure ($\varepsilon_{max,c} \approx 1.8 \cdot \varepsilon_{max,t}$) as depicted in Figure 6.32. Failure evolution did not significantly differ and after a linear increase up to $\varepsilon_t \approx 0.5$ % and $\varepsilon_c \approx 1.0$ %, stress-strain responses showed a gradual stiffness decrease up to brittle failure.

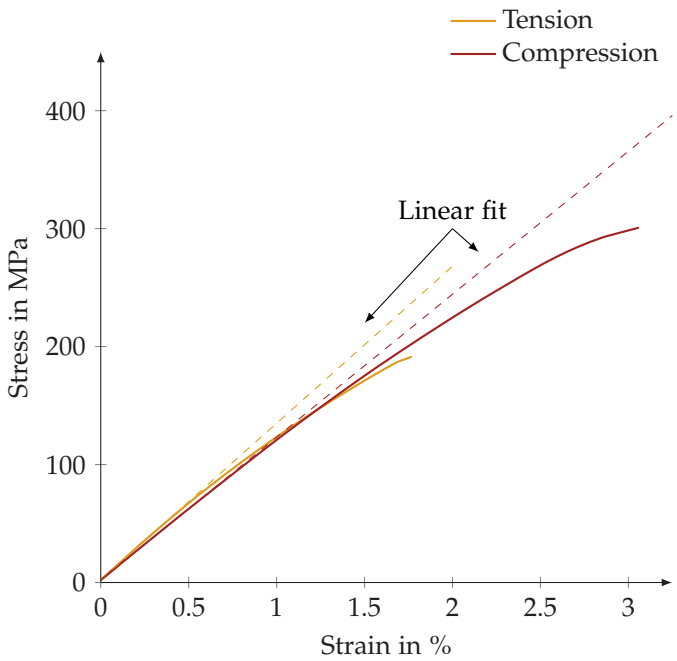


Figure 6.32: Representative stress-strain curves resulting from uniaxial tension and compression of discontinuous glass fibre SMC in 0°. Linear fit indicates the linear elastic material behaviour in the beginning of loading.

Figure 6.33 depicts a representative tensile stress-strain response of a Dico GF SMC specimen to further investigate damage evolution resulting from uniaxial tension. Strain fields, corresponding to selected points of the stress-strain curve (A – L), are shown in Figures 6.34 and 6.35.

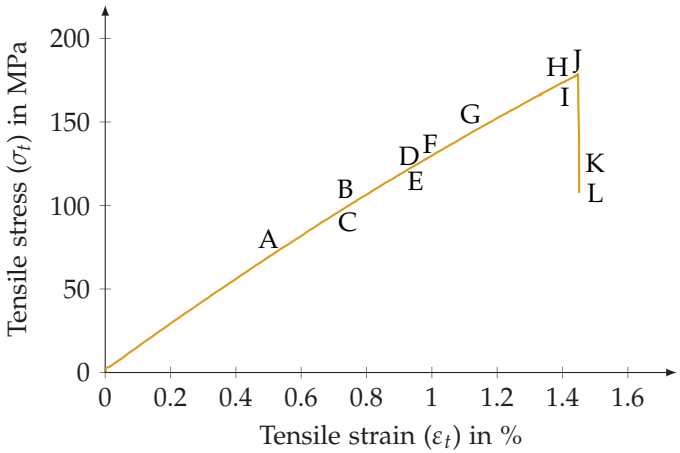


Figure 6.33: Representative $\sigma - \varepsilon$ curve resulting from uniaxial tension of discontinuous glass fibre SMC in 0°. Strain fields corresponding to points A – L are depicted in Figure 6.34 and Figure 6.35.

The slightly macroscopic non-linearity of the stress-strain evolution for tensile strains larger than $\approx 0.5\,\%$, was caused by the evolving damage of the specimen. As depicted in Figure 6.34 and Figure 6.35, the resulting strain field was homogeneous at the beginning of loading (point A). In point B, a local strain concentration on the left side of the specimen already indicated the location of final failure. The heterogeneity of the strain field evolved with a further increase in stress (point B – D). Local strain concentrations indicated highly localised damage of the Dico GF SMC specimen, linked to the formation and growth of matrix cracks perpendicular to loading, which was the main characteristic of the evolving damage in the Dico SMC exposed to tensile loads (point D). Crack growth was localised and occurred spontaneously (point B $\rightarrow$ C and point D $\rightarrow$ E). The two major cracks in the middle of the specimen grew from the edges to the centre of the specimen, agglomerated and led to final failure.

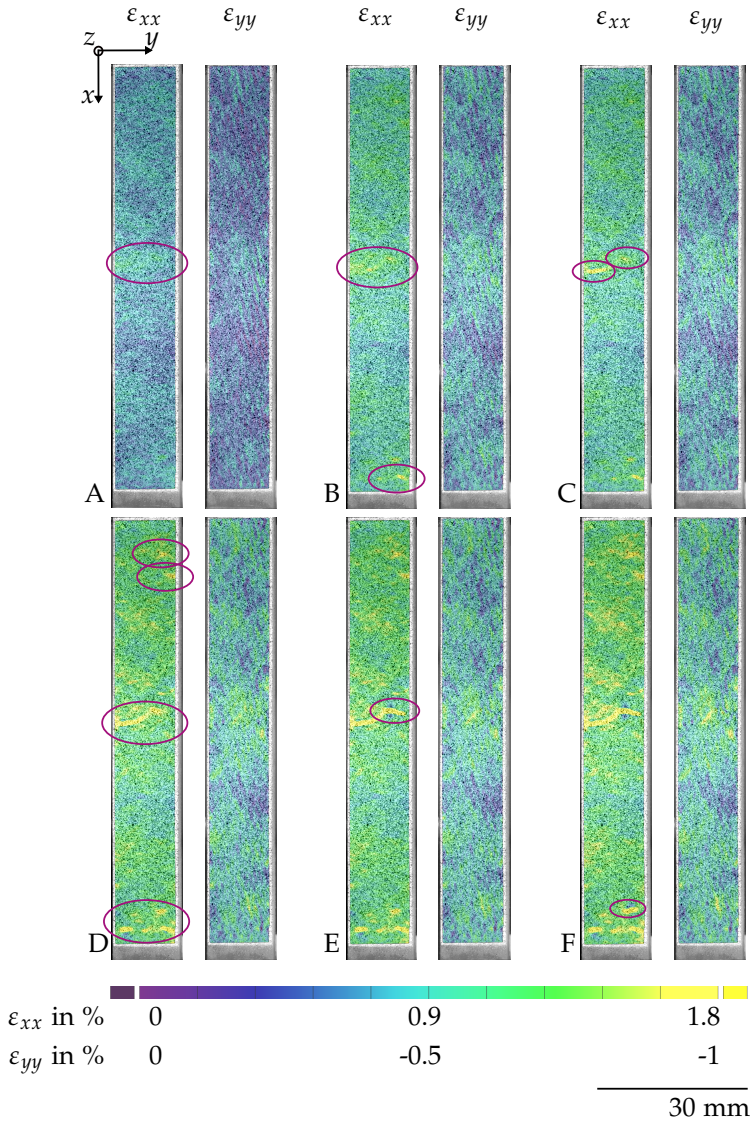


Figure 6.34: Strain fields (part I) resulting from uniaxial tension of discontinuous glass fibre SMC with the corresponding stress-strain evolution depicted in Figure 6.33.

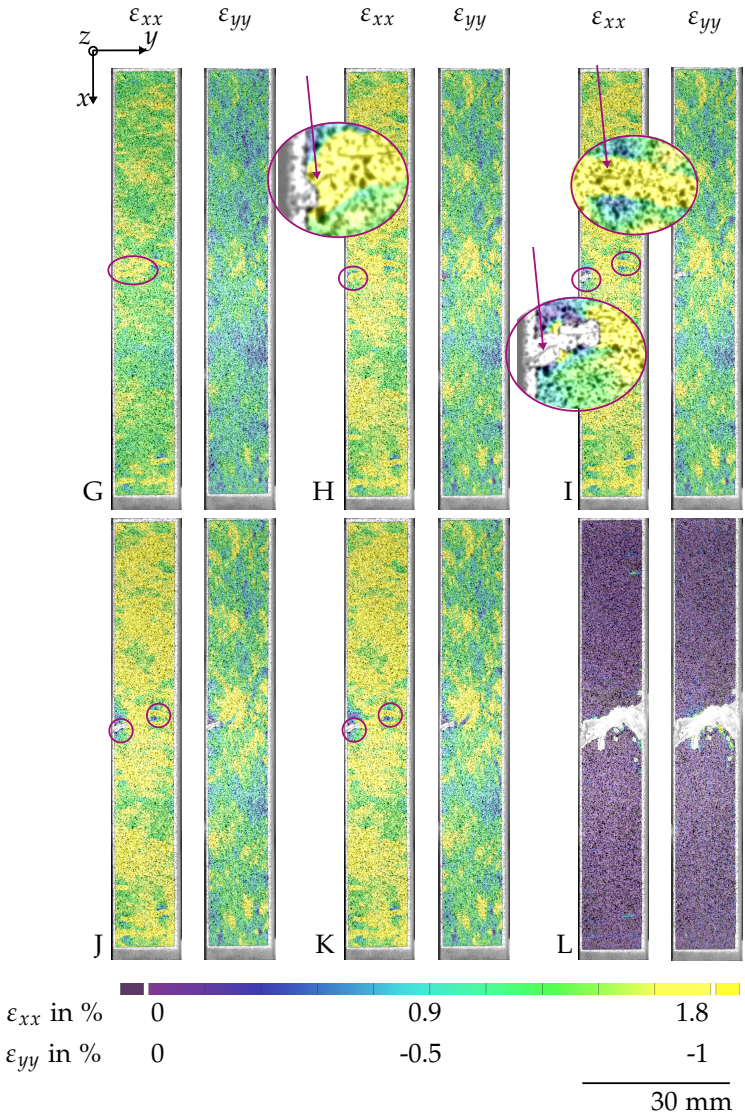


Figure 6.35: Strain fields (part II) resulting from uniaxial tension loading of discontinuous glass fibre SMC with the corresponding stress-strain evolution depicted in Figure 6.33. Arrows indication location of cracks.

Macroscopic post-mortem observation of a damaged SMC specimen, highlighted that interface failure between matrix and fibre bundles in terms of pseudo-delamination and pull-out of fibres bundles were dominating failure mechanisms (Figure 6.36).

Observation on the microscale by means of scanning electron microscopy (SEM) of a fractured surface (Figure 6.37) clearly shows matrix cracks, tending to align perpendicular to loading direction, at the surface of the specimen close to the damage zone. In the shell layers, which do not show the characteristic bundle structure, some individual fibres failed due to fibre breakage. In the core layers, interface failure (debonding) between the fibre bundles and matrix dominated the evolving damage (pseudo-delamination). Fibre breakage was only a secondary failure mechanism, as interface failure in the fracture zone was more likely to lead to a pull-out of entire fibre bundles.

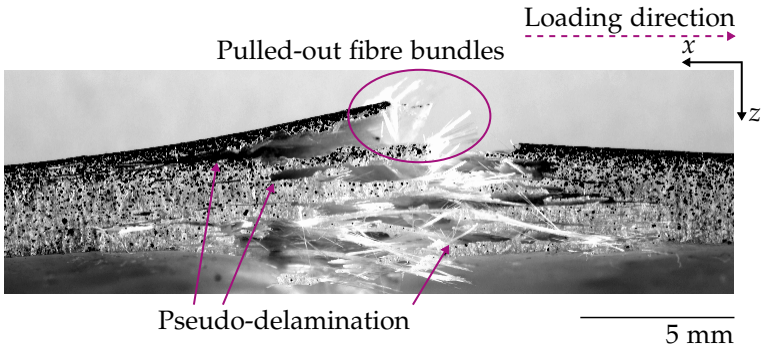


Figure 6.36: Macroscopic observation of fractured (post-mortem) discontinuous glass fibre SMC specimen (0°), which was exposed to uniaxial tension; side view (black colouration due to specimen preparation and for image correlation applied speckle pattern).

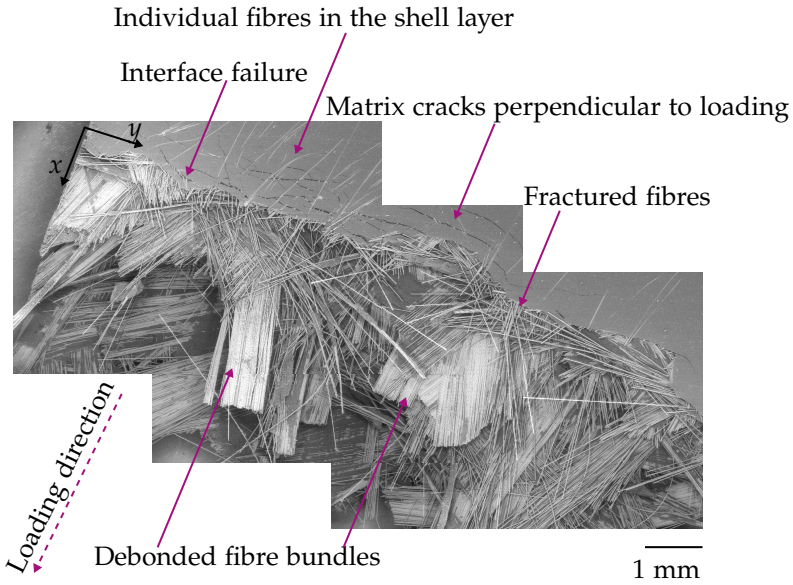


Figure 6.37: Microscopic observation (SEM) of fractured (post-mortem) discontinuous glass fibre SMC specimen (0°), which was exposed to uniaxial tension.

The stress-strain curve resulting from uniaxial compression of discontinuous glass fibre SMC, depicted in Figure 6.32, remained linear up to a compressive strain of $\approx 1\,\%$ before a slight decrease indicated initiation and evolution of failure within the specimen. Shortly before brittle fracture, stiffness decrease became more distinct. Dominating failure mechanism of Dico GF SMC composites exposed to compression was once again interface failure (pseudo-delamination). However, compared to tensile loading, significantly fewer planes of delamination were observed in post-mortem specimens. Compressive loading also led to shearing within the specimen due to broken fibres (Figure 6.38).

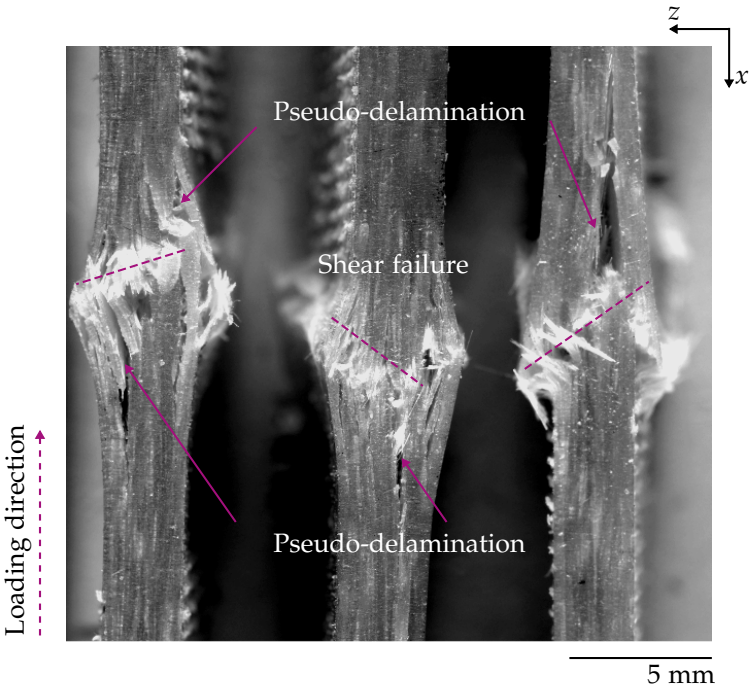


Figure 6.38: Macroscopic observation of fractured (post-mortem) discontinuous glass fibre SMC specimens (0°), which were exposed to uniaxial compression; side view.

6.3.3.2 Tensile and compressive properties of continuous carbon fibre SMC

In the following section, uniaxial tensile and compressive properties of continuous carbon fibre SMC in the fibre direction (0°) are presented, and failure evolution is described. Figure 6.39 summarises the tensile and compressive modulus of elasticity and tensile and compression strength of Co CF SMC loaded in the fibre direction.

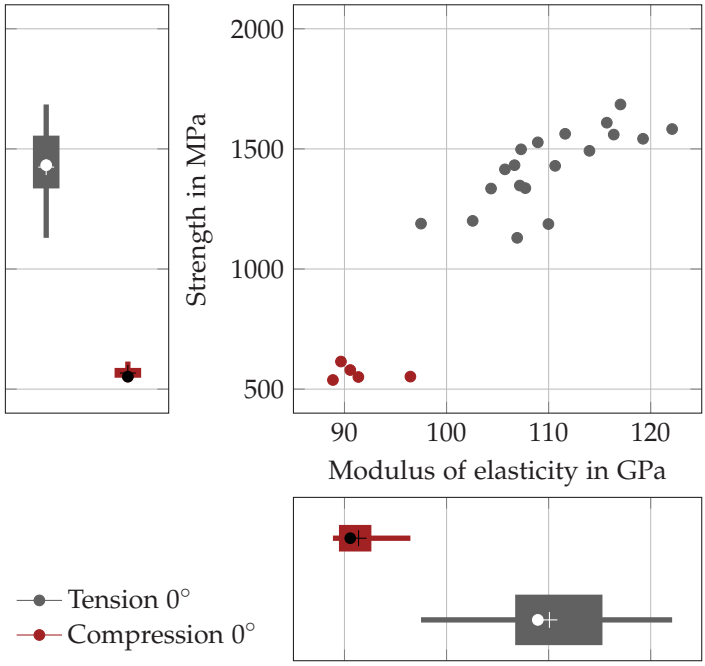


Figure 6.39: Tensile and compressive moduli of elasticity and tensile and compressive strength of continuous carbon fibre SMC in fibre direction (• = median, + = mean, box = 25^{th} to 75^{th} percentile; lines indicate minimum and maximum or 1.5 interquartile range, respectively).

Tensile modulus of elasticity of Co CF SMC exhibited a very high scatter (minimum measured stiffness = 97.5 GPa, maximum measured stiffness = 122.1 GPa). The same held true for tensile strength, which ranged from 1130 MPa to 1685 MPa. With a significantly lower compressive strength ($R_c \approx 0.4 \cdot R_t$), Co CF SMC was more sensitive to compressive loadings than to uniaxial tension (Figure 6.40 and Table 6.6). Tensile modulus of elasticity and tensile strength showed a slight positive correlation. No correlation could be observed for

compressive modulus of elasticity and compressive strength. The stress-strain evolution of continuous carbon fibre SMC loaded in tension or compression in the fibre direction was characterised by a steady increase of strain with increasing stress from beginning of loading until fracture (Figure 6.40). Continuous carbon fibre SMC experienced brittle failure.

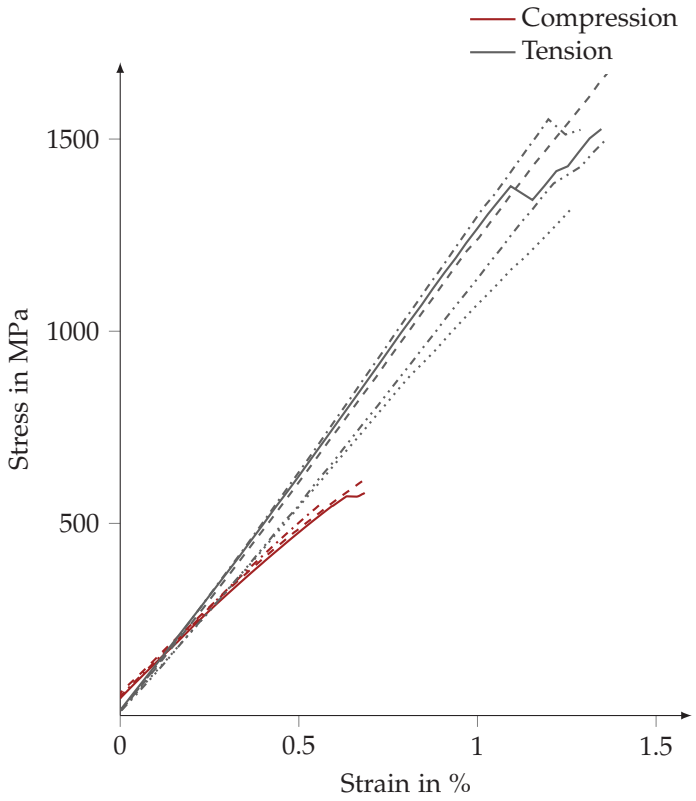


Figure 6.40: Stress-strain curves resulting from uniaxial tension and compression of continuous carbon fibre SMC (Co CF SMC) in 0°.

Two slightly different failure evolutions were observed if Co CF SMC was exposed to uniaxial tension. In the first case (type I), failure was characterised by splitting and individual fibre bundles failed in a very short time period due to inter-fibre fractures, which were reflected by small load drops in the stress-strain curve. Although it partially failed, the specimen could still maintain further loads. However, as soon as a critical load was reached, tensile specimens abruptly burst (Figure 6.41). Specimens, characterised by fibre misalignment were most likely to fail in the aforementioned way.

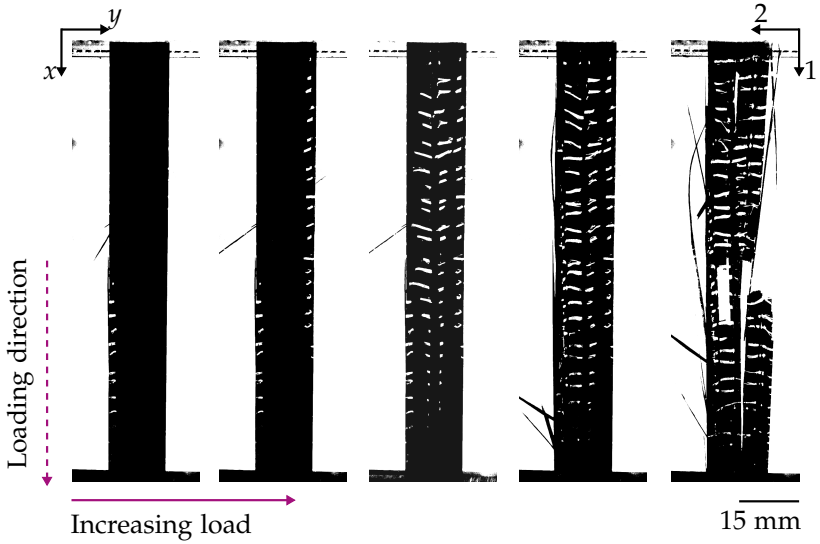


Figure 6.41: Damage evolution resulting from uniaxial tensile loading of continuous carbon fibre SMC. Failure was linked to inter-fibre fractures favoured due to fibre misalignment initiated at the edges.

Figure 6.42 depicts a representative stress-strain curve of the aforementioned failure type I of Co CF SMC, and significant points in stress-strain evolution are defined by the letters a – h. The corresponding images are shown in Figure 6.43. Failure is generally initiated at the edges, most likely due to misaligned fibre bundles (Figure 6.43 b and d). Failure progresses due to the growth of inter-fibre fractures and formation of new (inter-fibre) cracks (Figure 6.43 c, e, f and g).

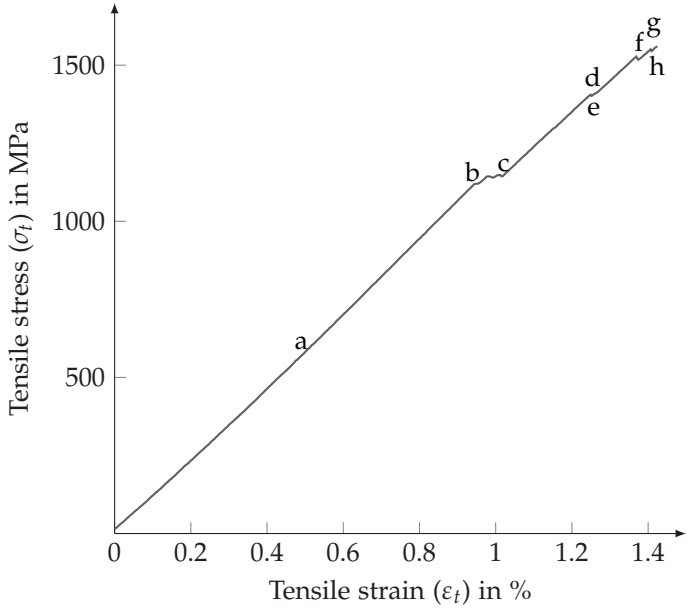


Figure 6.42: Representative tensile stress-strain curve of continuous carbon fibre SMC (Co CF SMC, 0°), which gradually failed. Images corresponding to points a – f are depicted in Figure 6.43.

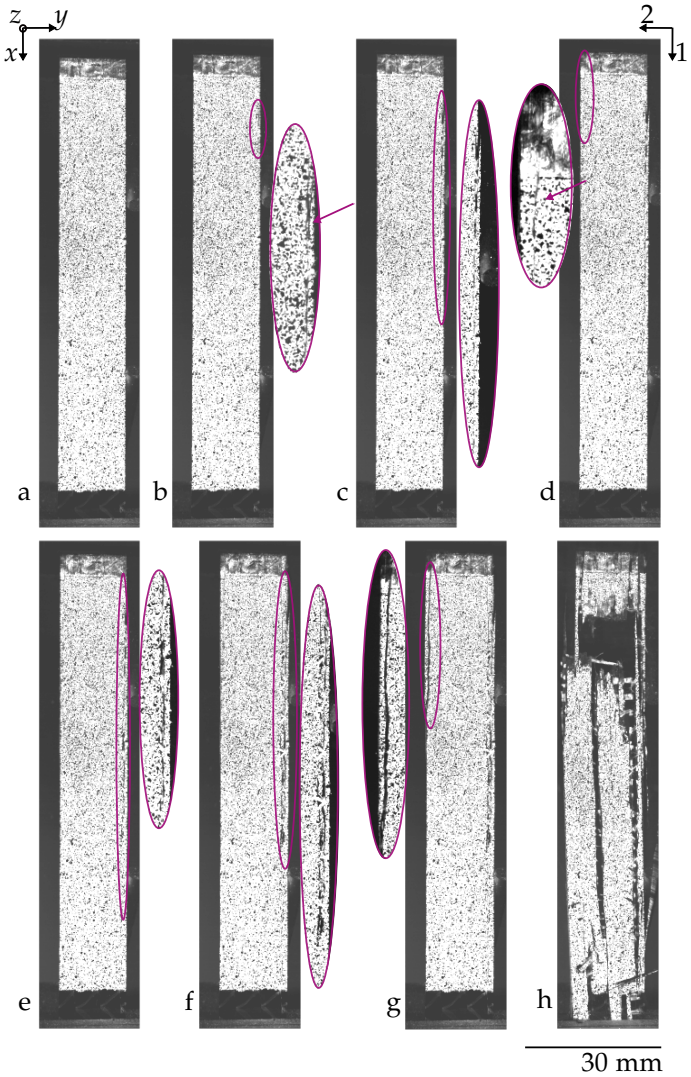


Figure 6.43: Damage evolution resulting from uniaxial tensile loading of continuous carbon fibre SMC in 0°, corresponding stress-strain response depicted in Figure 6.42. Arrows indicate locations of crack initiation.

The second type of failure of Co CF SMC was characterised by a spontaneous bursting of the specimen without indication and no preceding inter-fibre fractures visible at the macroscopic scale. A representative stress-strain evolution is depicted in Figure 6.44, and the strain fields corresponding to points A – F are shown in Figure 6.45. Uniaxial tension resulted in an anisotropic strain field considering strains in the $x-$ and $y-$ directions. Evolving strain fields were influenced by the paths of the stitching yarns (Figure 6.45) and were locally heterogeneous. Figure 6.46 summarises the failure mechanisms important to consider if continuous carbon fibre SMC is exposed to uniaxial tension.

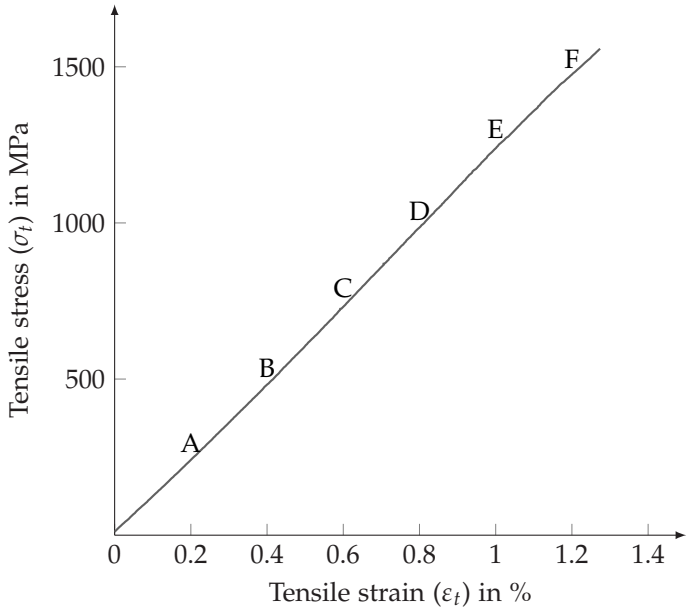


Figure 6.44: Representative tensile stress-strain curve of continuous carbon fibre SMC (Co CF SMC, 0°), which spontaneously failed. Corresponding strain fields in points A – F are depicted in Figure 6.41.

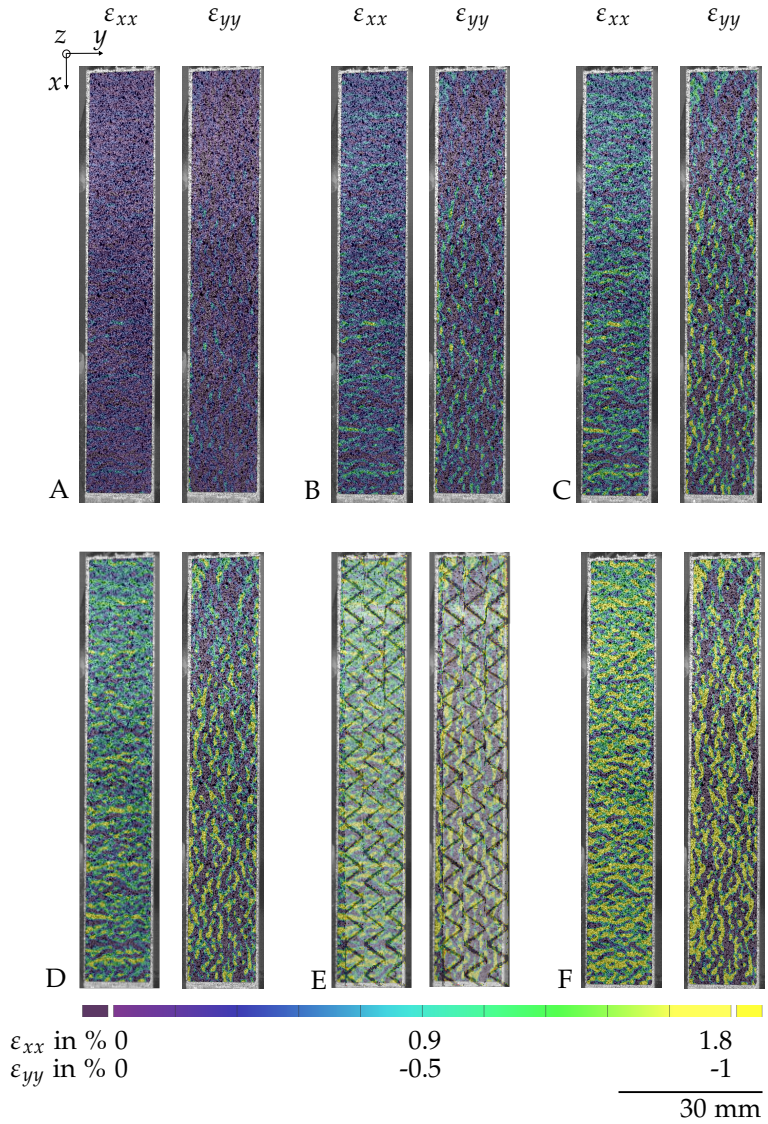


Figure 6.45: Evolution of strain field resulting from uniaxial tension of continuous carbon fibre SMC. E: resulting strain field with superposed pattern of stitching yarns.

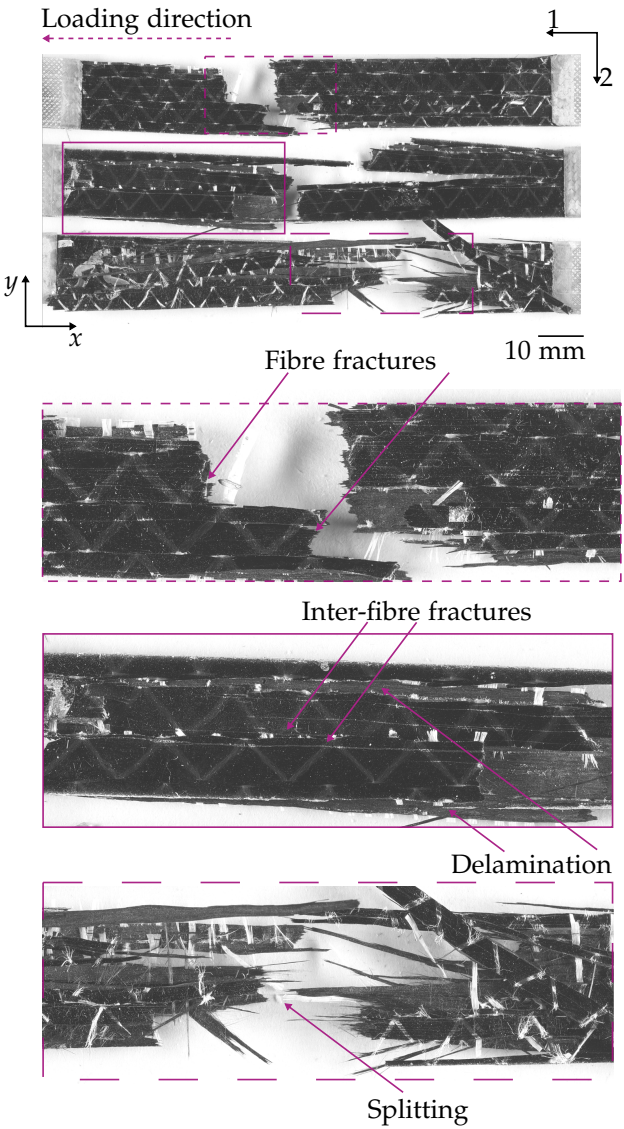


Figure 6.46: Macroscopic observation of fractured (post-mortem) continuous carbon fibre SMC specimens (0°), which were exposed to uniaxial tension (top view).

Uniaxial compression of Co CF SMC led to a linear increase of strain with increasing stress until fracture (Figure 6.40). The specimens failed abruptly at very low failure strains due the minimal load-bearing capacity of carbon fibres. Fibre buckling and fibre fractures dominated failure evolution. Compressive failure was also linked to delamination, and fractured specimens showed sheared layers of continuous carbon fibre SMC (Figure 6.47).

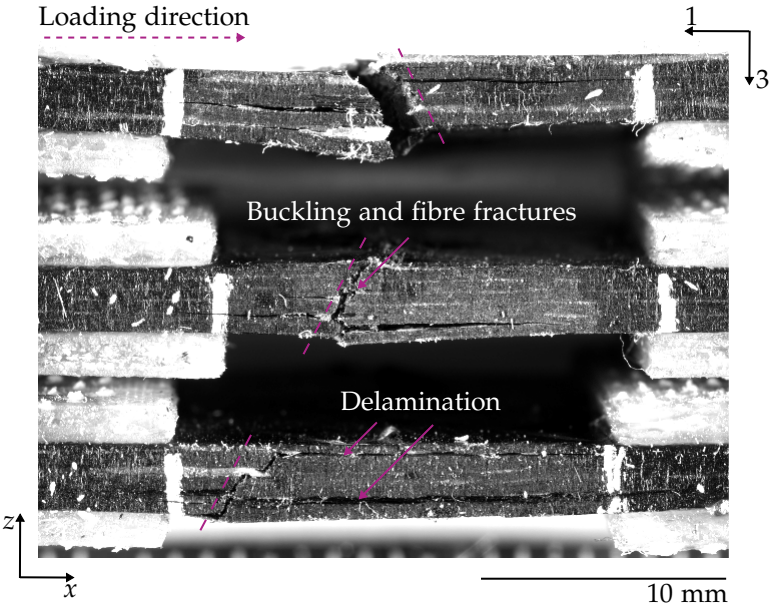


Figure 6.47: Macroscopic observation of fractured (post-mortem) continuous carbon fibre SMC specimens (0°), which were exposed to uniaxial compression (side view).

Tensile and compressive moduli of elasticity of Co CF SMC loaded perpendicular to fibre direction did not significantly differ (Figure 6.48). In addition, with respect to the pure UPPH resin, the fibrous

reinforcement did not lead to an enhanced tensile strength if loaded perpendicular to the fibres (Table 6.6). In general, tensile and compressive properties of Co CF SMC perpendicular to fibre direction were strongly determined by the properties of the UPPH resin. Compared to the pure resin specimens, elongation at tensile strength ($\varepsilon_{R,t}$) and elongation at (tensile) failure ($\varepsilon_{max,t}$) were significantly decreased due to the fibrous reinforcement (Figure 6.48).

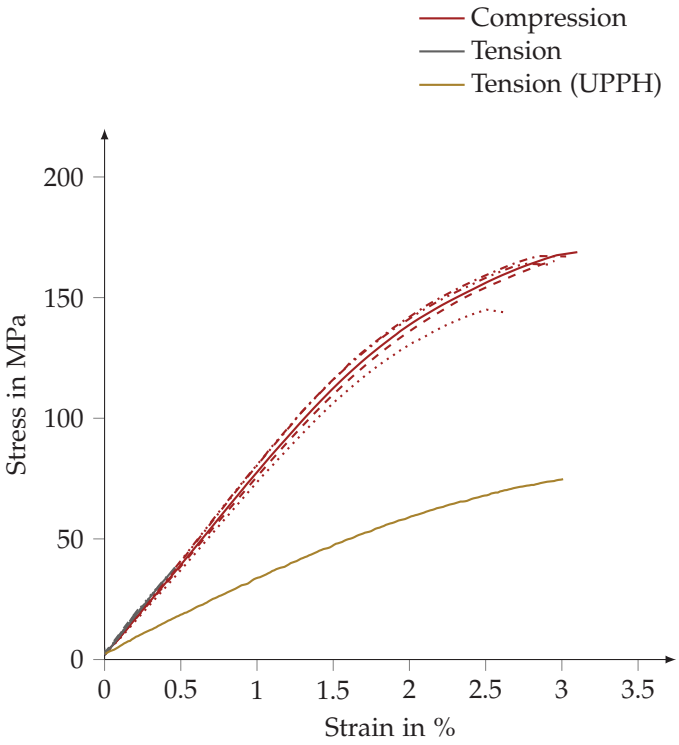


Figure 6.48: Stress-strain curves resulting from uniaxial tension and compression of continuous carbon fibre SMC (Co CF SMC) in 90° and representative stress-strain curve resulting from uniaxial tension of unsaturated polyester-polyurethane hybrid resin system.

Table 6.6: Tensile and compressive properties of continuous carbon fibre SMC with tensile and compressive modulus of elasticity (E_t and (E_c), Poisson's ratio (ν_t), tensile and compressive strength (R_t and R_c), elongation at tensile or compressive strength (ε_R) and failure strain (ε_{max}) corresponding to a decrease of sustained load to $0.8 \cdot F_{max}$ of the preceding F_{max}. Variable n indicates number of evaluated specimens.

		Tension 0°	Compression 0°	Tension 90°	Compression 90°
E		(n=19)	(n=5)	(n=11)	(n=8)
$\bar{x}$	in GPa	110.1	91.4	8.3	7.5
μ	in GPa	6.1	3.0	0.2	0.3
CV	in %	5.6	3.3	2.2	3.5
ν_t		(n=19)	-	(n=11)	-
$\bar{x}$	-	0.32	-	0.03	-
μ	-	0.02	-	0.02	-
CV	in %	5.3	-	52.0	-
R		(n=19)	(n=5)	(n=11)	(n=8)
$\bar{x}$	in MPa	1424	567	34	163
μ	in MPa	162	31	5	9
CV	in %	11.3	5.4	13.7	5.4
ε_R		(n=19)	(n=3)	(n=9)	(n=8)
$\bar{x}$	in %	1.3	0.6	0.4	2.9
μ	in %	0.1	0.1	0.1	0.2
CV	in %	6.8	9.3	25.4	7.3
ε_{max}		(n=19)	(n=3)	(n=9)	(n=8)
$\bar{x}$	in %	1.3	0.6	0.4	2.9
μ	in %	0.1	0.05	0.1	0.2
CV	in %	6.0	7.5	25.4	6.5

6.3.3.3 Tensile and compressive properties of continuous-discontinuous glass/carbon fibre SMC

In order to determine the effect of a continuous reinforcement of discontinuous glass fibre SMC, hybrid SMC sheets featuring a discontinuous glass fibre reinforced core and two continuously carbon fibre reinforced face sheets have been considered for tensile and compression testing. Allowing for a valuable comparison, mechanical testing was carried out with the same specimen geometry and testing parameters. Tensile and compressive properties of hybrid CoDico SMC mechanically loaded in fibre direction of the continuous reinforcement (0°) are depicted in Figure 6.49. Notably, in contrast to the pure discontinuous glass fibre SMC, the material flow during compression moulding affected the mechanical performance and flow region specimens of the hybrid SMC showed slightly lower tensile and compressive stiffness. Although the variations were not significant, they are a first indication that material flow of the discontinuous SMC composite may influence mechanical performance of hybrid SMC composites. The slight decrease in tensile strength ($-10\,\%$), observed for discontinuously reinforced SMC flow region specimens (Figure 6.26) was less important due to the hybridisation ($-5\,\%$). In addition, all aforementioned observations were superimposed by a significant scatter in experimental results. The hybrid CoDico GF/CF SMC composite was characterised by a tension-compression anisotropy with tensile modulus of elasticity and tensile strength being significantly higher than the compressive counterparts (Figure 6.49). With no distinction between charge and flow region specimens, $E_c \approx 0.87 \cdot E_t$ and $R_c \approx 0.55 \cdot R_t$ (Table 6.7). These variations reflect the material properties of the continuous carbon fibre SMC described in section 6.3.3.2, but are less pronounced. Whereas tensile modulus of elasticity and tensile strength showed a positive correlation, no

relation was observed in terms of uniaxial compression. If loaded perpendicular to the fibre direction of the continuous reinforcement (90°), tensile and compressive moduli showed no significant difference. Comparable to the properties of pure continuous carbon fibre SMC loaded perpendicular to fibre direction, compressive strength was higher than tensile strength (Figure 6.50).

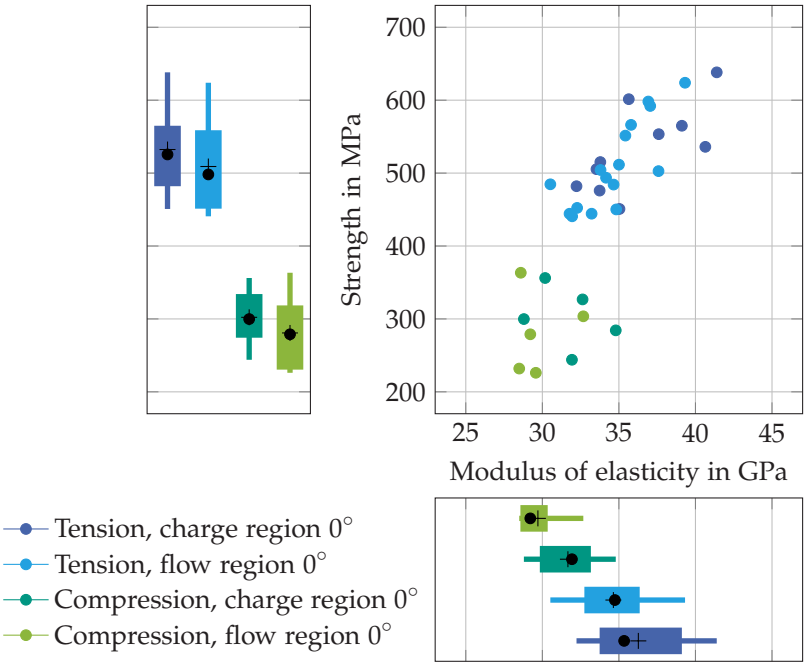


Figure 6.49: Tensile and compressive moduli of elasticity and tensile and compressive strength of continuous-discontinuous glass/carbon fibre SMC in fibre direction, 0°, (• = median, + = mean, box = 25^{th} to 75^{th} percentile; lines indicate minimum and maximum or 1.5 interquartile range, respectively).

Specimens extracted from the flow region in 90° showed marginally higher mechanical properties in terms of tensile stiffness and strength (Figure 6.50 and Table 6.8), as compared to charge region specimens.

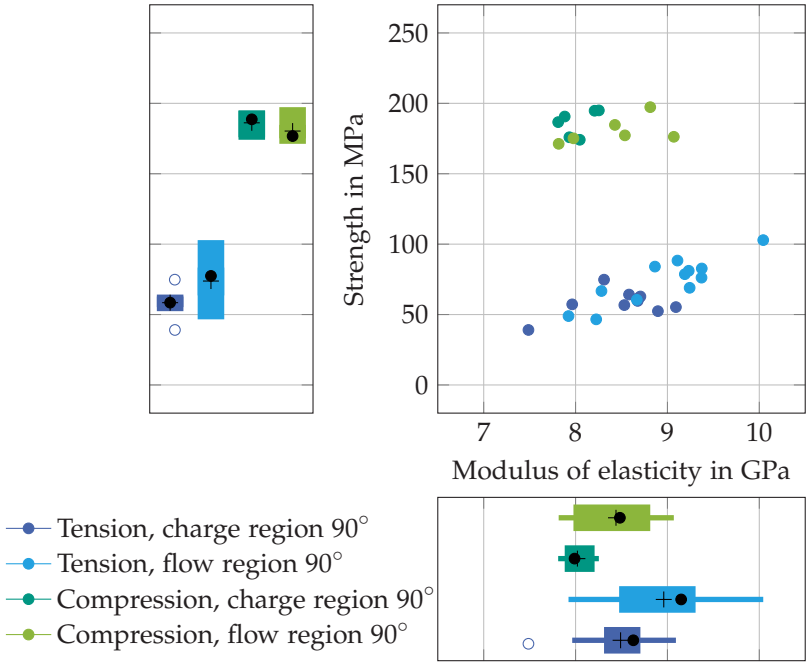


Figure 6.50: Tensile and compressive moduli of elasticity and tensile and compressive strength of continuous-discontinuous glass/carbon fibre SMC perpendicular to fibre direction, 90°, (• = median, + = mean, box = 25^{th} to 75^{th} percentile; lines indicate minimum and maximum or 1.5 interquartile range, respectively, ○ = outlier).

Specimens featuring a higher tensile modulus of elasticity also tended to show increased tensile strength, and a slight positive correlation was observed in terms of tensile loading. No correlation was observed between compressive modulus of elasticity and compressive strength.

Table 6.7: Tensile and compressive properties of continuous-discontinuous glass/carbon fibre SMC in fibre direction of the continuous component with tensile and compressive modulus of elasticity (E), Poisson's ratio (ν_t), tensile and compressive strength (R), elongation at tensile or compressive strength (ε_R) and failure strain (ε_{max}) corresponding to a decrease of sustained load to 0.8· preceding F_{max}. Variable n indicates number of evaluated specimens.

		Tension Charge region 0°	Tension Flow region 0°	Compression Charge region 0°	Compression Flow region 0°
E		(n=10)	(n=16)	(n=5)	(n=5)
$\bar{x}$	in GPa	36.3	34.6	31.7	29.7
μ	in GPa	3.2	2.4	2.3	1.7
CV	in %	8.9	6.9	7.3	5.8
ν_t		(n=10)	(n=16)	-	-
$\bar{x}$	-	0.37	0.37	-	-
μ	-	0.02	0.02	-	-
CV	in %	5.3	4.3	-	-
R		(n=10)	(n=16)	(n=5)	(n=5)
$\bar{x}$	in MPa	532	509	302	281
μ	in MPa	58.6	60.2	42.5	56.4
CV	in %	11.0	11.8	15.5	20.1
ε_R		(n=5)	(n=10)	-	-
$\bar{x}$	in %	1.5	1.5	-	-
μ	in %	0.1	0.1	-	-
CV	in %	8.6	5.8	-	-
ε_{max}		(n=5)	(n=10)	-	-
$\bar{x}$	in %	1.5	1.5	-	-
μ	in %	0.1	0.1	-	-
CV	in %	7.6	5.9	-	-

Table 6.8: Tensile and compressive properties of continuous-discontinuous glass/carbon fibre SMC perpendicular to fibre direction of the continuous component with tensile and compressive modulus of elasticity (E), Poisson's ratio (ν_t), tensile and compressive strength (R), elongation at tensile or compressive strength (ε_R) and failure strain (ε_{max}) corresponding to a decrease of sustained load to 0.8· preceding F_{max}. Variable n indicates number of evaluated specimens.

		Tension Charge region 90°	Tension Flow region 90°	Compression Charge region 90°	Compression Flow region 90°
E		(n=10)	(n=12)	(n=6)	(n=6)
$\bar{x}$	in GPa	8.5	9.0	8.0	8.4
μ	in GPa	0.5	0.6	0.2	0.5
CV	in %	5.5	6.7	2.2	5.7
ν_t		(n=10)	(n=12)	-	-
$\bar{x}$	-	0.1	0.1	-	-
μ	-	0.01	0.01	-	-
CV	in %	8.2	5.8	-	-
R		(n=10)	(n=12)	(n=6)	(n=6)
$\bar{x}$	in MPa	58	74	186	180
μ	in MPa	9.2	16.3	9.2	9.4
CV	in %	15.7	22.1	5.0	5.2
ε_R		(n=8)	(n=10)	(n=6)	(n=6)
$\bar{x}$	in %	1.0	1.2	3.0	2.7
μ	in %	0.2	0.3	0.2	0.2
CV	in %	24.6	25.6	6.8	7.8
ε_{max}		(n=8)	(n=10)	(n=6)	(n=6)
$\bar{x}$	in %	1.0	1.2	3.0	2.8
μ	in %	0.2	0.3	0.2	0.3
CV	in %	23.1	26.0	7.0	9.4

Figure 6.51 shows representative tensile stress-strain curves of hybrid CoDico GF/CF SMC in 0° and 90°. In qualitative terms, uniaxial tension in the fibre direction of the continuous component (0°) led to a stress-strain evolution comparable to the behaviour of pure continuously carbon fibre reinforced SMC. Hence, the continuous component determined the evolution of the stress-strain response. For some specimens, small load drops indicated, that failure evolved partially. However, final failure was characterised by an abrupt and brittle fracture of the specimens.

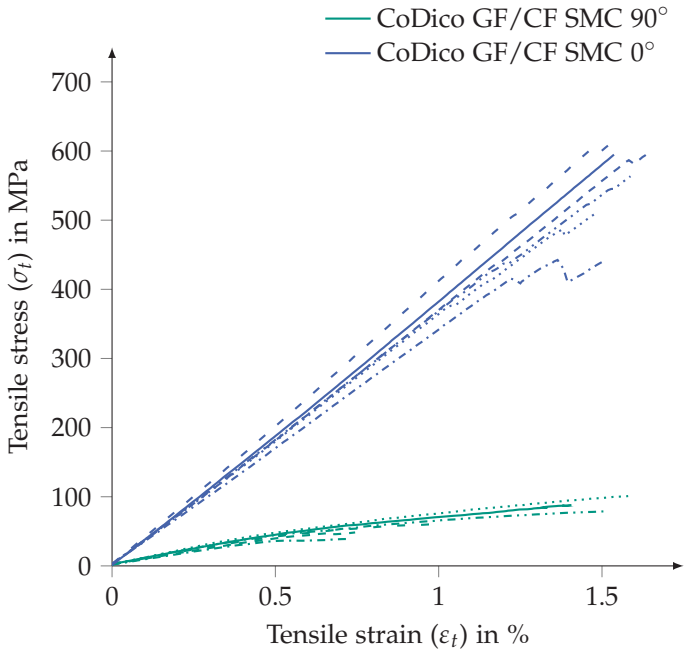


Figure 6.51: Representative stress-strain curves resulting from uniaxial tension of continuous-discontinuous glass/carbon fibre SMC (CoDico GF SMC) in 0° and 90°.

Loaded perpendicular to the fibre direction of the continuous component (90°), the stress-strain curve of hybrid CoDico GF/CF SMC showed a linear evolution up to an elongation of $\varepsilon_t \approx 0.5\,\%$, followed by a gradual decrease and brittle failure. The decrease in stiffness slightly reflected the behaviour of the discontinuous component. Assuming that the discontinuous core maintained tensile loads after failure of the continuous face sheets, hybridisation increased tensile strength and tensile failure strain compared to pure Co CF SMC (Figure 6.52).

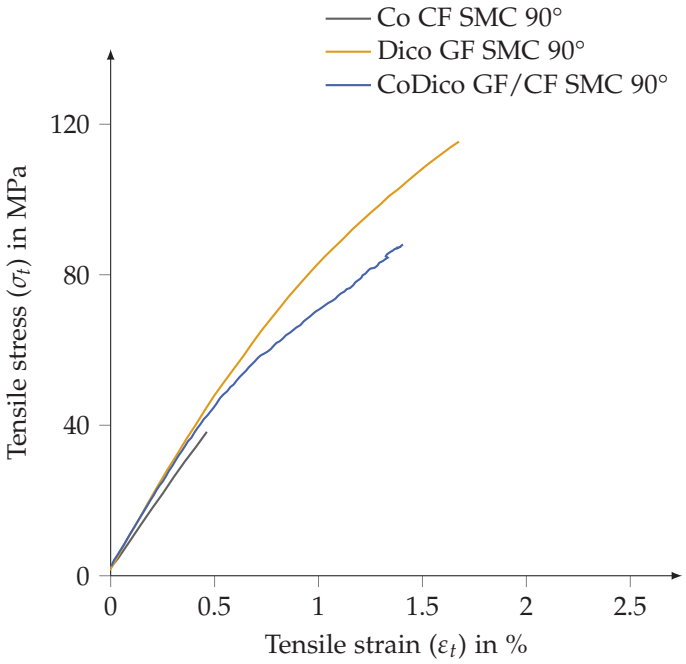


Figure 6.52: Representative stress-strain curves resulting from uniaxial tension of continuous carbon fibre SMC (Co CF SMC), discontinuous glass fibre SMC (Dico GF SMC) and continuous-discontinuous glass/carbon fibre SMC (CoDico GF/CF SMC) in 90°.

In the following, the damage evolution of a hybrid CoDico GF/CF SMC loaded in fibre direction of the continuous component (0°) is considered in detail. For this purpose, Figure 6.53 depicts a representative tensile stress-strain curve, and strain fields corresponding to distinct points (A – H) are shown in Figure 6.54.

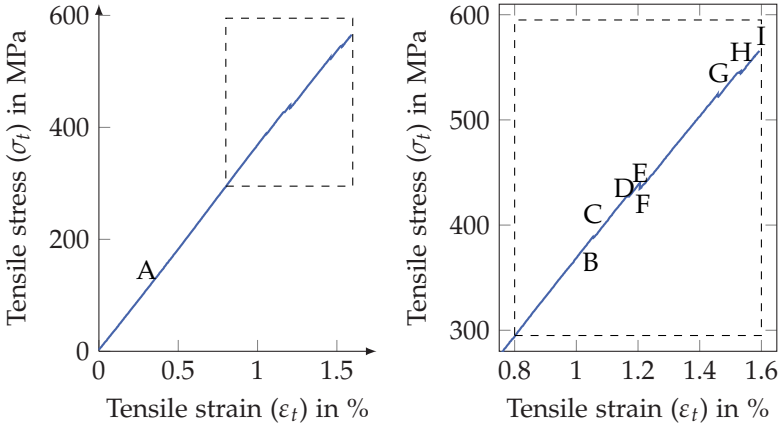


Figure 6.53: Representative $\sigma - \varepsilon$ curve resulting from uniaxial tension of continuous-discontinuous glass/carbon fibre SMC in 0°. Corresponding strain fields to points A – H are depicted in Figure 6.54.

As depicted in Figure 6.54, strains resulting from deformation in $x-$ and $y-$ directions (ε_{xx} and ε_{yy}) showed a homogeneous evolution at the beginning of loading (point A). As load increased, lateral strains (ε_{yy}) became highly heterogeneous (point B) and reflected the pattern of the stitching yarns (Figure 6.56). Strain localisations at the edges of the specimen indicate points of failure initiation (point C). In these mostly resin-rich regions, where continuous carbon fibre bundles were sheared and pushed apart during compression moulding such that the discontinuous glass fibre SMC was locally no longer reinforced, uniaxial tension led to elevated lateral strains.

Furthermore, the indicated sections were characterised by misaligned fibre bundles, coinciding with the edge of the specimen.

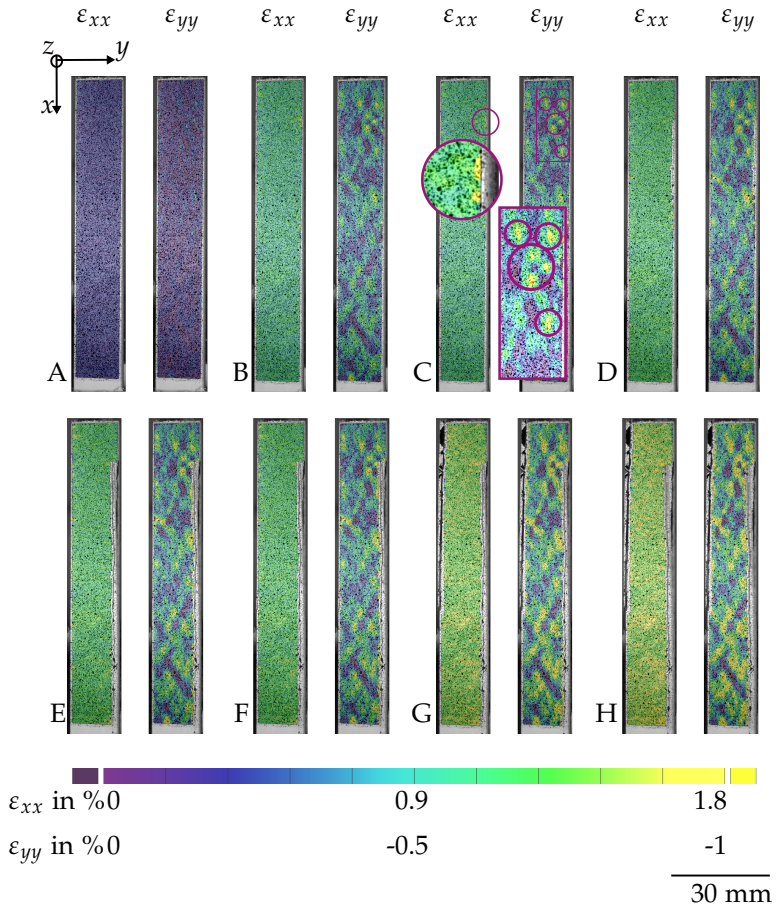


Figure 6.54: Evolving strain field resulting from uniaxial tension of continuous-discontinuous glass/carbon fibre SMC.

Figure 6.55 shows a representative CoDico SMC tensile specimen, which is characterised by fibre misalignment in the face sheets and resin-rich regions at the surface resulting from manufacturing.

Initiated by inter-fibre fracture, the sudden appearance and growth of cracks was linked to small load drops in the stress-strain curve, indicating partial failure of the specimen (point D). However, the specimen was still able to maintain further load, and the stress-strain curve still showed an increasing evolution. In the following, inter-fibre fractures propagated easily (Figure 6.54 points E – H). Crack propagation and splitting between individual carbon fibre bundles was linked to a macroscopic interlaminar delamination between the discontinuous and continuous component. With a further increase in load, the hybrid continuous-discontinuous SMC specimen was thus partially weakened, and the final macroscopic failure was marked by a brittle fracture based on fibre fractures of the continuous component and local failure of the discontinuous part due to pseudo-delamination (Figure 6.57).

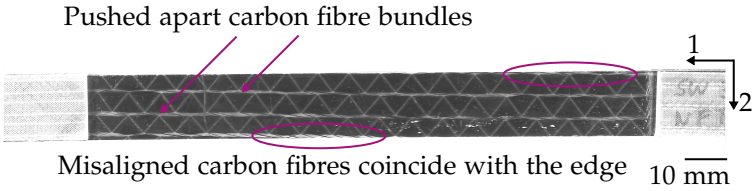


Figure 6.55: Representative tensile specimen of hybrid continuous/discontinuous glass/carbon fibre SMC specimens showing misaligned carbon fibres and pushed apart of carbon fibre bundles.

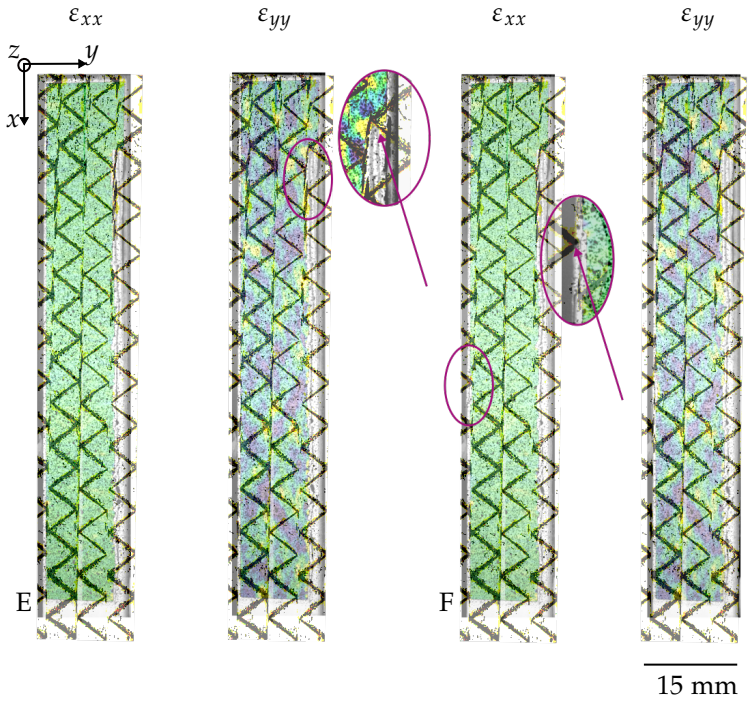


Figure 6.56: Superposition of strain field resulting from uniaxial tension of continuous-discontinuous glass/carbon fibre SMC with pattern of stitching yarns.

Figures 6.58 and 6.59 depict a side view and a top view of fractured (post-mortem) CoDico GF/CF SMC specimens. The multiple failure mechanisms described in the preceding section are clearly visible. In addition, delamination between the continuous and discontinuous component (interlaminar delamination) and within the continuous component (intralaminar delamination) can be clearly seen. In Figure 6.60, spalling of the matrix can also be identified as a result of evolving damage.

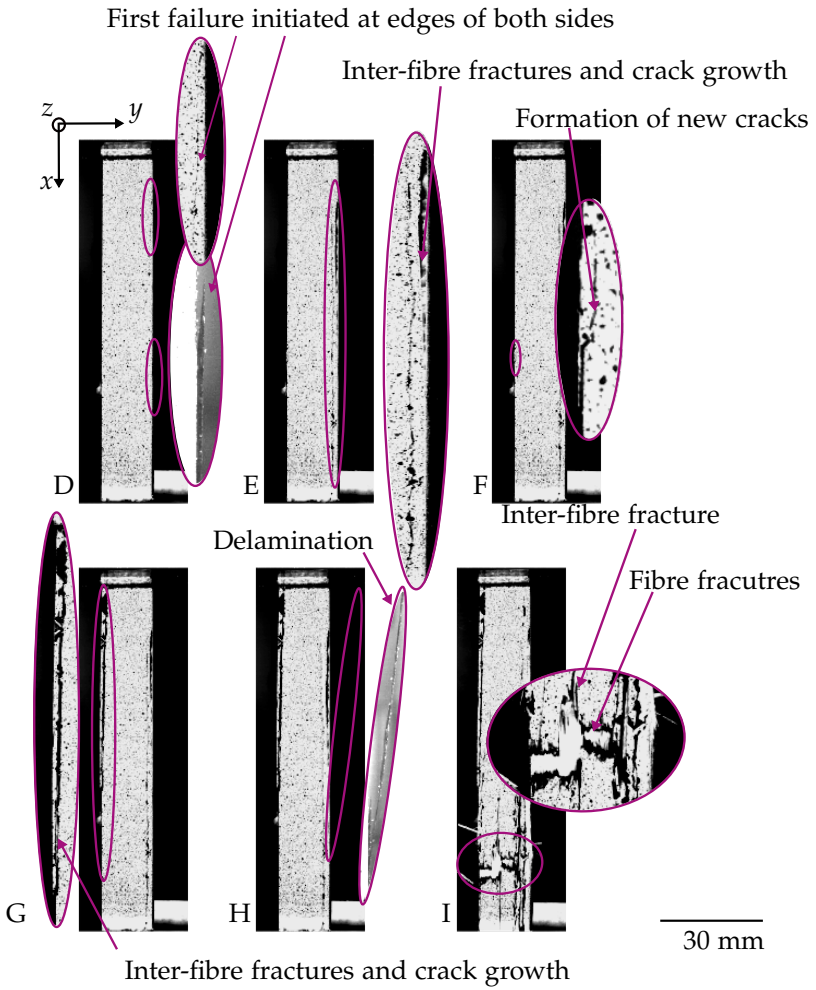


Figure 6.57: Damage evolution resulting from uniaxial tension of continuous-discontinuous glass/carbon fibre SMC.

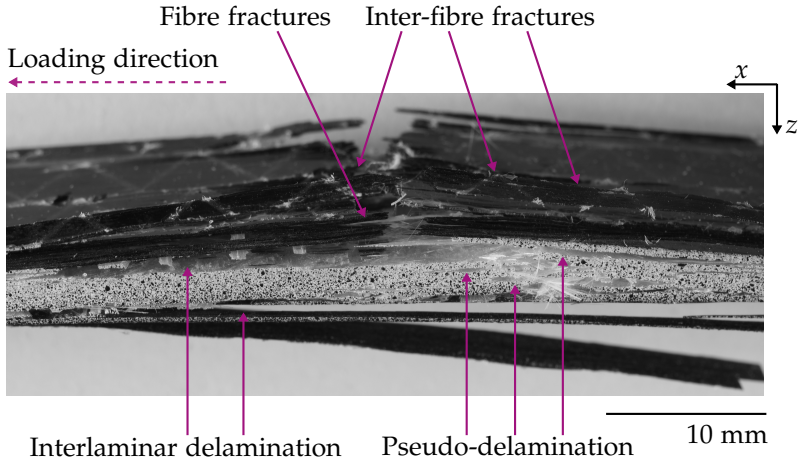


Figure 6.58: Fractured (post-mortem) hybrid continuous-discontinuous glass/carbon fibre SMC specimen which was exposed to uniaxial tension, side view.

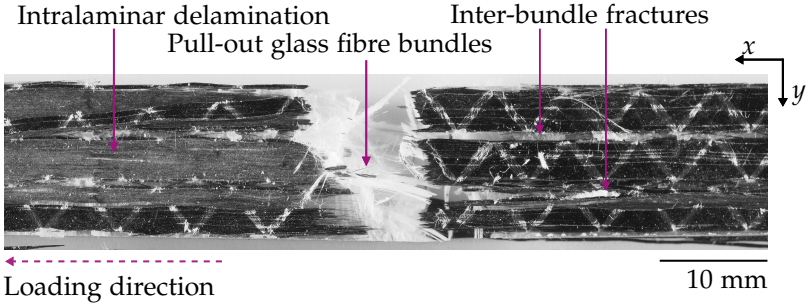


Figure 6.59: Fractured (post-mortem) hybrid continuous-discontinuous glass/carbon fibre SMC specimen which was exposed to uniaxial tension, top view.

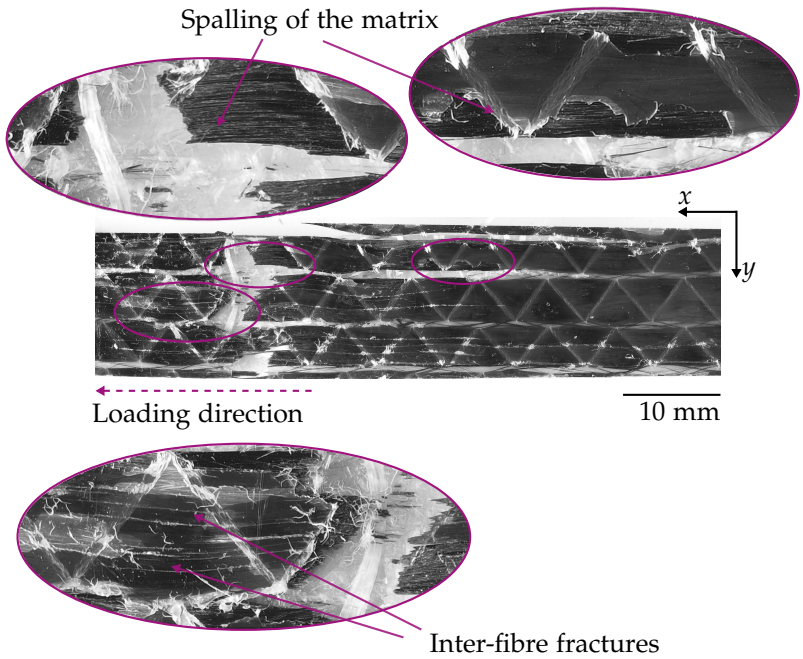


Figure 6.60: Fractured (post-mortem) hybrid continuous-discontinuous glass/carbon fibre SMC specimen which was exposed to uniaxial tension, top view (2).

Scanning electron microscopy (SEM) investigations of a post-mortem specimen showed that macroscopically visible inter-bundle fractures were accompanied by inter-fibre fractures of the continuous material (Figure 6.61 and Figure 6.62). In addition, matrix cracks, which grow perpendicular to the tensile direction, were present (Figure 6.61).

Interface failure between fibres and matrix as well as breakage of individual glass fibres determined failure of the discontinuous component in the transition zone. Within the core, the discontinuous material mainly failed due to intralaminar pseudo-delamination, hence matrix cracking and interface failure. Figure 6.61 depicts a fractured

CoDico SMC specimen with a higher magnification, which allows one to clearly identify inter-fibre fractures within the continuous component, not only present on a bundle scale but also separating individual carbon fibre filaments.

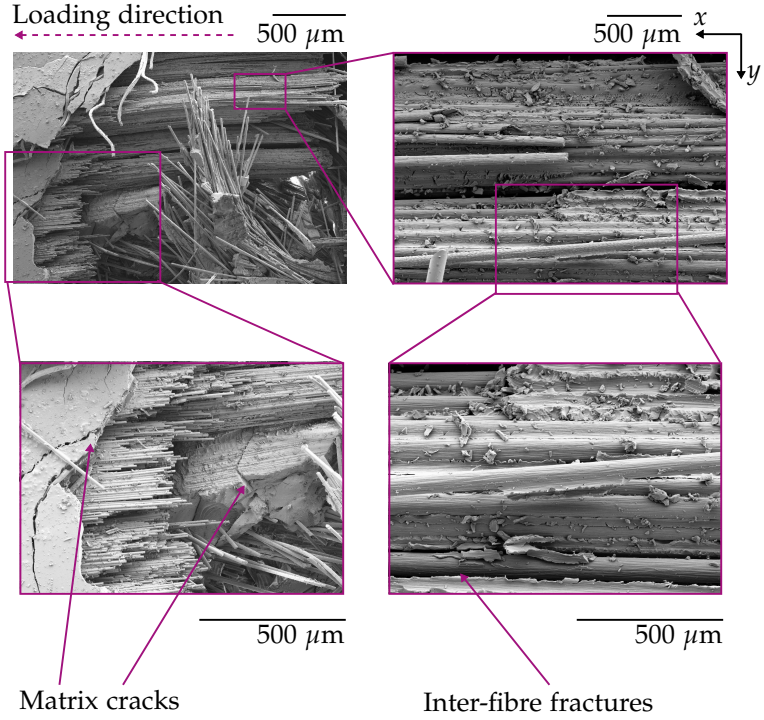


Figure 6.61: Detailed SEM observation of continuous component of fractured (post-mortem) continuous-discontinuous glass/carbon fibre SMC which was exposed to uniaxial tension.

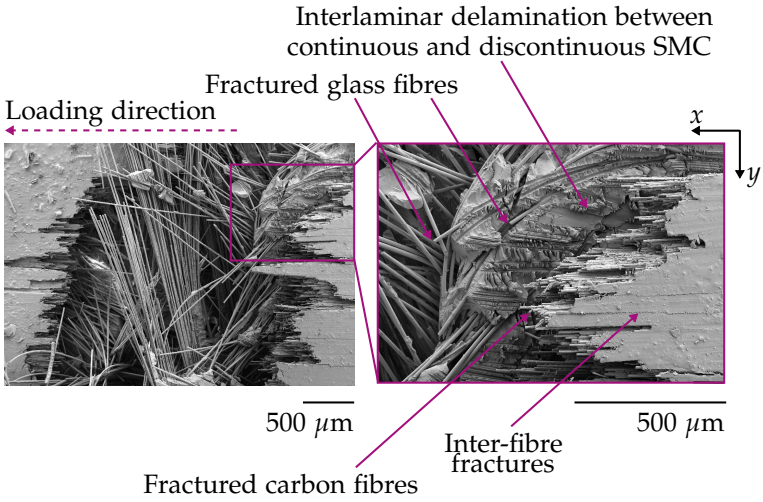


Figure 6.62: SEM investigation of fractured (post-mortem) continuous-discontinuous glass/carbon fibre SMC specimen which was exposed to uniaxial tension.

In the following, the damage evolution and failure mechanisms of hybrid CoDico SMC exposed to uniaxial compression are described. The representative stress-strain curve depicted in Figure 6.63 refers to the displacement of the crosshead. Due to the early and partial failure of the continuous face layers, strain measurement with the tactile clip-on extensometer was not possible until fracture.

Comparable to the presentation of damage evolution resulting from uniaxial tension, strain fields corresponding to significant points of the representative compressive stress-strain curve are shown in Figure 6.64.

If CoDico SMC (0°) was exposed to uniaxial compression, the resulting strain field was slightly heterogeneous before first failure was initiated (point A). In addition, the triangular shape of local strain

concentrations reflected the pattern of the stitching yarns (Figure 6.65 point A). Damage was initiated by an abrupt failure of continuous carbon fibre bundles due to fibre fractures (point B) visible on the macroscopic scale. The fibre fractures were followed by an inter-fibre failure between different fibres, preferably between different fibre bundles (point B and C). Fractured fibres led to a local inter-laminar delamination (point D), to a spalling of the matrix and to a progressive weakening of the specimen, which started to bend slightly (point E). If the applied load exceeded the residual compressive strength of the laminate, final failure was suddenly initiated. It could mainly be characterised by intralaminar pseudo-delamination of the discontinuous glass fibre SMC (point F). Localisation of fibre and inter-fibre fractures as well as crack propagation were linked to the pattern of the stitching yarns (Figure 6.65 point F).

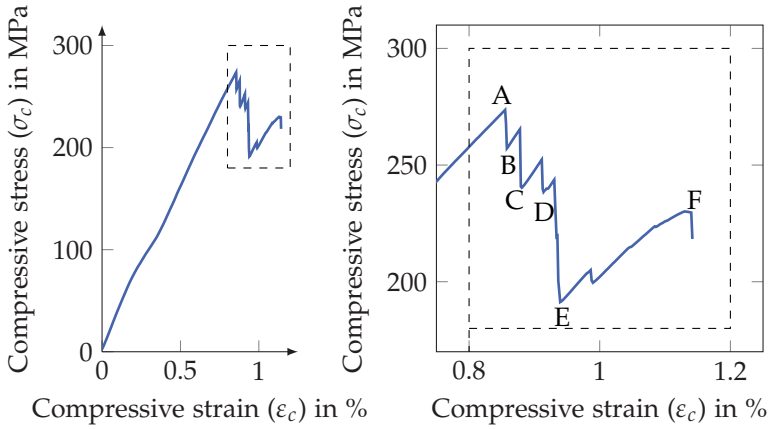


Figure 6.63: Representative stress-strain curve resulting from uniaxial compression of continuous-discontinuous glass/carbon fibre SMC. Corresponding strain fields in points A – F depicted in Figure 6.64 and magnification of selected strain fields in Figure 6.65.

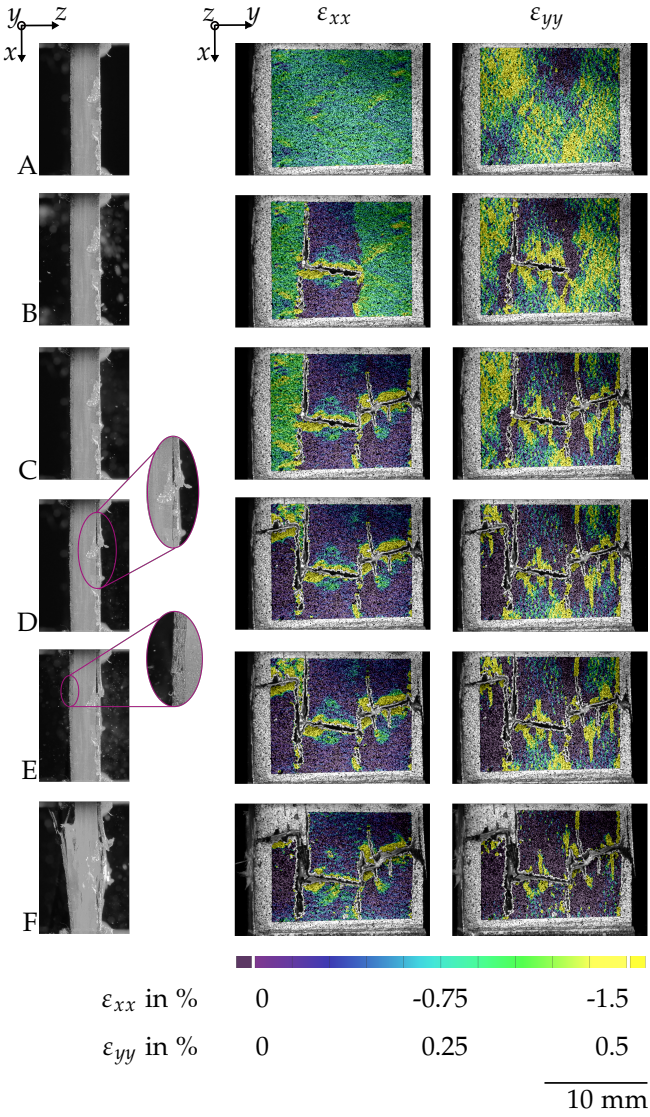


Figure 6.64: Evolving strain fields and damage evolution (side and top view) resulting from uniaxial compression of continuous-discontinuous glass/carbon fibre SMC.

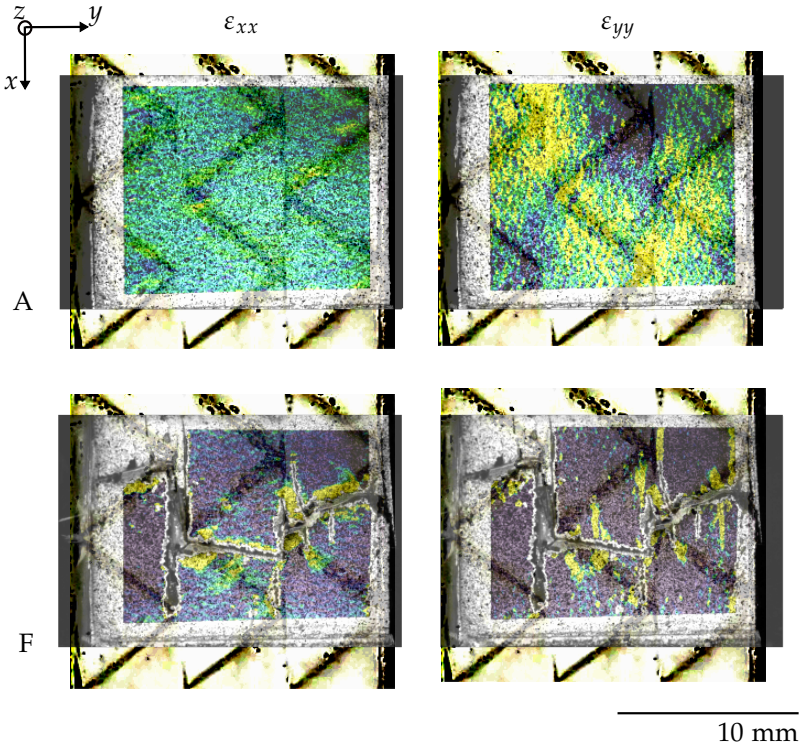


Figure 6.65: Strain field resulting from uniaxial compression of hybrid continuous-discontinuous glass/carbon fibre SMC superposed by localisation and pattern of stitching yarns, magnification of selected images of Figure 6.64.

Post-mortem observations of hybrid CoDico SMC specimens enabled clear identification of the different stages of failure resulting from uniaxial compression.

In Figure 6.66, the location of fibre fractures and resulting crack propagation paths are clearly visible. Uniaxial compressive loading also led to a localised spalling of the matrix. A side-view of fractured

specimens (Figure 6.67) clearly depicts delamination between the continuous and discontinuous component (interlaminar delamination), resulting from early fibre breakage of the continuous face layers (Figure 6.64: points D – F). Failure of the Dico GF SMC in the core of the hybrid CoDico was defined by shearing and pseudo-delamination.

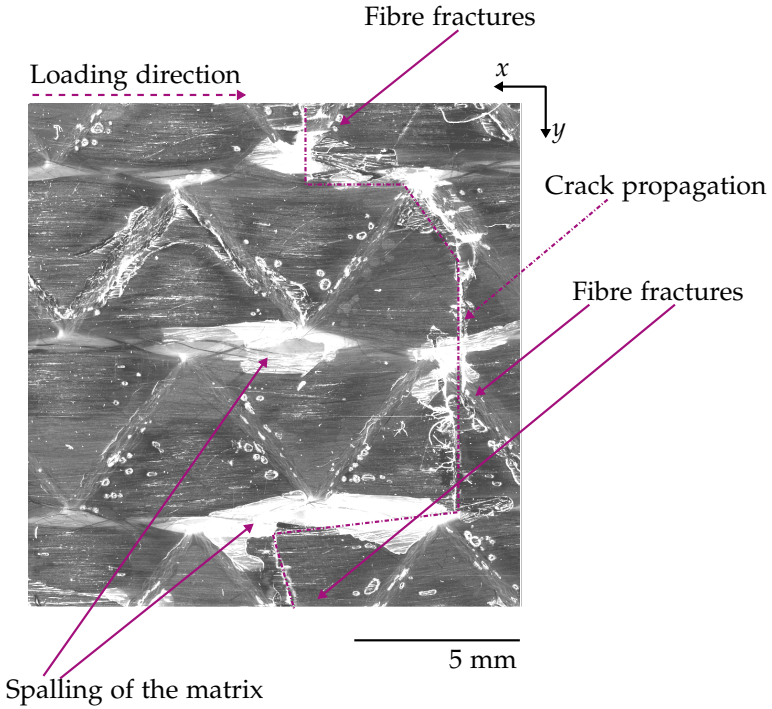


Figure 6.66: Fractured (post-mortem) continuous-discontinuous glass/carbon fibre SMC specimen, which was exposed to uniaxial compression, top view.

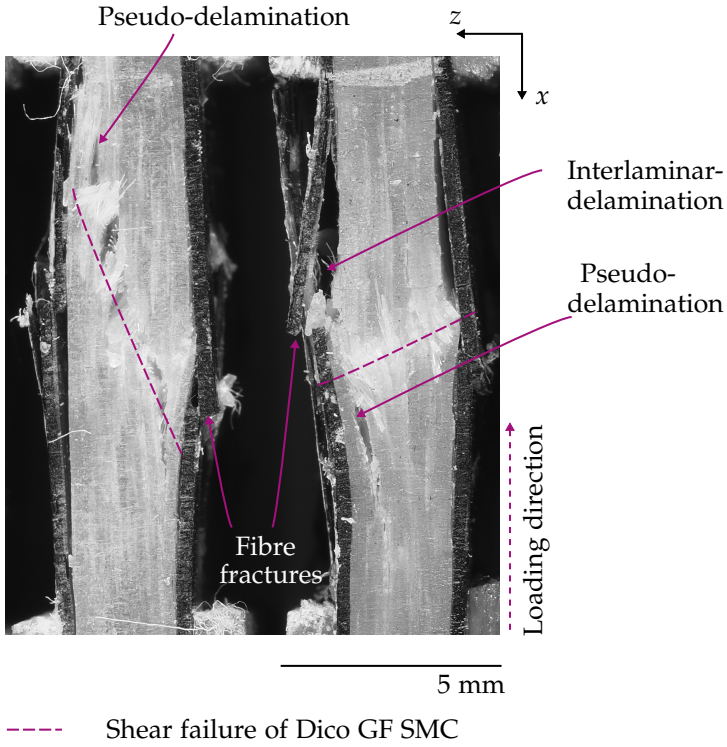


Figure 6.67: Fractured (post-mortem) continuous-discontinuous glass/carbon fibre SMC specimens, which were exposed to uniaxial compression, side view.

6.3.4 Out-of-plane loading of SMC composites

The following section presents the flexural properties of discontinuous glass fibre SMC, continuous carbon fibre SMC and hybrid continuous-discontinuous glass/carbon fibre SMC. In addition, damage mechanisms and failure evolution of the considered SMC materials exposed to out-of-plane loads are displayed.

6.3.4.1 Flexural properties of discontinuous glass fibre SMC

Discontinuous glass fibre SMC exhibited a flexural modulus of elasticity of 12.6 GPa (μ = 0.8 GPa, CV = 6.4%). Hence no difference in material stiffness compared to in-plane loadings was observed. With an average tensile strength of 283 MPa, R_t<R_f<R_c holds true. The superposition of tensile and compressive strains resulting from out-of-plane loadings explains this finding. Discontinuous glass fibre SMC exposed to three-point bending loadings was able to maintain high deflections. However, deviation between strain at flexural strength ($\varepsilon_{R,f}$) and strain at failure ($\varepsilon_{max,f}$) was marginal (Table 6.5), indicating brittle failure.

Figure 6.68 shows a representative stress-strain response resulting from three-point bending of Dico GF SMC.

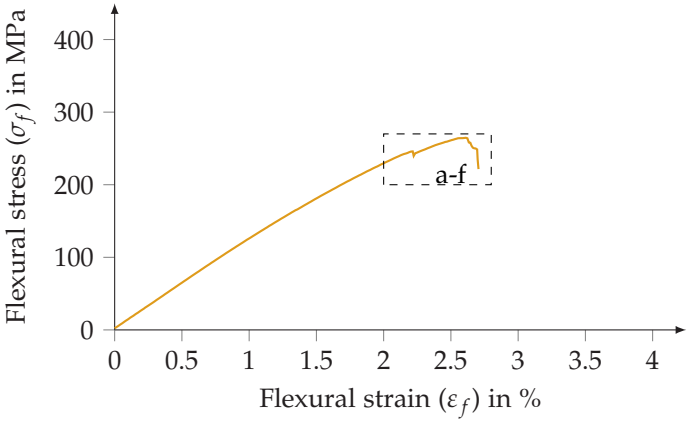


Figure 6.68: Representative stress-strain curve resulting from three-point bending of discontinuous glass fibre SMC.

In Figure 6.69, failure evolution shortly prior to final fracture is displayed. Flexural loading initially led to failure resulting from tensile strains at the lower side of the specimen (point b), characterised by a chipping off of the boundary layers (Chaturvedi et al., 1983) (point c). With a further increase in load, crack propagation preferably in the thickness direction of the specimen was observed (point d) leading to a loss of load-bearing capacities and a gradual stiffness decrease in the stress-strain curve. The formation of cracks within the specimen and an abrupt failure due to intra-laminar delamination (in-plane failure) (points e and f) marked the final failure of discontinuous glass fibre SMC specimens exposed to flexural loads.

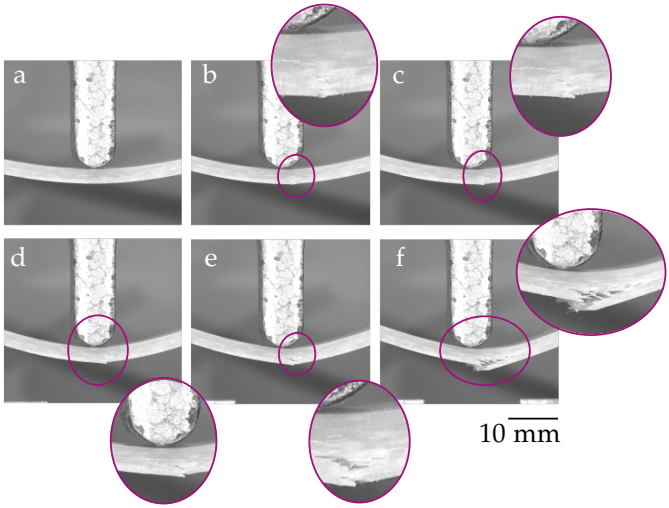


Figure 6.69: Failure evolution of discontinuous glass fibre SMC exposed to three-point bending, side view.

6.3.4.2 Flexural properties of continuous carbon fibre SMC

Continuous carbon fibre SMC was very sensitive to shear failure if span-to-thickness ratio was not sufficiently large (Figure 6.5). For the considered span-to-thickness ratio of 32:1, investigations led to a flexural modulus which featured only approximately 0.9 of the stiffness resulting from tensile loadings ($\bar{x}$ = 101.3 GPa). It is thus critical to say whether the determined value can be considered as flexural modulus of elasticity or should better be described as apparent flexural modulus of elasticity, with a higher span-to-thickness ratio possibly leading to a value closer to the tensile modulus of elasticity of the material. However, an increase in span-to-thickness ratio to 40:1 only slightly increased flexural modulus of elasticity, and given the observed variations, this increase was not significant. The flexural strength of continuous carbon fibre SMC was not as high as the tensile strength of the material, but it significantly exceeded compressive strength, indicating the simultaneous presence of tensile and compressive stresses and strains.

Figure 6.70 depicts representative stress-strain curves of continuous carbon fibre SMC exposed to three-point bending, and Figure 6.71 demonstrates significant points of failure evolution shortly prior to failure.

Continuous carbon fibre SMC exhibited generally a linear stress-strain response if exposed to bending loads, and failure was linked to an abrupt load drop. No significant variation between strain at flexural strength ($\varepsilon_{R,f}$) and flexural failure strain ($\varepsilon_{max,f}$) was observed (Table 6.9). Failure was initiated by fibre fractures due to compressive stresses at the upper side of the specimen (point a). The initiation of failure was linked with a load drop in the stress-strain evolution;

however, specimens were still able to maintain load. With increasing deflection and hence loading, fibre breakage and kinking became more important (point b). A crack below the loading nose formed (point c) and propagated in thickness direction of the specimen linked to localised delamination (points c – f).

Table 6.9: Flexural properties of continuous carbon fibre SMC in fibre direction (0°) for a span-to-thickness ratio of 32:1, with flexural modulus of elasticity (E_f), flexural strength (R_f), elongation at flexural strength ($\varepsilon_{R,f}$) and flexural failure strain ($\varepsilon_{max,f}$) corresponding to a decrease of sustained load to 0.8· preceding F_{max}. Variable n indicates number of evaluated specimens n.

E_f		(n=6)	R_f		(n=6)
$\bar{x}$	in GPa	101.3	$\bar{x}$	in MPa	947
μ	in GPa	3.8	μ	in MPa	62
CV	in %	3.7	CV	in %	6.5

$\varepsilon_{R,f}$		(n=6)	$\varepsilon_{max,f}$		(n=6)
$\bar{x}$	in %	0.94	$\bar{x}$	in %	1.0
μ	in %	0.1	μ	in %	0.1
CV	in %	7.7	CV	in %	13.0

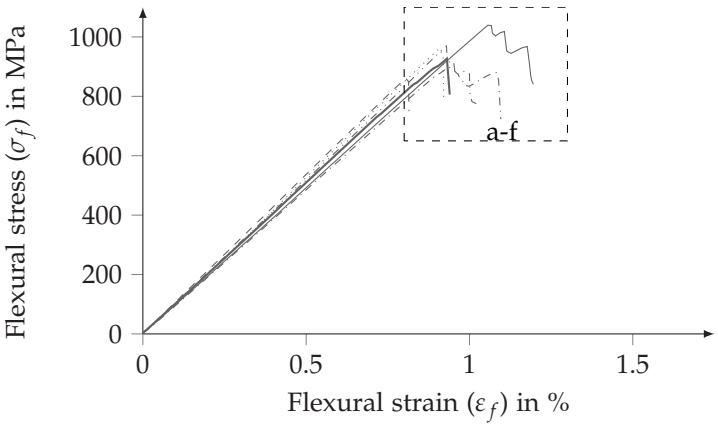


Figure 6.70: Representative stress-strain curves resulting from three-point bending of continuous carbon fibre SMC in fibre direction (0°).

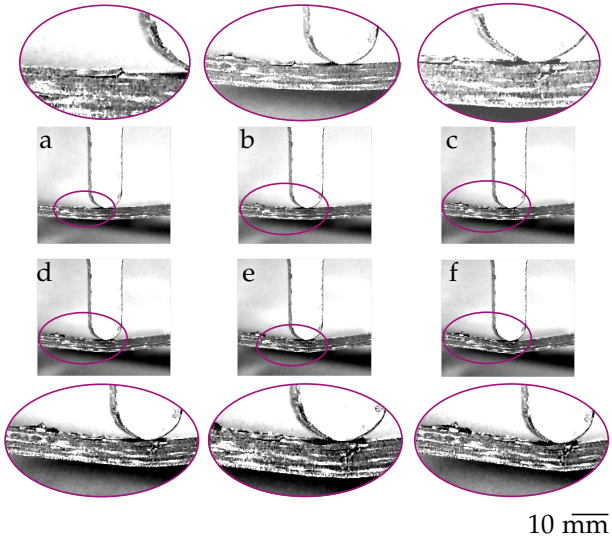


Figure 6.71: Failure evolution of continuous carbon fibre SMC exposed to three-point bending, side view.

6.3.4.3 Flexural properties of continuous-discontinuous glass/carbon fibre SMC

The flexural properties of hybrid CoDico SMC were determined by means of three-point bending tests with the same test setup and specimen geometry considered for the individual materials. Mechanical material properties are summarised in Table 6.10. Figure 6.72 depicts representative stress-strain curves of CoDico GF/CF SMC resulting from three-point bending and Figure 6.73 presents significant points of failure evolution. Exposed to flexural loads, CoDico GF/CF SMC showed a linear stress-strain evolution comparable to continuous carbon fibre SMC; hence the continuous face layers dominated resulting material behaviour. After reaching flexural strength, specimens showed an abrupt damage, and strain at flexural strength ($\varepsilon_{R,f}$) was approximately the same as the defined failure strain ($\varepsilon_{max,f}$). Flexural failure of hybrid CoDico SMC was initiated by fibre breakage of the continuous carbon fibres on the upper side of the specimen due to compressive stresses (point a). Failure progressed with local interlaminar delamination (point b) and fibre breakage on the lower surface (point c). The discontinuous glass fibre core layer partially failed (point d), most likely due to compressive failure, since it was locally no longer reinforced due to the failure and delamination of the continuous carbon fibre reinforced layer at the upper surface. Subsequently, tensile stresses led to tensile failure on the lower surface of the continuous carbon fibre SMC, which was also linked to delamination (Figure 6.73 d and e). At the end of the loading, the continuous component failed abruptly and in a highly localised manner, marked by fibre fractures and splitting in the lower surface. The glass fibre reinforced core layers remained almost intact, since the continuous carbon fibre reinforced shell layers received the majority of the load until failure (Dong and Davies, 2012).

Table 6.10: Flexural properties of continuous-discontinuous glass/carbon fibre SMC (0°) for a span-to-thickness ratio of 32:1, with flexural modulus of elasticity (E_f), flexural strength (R_f), elongation at flexural strength ($\varepsilon_{R,f}$) and flexural failure strain ($\varepsilon_{max,f}$) corresponding to a decrease of sustained load to 0.8· preceding F_{max} (*for one considered specimen load dropped only to 0.83·F_{max}). Variable n indicates number of evaluated specimens.

E_f		(n=6)	R_f		(n=6)
$\bar{x}$	in GPa	59.3	$\bar{x}$	in MPa	570
μ	in GPa	4.4	μ	in MPa	75
CV	in %	7.4	CV	in %	13.2

$\varepsilon_{R,f}$		(n=6)	$\varepsilon_{max,f}$		(n=6)*
$\bar{x}$	in %	1.0	$\bar{x}$	in%	1.1
μ	in %	0.2	μ	in %	0.2
CV	in %	14.4	CV	in %	22.2

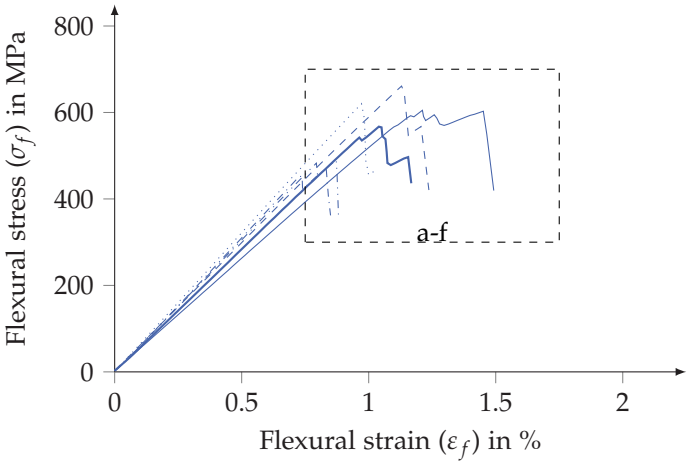


Figure 6.72: Representative stress-strain curves resulting from three-point bending of continuous-discontinuous glass/carbon fibre SMC.

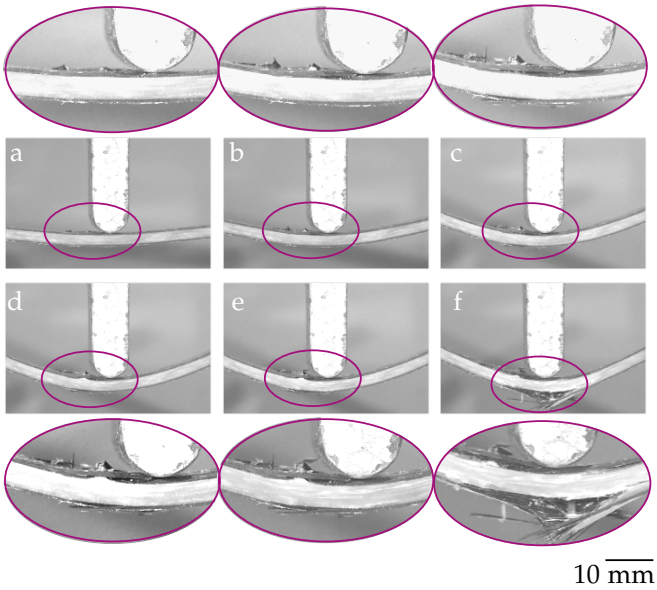


Figure 6.73: Failure evolution of continuous-discontinuous glass/carbon fibre SMC exposed to three-point bending, side view.

6.4 Mechanical properties and failure at the structure level

In the following section, the mechanical properties and damage evolution resulting from quasi-static and dynamic puncture are presented. Attention falls mainly on the interaction of damage mechanisms and the stress-strain responses of the different SMC composites resulting from puncture loading. Puncture properties were evaluated in terms of maximum sustained load (referred to as maximum load or strength, F_{max}) and puncture energy (E_p), which equals the absorbed

energy of the specimen during quasi-static or dynamic loading. Puncture energy was computed as follows

$$E_p = \int_0^{x_p} F dx, \tag{6.2}$$

with the force F and the deflection x. A numerical approximation of this integration was completed by applying a trapezoid rule. To mitigate or eliminate the aspect of friction between the striker and the punctured surface, the puncture energy was calculated up to the puncture deflection (x_p) according to EN ISO 6603-2 (2000). Within this ISO standard x_p is defined as the position at which the instantaneous measured load is half of the precedent maximum load occurred during puncture. In addition, energy at maximum load ($E_{F_{max}}$) was calculated, taking into account Equation 6.2 within the bounds $0 < x < x_{F_{max}}$. In the dynamic loading case, the filtered force-deflection response was considered to calculate puncture energy and to define the maximum sustained load of the specimen.

6.4.1 Puncture properties of discontinuous glass fibre SMC

For structural observations, charge and flow region specimens of discontinuous glass fibre SMC have been considered. Investigations of rate dependent behaviour were based on puncture testing carried out in quasi-static and dynamic manner. Maximum load, puncture energy, energy at maximum load and corresponding deflections have been evaluated and are presented in Figure 6.74 and Table 6.11.

Table 6.11: Quasi-static and dynamic puncture properties of discontinuous glass fibre SMC.

		Charge region Quasi-static	Flow region Quasi-static	Charge region Dynamic	Flow region Dynamic
S		(n=6)	(n=6)	(n=6)	(n=6)
$\bar{x}$	in N mm^{-1}	421	434	993	1009
μ	in N mm^{-1}	51	49	122	75
CV	in %	12.1	11.3	12.3	7.5
F_{max}		(n=6)	(n=6)	(n=6)	(n=6)
$\bar{x}$	in N	2849	3003	4533	4812
μ	in N	277	268	767	407
CV	in %	9.7	8.9	16.9	8.5
$E_{F_{max}}$		(n=6)	(n=6)	(n=6)	(n=6)
$\bar{x}$	in J	14.5	11.9	16.8	18.2
μ	in J	1.7	1.6	3.9	3.0
CV	in %	11.9	13.3	23.3	16.5
E_p		(n=6)	(n=6)	(n=6)	(n=6)
$\bar{x}$	in J	23.8	23.2	35.3	35.1
μ	in J	2.6	1.6	5.4	2.1
CV	in %	10.8	6.9	15.2	6.0
$d_{F_{max}}$		(n=6)	(n=6)	(n=6)	(n=6)
$\bar{x}$	in mm	7.3	6.8	8.0	7.9
μ	in mm	1.0	0.3	0.4	0.5
CV	in %	13.1	3.6	4.9	6.0
d_{E_p}		(n=6)	(n=6)	(n=6)	(n=6)
$\bar{x}$	in mm	13.4	12.4	13.5	12.7
μ	in mm	0.8	0.4	0.6	0.7
CV	in %	5.7	3.0	4.6	5.8

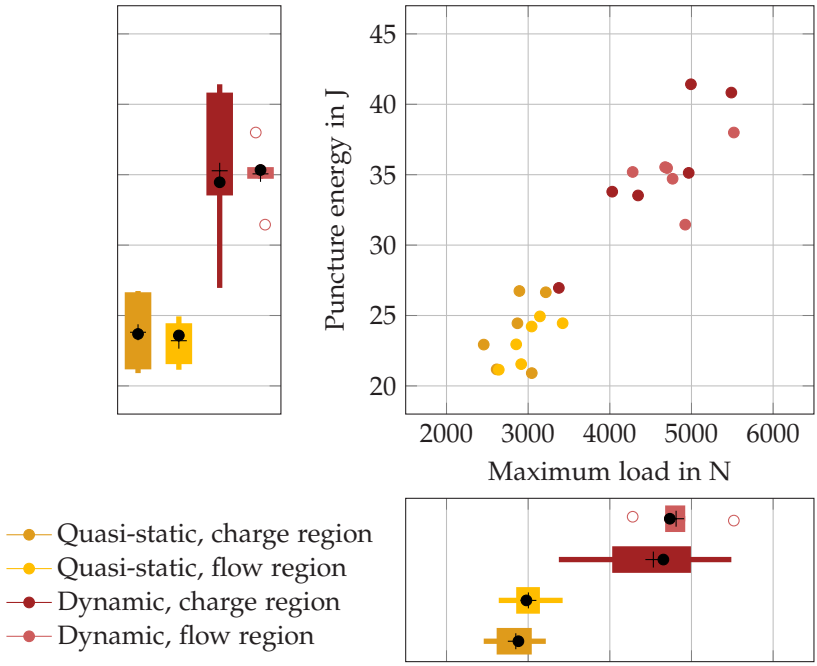


Figure 6.74: Quasi-static and dynamic puncture properties of discontinuous glass fibre SMC (• = median, + = mean, box indicates 25^{th} to 75^{th} percentile; lines indicate minimum and maximum or 1.5 interquartile range, respectively; ○ = outlier).

Maximum load and puncture energy of Dico GF SMC did not significantly differ for charge, as compared to flow region specimens. Mechanical performance showed higher scatter in terms of a dynamic puncture. With an increase of 60 % in maximum sustained load, Dico GF SMC exhibited positive rate dependence. Energy absorption capability (E_p) showed an increase of 48 % and 51 % for charge or flow region specimens, respectively. Specimens, which sustained a high load during quasi-static or dynamic puncture also showed higher energy absorption capability (Figure 6.74). No significant difference was observed considering deflection at maximum load and puncture

deflection, regardless of puncture velocity and specimen type. The slope of the load-deflection response was fitted by a least squares fit (as presented in section 4.2.2.1) in the range of $1 < d < 2$ to evaluate the puncture stiffness (S). In the dynamic loading case, the slope of force-deflection response was fitted in the same manner, beyond the dynamic offset in the same deflection range. With an increase from $427\,\mathrm{N\,mm^{-1}}$ ($\mu = 48\,\mathrm{N\,mm^{-1}}$, CV = 11.2 %) to $1001\,\mathrm{N\,mm^{-1}}$ ($\mu = 97\,\mathrm{N\,mm^{-1}}$, CV = 9.7 %), Dico GF SMC exhibited a significant rate dependence in terms of puncture stiffness.

Figure 6.75 shows representative force-deflection as well as energy-deflection responses resulting from quasi-static and dynamic puncture of charge and flow region Dico GF SMC specimens. In general, the force-deflection and energy-deflection response can be divided into six distinct regions, already defined by Kau (1990) and Knakal and Ireland (1986). In the following, the quasi-static material response is described in a detailed way. At the beginning of loading (section I), a common trend was seen for the Dico SMC specimen punctured in a quasi-static manner, and at lower contact forces, the contact response was of a power law form. Within this first part, indentation took place (Hertzian contact) (Sutherland and Soares, 2005). The following section was defined by a linear increase (section II) until a yield point. This point indicated a transition of the force-deflection curve from linear increase to an increase with reduced slope, due to initiation of failure. In the following, the force-deflection response was characterised by small load drops, which indicated evolving damage based on crack formation and growths. Force increased to peak load (section III), where peak was defined by a plateau rather than a distinct point if the specimens were punctured in a quasi-static manner. After peak, the load decreased gradually due to the formation and the growth of a widespread crack network; however,

the specimen retained its structural integrity (section IV). In section V the striker penetrated through the punctured specimen, and the last section (section VI) of the force-deflection response resulted from friction between the striker and the specimen.

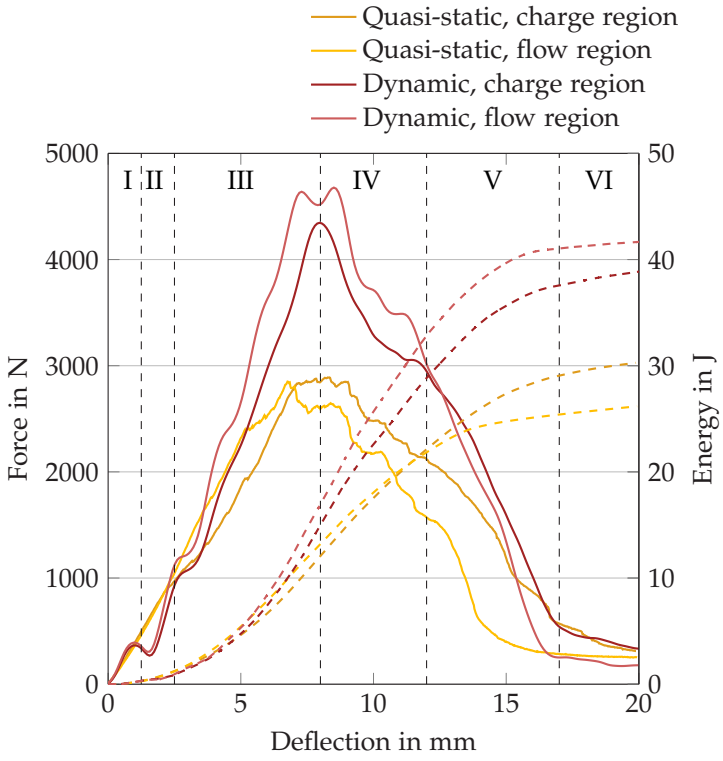


Figure 6.75: Force-deflection and energy-deflection curves resulting from quasi-static and dynamic puncture of discontinuous glass fibre SMC. Individual sections can be defined as follows: I: dynamic offset; II: yield; III: peak; IV: failure; V: penetration; and VI: friction.

The dynamic force-deflection response shows qualitatively the same characteristics. However, the initial part is defined by a dynamic offset (I) (Knakal and Ireland, 1986), which may have arisen from the apparatus and the specimen itself (e.g. influenced by its stiffness). Independent of loading rate, energy absorptions started beyond the yield point in a decisive way, since at the beginning of impact, elastic deformation did not contribute to energy absorption. As soon as cracks were initiated at the bottom side of the specimen, energy absorption became more important because of the formation of new surfaces, which absorbed energy induced by the striker. Energy absorption was most important beyond peak load until specimens were fully punctured by the striker (section IV and V). The energy-deflection curves reached a plateau, and in this phase energy was only dissipated due to frictional sliding between the specimen and shaft of the striker. Beyond maximum load, specimens punctured in a dynamic manner absorbed significantly more energy. Results presented by Trauth et al. (2018) indicate a rate dependence of interface properties of UPPH-based SMC composites reinforced with glass fibres enhancing energy absorption capability at higher loading rates.

Figure 6.76 depicts a representative force-deflection response of a Dico GF SMC specimen punctured in a quasi-static manner, in detail. Damage evolution was investigated through in-situ images captured with a camera positioned below the fixture. For significant steps in the force-deflection evolution, the corresponding images can be found in Figure 6.78. In addition crack growth was quantified by image processing (Figure 6.77).

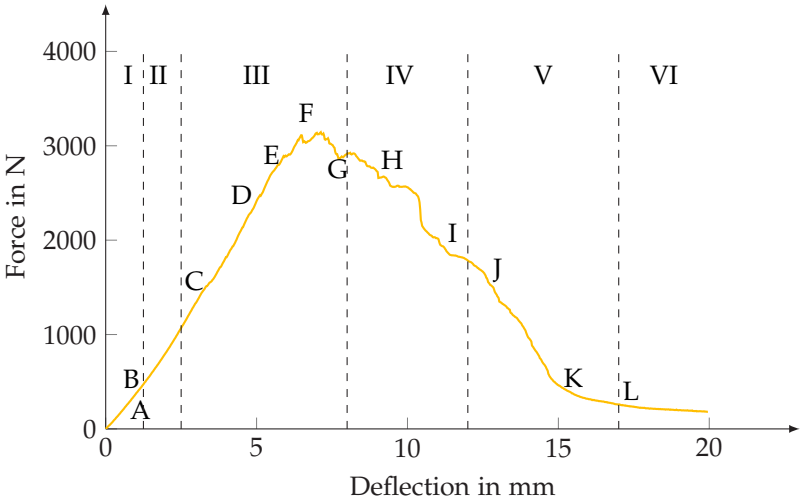


Figure 6.76: Representative force-deflection response resulting from quasi-static puncture of a discontinuous glass fibre SMC flow region specimen.

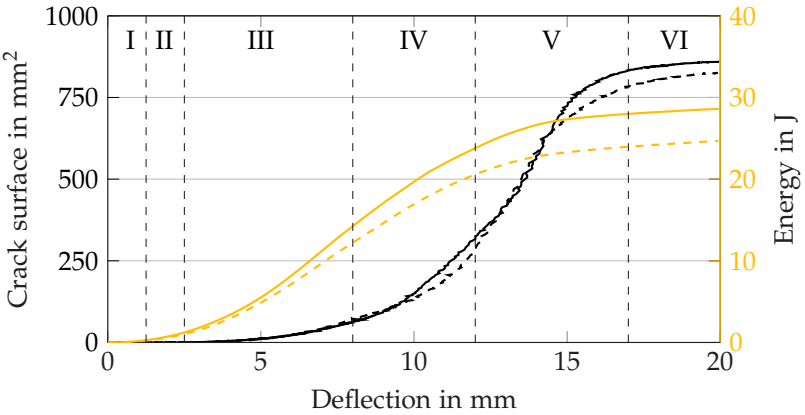


Figure 6.77: Evolution of crack volume with increasing deflection and corresponding energy-deflection response of two representative discontinuous glass fibre SMC specimens.

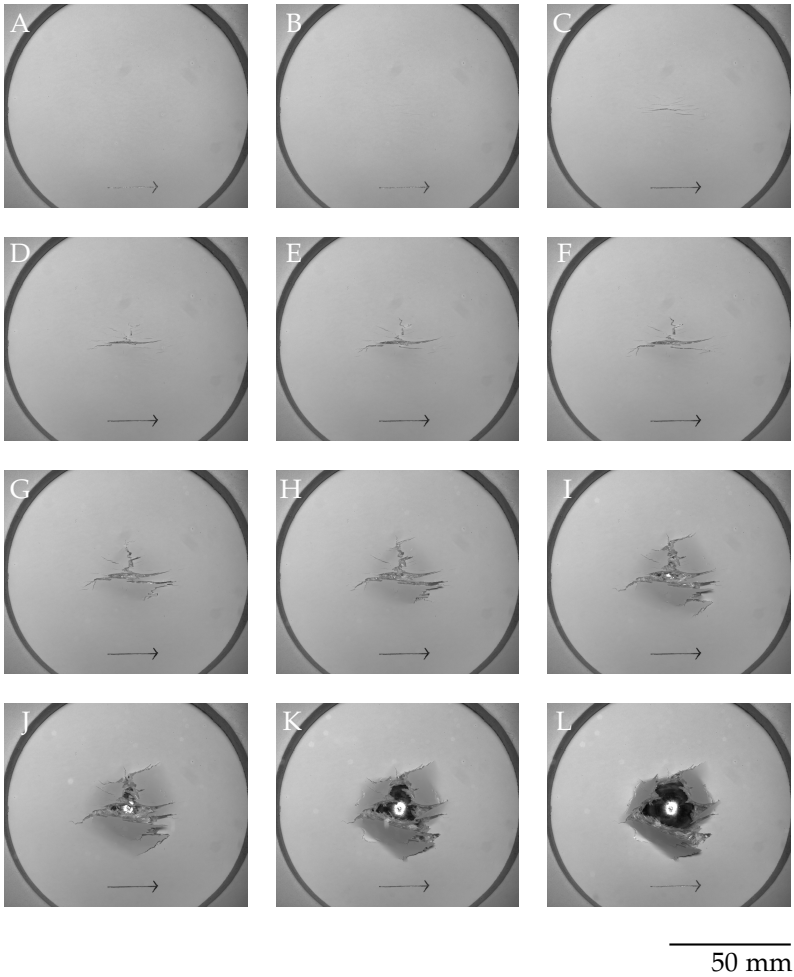


Figure 6.78: Failure evolution resulting from quasi-static puncture of discontinuous glass fibre SMC; flow region specimen, arrow indicating flow direction.

The rising portion of the force-deflection curve resulting from quasi-static puncture of Dico GF SMC started with a linear increase in deflection with increasing force, which was not linked to visible damage at the lower surface (point A and B). The decrease in stiffness in point C resulted from partial failure of the specimen at the lower surface due to the formation of cracks, tending to be oriented in flow direction, which was linked to first crack initiation events, as depicted in Figure 6.77. A further increase in force (points C – F, section III) led to crack growth and the continual formation of new (radial) cracks, but the crack-network was dominated by two major perpendicular radial cracks. Up to maximum load, the crack network further grew. From point F, the force significantly decreased as a result of important failure of the specimen, which was marked by abrupt crack growth (points G – I, section IV). Crack formation and growth rate increased significantly during this stage of puncture. In section V (points J – L) the specimen was penetrated. Penetration was linked to important further crack initiation and growth, before the shaft of the striker slid along the punctured surface in section VI. In this phase, energy was dissipated due to frictional sliding between the specimen and shaft of the striker. Post-mortem observation of the specimens highlighted some small circumferential cracks, which resulted from clamping.

In a comparable way, damage evolution resulting from dynamic puncture was captured by means of high-speed imagery during the impact event. Figure 6.79 highlights distinctive points of a representative force-deflection response, while Figure 6.80 depicts the corresponding high-speed images.

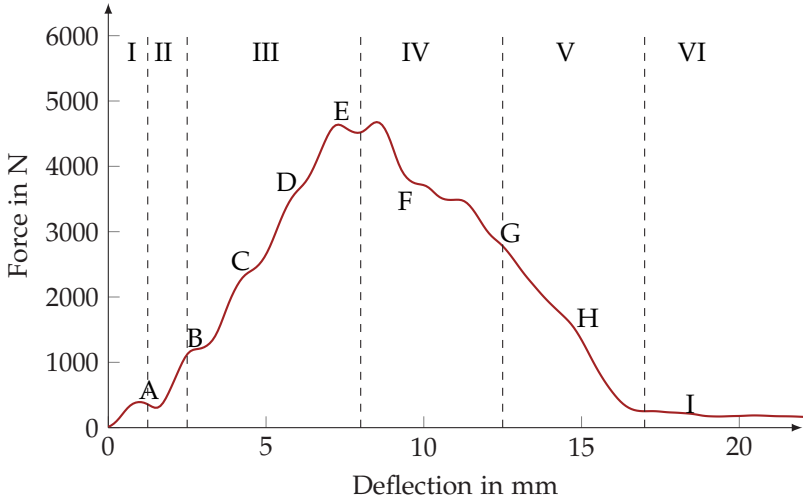


Figure 6.79: Representative dynamic force-deflection response of discontinuous glass fibre SMC flow region specimen.

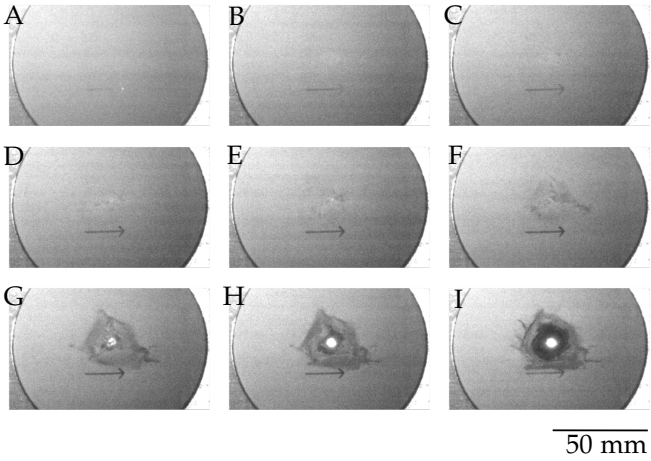


Figure 6.80: Damage evolution resulting from dynamic puncture of discontinuous glass fibre SMC flow region specimen; arrow indicating flow direction.

Considering dynamic puncture, the small drops in force in the rising part of the curve resulted from test setup and wave reflections; they do not reflect material behaviour, as the location of these load drops were reproducible for different specimens (Trauth et al., 2018). The first visible damage occurred in point C (at yield). In the following section, cracks started to grow, usually in flow direction. After reaching maximum force, load dropped due to sudden crack growth and formation at the lower surface (points E – G). In the following the striker penetrated through the specimen (points G – I).

6.4.2 Puncture properties of continuous carbon fibre SMC

Continuous carbon fibre SMC exhibited a significant negative rate dependence. Maximum load (F_{max}) and puncture energy (E_p) showed a characteristic decrease of $-13\,\%$ and $-21\,\%$, respectively, if specimens were punctured in a dynamic manner (Table 6.12). No correlation between maximum sustained load and absorbed energy could be observed (Figure 6.81).

Different failure modes were observed for Co CF SMC punctured in a quasi-static manner, which significantly influenced damage absorption capability. As a consequence, puncture energy exhibited a very high scatter (Figure 6.81). A first failure type was characterised by an abrupt load drop after reaching maximum load to a force value, which was significantly lower than peak force and below $F_{max}/2$. Considering the second type, load also abruptly decreased after peak load; however, force-deflection response showed a distinct plateau. For certain specimens, defined by the third failure type, load did not drop below $0.5 \cdot F_{max}$. These specimens have not been considered

to calculate puncture energy or puncture deflection. Due to the early onset of failure, stiffness of continuous carbon fibre SMC was evaluated in the range of $0.25 < d < 1$, with a least squares fit. In the dynamic loading case, the slope of the force-deflection response was fitted in the same manner for a deflection of $\approx 1 < d < 2$, due to a dynamic offset. The stiffness of continuous carbon fibre SMC exposed to quasi-static or dynamic puncture did not show significant variation (Table 6.12).

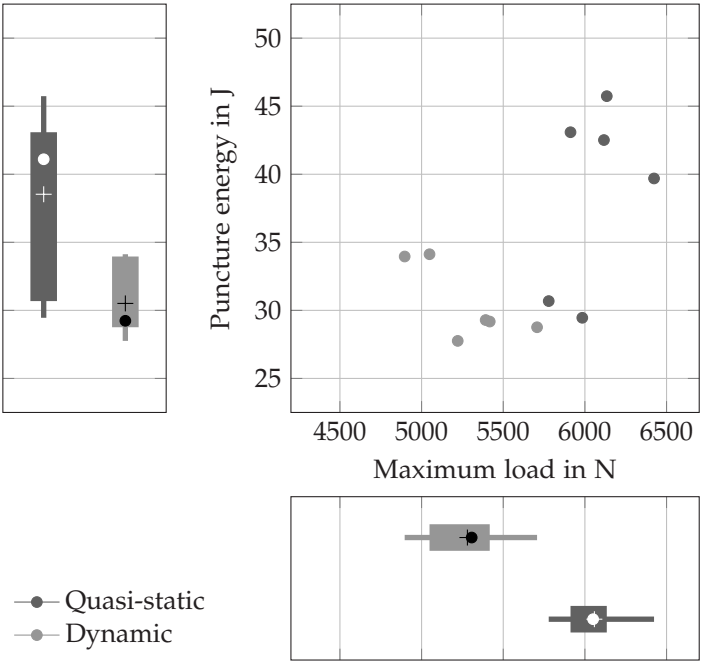


Figure 6.81: Quasi-static and dynamic puncture properties of continuous carbon fibre SMC (• = median, + = mean, box indicates 25^{th} to 75^{th} percentile; lines indicate minimum and maximum or 1.5 interquartile range, respectively).

Table 6.12: Quasi-static and dynamic puncture properties of continuous carbon fibre SMC.

		Quasi-static	Dynamic			Quasi-static	Dynamic
F_{max}		(n=8)	(n=6)	S		(n=8)	(n=6)
$\bar{x}$	in N	6058	5281	$\bar{x}$	in N mm^{-1}	901	940
μ	in N	200	289	μ	in N mm^{-1}	23	76
CV	in %	3.3	5.5	CV	in %	2.6	8.1
$E_{F_{max}}$		(n=8)	(n=6)	E_p		(n=6)	(n=6)
$\bar{x}$	inJ	32.3	19.5	$\bar{x}$	in J	38.5	30.5
μ	in J	6.7	2.0	μ	in J	6.8	2.8
CV	in %	11.4	10.1	CV	in %	17.8	9.1
$\mathrm{d}_{F_{max}}$		(n=8)	(n=6)	d_{E_p}		(n=6)	(n=6)
$\bar{x}$	in mm	9.1	7.4	$\bar{x}$	in mm	11.3	10.0
μ	in mm	0.7	0.3	μ	in mm	1.7	1.10
CV	in %	7.9	3.9	CV	in %	14.6	11.1

Figure 6.82 depicts representative force-deflection responses resulting from quasi-static and dynamic puncture of continuous carbon fibre SMC. The damage evolution of a selected continuous carbon fibre SMC punctured in a quasi-static manner is depicted in Figure 6.84, with corresponding images shown in Figure 6.83.

In general, first part of the force-deflection evolution was characterised by a steady (linear) increase in force for an increase of deflection up to peak load (sections I – III). A yield point could be identified at low deflections (section I, $d \approx 1\,\mathrm{mm}$). After yield, a decrease in stiffness due to the onset of failure at the lower surface of the specimens was observed (section III). Gradual failure led to a further decrease in stiffness up to peak load. Peak was linked to marginally lower deflection in the dynamic loading case. Beyond peak load, the specimens failed abruptly and were suddenly no longer able to

maintain loads (section IV). The prompt failure was also reflected by a kinking of the energy-deflection evolution. With only a slight increase from deflection at maximum load ($d_{F_{max}}$) to puncture deflection (d_p), continuous carbon fibre SMC showed low damage tolerance, with a localised puncture loading independent from loading rate (Table 6.12). The end of the puncture event (sections V and VI) was defined by penetration of the striker and friction.

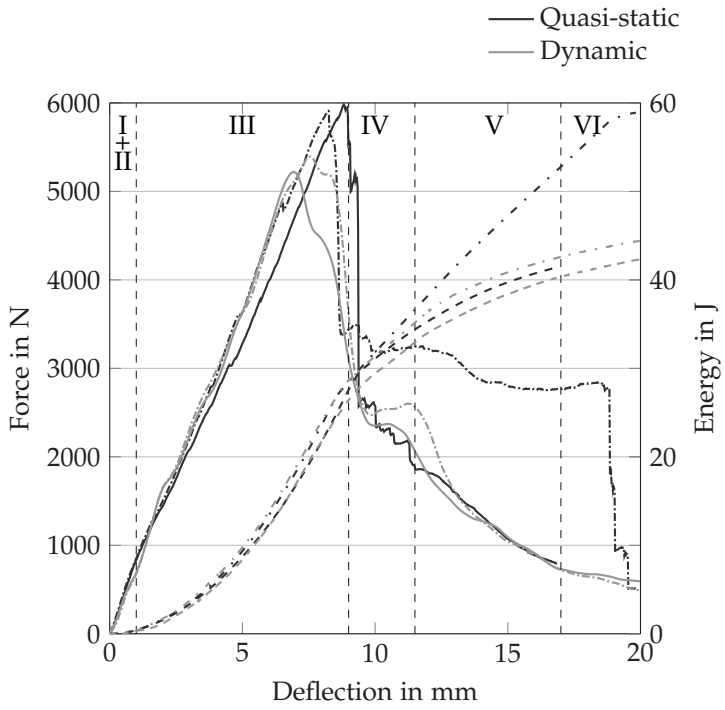


Figure 6.82: Representative force-deflection and energy-deflection response resulting from quasi-static and dynamic puncture of continuous carbon fibre SMC. Individual sections can be defined as follows: I: dynamic offset; II: yield; III: peak; IV: failure; V: penetration; and VI: friction.

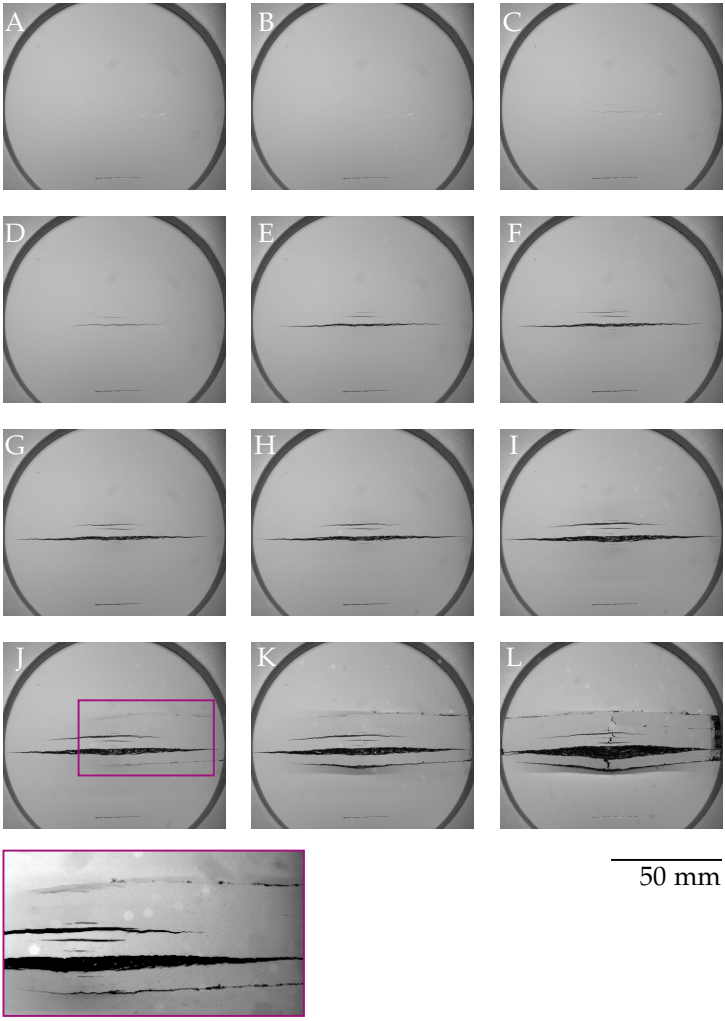


Figure 6.83: Damage evolution resulting from quasi-static puncture of continuous carbon fibre SMC.

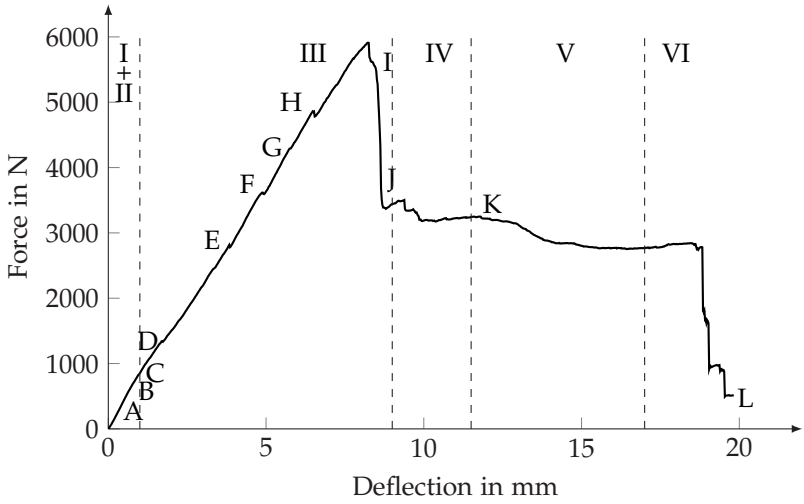


Figure 6.84: Representative force-deflection response resulting from quasi-static puncture of continuous glass fibre SMC.

Starting with a linear increase of the force-deflection response, an early formation of cracks in the fibre direction at the lower surface (points A – C, section I) slightly influenced the specimen's stiffness. In the beginning, damage was marginal, but as force increased, more cracks formed (starting from point C), and energy absorption became more important (section II). The small load drops in points D – H characterised abrupt, stepwise and instable crack growth linked to important energy absorption based in the formation of new surfaces (section III). Most important was the major crack in the middle of the specimen below the striker. Cracks grew easily in the fibre direction up to clamping (I), and the following load drop (I→J) was marked by a significant fracture of the specimen and the formation of inter-fibre cracks starting from clamping. The striker started to push through the specimen. Final failure was based on fibre breakage and linked to a significant load drop (point L).

The force-deflection evolution of a continuous carbon fibre SMC specimen punctured in a dynamic manner is qualitatively comparable to the quasi-static response (Figure 6.85 and 6.86).

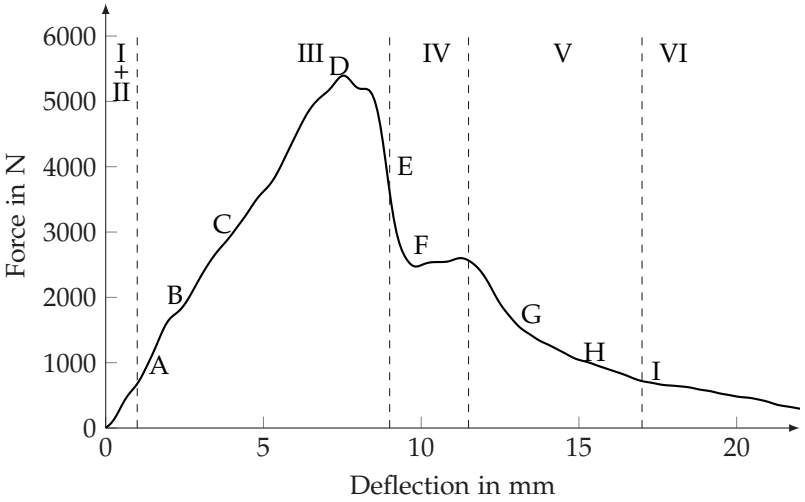


Figure 6.85: Representative force-deflection response resulting from dynamic puncture of continuous glass fibre SMC.

The initial increase in load with increasing displacement led to the formation of numerous small cracks at the lower surface, oriented in the fibre direction (points A – C, section II). Fibre breakage and the formation of cracks perpendicular to fibre direction were more important if Co CF SMC was punctured in a dynamic manner, and the important load drop in point D was linked to fibre fracture in the bottom layer. As soon as peak load was reached, the specimen was no longer able to maintain loads and the force-deflection response dropped significantly. In the following, the striker penetrated through the specimen, and energy absorption mainly resulted due to friction.

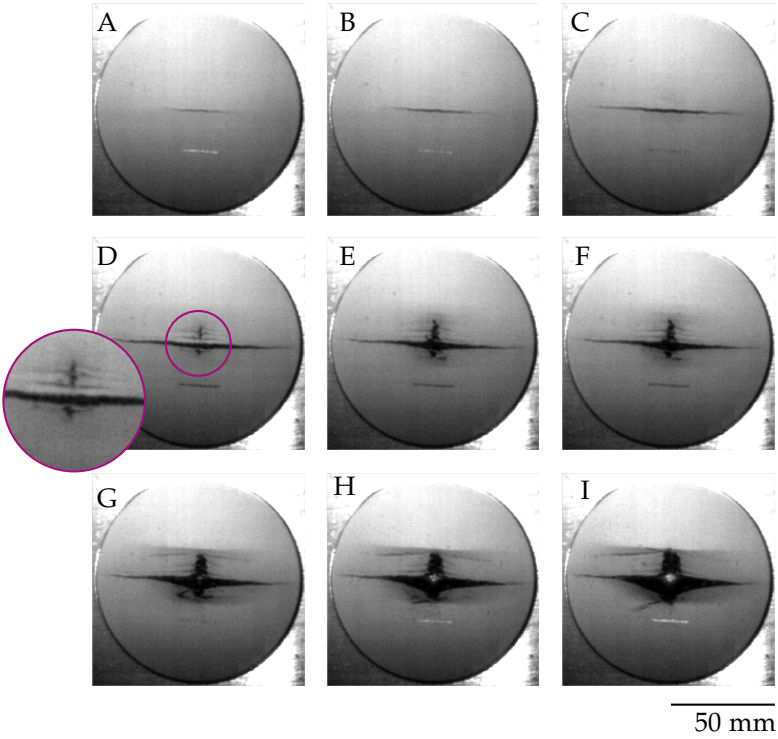


Figure 6.86: Damage evolution resulting from dynamic puncture of continuous carbon fibre SMC.

6.4.3 Puncture properties of continuous-discontinuous glass/carbon fibre SMC

Hybrid CoDico GF/CF SMC specimens were punctured in the same manner as the specimens made from the individual components, to enable evaluation of a hybridisation effect on structural properties. Charge and flow region specimens have been considered for evaluation, and Figure 6.87 and Table 6.13 depict the experimentally determined puncture properties of CoDico GF/CF SMC.

In contrast to Dico GF SMC, which showed no significant difference in mechanical performance of charge and flow region specimens (Figure 6.74 and Table 6.11), puncture energy (E_p) of CoDico GF/CF SMC was significantly lower for specimens extracted from flow region (Figure 6.87). The same trend was observed for maximum load; however, the difference was not significant for quasi-static puncture. With an increase of maximum load of 38 % and 28 % for charge and flow region specimens, CoDico GF/CF SMC exhibited a positive rate dependence, which was less distinct than for pure Dico GF SMC. Energy absorption capability increased for higher loading speeds 14 % and 23 % for charge and flow region specimens, respectively.

Stiffness of the CoDico GF/CF SMC specimens was evaluated in the range of $1 < d < 2$ in the quasi-static and dynamic loading case by a least squares fit. If punctured in a quasi-static manner, the stiffness of the hybrid CoDico GF/CF SMC was in between the observed values of Dico GF and Co CF SMC. If punctured in a dynamic manner, stiffness increased ($\approx$ 48 %). A positive correlation characterises the relation between maximum sustained load and absorbed energy for the two considered velocities (Figure 6.87).

Table 6.13: Quasi-static and dynamic puncture properties of continuous-discontinuous glass/carbon fibre SMC.

		Charge region Quasi-static	Flow region Quasi-static	Charge region Dynamic	Flow region Dynamic
S		(n=6)	(n=6)	(n=6)	(n=6)
$\bar{x}$	in N mm^{-1}	735	694	1065	1057
μ	in N mm^{-1}	35	51	64	115
CV	in %	4.7	7.4	6.0	10.9
F_{max}		(n=6)	(n=6)	(n=6)	(n=6)
$\bar{x}$	in N	4060	3916	5584	5021
μ	in N	235	162	415	457
CV	in %	5.8	4.1	7.4	9.1
$E_{F_{max}}$		(n=6)	(n=6)	(n=6)	(n=6)
$\bar{x}$	in J	24.9	20.0	24.2	17.4
μ	in J	1.6	5.4	3.6	2.7
CV	in %	6.3	26.9	14.7	15.2
E_p		(n=6)	(n=6)	(n=6)	(n=6)
$\bar{x}$	in J	34.3	29.2	39.1	35.9
μ	in J	3.0	1.0	1.9	2.7
CV	in %	8.7	3.6	4.7	7.6
$d_{F_{max}}$		(n=6)	(n=6)	(n=6)	(n=6)
$\bar{x}$	in mm	7.8	8.4	8.2	6.9
μ	in mm	1.0	1.2	0.7	0.4
CV	in %	12.9	14.6	8.5	5.9
d_{E_p}		(n=6)	(n=6)	(n=6)	(n=6)
$\bar{x}$	in mm	12.8	11.5	11.7	11.7
μ	in mm	0.7	0.6	0.6	0.8
CV	in %	5.6	4.8	5.1	6.5

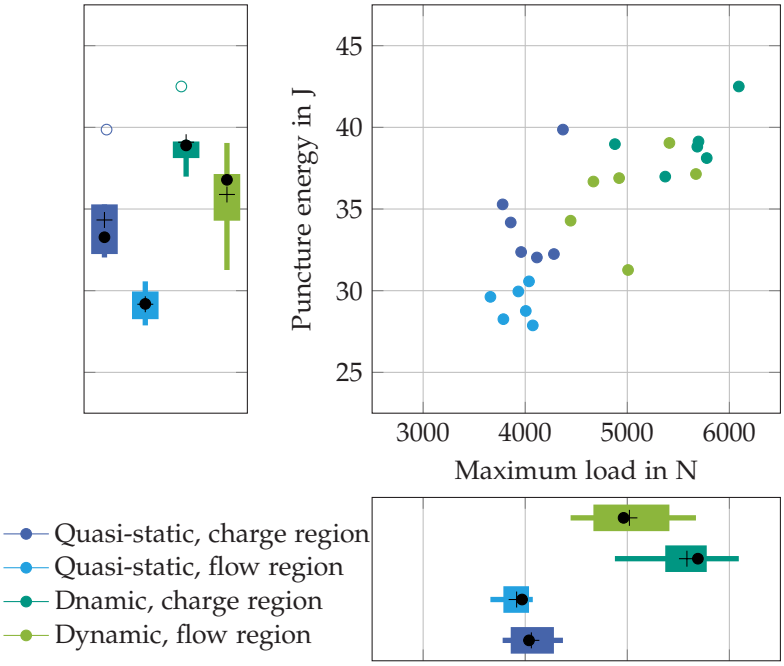


Figure 6.87: Quasi-static and dynamic puncture properties of continuous-discontinuous glass/carbon fibre SMC (• = median, + = mean, box indicates 25^{th} to 75^{th} percentile; lines indicate minimum and maximum or 1.5 interquartile range, respectively, ○ = outlier).

The force-deflection response, independent of loading rate, qualitatively showed the same evolution as defined for the Dico GF SMC and the Co CF SMC (Figure 6.88).

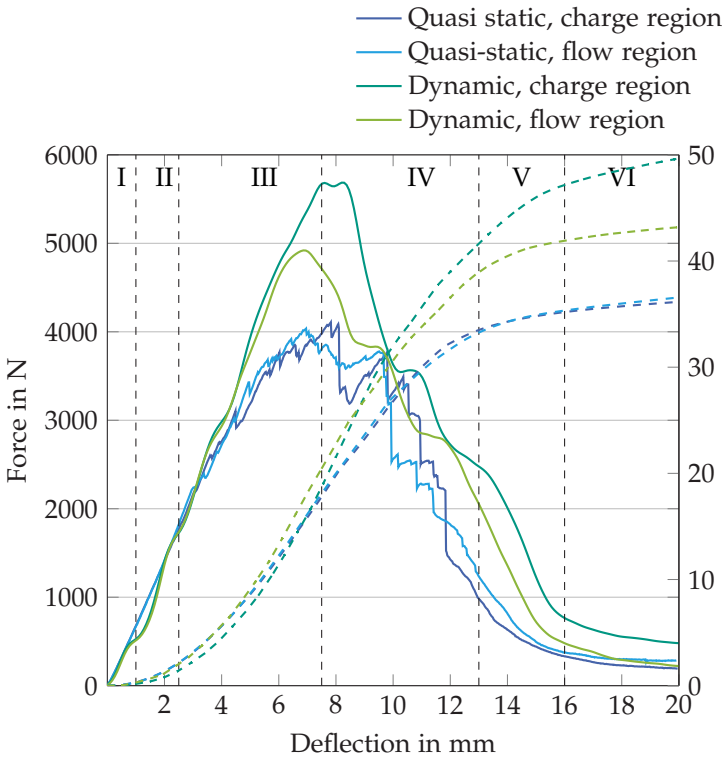


Figure 6.88: Representative force-deflection and energy-deflection responses resulting from quasi-static and dynamic puncture of continuous-discontinuous glass/carbon fibre SMC. Individual sections can be defined as follows: I: dynamic offset; II: yield; III: peak; IV: failure; V: penetration; and VI: friction.

After a linear increase up to yield (section I and II), stiffness started to decrease due to failure initiation at the lower surface (section III). From this point, damage of the specimen became evident due to numerous small load drops in the force-deflection response. Energy absorption became more important during this stage of loading, but did not quantitatively differ for different loading rates. The decreasing part of the force-deflection evolution was characterised

by a stepwise decrease independent of loading rate, which indicated partial and subsequent failure of the specimen consisting of different layers (section IV). Energy-deflection responses beyond peak (section IV) indicated that specimens punctured in a dynamic manner were able to absorb more energy than was the case with a quasi-static loading of the material. This tendency was already observed for Dico GF SMC composites, and it is highly possible that failure mechanisms of CoDico GF/CF SMC also differ with respect to loading rate. It is conceivable that the difference in energy absorption capability most probably resulted from the rate dependent failure evolution of the Dico GF SMC composite or the interface properties between the continuous and discontinuous components. In the end, the striker penetrated the specimen (section V). Load did not decrease to zero due to frictional effects (section VI).

With a significant increase from deflection at maximum load ($d_{F_{max}}$) to puncture deflection (d_p), CoDico GF/CF SMC featured better damage tolerance than did Co CF SMC (Table 6.13 and 6.12). The discontinuously reinforced core of the hybrid CoDico GF/CF SMC enhanced damage tolerance, preventing sudden failure of the specimen as soon as peak load was reached.

Figures 6.89 and 6.91 detail a representative force-deflection response and significant points in terms of damage evolution resulting from quasi-static puncture of the hybrid CoDico GF/CF SMC. Evolution of crack volume is depicted in Figure 6.90 to allow a quantitative evaluation of the evolving damage.

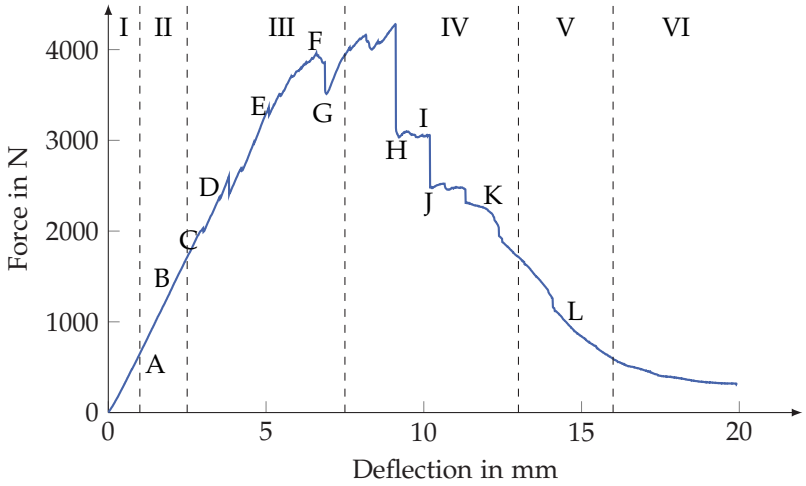


Figure 6.89: Representative force-deflection response resulting from quasi-static puncture of continuous-discontinuous glass/carbon fibre SMC. Images corresponding to points A – L appear in Figure 6.91.

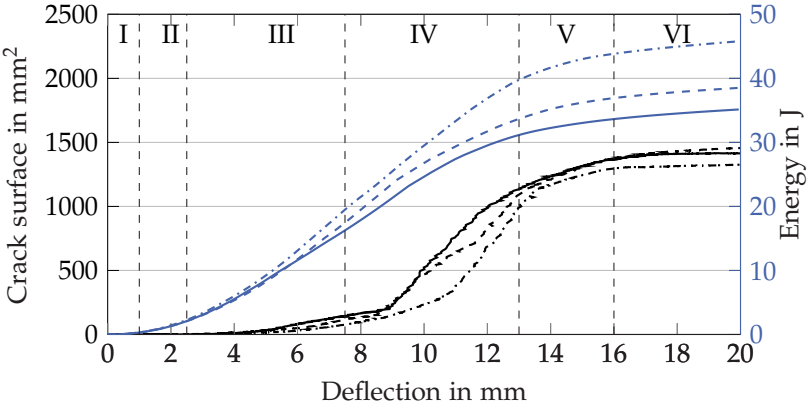


Figure 6.90: Evolution of crack volume with increasing deflection and corresponding energy-deflection response of three representative continuous-discontinuous glass/carbon fibre SMC specimens.

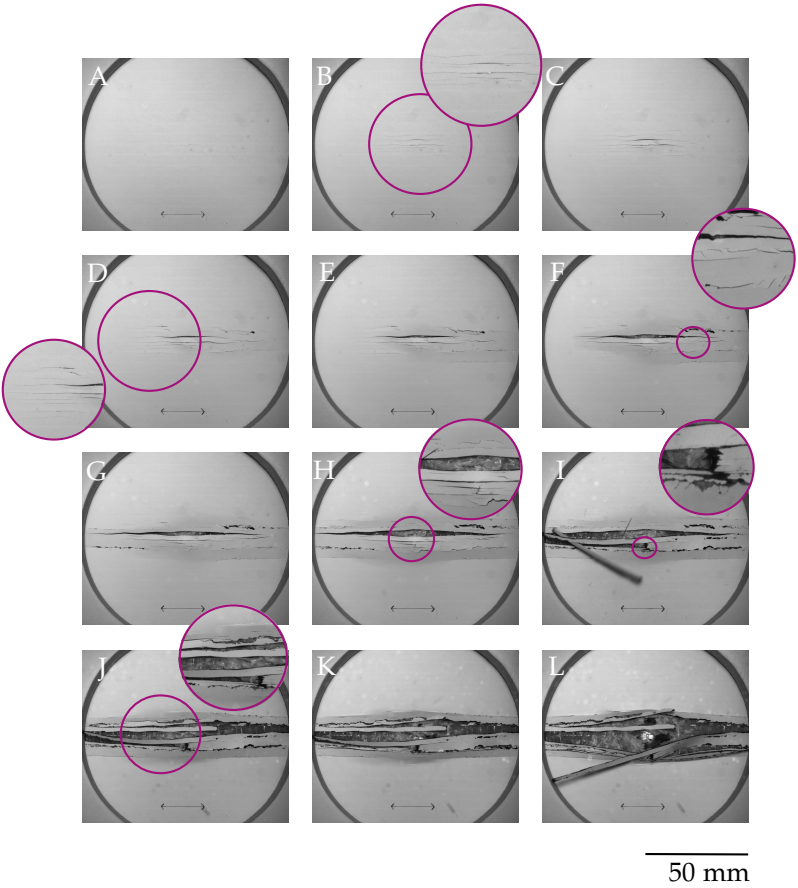


Figure 6.91: Damage evolution resulting from quasi-static puncture of hybrid continuous-discontinuous glass/carbon fibre SMC.

Starting with a steady (linear) increase (points A – C) due to the formation of small cracks at the lower surface in the direction of the fibres of the continuous carbon fibre SMC, failure became visible at lower deflections compared to the discontinuous glass fibre SMC. Nevertheless, the stiffness of the specimen was not affected during

this stage of loading (yield corresponds to point C), in contrast to an early decrease in stiffness of the Co CF SMC. The small load drops in points C, D and E resulted from abrupt crack formation and growth, mainly in fibre direction of the continuous component. Compared to the pure Co CF SMC, the crack network which formed at the lower surface of the hybrid CoDico GF/CF SMC specimen consisted of a larger number of rather small cracks. The cracks parallel to the fibre direction of the continuous face sheets propagated easily up to clamping. This progression was linked to significant load drops in point G. Beyond peak the evolution of the force-deflection response was marked by fibre breakage (points H and I) and delamination between the continuously and discontinuously reinforced layers of the CoDico GF/CF SMC (point J). From point K to the end of the force-deflection curve, evolution was determined by the striker pushing through the specimen and friction.

Figure 6.92 presents the post-mortem observations of fractured CoDico GF/CF SMC specimens, which were punctured in a quasi-static manner. The failure of the discontinuous component was determined by pseudo-delamination. Interlaminar (interlayer) and intralaminar (intralayer) delamination within the continuous components were also important failure mechanisms accompanied by inter-fibre fractures within the continuous component.

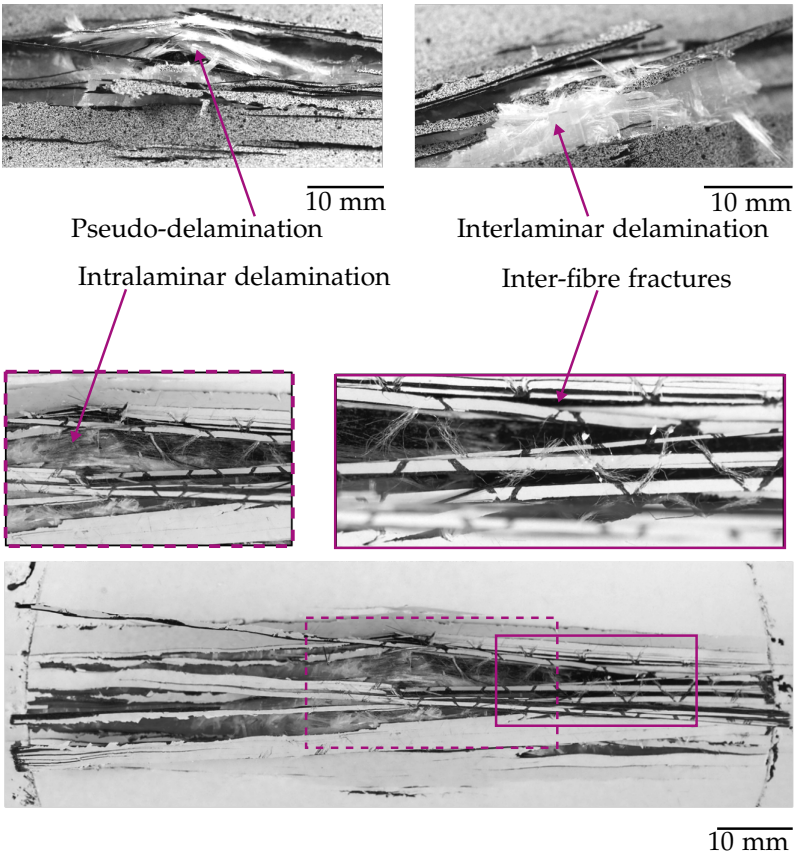


Figure 6.92: Damage region of a continuous-discontinuous glass/carbon fibre SMC specimen, punctured in a quasi-static manner.

The damage evolution of a representative hybrid CoDico GF/CF SMC specimen punctured in a dynamic manner is depicted in Figure 6.93, with corresponding images of damage evolution shown in Figure 6.94. Force-deflection evolution was characterised by a steady increase up to peak load. Several small cracks aligned in fibre direction of the continuous component formed (points A – C) and grew up to clamping. However, the formation of these cracks did not macroscopically influence the structural stiffness of the component. The significant load drop beyond peak load was characterised by a growth and spreading of the cracks formed within the continuous material. Delamination took place locally (points E – G). After reaching a small plateau (point G), the specimen suddenly failed due to the bursting of the continuous face sheet at the lower surface.

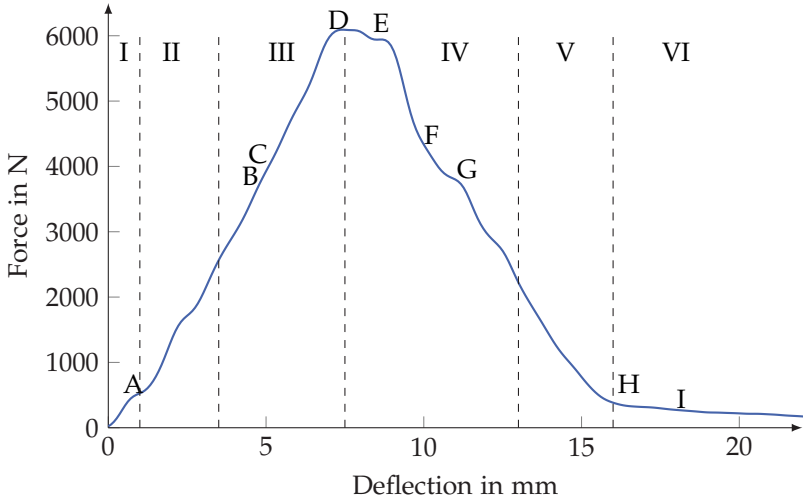


Figure 6.93: Representative force-deflection response resulting from dynamic puncture of continuous-discontinuous glass/carbon fibre SMC.

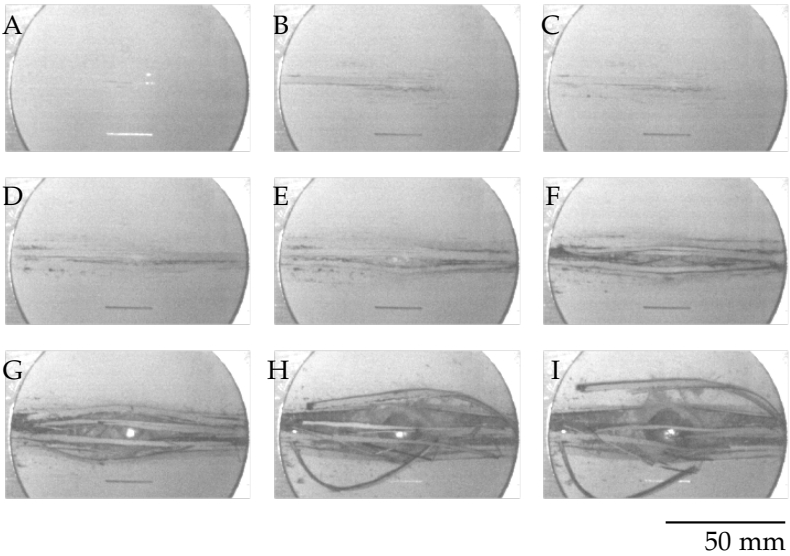


Figure 6.94: Damage evolution resulting from dynamic puncture of hybrid continuous-discontinuous glass/carbon fibre SMC.

Macroscopic post-mortem observation of hybrid CoDico GF/CF SMC specimens punctured in a dynamic manner (Figure 6.95) clearly indicated that interlaminar delamination played a more pronounced role than did damage mechanisms resulting from quasi-static puncture. In addition, pull-out of (glass) fibre bundles was the dominating failure mechanism of the discontinuous component (Figure 6.95).

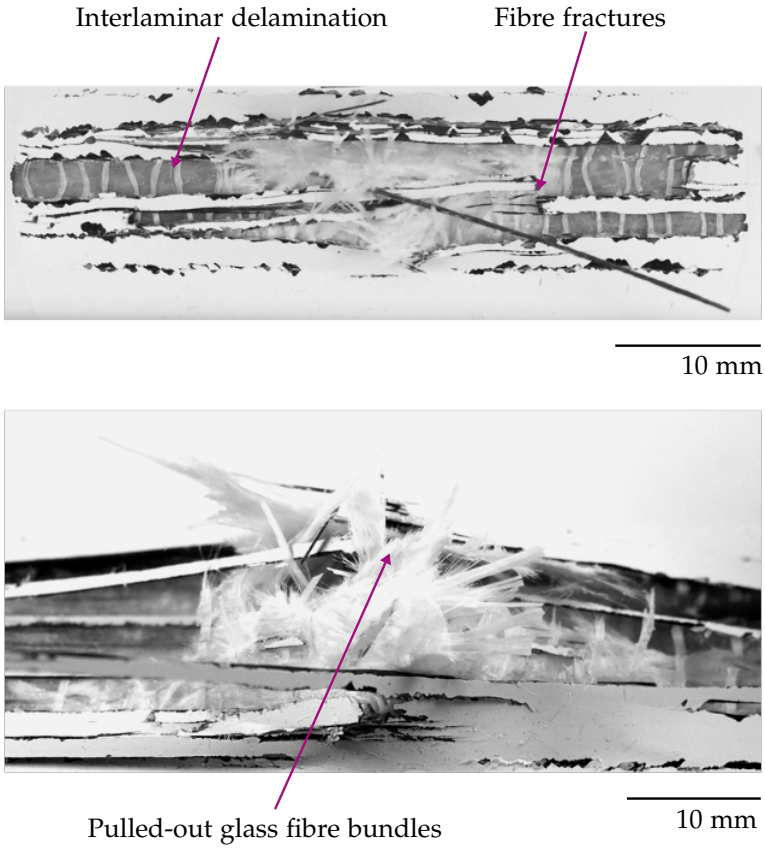


Figure 6.95: Damage region of a continuous-discontinuous glass/carbon fibre SMC specimen, punctured in a dynamic manner showing interlaminar delamination between the continuous and discontinuous component as well as pulled-out fibre bundles of the discontinuous component.

6.5 Mechanical properties and failure at the component level

Component properties were determined to investigate the effect of hybridisation on component scale, with load case simulating near-service loadings. Having approximately the same density (as described in sections 6.2.1.1 and 6.2.1.2), the component made from pure discontinuous glass fibre SMC and the locally reinforced parts realised with continuous carbon fibre SMC feature the same weight. In addition, the geometry was unchanged. As explained in section 4.4, the load data from the load cell and deflection data measured via a tactile transducer, positioned in the middle below the component, were recorded. Since all tests were carried out in a deflection-controlled manner, the deflection data of the specimens are identical with one another except for the maximum deflection at breakage. The measured force, however, differed and is considered in the following.

Figure 6.96 clearly shows that for components with local reinforcement the load increase over deflection was higher (i.e. the stiffness of the parts significantly increased due to the incorporation of a local reinforcement). At the last loading stage, corresponding to a maximum deflection of 5 mm, the specimens with continuous carbon fibre reinforcements carried an average load surplus of 946 N, in comparison to specimens without local reinforcement. That shift corresponds to an increase in strength of 32 %. Initial stiffness showed a more important scatter for the hybrid CoDico GF/CF SMC component (23 %) compared to the pure Dico SMC demonstrator parts, exhibiting a scatter in initial stiffness of only 3 %. The force-deflection response of the Dico and CoDico GF/CF SMC demonstrator parts were characterised by a gradual decrease, indicating a slight degradation of components' stiffness, resulting from increasing damage

to the component due to loading. The force-deflection response of the hybrid CoDico GF/CF SMC demonstrator parts showed only a slight decrease within the first three cycles, then increased in a linear way up to cycle 8. Load at failure was significantly higher for locally reinforced components (739 N, increase of 17 %), but deflection at failure decreased from an average of 9.0 mm for purely discontinuous glass fibre SMC demonstrator parts to 7.6 mm if hybridisation took place (decrease of 1.4 mm, 15 %). In addition, the scatter of fracture strength was significantly reduced due to the local reinforcement (Dico GF SMC μ = 226 N, CoDico GF/CF SMC μ = 88 N).

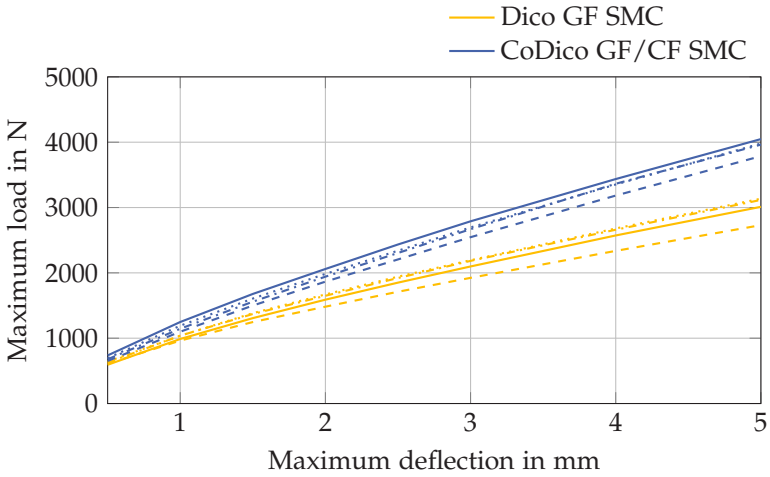


Figure 6.96: Evolution of maximum force during four-point bending loading of discontinuously (Dico) and continuously-discontinuously (CoDico) reinforced demonstrator part evaluated at maximum deflection of each cycle.

Figure 6.97 depicts the stiffness of the components determined for every cycle according to Equation 4.5. In general, stiffness decreased for the Dico GF SMC and CoDico GF/CF SMC demonstrator parts

with every cycle from the beginning of loading. Local reinforcement increased initial stiffness 23 % from an average value of 1247 N mm^{-1} to 1538 N mm^{-1}. However, initial stiffness of the hybrid CoDico GF/CF SMC demonstrator parts showed a significantly higher scatter, with CV = 9.5 %, compared to a variation of CV = 1.2 % for the purely discontinuous glass fibre SMC components.

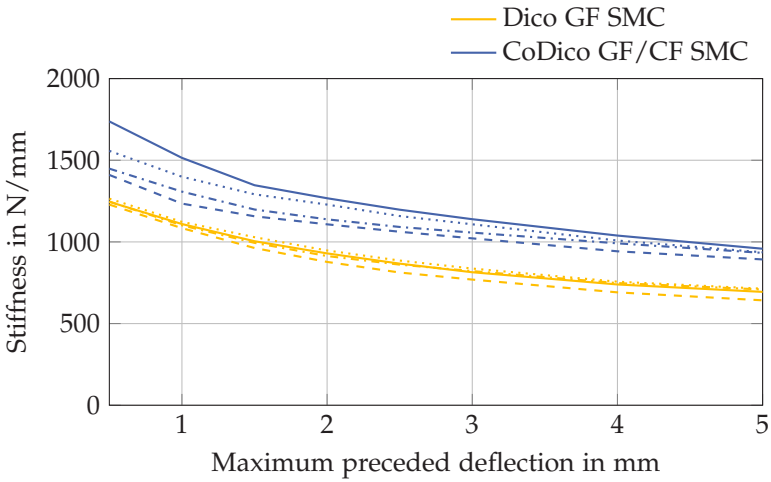


Figure 6.97: Evolution of stiffness during four-point bending loading of discontinuously (Dico) and continuously-discontinuously (CoDico) reinforced demonstrator part evaluated at maximum deflection of each cycle.

Considering damage evolution, lower values of D (damage parameter) at equal stages for the locally reinforced components were observed (Figure 6.98). Comparably to stiffness evolution during cyclic loading, locally reinforced components showed a slightly higher scatter in evolving damage.

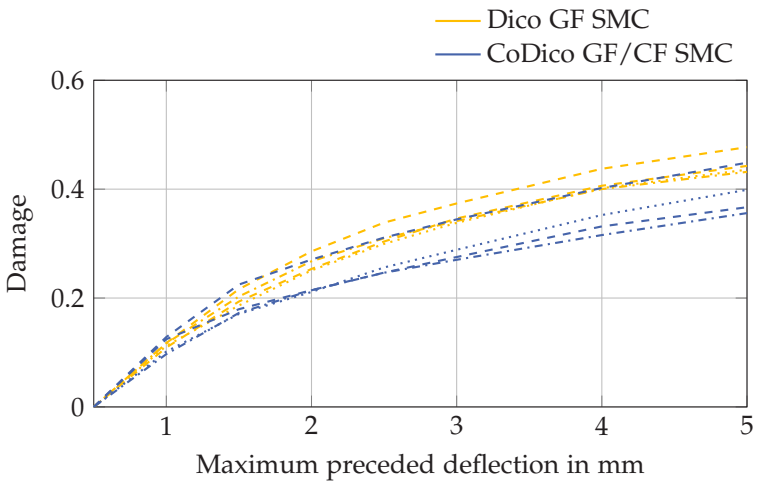


Figure 6.98: Evolution of damage during four-point bending loading of discontinuously (Dico) and continuously-discontinuously (CoDico) reinforced demonstrator part evaluated at maximum deflection of each cycle.

6.6 Analytical stiffness prediction

In the following section, the results of analytical modelling to predict the stiffness of discontinuous glass fibre SMC, continuous carbon fibre SMC and continuous-discontinuous glass/carbon fibre SMC are presented.

6.6.1 Analytical stiffness prediction of discontinuous glass fibre SMC

To analytically describe the stiffness of the discontinuous glass fibre SMC based on the Halpin–Tsai equations and Mori–Tanaka homogenisation approach (section 5.2.2.2), the material properties listed in Table 6.14 have been taken into consideration.

Table 6.14: Input parameters and material data of discontinuous glass fibre SMC.

Parameter	Value	Reference
E_M	3.45 GPa	Experimentally determined (section 6.3.1)
E_F	73 GPa	CES EduPack, 2017
ν_F	0.22	CES EduPack, 2017
ν_m	0.38	Experimentally determined (section 6.3.1)
ϕ_F (Mori–Tanaka)	24.2 vol.%	Experimentally determined (section 6.2.1)
ϕ_F (Halpin–Tsai) (1D)	26.6 vol.%	Experimentally determined (section 6.2.1)
ϕ_F (Halpin–Tsai) (2D)	24.9 vol.%	Experimentally determined (section 6.2.1)

Figure 6.99 and Figure 6.100 depict the analytically determined tensile modulus of elasticity and shear modulus considering different aspect ratios of the fibrous reinforcement (l/d) and a fibre volume content of 20, 25 or 30 vol.%, respectively. These values reflect the variation of the experimentally determined fibre volume content of the sheets considered within this dissertation.

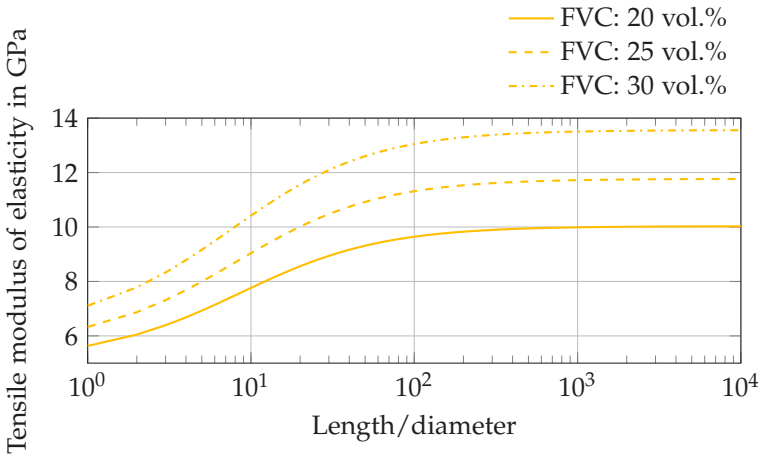


Figure 6.99: Tensile modulus of elasticity of discontinuous glass fibre SMC. Prediction based on Halpin–Tsai equations.

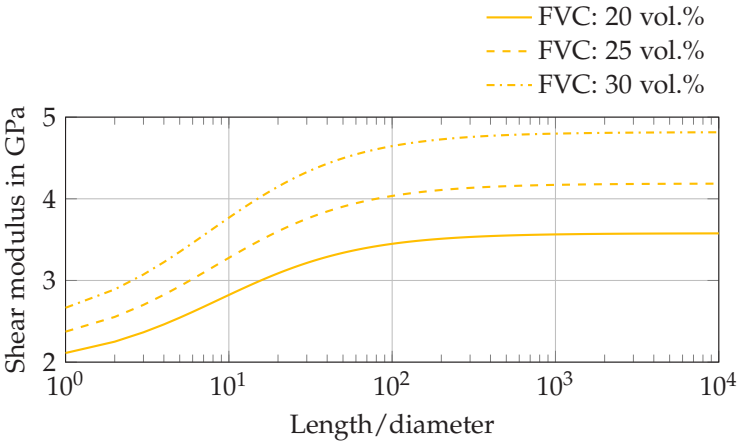


Figure 6.100: Shear modulus of discontinuous glass fibre SMC. Prediction based on Halpin–Tsai equations.

Considering the diameter of a glass fibre filament of 13.5 µm (Johns Manville, 2018) and the length of the filament in a standard SMC of 25.4 mm, the corresponding value of l/d equals 1881.5. For a fibre volume content of 26.6 vol.% (average value of all considered 1D Dico SMC sheets) predicted tensile modulus of elasticity and shear modulus equal 12.3 GPa and 4.4 GPa, respectively. Given the average fibre volume content of 2D Dico GF SMC sheets, predicted tensile modulus of elasticity and shear modulus are equal to 11.7 GPa and 4.2 GPa, respectively. Figures 6.102 and 6.103 demonstrate the analytically determined tensile modulus of elasticity of the discontinuous glass fibre SMC specimen extracted in flow direction and perpendicular to flow, based on the Mori–Tanaka approach. E_0 and E_{90} consider the stiffness in the $y-$ and $x-$ directions according to the convention presented in Figure 6.101.

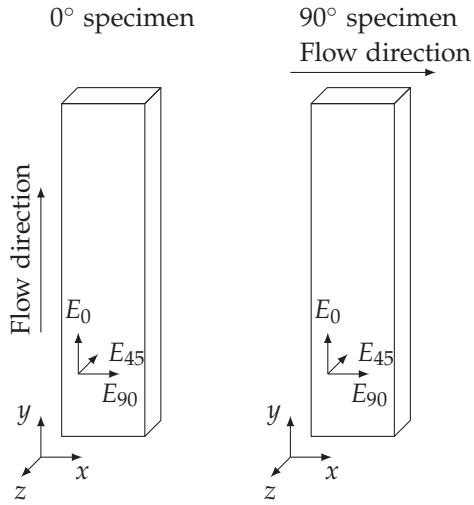


Figure 6.101: Orientation and convention of coordinate system to define elastic moduli based on Mori–Tanaka approach with fibre orientation tensors.

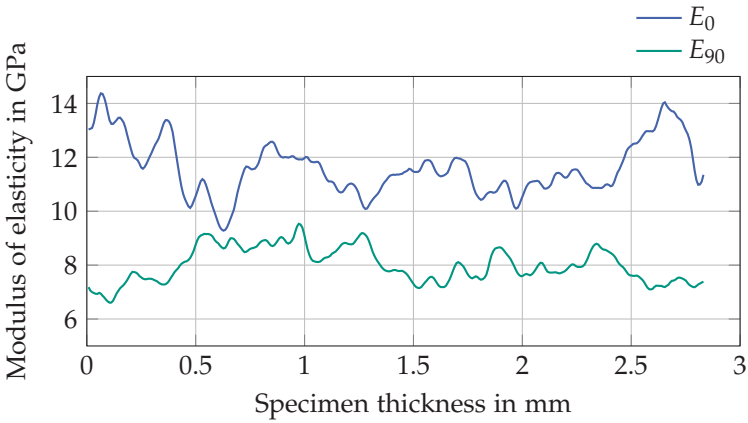


Figure 6.102: Modulus of elasticity of a specimen extracted in flow direction. Calculations based on Mori–Tanaka homogenisation and orientation averages.

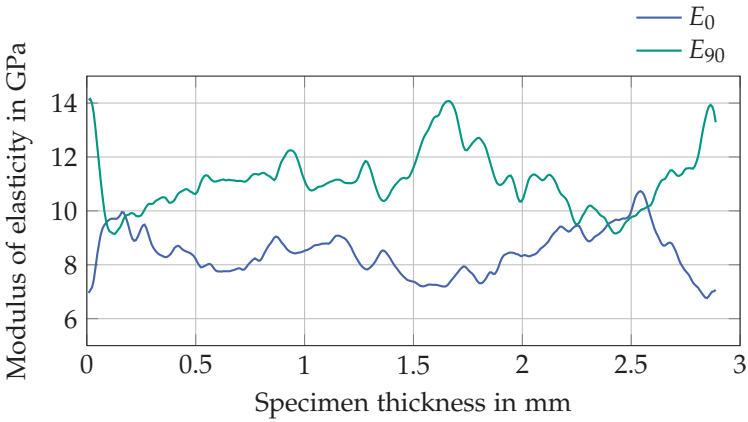


Figure 6.103: Modulus of elasticity of a specimen extracted perpendicular to flow direction. Calculations based on Mori–Tanaka homogenisation and orientation averages.

The calculations depend on a fibre volume content of 24.2 vol.%. This value was experimentally determined by means of thermogravimetric analysis of specimens extracted from the same sheet as the investigated specimens. Accuracy of the Mori–Tanaka homogenisation approach was evaluated with a comparison of analytically determined and experimentally measured stiffness. For this purpose, the (scanned) specimens were mechanically loaded in uniaxial tension to determine an experimental value of the tensile modulus of elasticity. Specimens were mechanically clamped with a clamping distance of 50 mm. Gauge length was set to 20 mm, and strains were measured with an extensometer. Tensile modulus of elasticity was determined in the strain range of 0.05 % to 0.25 %. Each specimen was loaded three times, up to a maximum strain of 0.35 % and tensile modulus of elasticity was determined on the rising slope using Equation 4.10 presented in section 4.5. The experimentally determined values were 12.16 GPa (μ = 0.015 GPa, CV = 0.13 %) for the specimen extracted parallel to flow direction and 8.75 GPa (μ = 0.10 GPa, CV = 1.18 %) for the specimen perpendicular to flow direction. Table 6.15 lists the experimentally and analytically determined values of the tensile modulus of elasticity for the two considered specimens.

Table 6.15: Comparison of analytically (Mori–Tanaka approach) and experimentally determined tensile modulus of elasticity.

Orientation of specimen	Parameter	Mori–Tanaka	Experiment	Deviation
Parallel to flow	E_0	11.74 GPa	12.16 GPa	3.6 %
	E_{90}	8.07 GPa		
Perpendicular to flow	E_0	8.54 GPa	8.75 GPa	2.5 %
	E_{90}	11.21 GPa		

Stiffness of individual slices was estimated with the Mori–Tanaka approach combined with the parallel axis theorem, assuming that the neutral axis coincides with the central axis of the specimen, enabled to define a flexural modulus of elasticity. The accuracy of the estimated stiffness was also evaluated through an experimental comparison. For this purpose, the specimens were loaded in three-point bending (L/h = 20) up to a maximum deflection of 0.25 %, and flexural modulus of elasticity was determined three times for one specimen.

The experimentally determined values were 13.53 GPa (μ = 0.51 GPa CV = 3.74 %) for the specimen extracted parallel to flow direction and 9.05 GPa (μ = 0.20 GPa, CV = 1.12 %) for the specimen perpendicular to flow direction. In Table 6.16 the average mean value of the experimentally measured flexural modulus of elasticity is compared with the analytically determined value.

Table 6.16: Comparison of analytically (Mori–Tanaka approach and parallel axis theorem) and experimentally determined flexural modulus of elasticity.

Orientation of specimen	Parameter	Mori–Tanaka	Experiment	Deviation
Parallel to flow	E_0	12.17 GPa	13.54 GPa	11.18 %
Perpendicular to flow	E_0	8.63 GPa	9.05 GPa	4.87 %

6.6.2 Analytical stiffness prediction of continuous carbon fibre SMC

The material properties listed in Table 6.17 have been considered to analytically describe the tensile modulus of elasticity in the fibre direction (0°). Figure 6.104 clearly shows that the RoM slightly overestimates elastic material behaviour in the fibre direction.

Table 6.17: Input parameters and material data of continuous carbon fibre SMC.

Parameter	Value	Reference
E_M	3.45 GPa	Experimentally determined (section 6.3.1)
E_F	242 GPa	Zoltek, 2018a
ν_F	0.2	CES EduPack, 2017
ν_M	0.38	Experimentally determined (section 6.3.1)

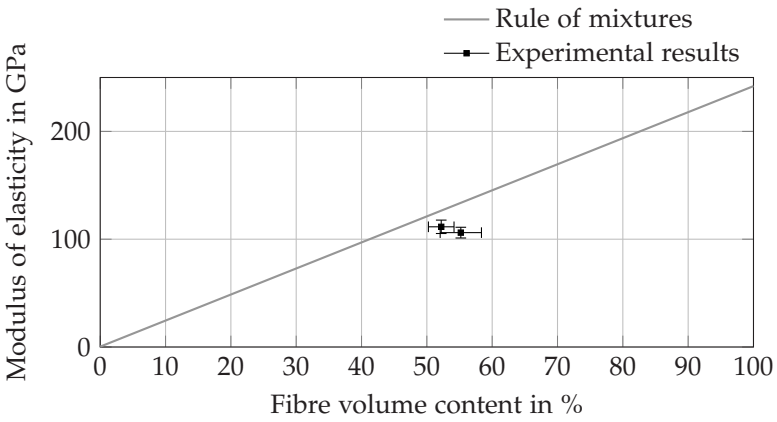


Figure 6.104: Longitudinal tensile modulus of elasticity of continuous carbon fibre SMC (0°) based on rule of mixtures.

Considering an FVC of 52.2 vol.% or 55.2 vol.% (sheet 1 and sheet 2) the predicted tensile modulus of elasticity is 128 GPa and 135 GPa, respectively. Taking into account the experimentally determined average value of 110.1 GPa this equals a deviation of 21.8 % and 15.5 %.

6.6.3 Analytical stiffness prediction of continuous-discontinuous glass/carbon fibre SMC

6.6.3.1 Tensile and compressive modulus of elasticity

The rule of hybrid mixtures (RohM) is an appropriate tool to predict the tensile modulus of elasticity of a hybrid composite. Since an analytical approach to predict the tensile modulus of elasticity of the continuous carbon fibre SMC composite (Figure 6.104) slightly overestimates material properties, the tensile and compressive modulus of the continuous carbon fibre SMC and the discontinuous glass fibre SMC were considered as input parameters.

The resulting stiffness of the hybrid laminate can be predicted by applying the RohM (Equation 5.44) as shown in Figure 6.105. To account for the scatter in material properties of SMC composites, calculation is based either on the arithmetic mean value or on the 25^{th} and 75^{th} percentile.

The experimental results depicted in Figure 6.105 depend on an average thickness of the hybrid specimens h = 2.91 mm and a thickness of the face sheets of h_f = 0.33 mm. Hence, $(2 \cdot h_f)/h \approx$ 0.22-0.23.

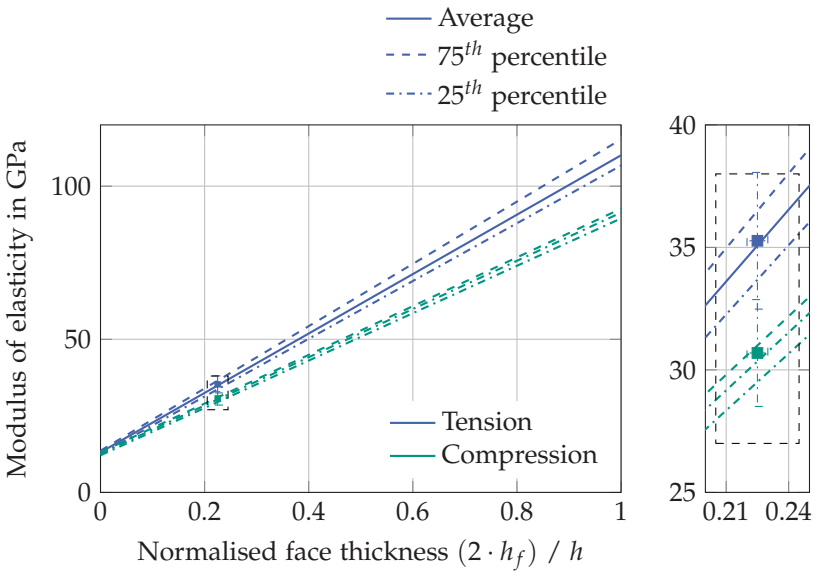


Figure 6.105: Tensile modulus of elasticity in fibre direction of the continuous component. Calculations based on hybrid rule of mixtures.

6.6.3.2 Flexural modulus of elasticity

The flexural stiffness of the hybrid CoDico GF/CF SMC laminate has been analytically modelled based on the classical laminate theory (CLT) (described in section 5.4.2). A symmetric and an asymmetric lay-up, due to the tension-compression anisotropy of the continuous material, were considered. Flexural rigidity resulting from a symmetric and an asymmetric lay-up are presented below. The analytical predictions based on the material parameters that appear in Table 6.18.

Table 6.18: Input parameters and material data of the discontinuous glass fibre SMC and continuous carbon fibre SMC considered for CLT.

Parameter	Value	Reference
$E_{11,Co,t}$ (average, tension)	110.08 GPa	Experimentally determined (section 6.3.3.2)
$E_{11,Co,c}$ (average, compression)	91.38 GPa	Experimentally determined (section 6.3.3.2)
$E_{22,Co,t}$ (average, tension)	8.31 GPa	Experimentally determined (section 6.3.3.2)
$E_{22,Co,c}$ (average, compression)	7.51 GPa	Experimentally determined (section 6.3.3.2)
$\nu_{12,Co}$	0.32	Experimentally determined (section 6.3.3.2)
$G_{12,F}$	105 GPa	CES EduPack, 2017
ϕ_F	53.4 vol.%	Experimentally determined (section 6.2.1)
$G_{12,Co}$	4.80 GPa	Förster and Knappe, 1971
$E_{11,Dico,t}$ (average, tension)	13.09 GPa	Experimentally determined (section 6.3.2.1)
$E_{22,Dico,t}$ (average, tension)	9.48 GPa	Experimentally determined (section 6.3.2.1)
$\nu_{12,Dico}$	0.38	Experimentally determined (section 6.3.2.1)
$G_{12,Dico}$	4.37 GPa	Experimentally determined (section 6.6.1)

In order to determine the shear modulus of the discontinuous glass fibre SMC ($G_{12,Dico}$), results obtained by the Halpin–Tsai approach depicted in Figure 6.100 were considered. The analytically predicted value of $G_{12,Dico}$= 4.37 GPa is within the boundaries described in CES EduPack (2017) considering a 40 wt.% glass fibre SMC (unsaturated polyester resin-based). Förster and Knappe (1971) presented a method to estimate the shear modulus of a unidirectionally carbon fibre reinforced lamina.

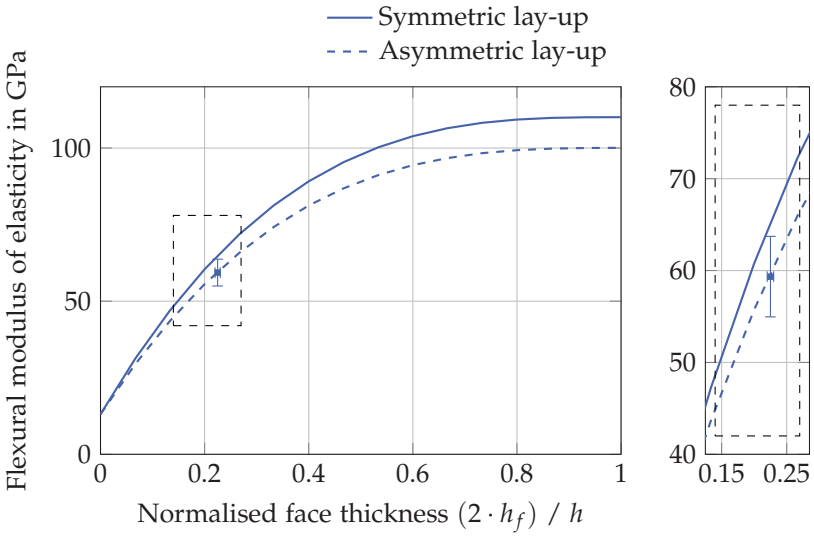


Figure 6.106: Flexural modulus of elasticity of continuous-discontinuous glass/carbon fibre SMC, predicted by classical laminate theory described in section 5.3.

As clearly depicted in Figure 6.106, the CLT based on a symmetric lay-up of the hybrid CoDico GF/CF SMC (assuming that tensile and compressive modulus of elasticity of the continuous component are equal) overestimates flexural stiffness ($E_{f,CLT,sym}$ = 64.06 GPa). Given the tension-compression anisotropy, the CLT (asymmetric lay-up) precisely predicts the resulting stiffness of the hybrid CoDico GF/CF SMC ($E_{f,CLT,asym}$ = 58.84 GPa). The experimentally determined arithmetic average equals E_f = 59.34 GPa, hence, deviation is below 1 %.

7 Discussion

The following section discusses the results presented in chapter 6. First, an evaluation of experimental methods is offered. Next, the particularity of the unsaturated polyester-polyurethane two-step curing hybrid resin system is addressed. The third part is based on the vertical characterisation strategy defined in chapter 4 and focusses on micromechanical observations followed by reasons explaining the observed mechanical behaviour of the individual and hybrid material, always linked to failure evolution and damage mechanisms. Attention is drawn primarily to the effect of hybridisation. In addition, tools to model stiffness and strength of the individual material, but more important of the hybrid material in an analytical way are evaluated in terms of complexity and accuracy of predictions.

7.1 Testing methodology and preliminary studies

This work has undertaken a deep investigation to determine the influence of the specimen's geometry on resulting mechanical properties. Tensile tests with different rectangular and dog-bone shaped specimens were carried out to define a possible influence of specimen geometry on the resulting material performance. Relative properties were compared to account for variations in the fibre volume content of different sheets and specimens, which were extracted from two-dimensional (2D) flow sheets with planar isotropic fibre orientation

(as shown in Figure 6.25). As stated in Marissen and Linsen (1999), smaller SMC specimens feature more cut fibres within the gauge section and less efficient reinforcement, deceasing the experimentally determined flexural stiffness and strength of the material. The relative stiffness of rectangular specimens featuring a width of 30 mm and a clamping distance of 100 mm (geometry R 2.1) was slightly lower than the stiffness of the same specimen type, clamped at a distance of 130 mm with the same gauge section (10×70 mm^2). Calculations of technical strains by averaging local displacement values considering a larger surface of the specimen may falsify results due to local strain concentrations (overestimation of average strains) near clamping (St. Venant's principle). However, relative material properties determined with slightly different geometries of the specimens did not significantly differ, and small variations can be based on structural rather than on statistical effects, as indicated by Varna et al. (1992).

The effect of the specimen's geometry on the relative strength of the discontinuous SMC material was slightly more important with larger specimens featuring lower strength (specimen geometry R 2 and B 2 in Figure 6.2). However, decreases were marginal (below 5 %) and not significant if scatter is considered. A possible explanation of this finding might be a size effect, commonly known for composite materials (Sutherland et al., 1999). The microstructure of a composite is important in determining the defects that may give rise to a size effect. At the microlevel, a decrease in fibre diameter was observed to lead to higher strength values (Griffith, 1921). Size effects on the specimen scale indicated that in smaller specimens, the probability of the occurrence of internal flaws or defects is lower than in larger ones. Hence, material strength might increase due to a size effect (Wisnom, 1999), for example. Size effects may explain the findings of this present dissertation.

Due to the heterogeneous microstructure, mechanical characterisation of discontinuous SMC materials was generally determined by a significant scatter. Taking stereo digital image correlation into consideration helped to deduce global information on strains resulting from mechanical loads. Conventional strain measurement techniques, such as strain gauges or extensometers, determine only local displacements, and evaluated strains depend strongly on the local microstructure of the contact zone. A parameter study pointed out that within appropriate bounds, measuring of displacement fields by means of digital image correlation to deduce strains was robust and reliable (Table 6.3).

7.2 Material behaviour of unsaturated polyester-polyurethane two-step curing hybrid resin system

The moulded unsaturated polyester-polyurethane two-step curing (UPPH) hybrid resin sheets exhibited high porosity, although the individual components were mixed in a vacuum to reduce the amount of air within the mixture. For this reason, tensile strength was characterised by a very high scatter, induced due to failure initiation at pores. Hence, the determined values should be considered with caution. Elastic properties (tensile modulus of elasticity and Poisson's ratio) which were important for modelling of material properties of the discontinuous and continuous SMC composites, however, could be determined precisely and matched very well with experimentally determined values of the same resin system presented by Kehrer et al. (2018).

Exposed to uniaxial compression, the rectangular specimens bent easily, and compressive failure strain could not be determined. Compressive strength was defined as the stress corresponding to the point in stress-strain response where the bending factor (b_f) reached a value of 0.1 (Figure 6.24).

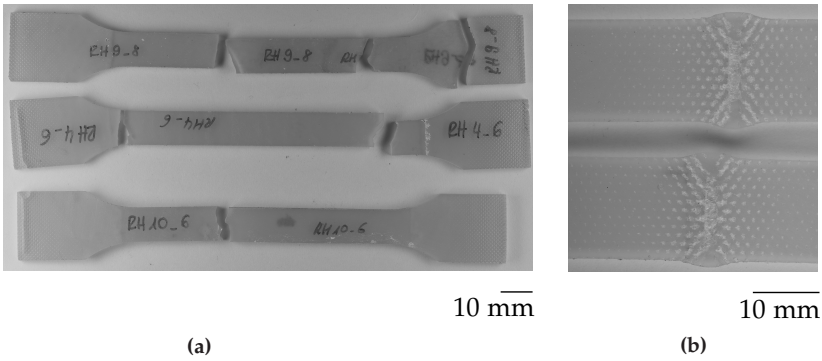


Figure 7.1: Damaged unsaturated polyester-polyurethane hybrid resin specimens, exposed to tensile loadings showing numerous fractures (a) and exposed to compressive loadings showing high plastic deformation (b).

Considering the experimental results, the unsaturated polyester-polyurethane hybrid two-step curing resin system exhibited a tension-compression anisotropy. Tensile loading led to a brittle failure of the specimens due to cracking, most probably simultaneously at different points (Figure 7.1a), whereas specimens featured a high plastic deformation if loaded in compression (Figure 7.1b) and did not fail even for a very small clamping distance ($\approx 5\,\mathrm{mm}$).

7.3 Discontinuous glass fibre SMC

7.3.1 Microstructural aspects of discontinuous glass fibre SMC

The discussion of microstructural aspects is based on the results presented in section 6.2. In the following, process-induced characteristics of fibre volume content and fibre orientation of the discontinuous glass fibre SMC composite are discussed as a starting point to relate the characteristic microstructure to the observed material properties.

Fibre volume content

Discontinuous glass fibre reinforced SMC sheets showed a higher average fibre volume content (26.6 vol.%) than the nominal fibre volume content of approximately 23 vol.%. The variation may be explained by the height of the resin film. Generally, it is calculated to lead, in combination with the adapted velocity of the conveyor belt and cutting unit, to a desired fibres-to-resin ratio and thus to a nominal fibre content. Variations in the film height of the resin between the theoretically calculated and real value resulting from a distinct viscosity and shear properties of the considered resin system are possible. Correction factors may be considered, based on detailed experience with the processing of a specific resin system to counteract the non-negligible amount of resin pressed out at the edges of the sandwiched SMC mat, due to calendaring and rolling-up of the semi-finished material. However, no correction factors were applied to adapt the film height of the resin to manufacture the materials considered within this dissertation. Investigations of the fibre volume content of the discontinuous (one-dimensional [1D]) glass fibre SMC material showed variations in average fibre volume content (FVC)

within one campaign (21.5 vol.% to 28.2 vol.%). However, only one sheet featured an FVC below the nominal value of 23 vol.% (Figure 6.9). It is possible that this distinct sheet was moulded with a stack of semi-finished material which originated from the end or the edges of the SMC roll. This section might thus feature a process-related lower fibre content. Due to the characteristics of the SMC manufacturing process and the bundle structure of the fibrous reinforcement, a locally divergent FVC resulted from processing and was unavoidable. The heterogeneous microstructure and the length of the bundles, which clearly exceeded the diameter of the specimens considered for thermogravimetric analysis (TGA) examinations, may favour the observed variations in fibre volume content within one sheet, between approximately 4 vol.% and 10 vol.%.

Different regions of one sheet, for example charge and flow region, did not show a characteristic distribution of FVC (Figure 6.11). Therefore, a sufficiently large number of specimens extracted at different positions of one sheet precisely describes the average real fibre volume content and its variation within one sheet. This value is important to know in order to describe mechanical properties based on micromechanical approaches.

Computed tomography allowed for the definition of fibre volume content in a non-destructive manner. The determined values based on image processing of $\mu - CT$ data of two distinct specimens extracted from the same sheet, were equal to 33.7 vol.% and 34.5 vol.%, respectively. The experimentally determined FVC (TGA) of the considered sheet was equal to 24.2 vol.%. The difference in results between the two methods highlights an important point of microstructural analyses through image processing based on μ-CT data. If the resolution is not high enough or the thresholds are not appropriately

defined, individual fibres within one bundle cannot be individually tracked. Instead, entire fibre bundles are considered to define the FVC, although the fibre volume fraction in a bundle is only 65 % on average (Orgéas et al., 2011).

Based on the same semi-finished material, variations in terms of FVC did not significantly differ between 1D and 2D flow sheets. In addition, as no distinct difference in average FVC and intra- as well as inter-plaque variation were observed for two manufacturing campaigns (Figure 6.10), the introduced process to manufacture non-filled structural glass fibre SMC which premised on the hybrid resin system, is robust.

Standard SMC formulations consider a significant amount of fillers, which may be as high as 40 wt.% (Orgéas et al., 2011), to account for special requirements (e.g. flame retardancy or to improve surface quality). Fillers increase a material's density having no enhancing effect on the material properties in general. The discontinuous SMC composite considered within the present dissertation is referred to as structural SMC, featuring no fillers and a nominal fibre content of $\approx$ 41 wt.%. With an average density of 1.53 g cm^{-3}, it has a high lightweight potential since standard SMC formulations, based on comparable fibre content feature densities in the range of 1.75 g cm^{-3} to 1.95 g cm^{-3} (CES EduPack, 2017; Oldenbo et al., 2003).

Fibre orientation

The investigated discontinuous glass fibre SMC exhibited a significant anisotropy in terms of fibre orientation with distinctly formed shell and core layers (Figure 6.14 and 6.15), as typically known for SMC materials and stated for example by Kim et al. (1992) or Le et al. (2008). It is highly possible that the discontinuous glass fibre

SMC considered within this study deformed in uniform extension within the core layers, as described by Barone and Caulk (1985). The contact of the semi-finished material with the preheated mould led to faster movement of the material within the shell layers, usually in the bottom half, since the material's viscosity was decreased in the contact zone. Splitting of fibre bundles and curvature of fibres, observed within the shell layers, might be a result of the aforementioned flow phenomena and the severe shearing of the paste-rich boundary layers (Le et al., 2008). Furthermore, as stated by Odenberger et al. (2004) during the initial phase of flow, outer layers of the stack are not forced to remain outer layers and may also move axially. However, the investigated SMC was characterised by a slightly orthotropic fibre orientation, with a negligible amount of fibre bundles aligned in z-direction ($O_{zz} \approx 0$). This fibre orientation indicates that shear deformation of the bundles due to flow was negligible and the compression moulding process was preferably defined by a plug-flow of the material. Resulting from one-dimensional (1D) flow, a preferred orientation with more fibre bundles aligned parallel to flow direction was observed. The ratio of O_{yy}/O_{xx}, given values averaged over the thickness of the specimen, was equal to 1.79 for the specimens extracted in flow direction. With a ratio of $O_{yy}/O_{xx} = 1.18$ (Le et al., 2008) observed for compression moulded sheets without significant flow, anisotropy in terms of fibre orientation becomes clear for the SMC composite investigated within this dissertation.

7.3.2 Mechanical behaviour and damage evolution of discontinuous glass fibre SMC

Coupon level: Tensile, compressive and flexural properties
The mechanical properties of SMC composites depend strongly on manufacturing parameters and material flow (Taggart et al., 1979; Trauth et al., 2018, 2017a). The effect of fibre orientation was also observed within this dissertation, and 2D flown sheets featured planar isotropic material properties (Figure 6.25) with a factor of anisotropy of f_A = 1.05 in terms of tensile modulus of elasticity (E_t) and tensile strength (R_t). A 1D flow led to anisotropic material properties (Figure 6.26) and regardless of loading case, material properties in the flow direction (0°) were significantly enhanced, as compared to the material performance perpendicular to flow. Material flow during compression moulding aligned fibre bundles in the flow direction across the entire sheet, and no difference was observed in the mechanical material behaviour of charge and flow region specimens. Tensile, compressive and flexural modulus of elasticity featured a factor of anisotropy of f_A = 1.38, 1.37 and 1.38, respectively.

Anisotropy of strength was more severe, with f_A = 1.96 for tensile, f_A = 1.33 for compressive and f_A = 1.67 for flexural loads. In order to compare the effect of fibre orientation on different loading cases, it is important to consider, that free length (between the clamping) of specimens differed with respect to different testing procedures. Hence, the volume of the specimen exposed to load differed (especially in terms of uniaxial compression and tension). Variations in material properties (0°) were most important for tensile loads (CV was in the range of 17 % to 30 %, CV of R_c and R_f were below 15 % and 11 %, respectively). Especially in terms of strength, the observed anisotropy was more severe compared than the material investigated,

for example, by Taggart et al. (1979) (tensile strength: f_A = 1.32, compressive strength: 1.13 < f_A < 1.26). However, a more significant effect of flow on anisotropy was stated by Boylan and Castro (2003), with $f_A \approx 1.5$ for stiffness and $f_A \approx 2.6$ for tensile strength.

The aforementioned findings highlight the importance of determining the mechanical material properties of an SMC composite in strong interaction with preceding flow during compression moulding. Depending on the resin system, fibre type and mould geometry, the influence of material flow on resulting mechanical performance may significantly differ and cannot be generalised.

In terms of tensile modulus of elasticity, the investigated Dico GF SMC composite showed lower mechanical properties, compared to a 45 wt.% polyester- based SMC material investigated by Chaturvedi et al. (1983). The aforementioned material featured an average tensile modulus of 14.7 GPa, but no details were presented on manufacturing parameters, nor mould coverage or flow condition. The Dico UPPH-based GF SMC composites considered within this dissertation, featuring a comparable fibre content, were characterised by a slightly lower average tensile modulus of elasticity (13.1 GPa in flow direction and 9.5 GPa perpendicular to flow direction). However, considering scatter in mechanical testing, this deviation is not significant. The tensile modulus of elasticity of a vinylester-based SMC composite with a fibre weight content of 41 wt.% investigated by Trauth et al. (2017a) was equal to 11 GPa in the manufacturing direction and 9.4 GPa perpendicular to the direction of manufacturing. Since the sheets investigated by Trauth et al. (2017a) did not flow, anisotropy was less severe (f_A = 1.19). Featuring a comparable FVC, the presented UPPH-based 2D flow Dico SMC composites (R_t = 159 MPa) clearly outperformed the vinylester-based SMC composite in terms of

tensile strength (R_t = 100 MPa, Trauth et al., 2017a). However, slightly smaller specimens have been considered within this dissertation, and due to a 100 % mould coverage realised by Trauth et al. (2017a), entrapped air might present an explanation of the SMC composite's lower strength.
Determination of compressive properties was rarely carried out on SMC materials in the past. Database values presented in the CES EduPack (2017) indicate a compressive modulus of elasticity of a 40 wt.% glass fibre SMC, based on an unsaturated polyester of 11.6 GPa. This value ranges between the experimentally determined value of compressive modulus of elasticity in 0° ($E_c \approx$ 12.6 GPa) and 90° ($E_c \approx$ 9.2 GPa) for the material considered within this dissertation. A polyester-based SMC investigated by Taggart et al. (1979) featured comparable stiffness (E_c = 12.4 GPa), but at a lower fibre content (25 wt.%). In terms of compressive strength, indicated values range between 204 MPa to 284 MPa for a fibre volume content from 25 wt.% to 65 wt.% (Table 2.3). Although the indicated values might be inferior to the results obtained for specimens aligned perpendicular to flow within this dissertation, experimentally determined strength values perpendicular to flow ($\approx$ 225 MPa) were significantly lower than a 40 wt.% unsaturated polyester-based SMC (CES EduPack, 2017) due to a flow-induced anisotropic fibre orientation.

Compared to polyester-based SMC composites featuring a FWC of 25, 30 or 65 wt.% (investigated by Walrath et al., 1982) the UPPH-based material investigated within this dissertation showed a significantly higher flexural modulus of elasticity. However, compared to the flexural properties presented by Chaturvedi et al. (1983) (polyester-based SMC, FWC: 45 %), flexural modulus of elasticity was slightly lower but flexural strength exceeded the values presented by Chaturvedi et al. (1983).

Generally, comparison of quantitative material data of different SMC composites is difficult, since mould coverage and flow, as well as specimen orientation, specimen geometry and testing parameters, may significantly vary.

The investigated discontinuous UPPH-based SMC composite did not show significant variation in terms of tensile, compressive or flexural modulus of elasticity. Nevertheless, as generally known for SMC materials and stated, for example, by Taggart et al. (1979), Mrkonjic et al. (2015) or Trauth et al. (2017a) – and as summarised in Table 2.3 – the investigated UPPH based discontinuous glass fibre SMC also exhibited a significant tensile-compression asymmetry in terms of strength, and $R_t < R_f < R_c$ holds true. However, this finding has to be critically reflected with respect to specimen size. This special characteristic is important to consider when mechanical material properties are sought to be modelled (Feld et al., 2017; Oldenbo et al., 2004).

Exposed to tensile loads, damage of Dico GF SMC was characterised by a failure evolution well known for SMC materials, described by Derrien et al. (2000), Jendli et al. (2005) or Wang et al., 1983, for example. Nevertheless, the kinking of the stress-strain curve ('knee-point') was not as pronounced as for standard SMC materials as defined by Chaturvedi et al. (1983), for instance. The absence of fillers or the special UPPH resin system might present possible explanations. Elastic deformation of the investigated Dico GF SMC was followed by the formation of interfacial cracks most likely perpendicular to loading direction. Microcracks within the matrix started to propagate, but fibre bundles aligned perpendicular to loading direction impeded further crack growth. Cracks were forced to propagate around the fibres, and crack growth was hence more likely to happen

perpendicular to the loading direction. For this reason, earlier failure of specimens with fibres preferably aligned perpendicular to flow resulted, probably due to an easier spread of the cracks over the entire width of the specimen. This growth of cracks explains lower strength observed for 90° specimens ($\approx 0.5 \cdot R_t$ of 0° specimens). Observation of post-mortem specimens exposed to tensile loads furthermore indicated a change from individual fibre failure in the shell layers to fibre bundle pull-out and pseudo-delamination within the core (Figure 6.37). As indicated, material flow during moulding led to a separation of individual filaments from the bundle structure of the shell. In this part of the specimen, fibres were also more likely to be characterised by a distinct curvature, which locally changed the orientation of the fibres in the shell layers with respect to the direction of loading (Figure 6.17). Fibres in the shell layers tended to break as soon as strength of an individual fibre was exceeded. Due to the slightly different orientation of the fibres, the possibility of breakage differed for different fibres. Within the core, fibre bundles could maintain higher loads, as stresses were transferred within the bundle and distributed between multiple fibres. For this reason, fibre bundles did not break as easily as single fibres, if exposed to tensile loads but interface failure was more likely to happen, resulting in pull-out of fibre bundles or pseudo-delamination.

Exposed to uniaxial compression, specimens mainly failed due to shearing. Pseudo-delamination was not as important as for tensile loadings. Compressive loads counteracted crack growth and debonding, leading to higher damage tolerance of the SMC composite and explaining higher the compressive strength of SMC materials, also linked to higher failure strains.

Exposed to out-of-plane loads, Dico SMC was not significantly sensitive to shear strains, and even for a span-to-thickness ratio of 4:1, no pure shear failure was observed. Dico GF SMC exhibited a high damage tolerance if loaded in three-point bending, and high deflections were possible before failure strain was reached. Failure was highly localised below the loading nose, based on chipping of (Chaturvedi and Sierakowski, 1983) and failure between fibre bundles.

Modelling approaches

Applying a generalised rule of mixtures (RoM) to estimate the stiffness of the discontinuous glass fibre SMC, according to Equation 5.23, resulted in a modulus of elasticity of 7.9 GPa for an average fibre content of 25.2 vol.% (average mean value of investigated 2D SMC sheets, depicted in Figure 6.10). Hence, the predicted value significantly underestimates ($\approx -30\,\%$) the experimentally determined stiffness of a 2D GF SMC, and it is not recommended to be considered to analytically predict the stiffness of chopped fibre SMC composites.

The Halpin–Tsai approach was based on a small number of input parameters. However, this method does not generally account for fibre orientation, and the predicted stiffness is most likely to represent the material behaviour of a planar-isotropic SMC with no preferred fibre orientation resulting from material flow. With an experimentally determined average value of E_t = 11.6 GPa determined for 2D flow SMC sheets with an assumed planar-isotropic fibre orientation and no distinction made between charge and flow region specimens or 0° and 90°, the analytically determined value slightly (6 %) overestimated the stiffness of the material. However, this variation was not significant with respect to the intrinsic scatter of material properties

of SMC composites and it is important to mention that the Halpin–Tsai approach is easy to apply to gain a basic understanding of the mechanical performance of SMC materials not exposed to uniaxial flow during compression moulding.

Predictions based on the Mori–Tanaka approach allowed for a description of longitudinal and transverse stiffness of the material through consideration of information on fibre orientation gained by μ-CT observations. Deviations between experimentally and theoretically predicted values were marginal (below 4 %) and may have resulted from the value of fibre volume content considered for modelling. The average fibre volume content (determined by TGA) of the sheets from which specimens have been extracted was consulted to calculate the stiffness of the specimens. However, in reality the FVC was characterised by variations with respect to the specimen's thickness. A precise determination of fibre volume content is important to consider for this homogenisation approach, and it would be best to consider local fibre volume contents within different layers of the specimen according to the components of the FOTs. This method implies, however, that only small volumes of the material could be considered to achieve a sufficiently high resolution of the μ-CT images. Nevertheless, with regard to the small deviations, the Mori–Tanaka approach was an appropriate tool to predict the tensile modulus of elasticity of the one-dimensionally flown sheets, even though only an average fibre volume content of the sheet was considered.

Given the layered structure of the SMC materials, which results due to stacking of multiple layers of the semi-finished material prior to moulding, a summation of the stiffness of individual layers with respect to the neutral axis and a parallel axis theorem enhanced the

accuracy of the predicted flexural modulus (error decreased from 15.3 % based on a simple summation to 11.3 % based on a summation with parallel axis theorem). Nevertheless, variation between calculated and experimentally determined values was higher for flexural stiffness than for tensile properties. Observation by means of μ-CT was based on an alignment of the captured images to compensate for possible misalignment of the specimen within the computer tomograph. Hence, the surface layers were possibly (artificially) cropped for image processing and could not be evaluated in terms of fibre orientation. Since these layers most importantly influence flexural stiffness, the effect on estimated flexural modulus is more important compared to a possible induced error while predicting tensile modulus of elasticity.

Structure level: Puncture properties

Considering puncture properties of SMC composites, a wide literature review indicated that, so far, little attention has been paid to rate effects.

In Trauth et al. (2018), a positive rate dependence of puncture properties was observed for SMC composites based on the same UPPH resin system as considered within this dissertation with a comparable glass fibre reinforcement (41 wt.%, 25.4 mm long fibres). Maximum load and energy absorption capability significantly increased for higher loading rates for charge (65 % and 67 %) and flow region specimens (73 % and 64 %). The findings of Trauth et al. could be confirmed by the results of this study (section 6.4.1). Nevertheless, the increase in maximum load and puncture energy was slightly less important (increase in maximum load and puncture energy was $\approx$ 60 % and 50 %, respectively), which could be explained by the anisotropic fibre orientation of the 1D flow SMC sheets. In Trauth et al., 2018 2D

flow sheets have been considered for experimental investigations. In addition, intrinsic scatter is again important to consider.

Due to manufacturing of the SMC sheets in a compression moulding process, variations in thickness are possible which may influence the resulting puncture properties, and an exponential correlation between maximum load or absorbed energy and thickness of the specimen was observed for SMC materials (Kau, 1990; Lee et al., 1999), as affirmed in EN ISO 6603-2 (2000). Given the results of the present study, no significant influence of specimens' thickness on dynamic impact properties could be observed (coefficient of regression $r^2 < 0.5$). Variations in fibre volume content, hence variation in density and thus mass of the specimens, also did not significantly influence dynamic puncture properties ($r^2 < 0.3$).

Considering quasi-static puncture loads, strength and puncture energy correlated with $h^{1.98}$ and $h^{2.0}$, respectively. However, regression coefficients (r^2) were only 0.6 and 0.7, and variations in terms of thickness of the Dico GF SMC sheets ($\bar{h}$ = 2.85 mm, μ = 0.11 mm, CV = 3.83 %) were too small to significantly affect puncture properties. Due to a very localised loading, the highly heterogeneous microstructure had a more important effect on puncture properties.

Damage of discontinuous glass fibre SMC exposed to quasi-static and dynamic puncture was characterised by a comparable damage evolution. In general, it was mainly based on the formation of radial cracks initiated below the striker. A yield point could be defined for both loading rates, characterised by a decrease in stiffness, followed by a second linear load-deflection response, with a reduced slope. In-situ image capturing allowed for investigation of damage evolution, and this yield point was linked to damage initiation on the lower

surface, affecting the macroscopic stiffness of the material (Kau, 1990). Dico GF SMC specimens exposed to puncture loads did not fail abruptly, and no distinct point in the force-deflection response could be assigned to breaking. The failure was characterised by a gradual failure linked to a slight but steady decrease of the force-deflection evolution due to successive crack formation and growth, strongly dependent on fibre distribution and orientation.

In the dynamic loading case, due to a relatively low stiffness of the material, oscillation of the specimen resulted due to the impacting energy. Although this effect is normally less severe for lower impacting speeds (Cheresh and McMichael, 1986), the initial part of the load-deflection curve of the Dico GF SMC was characterised by a dynamic offset. Hence, calculation of the material's puncture stiffness is complex. The presented method to define puncture stiffness within this dissertation accounted for a possible indentation of the striker at the beginning of loading (Hertzian contact) and did not consider deflections below 1 mm in the quasi-static loading case. The same deflection range was considered for dynamic puncture for the sake of comparability and to take the dynamic offset into consideration.

The increase in maximum load and energy absorption capability were most likely based on different failure mechanisms, which determined the damage evolution of the material. Failure modes of glass fibre reinforced polymers may change with increasing loading rate (Okoli, 2001). A transition in failure modes of Dico GF SMC exposed to puncture was already observed by Trauth et al. (2018), with fibre pull-out and matrix cracking being more important at higher loading rates. In addition, the matrix properties significantly influence evolving damage, since the aforementioned failure mechanisms such as fibre pull-out, for example, strongly rely on the fibre-matrix interfacial

strength (Mallick, 2007). Jendli et al. (2005) also concluded that, exposed to higher loading rates, the fibre-matrix interface failure strength of SMC composites significantly increased.

7.4 Continuous carbon fibre SMC

7.4.1 Microstructural aspects of continuous carbon fibre SMC

The fibre volume content (FVC) of continuous carbon fibre SMC was generally higher than the nominal fibre content for the same reasons as described in section 7.3.1. Due to the continuous reinforcement, which somehow eliminates the effect of TGA specimen size, intra-plaque variations were lower than for the discontinuous material (below 5 % with the exception of one sheet). However, thinner sheets were characterised by a higher scatter. A possible explanation might be insufficient impregnation, which was most severe for the thinnest ($h \approx 1\,\text{mm}$) sheets, as depicted in Figure 7.2. Dry spots possibly resulted from a too small amount of resin on the upper and lower carrier foil during manufacturing of the semi-finished material. In addition, if pre-curing of the special UPPH resin system is not sufficiently controlled by heating and cooling down the SMC mat on the conveyor belt or due to a too long delay between manufacturing of the semi-finished material and the following compression moulding step, the material may be at risk to dry out. Since dry spots were not observed in such a significant amount on thicker Co CF SMC sheets, re-impregnation of thicker sheets (distribution of resin) might be possible during moulding.

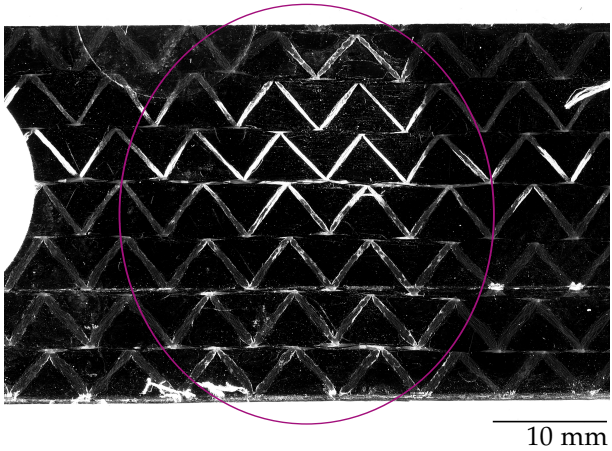


Figure 7.2: Dry spots on compression moulded continuous carbon fibre SMC sheet featuring a nominal thickness of 1 mm.

7.4.2 Mechanical behaviour and damage evolution of continuous carbon fibre SMC

Coupon level: Tensile, compressive and flexural properties

Manufacturing of continuous carbon fibre SMC, based on an adopted SMC process, is reliable and leads to a continuous carbon fibre composite with properties comparable to those of conventional unidirectional carbon fibre reinforced polymers (Trauth and Weidenmann, 2016). However, resulting material properties were determined by a significant scatter. Inhomogeneities in the material due to locally insufficient impregnation and thus variations in fibre volume content and fibre misalignment were the most important reasons for the observed scatter. Considering tensile loads, an increasing FVC did not automatically lead to enhanced tensile properties due to the aforementioned detrimental properties of the Co CF SMC sheets.

Furthermore, preliminary tests showed that mechanical performance tends to decrease if continuous carbon fibre SMC sheets were stored and mechanically loaded at a later time (Figure 6.4). The complex B-stage evolution combined with variable time frames between manufacturing of semi-finished materials and moulding or between testing campaigns may explain the observed tendencies. However, such investigations were not in the scope of this dissertation, and further investigation must be made to better understand the curing characteristics and ageing effects of Co CF SMC.

The mechanical material performance of the continuous carbon fibre SMC was significantly determined by a tension-compression anisotropy. As commonly stated in the literature (e.g. Serna Moreno et al., 2016; Soutis, 1997), compressive strength was significantly lower than tensile strength. The anisotropy most possibly resulted from shear mode deformation (fibre microbuckling or kinking) (Berbinau et al., 1999; Rosen, 1965). According to Naik and Kumar (1999) kinking is defined as a direct consequence of localised plastic microbuckling, coupled with low failure strain of the reinforcing material. This failure mode was first (analytically) described by Rosen (1965), who stated, that due to the small diameters of the individual fibres, described as slender columns, buckling is highly possible, although the composite may not tend to buckle on the macroscopic scale. A weak radial bond between the fibres further favours this failure mode if the composite is exposed to compressive loads (Hahn and Williams, 1986), and shear properties of the matrix become extremely important (Eyer et al., 2016). In contrast to tensile stiffness and strength, which are fibre-dominated properties of a continuous material, the matrix properties play a more decisive role if a unidirectional composite is loaded in compression. The low compressive strength of the continuous carbon fibre SMC is a limiting

parameter in designing hybrid CoDico SMC structures. With a ratio of $E_c/E_t \approx 0.8$ and $R_c/R_t \approx 0.4$, deviation between the tensile and compressive stiffness and strength of the investigated continuous carbon fibre SMC was more severe compared to values presented in the literature (e.g. $R_c/R_t \approx 0.6$ (Budiansky and Fleck, 1993). Limited compressive strength also resulted in early failure initiation due to compressive strains during out-of-plane loading of continuous carbon fibre SMC.

As depicted in Figure 7.3, in some cases Co CF SMC was characterised by a significant misalignment of the fibres with respect to axis of the sheet, hence loading direction. Possible sources of the resulting fibre misalignment are the feeding of the dry non-crimp fabric at the beginning of the conveyor belt, a shifting during manufacturing of the semi-finished material or an inaccurate placement of the semi-finished sheet on the cutting table or inside the mould, as well as stacking of different layers of the semi-finished material prior to moulding. In addition, extraction of the specimens for mechanical characterisation may also influence the fibre orientation within the specimens. Fibre misalignment significantly affects strength of unidirectionally reinforced composites, especially in terms of uniaxial compression (Wisnom, 1990). In addition, deviations from an ideal parallel fibre orientation of unidirectional fibre-reinforced composite with respect to loading direction reduces resistance to splitting (Hillig, 1994). Observation of failure evolution resulting from uniaxial tension indicated that Co CF SMC characterised by a distinct fibre misalignment likely failed due to the formation of inter-fibre cracks. Cracks were most likely initiated where misaligned fibre bundles met the edges of the specimens. The evolution of the stress-strain curve prior to final failure reflected successive crack formation and growth. If misalignment was not too pronounced, specimens likely failed due to fibre fractures and spontaneous bursting. The failure evolution of

continuous carbon fibre reinforced materials usually depends heavily on the fibre matrix interface (Hamada et al., 1997), which might also play an important role in the evolving damage of the investigated Co CF SMC composites within this dissertation, since a weak interface might favour the formation and growth of inter-fibre fractures.

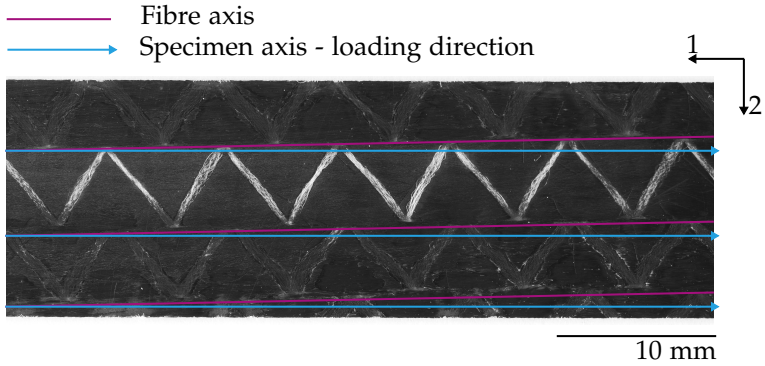


Figure 7.3: Macroscopic observation showing fibre misalignment of continuous carbon fibre SMC composite.

Additionally, the microstructure of continuous carbon fibre SMC was characterised by fibre waviness. It was defined by an out-of-plane ondulation resulting from the stitching yarns of the individual layers (Figure 7.4) and the stacking of several semi-finished sheets to obtain moulded plaques featuring different thicknesses. Fibre misalignment and fibre waviness (in- and out-of-plane misalignment) resulted from the organisation of fibres (multiple filaments) in bundles, which were held together by stitching yarns. Fibre waviness generally has a negative influence on material and laminate properties consisting of unidirectional carbon fibre reinforced layers (Adams and Hyer, 1994; Wisnom, 1990, 1999). It influences not only tensile but also compressive properties such that the greater the misalignment, the weaker and more compliant the laminate (Budiansky and Fleck, 1993;

Mrse and Piggott, 1993). Simulation of tensile and compressive failure of continuous carbon fibre reinforced materials loaded perpendicular to the fibre direction reveal that the tension fracture initiates as interfacial debonding and evolves as a result of interactions between interfacial debonding and matrix plastic deformation, while the compression failure is dominated by matrix damage (Lei et al., 2012).

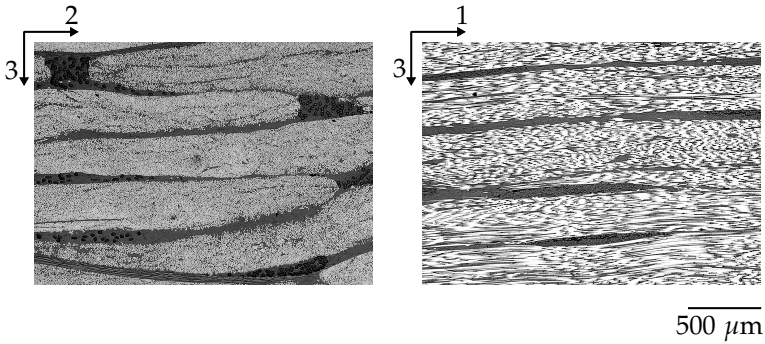


Figure 7.4: Microscopic observation of continuous carbon fibre SMC (axis 1 is parallel to the fibres) showing ondulation and fibre waviness.

Modelling approaches

With regard to the aforementioned microstructural particularities, analytical prediction of tensile modulus of elasticity in the fibre direction through the application of a rule of mixtures significantly overestimates the experimentally determined value by 20 %. Indeed, the Voigt bound is the upper bound of a predicted material property, assuming all fibres are perfectly aligned in the fibre direction. A misalignment of fibrous reinforcement decreases the resulting material stiffness, with an increasing misalignment angle. Taking into account that matrix failure strain ($\varepsilon_{max} \approx 3\,\%$) is higher than (carbon) fibre failure strain ($\varepsilon_{max} \approx 2\,\%$ CES EduPack, 2017),

and hence strength prediction according to Figure 2.5a, it was possible to estimate tensile strength of Co CF SMC featuring a FVC of 55 vol.%. With the described approach, analytically determined strength equals $\approx$ 2300 MPa. The average experimental value of 1424 MPa is 60 % lower. This significant deviation might underline the effect of fibre misalignment, ondulation and dry spots observed for the continuous carbon fibre SMC. In addition, the fibre strength defined by the supplier might be a result of fibre bundle and not single-fibre testing, hence deviating from real fibre properties. Considering the technical data sheet of the supplier, which lists the material properties of the non-crimp fabric in a unidirectional layup, as considered within this dissertation (Zoltek, 2018c), the average strength value of 1440 MPa (FVC of 55 vol.%) is in the same range as the experimentally defined value.

Structure level: Puncture properties

Puncture properties of carbon fibre reinforced composites show most likely no variation of mechanical performance due to a variation of loading rate (Caprino et al., 2003; Trauth et al., 2018), and a possible explanation might be the non-rate sensitivity of the carbon fibres (Zhou et al., 2010). The continuous carbon fibre SMC composite investigated within this dissertation even exhibited a slightly negative rate dependence in terms of strength and energy absorption capability. The parallel fibre bundles were no important obstacle for the striker, which easily punctured the specimen especially at higher loading rates, hence impacting energies, and failure was brittle and catastrophic.

The resulting force-deflection response, regardless of puncture velocity, was characterised by an increase to maximum load, which was followed by a sudden load drop. Failure was mainly based on the

formation and growth of inter-fibre cracks. Once initiated, fractures grew easily and spontaneously. A yield point leading to a slightly decreased slope in the quasi-static loading case, was hence linked to very low deflections (below 1 mm) and indicated the early onset of failure. For this reason, stiffness was defined by fitting the slope of the force-deflection response below a deflection of 1 mm.

In general, impact or puncture testing of continuously reinforced materials is based on laminates featuring a stacking sequence which deviates from a purely unidirectional reinforcement with only 0° plies (e.g. Belingardi and Vadori, 2002 and Li et al., 2002). The architecture of fibrous reinforcement of the Co CF SMC considered within this dissertation is not suitable to sustain puncture loads. However, puncture testing of Co CF SMC within this dissertation aimed to define a reference of puncture properties and to evaluate the effect of hybridisation in a subsequent step. For this reason, the same layup of the continuous carbon fibre SMC, considered for hybridisation (only 0°) was taken into account to deduce puncture properties.

7.5 Continuous-discontinuous glass/carbon fibre SMC

7.5.1 Microstructural aspects of continuous-discontinuous glass/carbon fibre SMC

The two different SMC composites (Dico GF and Co CF SMC) feature a comparable density of $\rho_{Dico} = 1.53\,\mathrm{g\,cm^{-3}}$ and $\rho_{Co} = 1.50\,\mathrm{g\,cm^{-3}}$. Hence, the density of the hybrid SMC had a similar magnitude.
Scanning electron microscopy (SEM), μ-CT and macroscopic observations enabled investigation of the microstructure of the hybrid

CoDico SMC composite (section 6.2). The results most importantly depicted a transition zone between the discontinuous and the continuous material, and no sharp or distinct interface was formed. The material flow of the discontinuous component locally pushed the continuous fibre bundles apart during moulding. The glass fibre bundles' individual fibres spread and separated from the bundles and showed a higher curvature in the transition zone, similar to the microstructure, which was observed for pure discontinuous glass fibre SMC. As known for standard SMC materials, bundle structure was not influenced in the core layers in terms of separation or curvature. Fibre orientation distribution within the discontinuous component of the hybrid SMC was comparable to the evolution of the components of the fibre orientation tensor over thickness of a pure discontinuous glass fibre material (Figure 6.19). Comparable average values were obtained ($O_{yy} \approx 0.6$ [flow direction] and $O_{xx} \approx 0.4$). The transition zone within the hybrid material featured a thickness of ≈ 0.5 mm (Figure 6.20).

As already discussed by Mallick (1986) and Corbridge et al. (2017), the misalignment of the continuous material, resulting from crossflow of the discontinuous component in a one-shot compression moulding process of hybrid SMC sheets, also negatively affected resulting material properties of the hybrid CoDico GF/CF SMC investigated within this dissertation. Failure evolution due to inter-fibre fracture was favoured by misaligned fibres meeting the edge of the specimen. Taking into account the manufacturing process presented within this dissertation, there was no significant cross-flow of the discontinuous material during moulding of the hybrid SMC sheets. However, hybrid SMC sheets were nevertheless characterised by a significant (local) spreading and fibre misalignment (Figure 6.22). Thus, although the stack of discontinuously reinforced semi-finished material

featured the same width as the mould, local cross-flow occurred. Since there was no stabilising mechanism (fixation) perpendicular to the fibre axis, shearing and pushing apart usually occurred between different continuous carbon fibre bundles.

7.5.2 Mechanical properties, damage evolution and hybridisation effect

7.5.2.1 Coupon level

The following section deals with the discussion of mechanical material properties and failure evolution of the CoDico GF/CF SMC at the coupon level. Different criteria to evaluate a hybridisation effect are discussed and the effect of hybridisation in terms of mechanical performance and damage evolution is considered.

Evaluation of hybridisation effects

The primary objective of hybrid composites is to enhance a distinct property of a material, structure or component which might be of mechanical, physical or thermal origin, for example. Within this dissertation, only mechanical properties were of interest. For this purpose, in terms of uniaxial loads, the effect of hybridisation was evaluated for material properties in the fibre direction of the continuous component. The arithmetic mean value of distinct properties was accounted for (with no difference between charge and flow region specimens) to evaluate the effect of hybridisation (EoH_2), and the mechanical performance of the Dico GF SMC was considered as a reference. Due to the brittle nature of continuous fibre reinforced composites, failure strain and deflection at failure of the Co CF SMC were considered references to evaluate a possible enhancement of damage tolerance resulting from hybridisation.

Taking a deviation from the rule of mixtures into consideration to evaluate an effect of hybridisation (EoH_1) is suitable only for uniaxial loadings. In addition, it is important to precisely describe the volume fractions occupied by the individual constituents, as stated by Phillips (1976). The thickness of the investigated hybrid CoDico GF/CF SMC sheets ($\bar{h}$ = 2.91 mm) featured only slight variations (μ = 0.06 mm, CV = 2.19 %). Nevertheless, the thickness of the continuous reinforcement was characterised by high variations. As depicted in Figure 6.22 and Figure 7.5, the pushing apart of the continuous carbon fibres in the transition zone, even locally, led to a disruption of the continuous reinforcement.

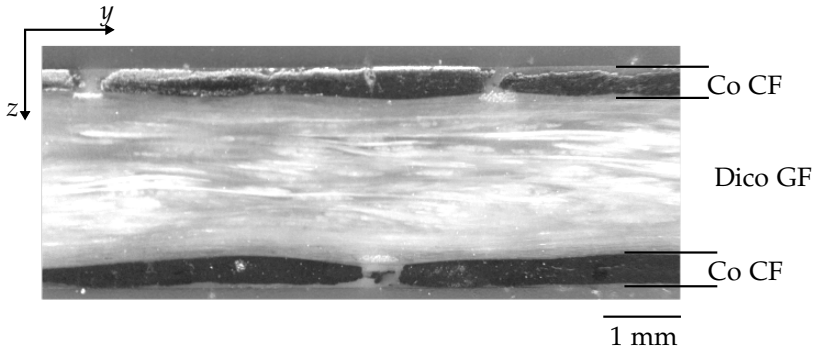


Figure 7.5: Section through a compression moulded continuous-discontinuous glass/carbon fibre SMC specimen to depict layered structure, spread carbon fibre bundles and variable thickness of the continuous reinforcement.

The inconsistency of continuous reinforcement, especially, complicated predictions of the material properties. Consequently, a thickness of 2 · 0.33 mm of the face sheets and h = 2.91 mm of the laminate was considered (hence $(2 \cdot h_f)/h$ = 0.23) to apply a rule of hybrid mixtures according to Equation 5.44. Furthermore, a variation of ± 0.05 mm was considered to define scatter whilst modelling material properties.

Tensile modulus of elasticity and tensile strength

When characterising hybrid composites, it is generally not recommended to measure displacements with strain gauges or an extensometer, since these techniques do not account for the variability of locally different material properties resulting from the anisotropic and heterogeneous microstructure of the material (Feraboli et al., 2009). Digital image correlation, however, provides an appropriate measurement technique to account for microstructural heterogeneities (Johanson et al., 2015; Selezneva and Lessard, 2015). It also offers a possibility to investigate damage evolution (Laurin et al., 2012). This contactless measurement technique also provides the important advantage, that a partial failure does not lead to distorted strain measurements which could result from a measurement with devices which have contact with the specimen (e.g. an extensometer). The following discussion of mechanical performance within this section is based on the results and findings presented in section 6.3.3.

As clearly indicated in Figure 7.6, which sums up the tensile properties of the two individual and the hybrid SMC composites, a linear correlation was observed for tensile modulus of elasticity and tensile strength due to hybridisation.

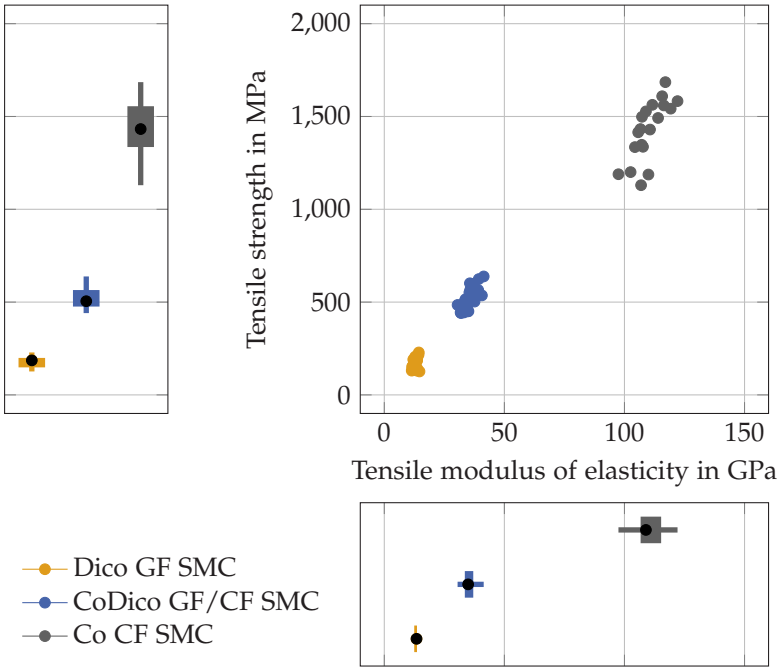


Figure 7.6: Tensile properties of continuous carbon fibre SMC, discontinuous glass fibre SMC and continuous-discontinuous glass/carbon fibre SMC to evaluate the hybridisation effect (● = median, box indicates 25^{th} to 75^{th} percentile; lines indicate minimum and maximum or 1.5 interquartile range, respectively).

Hybridisation of SMC composites within this study led to a significantly increased **tensile modulus of elasticity** (+169 %).

Earlier attempts to hybridise SMC materials also showed hybridisation effects in terms of tensile stiffness. With combined reinforcement based on chopped and continuous glass fibres, the tensile modulus of elasticity significantly increased with the increasing content of the continuous component. For a ratio of the two components comparable to the ratio of the hybrid SMC composites investigated

within this dissertation, a unidirectional reinforcement resulted in an average stiffness increase of 57 % (Sridharan, 1982). The effect of hybridisation was less pronounced than in the results of the present study, since only glass fibres were considered as reinforcement, featuring a significantly lower tensile modulus of elasticity compared to carbon fibres.

Sridharan (1982) pointed out that the ratio of continuously and discontinuously reinforced plies forming an interlayer hybrid SMC is the factor most responsible for the resulting stiffness of the hybrid material. The increase of stiffness was proportional to the volume content of the continuous component. Investigations by Trauth and Weidenmann (2016) resulted in a stiffness increase of 284 % if the ratio of continuous/discontinuous SMC was 1:2 and the continuous material was placed in the middle. For a ratio of 2:1 with two continuously carbon fibre reinforced face sheets, the stiffness increase was more substantial (647 %). A two-sided reinforcement of a standard SMC composite (based on a mixture of thermoset and thermoplastic resin system with 30 wt.% of glass fibres and 46 wt.% of fillers) by non-crimp carbon fibre fabrics in $\pm$ 45° configuration, led to a stiffness increase of 125 % (Gortner et al., 2015a). The effect of continuous reinforcement of the hybrid CoDico SMC investigated within this dissertation was more distinct. With a nominal thickness of the hybrid SMC sheets of 2 – 3 mm considered by Gortner et al. (2015a) and the thickness of each layer of the $\pm$ 45° reinforcing layers of $\approx$ 400 µm, the ratio of $(2 \cdot h_f)/h$ equalled 0.27 – 0.4 in the cited publication. Although this ratio of $(2 \cdot h_f)/h$ was slightly higher compared to the hybrid material considered within this study, the lower increase of stiffness resulted from the orientation of the carbon fibres, which were not aligned in loading direction ($\pm$ 45°).

A combination of a glass fibre SMC (based on an unsaturated polyester, with either 25 or 50 wt.% of glass fibres and a significant amount of fillers) with pre-impregnated carbon fibres, in a woven configuration, led to a stiffness increase of 20 % and 41 %, respectively. If unidirectional pre-impregnated carbon fibres were considered, the increase of tensile modulus was more distinct (100 %, 200 %) due to the alignment of carbon fibres in loading direction (Wulfsberg et al., 2014). No indication was made concerning ratio between the continuous and discontinuous components; hence, a direct comparison with the results obtained within the present dissertation is not possible.

The approach to hybridise SMC composites presented within this dissertation led furthermore to an almost tripled **tensile strength** (193 %, Figure 7.6). Given the aforementioned references, this effect was more distinct, as compared to a hybrid SMC composite reinforced solely by glass fibres (124 %, Sridharan, 1982). A hybridisation based on two $\pm$ 45° non-crimp fabrics increased tensile strength by 350 % (Gortner et al., 2015a). At a first glance, this value seems more remarkable compared to the results achieved by the hybridisation approach described within this dissertation, but with an average tensile strength of only $\approx$ 40 MPa of the pure discontinuous glass fibre SMC, the reference value to determine the effect of hybridisation was decisively lower.

A woven carbon fibre pre-impregnated fabric increased the tensile strength of discontinuous glass fibre SMC, featuring a fibre content of 25 wt.%/ 50 wt.%, respectively, 17 % and 33 %. A unidirectional carbon fibre pre-impregnated fabric increased tensile strength of the same discontinuous glass fibre SMC composites 167 % and 200 %. The architecture and orientation of the continuous reinforcement

determined effect of hybridisation (Wulfsberg et al., 2014). Considering a unidirectional reinforcement and a discontinuous glass fibre SMC featuring a FWC of 50 %, hybridisation was in the same range as the results of mechanical characterisation of the UPPH-based CoDico GF/CF SMC.

Modelling of tensile properties

A rule of hybrid mixtures (Equation 5.44), based on the properties of the individual components, was already frequently considered to determine and predict the stiffness of hybrid short fibre reinforced composites (Fu et al., 2000, 2001), particle-short fibre hybrid composites (Fu et al., 2002), hybrid composites based on a combination of unidirectional fibres and fabrics (Ikbal et al., 2016) and continuous fibre hybrids (Swolfs et al., 2014). As yet, little attention has been paid to analytical modelling of interlayer hybrid composites based on both continuous and discontinuous fibrous reinforcement.

Based on the experimental results of this dissertation, a rule of hybrid mixtures, presented in 5.44, enabled accurate prediction of the tensile stiffness of a hybrid CoDico SMC (Figure 6.105). If a ratio of $(2 \cdot h_f)/h = 0.23$ is considered, the analytically predicted stiffness value of 35.3 GPa matches very well with the experimentally determined value (Figure 6.49).

Presented by Zweben (1977), early attempts to predict the tensile strength of hybrid materials, derived from a combination of different fibre types in unidirectional configuration, were based on statistical analysis of failure mechanisms. A more basic estimation of the strength of a hybrid composite exposed to uniaxial loads may follow the rule of hybrid mixtures (presented in section 5.4.1), with the components P_{C1} and P_{C2} referring to the strength of the two individual

fibre reinforced materials combined in a laminate. However, as stated by Manders and Bader (1981), for instance, it is highly possible that in hybrid composites which feature only a low amount of the stiffer and more brittle component, where the predominating fraction is based on the less stiff and more ductile component, the hybrid might be able to carry additional loads after the brittle component has failed. Hence, a bilinear rule of hybrid mixtures might be more appropriate to estimate the strength of hybrid interlayer composites.

A bilinear rule of mixtures was already successfully applied to predict strength of hybrid materials based on a combination of different unidirectionally arranged fibre types (Manders and Bader, 1981). Recently, it was also considered to predict strength of hybrid glass/carbon composites reinforced by two different types of woven fabrics (plain weave glass and twill weave carbon) (Zhang et al., 2012) or satin weave carbon and plain weave glass fibre fabrics (Pandya et al., 2011). The approach of a bilinear rule of hybrid mixtures is now extended to hybrid composites based on continuous and discontinuous fibre reinforcements. The homogenised properties of the two components are considered as input parameters. Basically, the strength of a hybrid composite ($\sigma_{hyb,max}$) exposed to uniaxial in-plane loads, can be described according to the model presented in Figure 2.5a. The tensile strength for low fractions of the low elongation fibrous reinforcement C1 (in the case of this dissertation corresponding to the Co CF SMC face sheets) equals

$$\sigma_{hyb,max} = \sigma_{C2,max} \cdot (1 - \phi_{C1}), \tag{7.1}$$

with $\sigma_{C2,max}$ the tensile strength of $C2$ and with ϕ_{C1} the volume fraction of component C_1. If the volume fraction of C_1 increases, the strength of the hybrid composite is equal to

$$\sigma_{hyb,max} = \sigma_{C1,max} \cdot \phi_{C1} + \sigma_{C2}(\varepsilon_{C1,max}) \cdot (1 - \phi_{C1}). \tag{7.2}$$

Generally, $C1$ features a lower failure strain than $C2$, and $\varepsilon_{C1,max}$ represents the failure strain of the brittle component $C1$. The term $\sigma_{C2}(\varepsilon_{C1,max})$ refers to the stress within component $C2$ at the moment of failure of component $C1$, equal to the strain $\varepsilon_{C1,max}$, and is calculated by applying Hooke's law, hence assuming linear elastic behaviour of $C2$ up to failure of $C1$. This is an idealised assumption. The presented bilinear rule of hybrid mixtures predicted a tensile strength of 459 MPa of the CoDico GF/CF SMC. This value slightly underestimate the experimentally determined value, and a positive hybridisation effect (13 %) can be stated, as clearly depicted in Figure 7.7.

Analytically predicted tensile strength based on a linear rule of mixtures did not significantly differ from the strength value determined with a bilinear rule of mixtures since no important variation between failure strain of Dico GF and Co CF SMC resulted from uniaxial tension. The predicted tensile strength equalled 464 MPa (positive hybridisation effect of 12 %). The average value as well as the 25^{th} and the 75^{th} percentile are depicted to account for variations in mechanical performance and the strength of the individual components. For the sake of clarity, only average values are depicted to calculate the linear rule of hybrid mixtures.

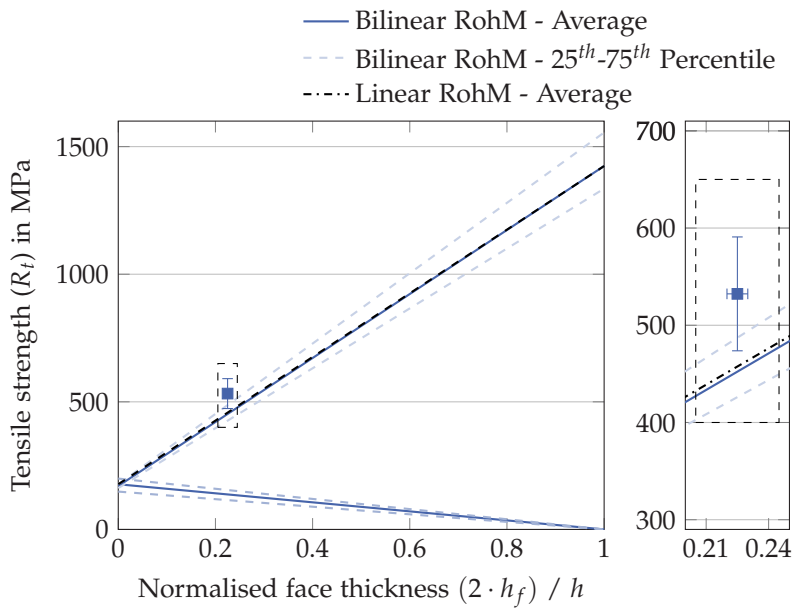


Figure 7.7: Prediction of tensile strength of hybrid continuous-discontinuous glass/carbon fibre SMC based on a linear rule of hybrid mixtures (RohM) and a bilinear rule of hybrid mixtures (bilinear RohM) with rectangle and error bars indicating experimentally determined values.

The strength of CoDico GF/CF SMC composites was mainly determined by the continuous component. Minimal and critical content of the reinforcing continuous material (equivalent to minimal and critical fibre content in a composite, defined by Kelly and Davies (1965), were extremely low. As depicted in Figure 7.8, stress-strain evolution of the hybrid CoDico SMC composite was mainly determined by the continuous carbon fibre SMC and showed a linear increase up to brittle fracture.

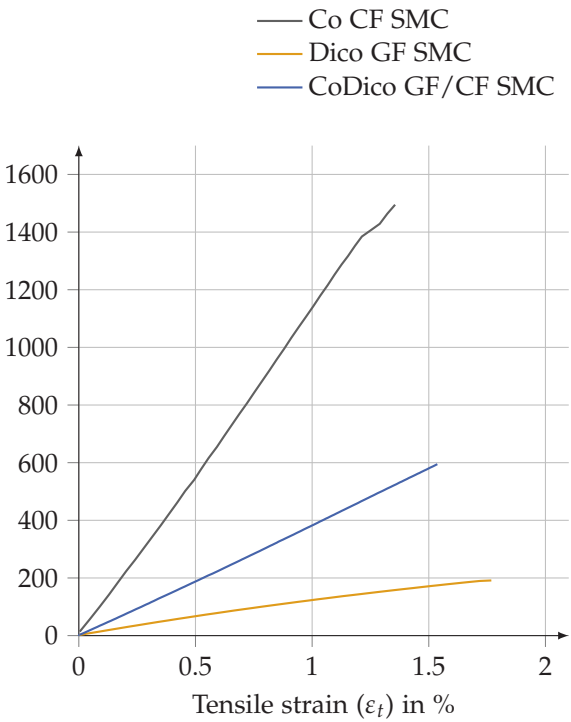


Figure 7.8: Representative stress-strain curves of discontinuous glass fibre, continuous carbon fibre and continuous-discontinuous glass/carbon fibre SMC resulting from uniaxial tension.

Small load drops (Figure 6.51), which resulted from partial failure of some specimens, did not influence the overall evolution of the stress-strain curve. The **tensile failure strain** of CoDico SMC composites was increased (15 % compared to failure strain of continuous carbon fibre SMC). In terms of hybrid composites, this effect is often described as pseudo-ductility (Hayashi, 1972). According to Ikbal et al. (2016), the hybrid structures may show some ductility because of their mixture of a certain amount of brittle carbon fibres combined with ductile glass fibres. Exhibiting a slightly enhanced

tensile failure strain of the discontinuous SMC composite, damage evolution in continuous carbon fibre reinforced parts of the material is constrained because of surrounding glass fibres. Hence, the carbon fibre reinforced part of the hybrid material may sustain greater strain before failure, and the (tensile) failure strain of hybrid configuration increases. However, ductility in general refers to a more gradual failure evolution. Considering that final failure of hybrid CoDico GF/CF SMC composites was still characterised by a catastrophic and brittle failure, pseudo-ductility, as defined by Swolfs et al. (2014), for example, might not be the appropriate term, and enhancement of failure strain is a better description of the observed effects.

Failure evolution resulting from uniaxial tension

Fibre orientation (misalignment) and inconsistency of the continuous face layers (pushed apart, leading to resin-rich regions) significantly determined the failure evolution of hybrid CoDico GF/CF SMC composites. For the investigated hybrid CoDico SMC composites, tensile failure stems from on a combination of damage mechanisms, characteristic of the discontinuous and the continuous components. As clearly depicted in Figure 7.8, no stiffness degradation, characteristic of the discontinuous component and resulting from evolving damage, was observed for the hybrid CoDico GF/CF SMC. Failure within the discontinuous glass fibre SMC, hence crack formation and growth, which might nevertheless be possibly present within the specimen, did not influence the global stress-strain response of the hybrid CoDico GF/CF SMC in a significant way. In the end of loading, the discontinuous component failed due to pseudo-delamination between different bundles, and the failure of the continuous phase was mainly defined by fibre fractures for small angles of misalignment. Damage was more likely to be defined by inter-fibre fractures and splitting for larger angles of misalignment. In addition,

(intra- and interlayer) delamination occurred. The superposition of failure mechanisms, characteristic of the individual components of a hybrid material has already been observed for comparable hybrid materials (Selmy et al., 2011).

The specific carbon fibre bundle structure, hence the characteristic pattern of the stitching yarns, significantly influenced evolving strains of the continuous carbon fibre SMC (Figure 7.9) and led to a locally highly heterogeneous strain field if the pure Co CF was loaded in tension. In contrast, the strain field of hybrid CoDico GF/CF SMC could most likely be described as homogeneous in the loading direction.

The resulting strain field (ε_{xx}) was thus strongly influenced by the discontinuously reinforced core layers. Local crack initiation and growth, characteristic for the failure of Dico GF SMC (Figure 6.34 and 6.35), was not observed at the surface layer of the hybrid CoDico SMC, and the resulting strain field remained globally and qualitatively homogeneous up to fracture. In contrast, transverse strains (ε_{yy}) were characterised by a highly heterogeneous evolution. Driven by slightly different Poisson's ratios of the continuous and discontinuous material (Co CF SMC: ν_t = 0.32 and Dico GF SMC ν_t = 0.38), differences in transverse strain, as clearly depicted in Figure 7.9 might be explained, resulting furthermore from inconsistent continuous reinforcement in the shell layers. In addition, the pushing apart of the carbon fibre bundles resulted in locally not continuously reinforced specimens, so transverse strains in these locations depend on the properties of the discontinuous material.

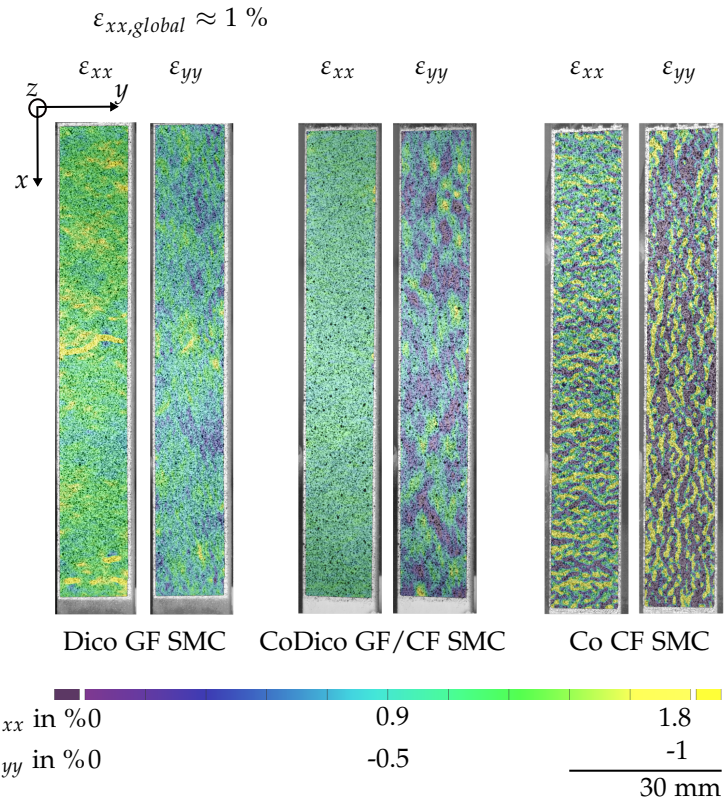


Figure 7.9: Strain fields resulting from uniaxial tension of discontinuous glass fibre SMC, continuous-discontinuous glass/carbon fibre hybrid SMC and continuous carbon fibre SMC corresponding to a global average strain $\varepsilon_{xx,global} \approx 1$ %.

Compressive modulus of elasticity and compressive strength

The compressive stiffness and strength of Dico GF SMC, Co CF SMC and CoDico GF/CF SMC are summarised in Figure 7.10.

The investigated hybrid CoDico GF/CF SMC composite exhibited a significant increase in **compressive modulus of elasticity** (143 %).

The resulting stiffness could accurately be predicted by a rule of hybrid mixtures described in Equation 5.44 and depicted in Figure 6.105. The effect of hybridisation was less significant than for a vinylester-based discontinuous glass fibre SMC reinforced by layers of continuous carbon fibre SMC (based on unsaturated polyester-polyurethane resin system). The described hybrid laminates, investigated by Trauth and Weidenmann (2016), were characterised by an increase of compressive modulus of elasticity of 240 % and 680 %, depending on the ratio of continuous-discontinuous material, respectively. Comparable to tensile properties, the effect of hybridisation on material's stiffness depended strongly on the ratio of the combined materials, with the continuous material dominating the enhancement of the global stiffness. In general, specimens investigated by Trauth and Weidenmann (2016) featured thicker continuous face layers with a ratio of $(2 \cdot h_f)/h \approx 0.3 – 0.6$; therefore, enhancement of material's stiffness was more significant than in the results presented within this dissertation. Since the continuous carbon fibre SMC exhibited an anisotropy in terms of tensile and compressive properties, compressive modulus of elasticity of the hybrid CoDico GF/CF SMC was also slightly lower than the tensile counterpart, and $E_c = 0.86 \cdot E_t$ held true for the hybrid CoDico SMC.

A hybridisation of the investigated SMC composites did not affect the **compressive strength** of the discontinuous SMC. A similar effect was stated by Ikbal et al. (2016) considering the compressive strength of a hybrid (unidirectional) glass and carbon fibres reinforced composite. A slight decrease of 2 % of compressive strength was even observed (Dico GF SMC R_c = 298 MPa and hybrid CoDico GF/CF SMC R_c = 292 MPa). This difference, however, resulted more likely from scatter in material properties of the two components. In contrast, Trauth and Weidenmann (2016) reported an increase of

63 % and 136 % considering the compressive strength of a hybrid CoDico SMC laminate. The specific layup, which consisted of several layers of the continuous carbon fibre reinforced prepreg considered as face layers significantly increased compressive strength within the aforementioned study.

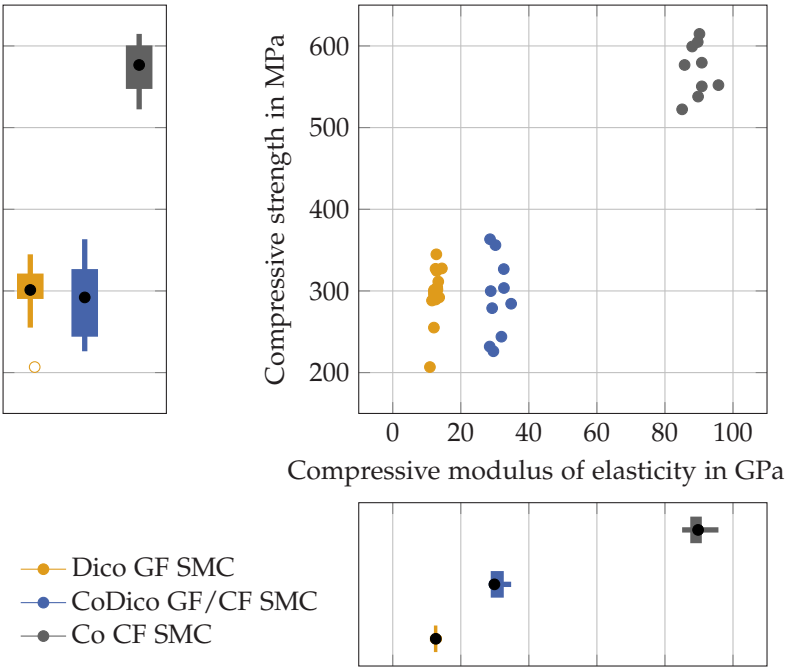


Figure 7.10: Compressive properties of discontinuous glass fibre SMC, continuous carbon fibre SMC and continuous-discontinuous glass/carbon fibre SMC (● = median, + = mean, box indicates 25^{th} to 75^{th} percentile; lines indicate minimum and maximum or 1.5 interquartile range, respectively, ○ = outlier).

In contrast, face sheets within this present dissertation consisted of only one layer of continuous carbon fibre reinforced prepreg. This approach resulted in a lower damage tolerance of the Co CF SMC

exposed to uniaxial compression. A positive hybridisation effect in terms of compressive strength (increase of $\approx 10\,\%$) was also reported by Pandya et al. (2011), based on investigation of the mechanical performance of hybrid materials made from unidirectional glass and carbon fibres.

Modelling of compressive properties

A linear and bilinear rule of hybrid mixtures to estimate the stiffness of the CoDico GF/CF SMC composite may also be considered for compressive loads, and Figure 7.11 depicts the results of the analytical modelling of the compressive strength of the hybrid SMC. Analytically determined compressive strength of hybrid CoDico GF/CF SMC by means of a linear rule of hybrid mixtures equalled 360 MPa. This value leads to a negative hybridisation effect (EoH_2: $-23.5\,\%$). Considering the bilinear rule of hybrid mixtures, the realised ratio of face sheet thickness to global thickness of the laminate may theoretically not enhance the mechanical performance of the hybrid CoDico GF/CF SMC in terms of strength, due to low compressive failure strain of the continuous component. Considering the idealised model of a bilinear rule of hybrid mixtures and the material properties of the individual components as input parameters, the realised ratio of $(2 \cdot h_f)/h \approx 0.23$ was too low to reach the critical or minimal content of continuous reinforcement to enhance compressive strength. The compressive properties of hybrid CoDico GF/CF SMC were hence mainly determined by the material properties of the discontinuous material, because of an early failure of the continuously reinforced face sheets linked to low failure strain. A negative hybridisation effect in terms of compressive strength was also reported by Piggott and Harris (1981), based on investigations of pultruded fibre composite rods made from polyester resin and mixtures of carbon, Kevlar and

glass fibres. Hence compressive loads are more critical to consider if a hybrid composite is sought.

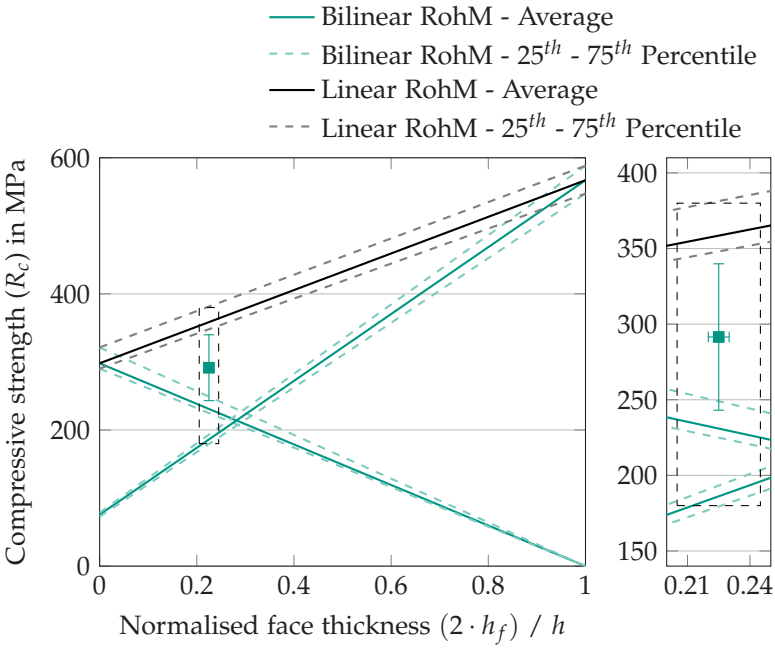


Figure 7.11: Prediction of compressive strength of hybrid continuous-discontinuous glass/carbon fibre SMC based on a (linear) rule of hybrid mixtures (RohM) and a bilinear rule of hybrid mixtures (bilinear RohM) with rectangle and error bars indicating experimentally determined values.

Failure evolution resulting from uniaxial compression

Measurement of compressive strains was not possible up to final failure, with the clip-on extensometer due to an early and partial failure of the continuous face sheets (slipping of the sensor). Digital image correlation on the front side of the specimen was confronted with the same difficulties, since facets got lost when first failure

occurred. Consequently, digital image correlation was applied to the side face of selected specimens to capture representative stress-strain curves of a hybrid CoDico SMC specimen resulting from uniaxial compression. In this manner, the global deformation of the specimen could be captured up to final failure, and Figure 7.12 depicts representative stress-strain curves of the Dico GF SMC, Co CF SMC and hybrid CoDico GF/CF SMC exposed to uniaxial compression, with the deformation of the hybrid CoDico GF/CF SMC determined by means of digital image correlation.

Evolution of the stress-strain response of the hybrid CoDico GF/CF SMC was mainly determined by the continuous component, featuring a steady (linear) increase from beginning of loading almost to (brittle and spontaneous) final failure. The **compressive failure strain** was approximately equal to 1.15 % (μ = 0.12 %, CV = 10.4 %) considering three specimens evaluated by means of digital image correlation on the side face. Hence, failure strain was doubled compared to the compressive failure strain of the Co CF SMC. However, first failure, which manifested in fibre breakage in the face layers, was linked to a compressive strain of $\varepsilon_c \approx 0.3\,\%$ (corresponding to point A in Figure 6.64). Since the continuous face sheets consisted of only one layer of the semi-finished continuous SMC material, microbuckling and fibre fracture may be linked to lower deflection, in comparison to the pure continuous carbon fibre specimen, which consisted of six layers of semi-finished Co CF SMC. Up to final failure, the CoDico GF/CF SMC was supported by the discontinuous component until compressive strength of the discontinuous component was reached.

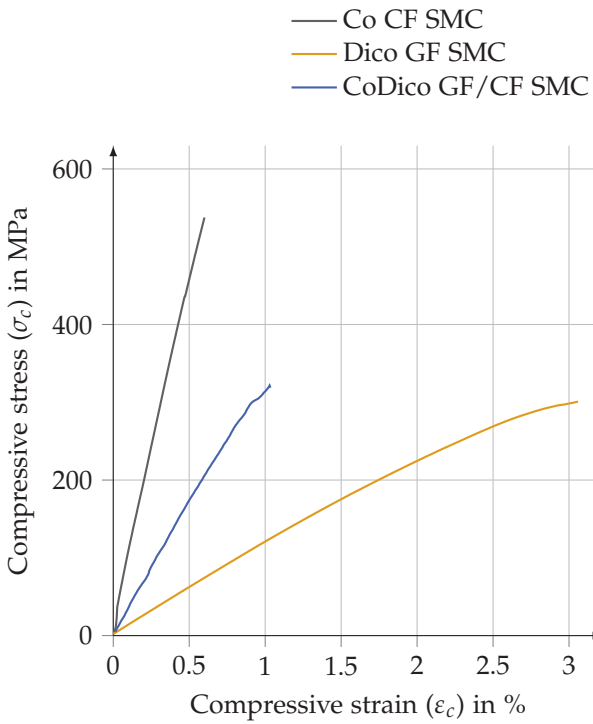


Figure 7.12: Representative stress-strain response of discontinuous glass fibre, continuous carbon fibre and continuous-discontinuous glass/carbon fibre SMC exposed to uniaxial compression.

Flexural modulus of elasticity and flexural strength

Flexural properties in terms of stiffness and strength of the two individual and the hybrid material are summarised in Figure 7.13. Flexural properties of the hybrid CoDico GF/CF SMC composites were characterised by a significant positive hybridisation effect. **Flexural modulus** increased 370 % (Figure 7.13). Exposed to flexural loads, the layer arrangement and stacking sequence of a hybrid laminate is the most important factor determining the global stiffness of the

laminate (Dong and Davies, 2012; Trauth and Weidenmann, 2016). In the present dissertation, the hybrid CoDico GF/CF SMC composite was designed to show optimised properties if exposed to out-of-plane (bending) loads. This loading reflects a realistic loading case of SMC components, for example in the automotive industry, which is determined by bending rather than uniaxial tension or compression and the continuous carbon fibre SMC face sheets maximised the possible theoretical enhancement of flexural stiffness. For the CoDico GF/CF SMC investigated in this dissertation, the increase in stiffness was more important compared than tensile and compressive loads. If carbon fibre reinforcements were considered as core layers, a less important increase in stiffness was observed (<30 % Wulfsberg et al., 2014, $\approx$ 60 % Trauth and Weidenmann, 2016). The observed stiffness increase of the hybrid CoDico GF/CF SMC was also more important than a two-sided reinforcement by a $\pm$ 45° non-crimp-fabric (190 %) reported by Gortner et al. (2015b). Although the reinforcing component featured a higher ratio with respect to the entire thickness of the specimen, the reinforcing effect was pronounced due to the non-unidirectional orientation of the carbon fibres within the face sheets. Depending on volume content of the continuous component considered as face layers, enhancement of flexural stiffness can be even pivotal. For a symmetrical lay-up with continuous carbon fibre reinforced face layers and a volume fraction of the continuous material of about 67 %, flexural modulus was 10 times as high as the reference value of the discontinuous material (Trauth and Weidenmann, 2016).

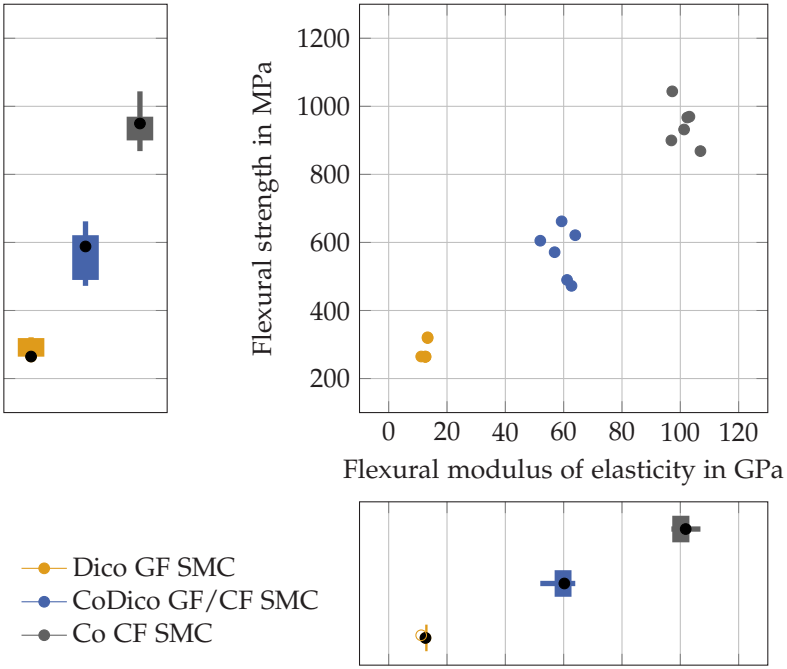


Figure 7.13: Flexural properties of discontinuous glass fibre SMC, continuous carbon fibre SMC and continuous-discontinuous glass/carbon fibre SMC (• = median, + = mean, box indicates 25^{th} to 75^{th} percentile; lines indicate minimum and maximum or 1.5 interquartile range, respectively).

The **flexural strength** of the investigated CoDico GF/CF SMC was twice as high as the corresponding value of Dico GF SMC due to the reinforcement by the continuous face sheets. A reinforcement based on ± 45° non-crimp fabric face layers was slightly more impactful than the results observed within this study (126 %, Gortner et al., 2015a). A possible explanation is the low compressive strength of continuous carbon fibre materials, limiting flexural strength. In addition, the material properties of CoDico GF/CF SMC were characterised by a significant scatter, and the aforementioned deviation is of less

importance if variation in mechanical performance is considered. Discontinuous glass fibre SMC, reinforced by either unidirectional or woven carbon fibre fabrics, yielded no significant increase in flexural strength with the reinforcing component within the core (Figure 2.24). This finding suggests, again, that in terms of flexural properties, the layup of hybrid materials and laminates is a very critical consideration.

Modelling approaches of flexural properties

In terms of modelling flexural properties, a rule of mixtures is not appropriate, since it does not account for a distinct stacking and non-uniform stress and strain distribution with respect to the thickness direction of the specimen. As depicted in Figure 6.106, stiffness predictions based on the classical laminate theory (CLT) could precisely estimate the flexural properties of the investigated interlayer CoDico GF/CF SMC composite. However, because of the tension-compression anisotropy of the continuous carbon fibres, an asymmetric lay-up has to be considered. For this purpose, three different materials have been defined as input parameters to account for the significant deviation in terms of the tensile and compressive stiffness of the continuous face layers. Considering a symmetric lay-up, flexural modulus of elasticity was overestimated.

In a study by Zhang et al. (2012), the flexural strength of a hybrid laminate (consisting of glass plain weave and carbon twill weave fabrics and an epoxy matrix with different stacking sequences) was also predicted by means of the classical laminate theory. The presented model considered an average modulus of elasticity ($(E_t + E_c)\ /2$) for each layer to define the [*abd*] matrix. Based on the aforementioned method, a similar approach was developed to approximate the flexural strength of the hybrid CoDico GF/CF SMC material investigated

within this dissertation. Observations of CoDico GF/CF SMC specimens exposed to flexural loads indicated that failure was initiated due to compressive stresses at the upper surface. However, the discontinuously reinforced core supported the specimen until final failure, which manifested through tensile failure on the lower surface (Co CF SMC). The flexural failure strain of hybrid SMC composites ranged between the compressive and tensile failure strain, indicating a superposition of different failure evolutions due to simultaneous compressive and tensile stresses. Modelling aimed to predict flexural properties of the hybrid material without knowing flexural stiffness and strength. Hence, considering compressive behaviour of the pure Co CF SMC, which predominates the flexural properties, a theoretical failure strain, resulting from superposition of tensile and compressive properties of $\varepsilon_{max,f,model} = (\varepsilon_{max,t,Co} + \varepsilon_{max,c,Co})/2$ was considered. It equalled 0.96 %. Compared to flexural failure strain of the Co CF SMC, which was in the range of 1 %, the proposed approach may be able to estimate the flexural properties of the hybrid material based on tensile and compressive properties, considered as input parameters. The predicted flexural strength of the CoDico GF/CF SMC was finally equal to $E_{f,CLT,CoDico} \cdot \varepsilon_{max,f,model}$, with $E_{f,CLT,CoDico}$ the predicted flexural modulus based on the (asymmetric) classical laminate theory. This very basic approach enabled accurate prediction of the flexural strength of the hybrid CoDico SMC (Figure 7.14) in a precise way.

However, it assumes a linear behaviour up to final failure and that the continuous face sheets dominate the evolution of the stress-strain curve (Figure 7.15). In order to highlight the effect of stacking of individual laminae to form a laminate, Figure 7.14 also depicts predicted strength values based on linear rules of hybrid mixtures assuming pure tensile, compressive or flexural failure of the two

components. A classical rule of hybrid mixtures approach (pure bending), which does not account for the stacking sequence of the laminate underestimates flexural strength by one third.

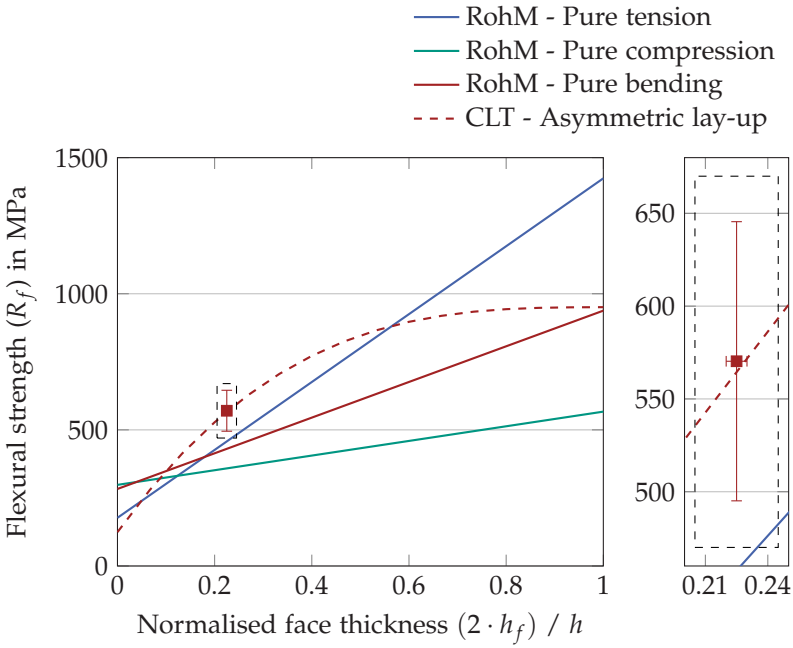


Figure 7.14: Prediction of flexural strength of hybrid continuous-discontinuous glass/carbon fibre SMC based on classic laminate theory compared with linear rule of hybrid mixtures, with rectangle and error bars indicating experimentally determined values.

Failure evolution resulting from three-point bending

Exposed to flexural loads, the stress-strain evolution of hybrid CoDico GF/CF SMC was mainly determined by the flexural stress-strain response of the continuous carbon fibre SMC (Figure 7.15).

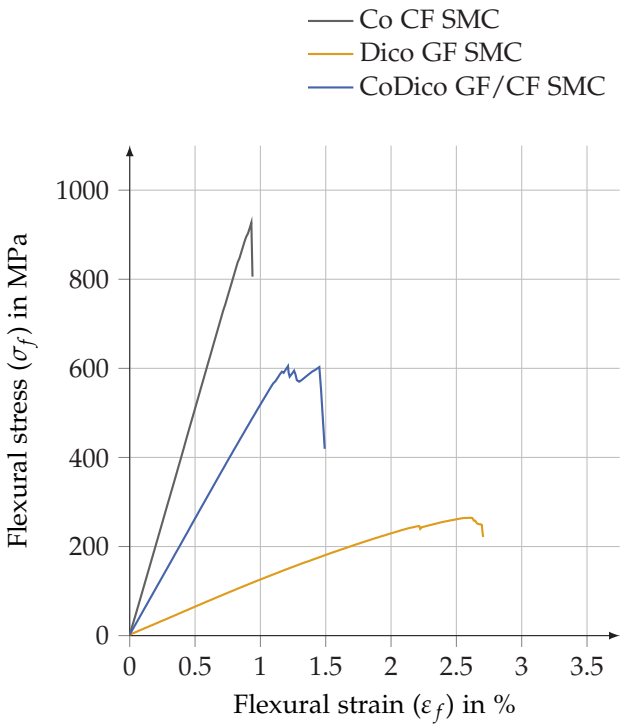


Figure 7.15: Representative stress-strain curves of discontinuous glass fibre, continuous carbon fibre and continuous-discontinuous glass/carbon fibre SMC exposed to three-point bending.

The failure mechanisms of Dico GF SMC and Co CF SMC are superposed if hybrid CoDico GF/CF SMC specimens are exposed to out-of-plane (flexural) loads. Compressive failure on the upper surface was a dominant failure mechanism, as already stated for different hybrid materials exposed to flexural loads (Dong and Davies, 2012). Failure evolution was then linked to local delamination, followed by a compressive failure on the upper side of the discontinuous core layer (which was locally no longer reinforced due to the failure and

delamination of the Co CF layer), tensile failure on the lower surface of the continuous carbon fibre SMC and delamination. These observations on damage evolution and failure mechanisms tie in with recently published results on investigations to characterise the failure mechanisms of hybrid CoDico GF/CF SMC exposed to flexural loads by Trauth et al. (2017b). Within the aforementioned study, three-point bending tests on different SMC composites were carried out, combined with acoustic emission analysis. The hybrid SMC featured continuously carbon fibre reinforced face sheets and a discontinuous glass fibre reinforced core. Pattern recognition was carried out applying a method similar to the approach presented by Sause et al. (2012). The results indicated, that clustering methods were generally able to assign acoustic emission signals to different failure mechanisms. Within the contribution by Trauth et al. (2017b), fibre breakage, interface failure and matrix failure were observed in μ-CT images of the post-mortem specimens and associated with the results of clustering. It was shown that the detected signals captured during a three-point bending test on a hybrid SMC specimen were nearly a superposition of the two bulk materials, considering the point clouds in feature space. Generally, the applied method led to a number of clusters that could be associated with the failure mechanisms observed with imaging methods. Even if validation methods must be improved, the assigned clusters were plausible and enabled deeper insight into the evolving damage of hybrid SMC materials exposed to flexural loads.

7.5.2.2 Structure level

Quasi-static and dynamic puncture of plates generally lead to a biaxial stress-state if the specimen is fully clamped. However, for a biaxial loading (superposition of bending and tension) with the impactor being small with respect to the unsupported area surrounding

the impact zone, the stress state at failure for a fixed configuration was defined to be dominated by plate bending for SMC composites (Roche and Kakarala, 1986). Puncture testing of SMC composites allowed for the investigation of structural properties to gain further understanding of the effect of hybridisation resulting from a more complex loading case. In reality, a comparable situation of loading may result from handling and assembling (low impact energies) or from the side impact of a vehicles, for example (Roche and Kakarala, 1986). The failure of composites exposed to impact situations or to puncture loadings is very complex and progressive. Generally, fibre reinforced polymers offer great mechanical performance if loaded in-plane. However, they are very susceptible to damage in the case of out-of-plane loads such as puncture. In the following structural properties of hybrid CoDico GF/CF SMC materials, rate dependence and possible variations of failure mechanisms resulting from an increase in loading speed are discussed based on the results presented in section 6.4.

Exposed to quasi-static puncture, hybrid CoDico GF/CF SMC exhibited significantly higher strength (maximum sustained load or failure load, respectively) (36 %) and energy absorption capability in terms of puncture energy (35 %) (Figure 7.16), compared to the puncture properties of pure discontinuous glass fibre SMC.

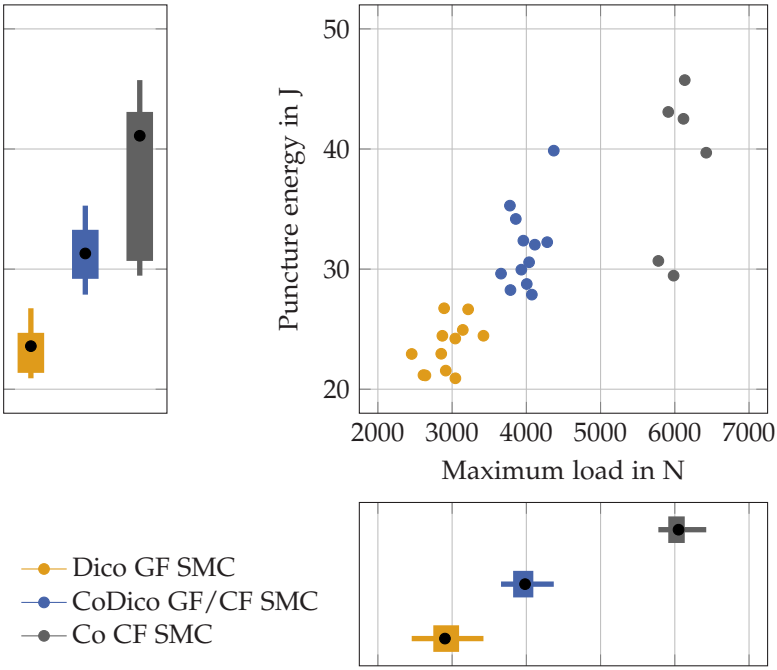


Figure 7.16: Quasi-static puncture properties of discontinuous glass fibre SMC, continuous carbon fibre SMC and continuous-discontinuous glass/carbon fibre SMC (• = median, + = mean, box indicates 25^{th} to 75^{th} percentile; lines indicate minimum and maximum or 1.5 interquartile range, respectively).

Investigating the quasi-static puncture properties of hybrid woven laminated hybrid composites, reinforced with different combinations of woven carbon, Kevlar and glass fibres suggested, that fibres placed in the outer layers played an important role in energy dissipation and in the damage mechanism of the structure (Bulut et al., 2016). Hence, the significant increase in maximum load reflects the effect of the continuous carbon fibre outer layers. Due to the specific layup with continuous carbon fibre face sheets, combined with the bending-dominated loading case, the Co CF SMC also mainly influenced the

stiffness of the structure, and the stiffness of the hybrid CoDico SMC was significantly increased (75 % for charge and 60 % for flow region specimens) due to the continuous face sheets, with respect to the stiffness exhibited by the Dico GF SMC. Approximately 72 % of puncture energy of hybrid CoDico charge region specimens was absorbed until maximum load. Flow region specimens featured a ratio of $E_{F_{max}} \; / \; E_p \; \approx \; 0.68$. With $E_{F_{max}} \; / \; E_p \; \approx \; 0.6$ (charge region specimens) and $E_{F_{max}} \; / \; E_p \; \approx \; 0.5$ (flow region specimens) for Dico GF SMC and ≈ 0.84 for Co CF SMC failure evolution. The resulting energy absorption of hybrid specimens thus emerged, due to a superposition of the two individual components. Continuous carbon fibre SMC exposed to (quasi-static) puncture loads failed in a very brittle spontaneous manner. Crack formation and growth up to peak load absorbed the energy of the impacting striker. Discontinuous glass fibre SMC exhibited a more gradual failure evolution. The initial force-deflection response of the hybrid CoDico GF/CF SMC was defined by important crack formation and growth within the continuous face sheets. However, as soon as the face sheets were no longer able to maintain loads, load transfer to the discontinuous core layers resulted in a more gradual and stepwise failure of the hybrid SMC (Figure 7.17). Force-deflection evolution of CoDico GF/CF SMC increased linearly up to a yield point, which was linked to higher forces compared to the Dico GF SMC but approximately the same deflection. The load further increased up to peak load, but damage was already initiated, and due to crack formation and growth the force-deflection evolution was characterised by significant load drops up to peak load. The significant drops were not observed to this extent for the continuous carbon fibre material, since for the hybrid CoDico GF/CF SMC failure in this stage was also linked to delamination.

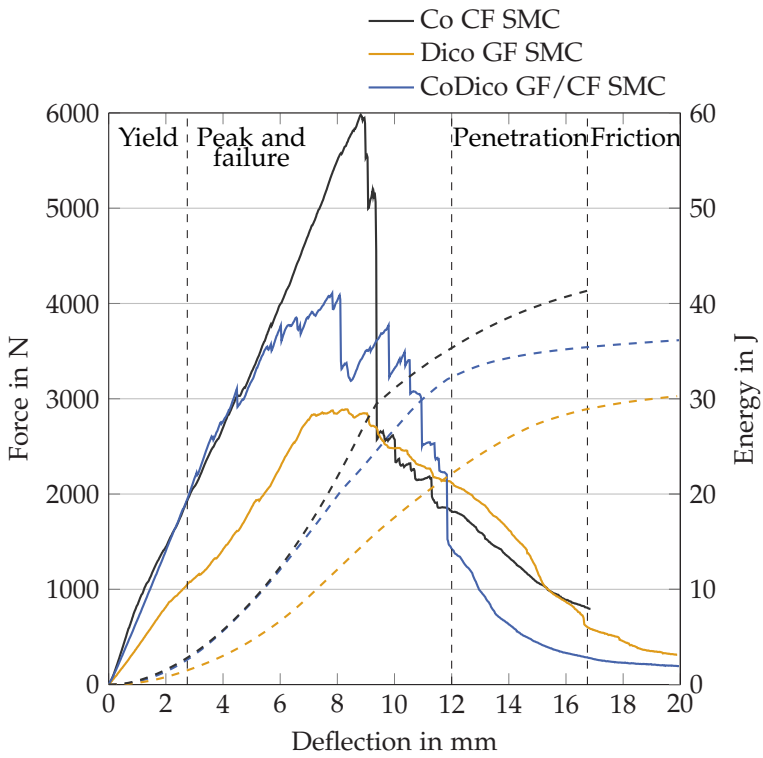


Figure 7.17: Quasi-static force-deflection and energy-deflection responses of discontinuous glass fibre SMC, continuous carbon fibre SMC and continuous-discontinuous glass/carbon fibre SMC.

In addition, failure evolution of the CoDico SMC was not characterised by a distinct point in the force-deflection evolution, as observed for the continuous carbon fibre SMC followed by a tremendous force drop, but was rather defined by several steps, indicating subsequent failure of the different components. Up to a deflection corresponding to the failure of the Co CF SMC (significant load drop), the energy absorption of Co CF SMC and CoDico GF/CF SMC did not significantly differ. Hence the energy absorption capability of

the hybrid CoDico GF/CF SMC was enhanced with respect to the discontinuous component up to peak load.

Recent studies have pointed out that hybrid composites present an effective way to increase dynamic puncture (Gortner et al., 2015a) and ballistic impact properties (Bandaru et al., 2015). The results of the present dissertation also indicated that maximum load was slightly increased for the hybrid CoDico GF/CF SMC composites with respect to the discontinuously reinforced material (13.5 %, Figure 7.18). However, the effect of reinforcement was less distinct than for quasi-static puncture. In the case of dynamic loading, the positive rate dependence of the Dico GF SMC was superposed with the negative rate dependence of the Co CF SMC; hence, rate dependent increase of puncture performance was less significant due to the lack of (or slightly negative) rate dependence of the carbon fibre SMC composite. Considering the Dico GF SMC as the reference energy absorption capability of the hybrid CoDico SMC only showed a marginal increase with increasing puncture velocity (7 %). However, with respect to the continuous carbon fibre SMC, absorbed energy increased 30 % for charge and 18 % for flow region specimens. The important difference between charge and flow region specimens, as indicated in the discussion of quasi-static puncture properties, possibly results from interface quality, which was probably influenced by material flow during compression moulding. Delamination may thus be favoured and linked to lower energy for flow region specimens. Absorbed energy up to peak load even differed by ≈ 40 %. Hybrid CoDico GF/CF SMC composites, which were punctured with a higher loading rate, were characterised by a more important delamination compared to specimens punctured in a quasi-static manner (Figure 6.95).

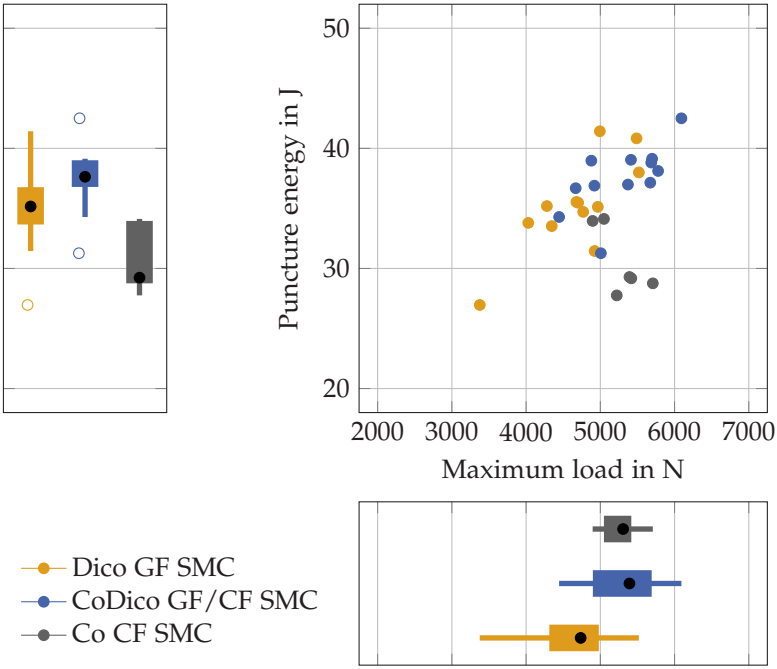


Figure 7.18: Dynamic puncture properties of discontinuous glass fibre SMC, continuous carbon fibre SMC and continuous-discontinuous glass/carbon fibre SMC (• = median, + = mean, box indicates 25^{th} to 75^{th} percentile; lines indicate minimum and maximum or 1.5 interquartile range, respectively, ○ = outlier).

Although material flow of the discontinuous component did not significantly influence quasi-static puncture properties, the resulting transition zone might show slightly different characteristics between the flow and charge region, becoming evident at higher loading rates. With $E_{F_{max}} \,/\, E_p \approx 0.6$ for charge and ≈ 0.5 for flow region specimens, energy absorption beyond peak load was slightly more important than in a quasi-static loading. The gradual failure of the hybrid CoDico GF/CF SMC shifted to a more abrupt failure evolution if

punctured in a dynamic manner, comparable to the force-deflection evolution of the Co CF SMC (Figure 7.19).

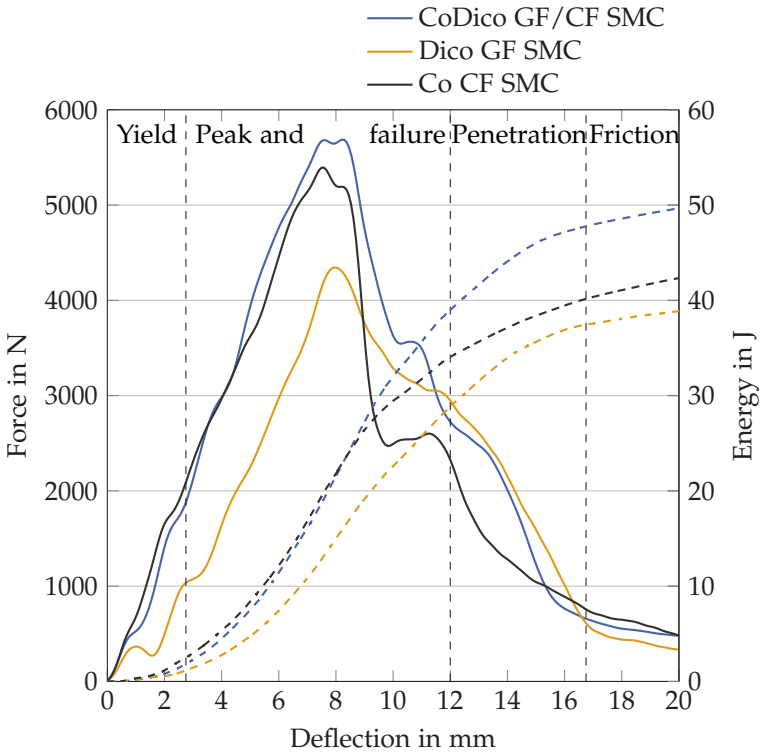


Figure 7.19: Dynamic force-deflection and energy-deflection responses of discontinuous glass fibre SMC, continuous carbon fibre SMC and continuous-discontinuous glass/carbon fibre SMC.

The literature (Gortner et al., 2015b) includes study results that refer to a more significant increase in maximum load (114 %) and energy intake (106 %) if a discontinuous glass fibre SMC was reinforced by two ± 45° non-crimp fabric face layers and punctured according to

EN ISO 6603-2 (2000). The effect of hybridisation might be more significant due to the architecture of the fibrous reinforcing in the shell layers, and the slightly higher ratio of face sheet thickness to laminate thickness (0.27 – 0.4). In addition, Gortner et al. compared maximum measured energy intake at the end of the impacting event and did not account for a falsification due to frictional effects. Nevertheless, it might be concluded that, due to the multi-axial loading, resulting from puncture testing, a unidirectional fibrous reinforcement in the face layers may not be the most efficient way to reinforce discontinuous composites, since mechanical performance perpendicular to fibre direction is extremely low.

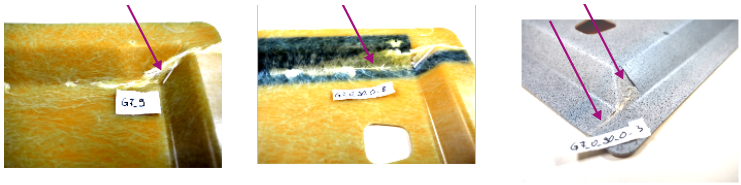
7.5.2.3 Component level

Component testing of Dico GF SMC and CoDico GF/CF SMC based demonstrator parts aimed to define damage evolution and material performance if exposed to near-service loads. In addition, manufacturing of demonstrator parts which are locally reinforced is one important objective of the International Research Training group (IRTG, GRK 2078). The characterisation of hybrid demonstrator parts is a necessary step to evaluate the performance and applicability of hybrid CoDico GF/CF SMC composites on a component level.

The components with local Co CF reinforcement generally featured superior mechanical performance with an increase in initial stiffness ($\approx$ 23 %) and strength ($\approx$ 32 %) compared to non-locally reinforced demonstrator parts. Initial stiffness was characterised by a certain scatter which was more important than variations in stiffness of the demonstrator part only based on Dico GF SMC. This scatter may be due to a process-induced difference based on a misalignment of the local reinforcement. However, considering the relatively

low number of investigated specimens, this result only shows a qualitative tendency.

Failure evolution was comparable for non-locally reinforced demonstrator parts and components featuring a local reinforcement. One major crack formed at the inclined side plane near the hole within the structure (Figure 7.20a). Damage was accompanied by delamination of the continuous reinforcement (Figure 7.20b). Fracture was most likely to propagate at the interface between local reinforcement and discontinuously reinforced material (Figure 7.20c).



(a) (b) (c)

Figure 7.20: Macroscopic observation of damaged demonstrator parts; demonstrator made from pure discontinuous glass fibre SMC showing one major crack (a); locally reinforced demonstrator part (bottom) showing one major crack and delamination within the crack region (b); and locally reinforced demonstrator part (top) showing a crack propagating at the interface of continuous and discontinuous reinforcement (c). Dimensioned drawing of the demonstrator part depicted in Figure 3.15.

In summary, one has to highlight that the local continuous reinforcement offered significant advantages in terms of stiffness and strength without sacrificing the benefits of components made only from Dico GF SMC regarding the design freedom. Additionally, taking into account that both components based on the same resin system and a ratio of 1/10 considering the price of glass/carbon fibres (CES EduPack, 2017), the material costs can be significantly reduced due to a local reinforcement in comparison to components based entirely on

a fibrous reinforcement made from carbon fibre reinforced composites. Furthermore, enhanced design freedom, which also enabled a demonstrator part with ribs, underlines one of the major advantages of the presented strategy to hybridise SMC composites.

8 Final remarks

In this final chapter, the main findings of this work are summarised, with the effect of hybridisation in central focus of the resume. It is then possible to draw a conclusion regarding the mechanical performance of the investigated hybrid continuous-discontinuous glass/carbon fibre SMC.

8.1 Summary

The investigated hybrid continuous-discontinuous glass/carbon fibre SMC material enabled a combination of the advantages of discontinuous fibre reinforced polymers, in terms of design freedom and low material and manufacturing cost, with the high specific stiffness and strength resulting from a continuous reinforcement. Although SMC composites, as they are known today, date to the 1960s and are used in wide-ranging applications, the potential of hybrid SMC materials has been subject to little research in the past. The presented approaches are either based solely on glass fibre reinforced composites with chopped and continuous fibre architectures, a combination of discontinuous materials with dry-textiles or expensive prepreg material as continuous component. Within this work and in the framework of the International Research Training Group, GRK 2078, which focusses on the integrated engineering of continuous-discontinuous long fibre reinforced polymer structures, an innovative approach aimed to combine a continuous carbon fibre reinforced

composite with a discontinuously glass fibre reinforced polymer, with both materials manufactured on a conventional SMC conveyor belt. An adapted process, developed at the Fraunhofer Institute for Chemical Technology (ICT) in Pfinztal Germany, was successfully implemented to manufacture continuous carbon fibre SMC sheets, which could be considered in a following step to manufacture hybrid SMC laminates, featuring a discontinuous glass fibre SMC core layer and two continuous carbon fibre face layers. In contrast to already existing approaches to develop a hybrid SMC composite, the presented approach offers the significant advantage of chemical similarity of the matrix to improve interface quality between the differently reinforced layers of the CoDico laminate. In addition, unidirectionally reinforced semi-finished sheets could be manufactured in a cost-efficient way on an adapted conventional SMC conveyor plant, which might permit the presented manufacturing process in industrial applications. It also enabled local reinforcement of three-dimensional components which featured enhanced mechanical performance compared to non-reinforced components made from discontinuous glass fibre SMC only.

The following overview of this study's results and findings takes up the research questions defined in section 2.5.

Microstructure and process-induced anisotropy of fibre orientation
Generally chopped, discontinuous fibre reinforced materials, such as SMC composites, are characterised by a heterogeneous microstructure, which arises due to manufacturing. The movement of the conveyor belt, but more importantly the geometry of the mould, initial mould coverage and resulting flow during moulding force the fibrous reinforcement to align in the flow direction. Hence, SMC composites might be characterised by a non-random fibre orientation. As a

consequence, material properties are anisotropic, and experimental characterisation has to be realised for specimens extracted featuring different orientations with respect to flow direction. In addition, fibre bundles at the edges or corners may be exposed to high deformation, and it is recommended not to extract specimens from the edges of the sheets to avoid possible falsification of experimentally determined mechanical performance. Structure-property relationships have been investigated for the continuously and discontinuously reinforced material from the micro- to the macroscale to identify the influence of manufacturing parameters on material properties. With μ-CT observations, valuable information regarding fibre orientation and interface between the continuous and discontinuous layers was gained. The observed discontinuous SMC composite was characterised by a significant shell-core effect. In the shell layers, fibre bundles were spread, separated from the bundles and tend to bend due to complex moulding kinematics and a non-uniform temperature distribution within the mould. Within the core, the fibrous reinforcement was organised in fibre bundles, featuring no significant curvature and usually aligned with flow. Determination of fibre orientation tensors allowed quantification of the flow-induced fibre orientation and delivery of input to analytically predict the stiffness of the material. The presented characterisation strategy enabled definition of anisotropy of mechanical performance resulting from process-induced fibre orientation and variations in fibre volume content within different discontinuous glass fibre SMC sheets. Anisotropic material properties resulted from one-dimensional (1D) flow of the semi-finished material. Nevertheless, no difference was observed in mechanical performance of charge and flow region specimens.

Microstructural observations of the interface between continuously and discontinuously reinforced SMC layers highlighted a significant transition zone. No distinct interface existed. Within the transition zone the discontinuous material forced the continuous carbon fibre bundles to spread. Spreading of the continuous carbon fibre bundles was also favoured due to a lack of a vertical connection between different bundles. Although the discontinuous SMC composite in the core filled the mould without significant flow perpendicular to the principal axis of the continuous reinforcement, slight fibre misalignment of the unidirectional carbon fibres resulted due to local crossflow. The positioning of the continuous non-crimp fabric on the conveyor belt, along with cutting and stacking of the semi-finished sheets prior to moulding, is crucial to avoid fibre misalignment. Not only mechanical properties, but also more important damage evolution and failure mechanisms strongly depended on fibre orientation of the continuous component.

Definition of appropriate measurement techniques and specimen geometries

Characterisation of discontinuous SMC materials was linked to a significant scatter resulting from the heterogeneous microstructure. Hence, it was extremely difficult to distinguish between an effect resulting from testing parameters and specimen geometry or from the heterogeneous microstructure. Statistical data evaluation helped to define material properties accounting for intrinsic variations.

The effect of specimen size on mechanical material properties was defined in a preliminary study. No significant difference was observed in specific stiffness resulting from tensile testing with different specimen geometries. Specific strength slightly decreased for larger specimens. In addition, preparation of edges after water-jet cutting

did not influence the quasi-static material performance of continuous SMC materials. Nevertheless, edge quality might influence cyclic properties of continuously reinforced materials, and it must be kept in mind to consider the edge quality again as soon as fatigue properties are sought to be defined.

Investigations in terms of image processing and data evaluation enabled the definition of appropriate testing parameters to successfully apply stereo digital image correlation on heterogeneous SMC materials. This full-field measurement technique allowed for a detailed characterisation of evolving strain fields and damage. Testing procedures defined within this dissertation were adapted to account for either a continuous or discontinuous reinforcement, as well as characterise hybrid CoDico SMC composites.

Evaluation of hybridisation effects

The rule of (hybrid) mixtures is generally not the best criterion to evaluate a hybridisation effect for every loading case (e.g. flexural properties or multiaxial loading cases). In order to account for specific loading cases, it is recommended to individually define a criterion to evaluate an effect of hybridisation. A basic approach is based on the identification of the variation of a distinct property of the hybrid composite with respect to a reference value defined by one individual component, for example.

In terms of stiffness, strength and energy absorption capability, the discontinuous glass fibre SMC was considered as reference, featuring the lowest mechanical performance. Considering damage tolerance, hence failure strain or maximum deflection, the continuous carbon fibre SMC material exhibited lower performance and was therefore

considered a reference to define hybridisation effects. Figure 8.1 presents an overview of the results concerning hybridisation effects.

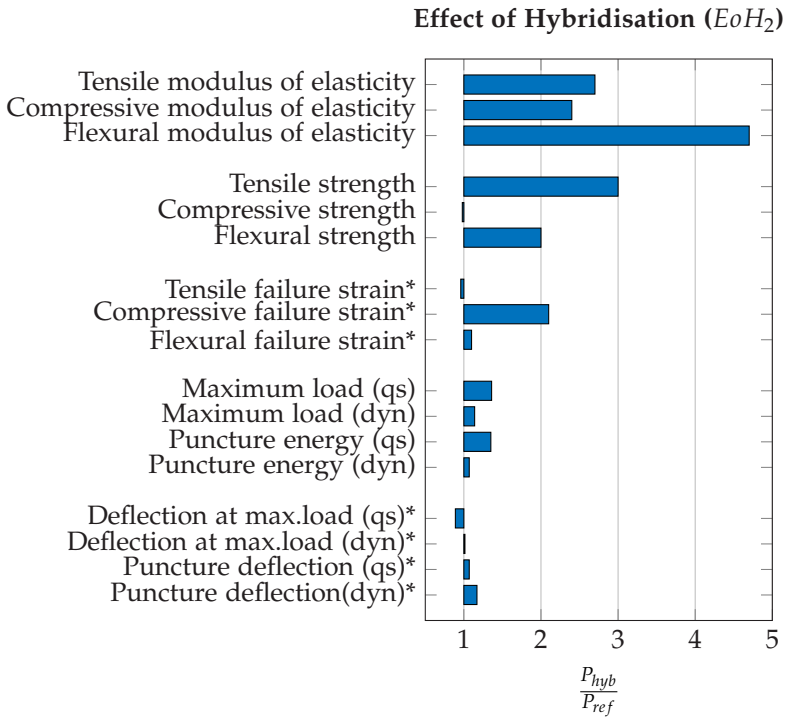


Figure 8.1: Effect of hybridisation of mechanical properties of continuous-discontinuous glass/carbon fibre SMC (for properties marked with *, the continuous carbon fibre SMC was considered as reference in all other cases of evaluation of hybridisation effects based on the enhancement of mechanical performance with respect to the property of the discontinuous SMC material).

In summary, for every considered loading case, regardless of whether material, structural or component properties were considered, stiffness, strength and energy absorption capability of the hybrid CoDico GF/CF SMC were characterised by a positive hybridisation effect

resulting from a continuous carbon fibre reinforcement. Considering a quasi-static loading, the only exception was compression strength, which was not affected by the continuous face layers due to the low compressive strength and failure strain of the continuous component exposed to compressive loads. Additionally, dynamic puncture properties in terms of maximum load and energy absorption were only slightly influenced by a continuous reinforcement due to a superposition of rate effects and limited damage tolerance of unidirectionally reinforced composites.

The failure strain of CoDico GF/CF SMC was enhanced with respect to the pure continuous carbon fibre SMC material linked to an increased damage tolerance if hybrid CoDico GF/CF SMC was exposed to tensile, compression and quasi-static and dynamic puncture loads. Hence, the continuous carbon fibre SMC, which exhibits in general low failure strains, was therefore reinforced by the discontinuous component.

Modelling approaches

In terms of analytical modelling, tensile and compressive moduli of elasticity could accurately be predicted by a rule of hybrid mixtures (RohM), considering the experimentally determined, hence homogenised, stiffness of the Dico GF SMC and Co CF SMC as input parameters (Figure 8.2). However it is crucial to precisely define the volume content of the different materials, which was especially complicated in the present study due to a highly heterogeneous thickness of the continuous face layers.

The tension-compression anisotropy of the Co CF SMC has to be considered to predict flexural stiffness of the hybrid CoDico GF/CF

SMC, and an asymmetric laminate resulted in the best results by means of classical laminate theory (CLT) (Figure 8.2).

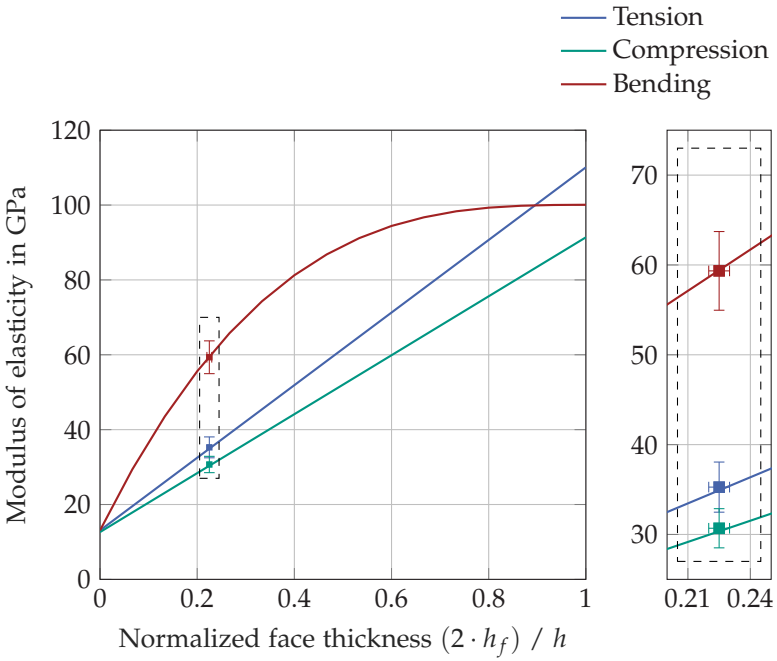


Figure 8.2: Analytically predicted tensile, compressive and flexural modulus of elasticity in fibre direction of the continuous component. Calculations based on rule of hybrid mixtures and classical laminate theory with rectangle and error bars indicating experimentally determined values.

A linear rule of hybrid mixtures also enabled precise prediction of the tensile strength of the hybrid CoDico SMC. Considering compressive loadings, a linear rule of hybrid mixtures overestimates mechanical performance. If a bilinear rule of hybrid mixture was taken into account, the investigated layup of the laminate and the ratio of face sheet thickness to global thickness of the laminate was not

sufficiently high to achieve a reinforcement effect. Compressive strength, predicted with a bilinear rule of mixtures, was significantly lower than the experimentally determined value. Flexural strength of the hybrid CoDico GF/CF SMC could accurately be predicted by an analytical approach based on the classical laminate theory and the observed failure evolution of the hybrid CoDico SMC composite exposed to flexural loads. The tensile and compressive moduli of elasticity and the failure strains of the continuous component as well as the tensile modulus of elasticity of the discontinuous component were considered as input parameters.

Damage mechanisms and failure evolution
Evolving damage and failure mechanisms of the investigated CoDico GF/CF SMC were determined from a superposition of failure of the two individual components.

Damage evolution of the pure discontinuous glass fibre SMC was determined by the formation of matrix cracks followed by crack growth and accumulation of cracks resulting in final failure. Failure differed between the core layers (matrix cracking perpendicular to loading direction and fibre breakage of individual fibres) and the shell layers (debonding and pull-out of fibre bundles and pseudo-delamination).

Failure of the carbon fibre SMC material significantly depended on loading case. For uniaxial tension, inter-fibre fractures and splitting of different fibre bundles were the dominant mechanisms to absorb energy. Fibre misalignment had an important effect on failure evolution, and especially for the hybrid CoDico GF/CF SMC materials exposed to tensile loadings, damage was initiated where misaligned carbon fibre bundles met the edges of the specimen.

For compressive loads, early microbuckling and the low compressive strength of the continuous carbon fibre SMC prevented a positive hybridisation effect.

In terms of flexural loadings, the lay-up of the laminate and the greatest distance of the continuous material from the neutral axis explains the disproportionate increase in the flexural stiffness and strength of the hybrid material. Generally, the tension-compression anisotropy, observed for the Co CF SMC, significantly influenced the flexural behaviour of hybrid SMC. Firstly, failure was initiated by compressive strains and fibre breakage on the upper surface, followed by compressive failure of the discontinuous material and final failure at the lower surface (fibre breakage linked to splitting hence inter-fibre fractures of the continuous component and delamination).

8.2 Conclusion

Hybridisation with more than one fibre type within a common matrix in an interlayer configuration leads to another dimension of the potential versatility of fibre reinforced composite materials. Hybrid SMC composites, which consisted of two continuously reinforced face sheets and a discontinuous glass fibre SMC within the core, enabled greater control of specific properties, achieving a more favourable balance between the advantages and disadvantages of the two individual materials, for example the low failure strain of the continuous component and low stiffness and strength of the chopped glass fibre SMC. The main goal of this dissertation was to provide a fundamental understanding of material, structural and component properties of hybrid CoDico glass/carbon fibre SMC to move towards the implementation of hybrid SMC structures in technical applications that

involve varied loading cases. A vertical characterisation strategy started from the coupon level and highlighted characteristics on the micro-, meso- and macroscale of the individual and the hybrid composites. On each level, a horizontal characterisation strategy was intended to investigate the two individual materials in a first step and to deduce, in the following, effects of hybridisation in terms of mechanical behaviour and failure evolution due to an experimental characterisation of the hybrid material.

Microstructural characteristics at the interface, as well as fibre orientation resulting from manufacturing, have been considered in detail, indicating a transition zone between the two components. The following characterisation on the coupon level indicated a significant increase of tensile (+169 %), compressive (+143 %), and flexural (+370 %) modulus of elasticity. In terms of tensile and compressive loads volume fraction of the two individual materials and especially the elastic properties of the continuous carbon fibre SMC influences the stiffness of the hybrid CoDico SMC, which could be analytically predicted by a rule of hybrid mixtures. Due to the specific layup of the laminate, the increase of flexural modulus of elasticity was most significant. A precise prediction of resulting properties of the hybrid CoDico SMC strongly relied on the consideration of the tension-compression anisotropy of the continuous carbon fibre SMC.

The tensile strength of the hybrid CoDico SMC was three times as high (+193 %) as the tensile strength of the pure discontinuous glass fibre SMC. A linear and bilinear rule of hybrid mixtures, which slightly underestimated the tensile strength of the hybrid CoDico SMC, highlighted a positive hybridisation effect. The continuous face layers determined failure evolution. The hybrid CoDico SMC failed due to inter-fibre failure linked to delamination and a partial

weakening of the specimen. In the end, the discontinuous glass fibre SMC failed due to pseudo-delamination. Failure strain was slightly increased (+15 %) due to hybridisation; taking the continuous carbon fibre SMC as reference, however, no pseudo-ductility was observed. Hybridisation had no effect on compressive strength, since continuous carbon fibre SMC featured a low damage tolerance if exposed to uniaxial compression. The effect was even more severe since the continuous face sheet was built up from only one layer of continuous carbon fibre SMC. Microbuckling of the surface layer linked to delamination and pseudo-delamination within the discontinuous glass fibre SMC core were the most important failure mechanisms. The flexural strength of the hybrid CoDico SMC was twice as high (+126 %) as that of the discontinuous glass fibre SMC. An adaption of the classical laminate theory, taking a theoretical failure strain into account, which results from a superposition of tensile and compressive failure strain, enabled accurate prediction of flexural strength of a hybrid CoDico SMC.

The subsequent characterisation at the structure level provided further information on puncture properties considering rate effects and underlined perspectives to consider hybrid SMC composites, featuring a local continuous reinforcement, for different technical applications. Exposed to quasi-static puncture, hybrid CoDico SMC exhibited a significantly higher maximum load (+34 %) and puncture energy (+35 %) than did pure discontinuous glass fibre SMC. Dynamic puncture led to a superposition of a positive rate dependence of the discontinuous glass fibre SMC and a non-rate dependence of the continuous carbon fibre SMC, which resulted in a less notable increase in terms of maximum load (+7 %) and puncture energy (+14 %) of the hybrid CoDico SMC.

Four-point bending testing on a component scale indicated that a local continuous reinforcement of a discontinuous glass fibre SMC component significantly enhanced stiffness (+23 %) and load at failure (+17 %), whereby the weight and geometry of the considered component were not changed.

In general, hybrid CoDico glass/carbon fibre SMC composites offer the possibility to attain properties of the hybrid material, which are more than the sum of the properties of the individual components if the hybrid composite features an appropriate design accounting for a well-defined loading case in terms of the ratio of the individual materials and stacking sequence of the laminate.

Bibliography

Abrams, L. M. (2001). Processing studies in sheet molding compound compression molding. Dissertation. Columbus, Ohio: The Ohio State University.

Adams, D. and Hyer, M. (1994). Effects of Layer Waviness on the Compression Response of Laminates. In: *Compression Response of Composite Structures*. Ed. by S. Groves and A. Highsmith. West Conshohocken, PA: ASTM International, 65–77.

Adams, D. O. and Adams, D. F. (2002). Tabbing Guide for Composite Test Specimen. U.S. Department of Transportation - Federal Aviation Administration, Washington, D.C.

Advani, S. G. and Tucker, C. L. (1990). A numerical simulation of short fiber orientation in compression molding. *Polymer Composites* 11(3), 164–173. ISSN: 02728397. DOI: 10.1002/pc.750110305.

Advani, S. G. and Tucker III, C. L. (1978). The use of tensors to describe and predict fiber orientation in short fiber composites. *Journal of Rheology* 31(8), 751–784. DOI: 10.1122/1.549945.

Affdl, J. C. H. and Kardos, J. L. (1976). The Halpin-Tsai equations: A review. *Polymer Engineering & Science* 16(5), 344–352. ISSN: 1548-2634. DOI: 10.1002/pen.760160512.

Agrawal, S., Singh, K. K. and Sarkar, P. K. (2014). Impact damage on fibre-reinforced polymer matrix composite – A review. *Journal of Composite Materials* 48(3), 317–332. ISSN: 0021-9983. DOI: 10.1177/0021998312472217.

Akiyama, K. (2011). Development of Prepreg Compression Molding technology (Presentation). Troy, MI.

Asadi, A., Miller, M., Sultana, S., Moon, R. J. and Kalaitzidou, K. (2016). Introducing cellulose nanocrystals in sheet molding compounds (SMC). *Composites Part A: Applied Science and Manufacturing* 88, 206–215. ISSN: 1359-835X. DOI: 10.1016/j.compositesa.2016.05.033.

Ashby, M. (2006). Materials Selection in Mechanical Design: Das Original mit Übersetzungshilfen. 1st ed. München: Springer Spektrum. ISBN: 978-3-8274-1762-6.

ASTM D3039/D3039M (2017). Standard Test Method for Tensile Properties of Polymer Matrix Composite Materials. West Conshohocken, PA: ASTM International.

ASTM D5687/D5687M-95 (2015). Standard Guide for Preparation of Flat Composite Panels with Processing Guidelines for Specimen Preparation. West Conshohocken, PA: ASTM International.

ASTM D7264/D7264M (2015). Standard Test Method for Flexural Properties of Polymer Matrix Composite Materials. West Conshohocken, PA: ASTM International.

ASTM E111 (2010). Standard Test Method for Young's Modulus, Tangent Modulus, and Chord Modulus. West Conshohocken, PA: ASTM International.

Aveston, J. and Kelly, A. (1973). Theory of multiple fracture of fibrous composites. *Journal of Materials Science* 8(3), 352–362. ISSN: 1573-4803. DOI: 10.1007/BF00550155.

AVK - Industrievereinigung Verstärkte Kunststoffe e.V., ed. (2013). Handbuch Faserverbundkunststoffe/Composites: Grundlagen, Verarbeitung, Anwendungen. 4th ed. Springer Fachmedien Wiesbaden: Springer Vieweg. DOI: 10.1007/978-3-658-02755-1.

AZO Materials (2018). E-Glass Fibre. URL: `https://www.azom.com/article.aspx?ArticleID=764` (Accessed: 06 June 2018).

Bandaru, A. K., Vetiyatil, L. and Ahmad, S. (2015). The effect of hybridization on the ballistic impact behavior of hybrid composite armors. *Composites Part B: Engineering* 76(Supplement C), 300–319. ISSN: 13598368. DOI: 10.1016/j.compositesb.2015.03.012.

Barone, M. R. and Caulk, D. A. (1985). Kinematics of flow in sheet molding compounds. *Polymer Composites* 6(2), 105–109. ISSN: 02728397. DOI: 10.1002/pc.750060208.

Belingardi, G. and Vadori, R. (2002). Low velocity impact tests of laminate glass-fiber-epoxy matrix composite material plates. *International Journal of Impact Engineering* 27(2), 213–229. ISSN: 0734-743X. DOI: 10.1016/S0734-743X(01)00040-9.

Benveniste, Y. (1987). A new approach to the application of Mori-Tanaka's theory in composite materials. *Mechanics of Materials* 6(2), 147–157. ISSN: 0167-6636. DOI: 10.1016/0167-6636(87)90005-6.

Benveniste, Y. and Dvorak, G. J. (1990). On a Correspondence Between Mechanical and Thermal Effects in Two-Phase Composites. In: *Micromechanics and Inhomogeneity: The Toshio Mura 65th Anniversary Volume*. Ed. by G. J. Weng, M. Taya and H. Abé. Springer, 65–81. ISBN: 978-1-4613-8919-4. DOI: 10.1007/978-1-4613-8919-4_4.

Berbinau, P., Soutis, C. and Guz, I. A. (1999). Compressive failure of 0-degree unidirectional carbon-fibre-reinforced plastic (CFRP) laminates by fibre microbuckling. *Composites Science and Technology* 59(9), 1451–1455. ISSN: 0266-3538. DOI: 10.1016/S0266-3538(98)00181-X.

Bernstorff, B. von and Ehrenstein, G. W. (1990). Failure mechanism in SMC subjected to alternating stresses. *Journal of Materials Science* 25(9), 4087–4097. ISSN: 1573-4803. DOI: 10.1007/BF00582486.

Berreur, L., Maillard, B. de and Nosperger, S. (2002). L'industrie française des matériaux composites - Des enjeux prioritaires pour un développement durable: Etude stratégique. URL: `https://archives.entreprises.gouv.fr/2012/www.industrie.gouv.fr/biblioth/docu/dossiers/sect/pdf/rapfinal_long.pdf` (Accessed: 31 Oct. 2018).

Bert, C. W. and Kline, R. A. (1985). Composite-material mechanics: Properties of planar-random fiber composites. *Polymer Composites* 6(3), 133–141. ISSN: 1548-0569. DOI: 10.1002/pc.750060302.

Böhlke, T., Kärger, L., Weidenmann, K. A. and Henning, F. (2016). Continuous-discontinuous long fiber-reinforced polymer structures: Modeling, characterization and validation (Presentation). AFBW AG Composite-Simulation. Karlsruhe.

Boylan, S. and Castro, J. M. (2003). Effect of reinforcement type and length on physical properties, surface quality, and cycle time for sheet molding compound (SMC) compression molded parts. *Journal of Applied Polymer Science* 90(9), 2557–2571. ISSN: 1097-4628. DOI: 10.1002/app.12726.

Bruderick, M., Denton, D., Shinedling, M. and Kiesel, M. (2003). Application of Carbon Fiber SMC for the Dodge Viper. URL: `http://www.quantumcomposites.com/pdf/papers/Viper-SPE-Paper.pdf` (Accessed: 24 Jan. 2018).

Brylka, B. (2017). Charakterisierung und Modellierung der Steifigkeit von langfaserverstärktem Polypropylen. Dissertation. Karlsruhe: Karlsruhe Institute of Technology.

Bücheler, D. (2018). Locally continuous-fiber reinforced sheet molding compound. Dissertation. Karlsruhe: Karlsruhe Institute of Technology.

Bücheler, D. and Henning, F. (2016). Hybrid resin improves position and alignment of continuously reinforced prepreg during compression co-molding with sheet molding compound. In: *Proceeding of the 17th European Conference on Composite Materials; Munich; Germany;* Aachen: European Society for Composite Materials (ESCM).

Bücheler, D., Kaiser, A. and Henning, F. (2016). Using thermogravimetric analysis to determine carbon fiber weight percentage of fiber-reinforced plastics. *Composites Part B: Engineering* 106, 218–223. ISSN: 13598368. DOI: 10.1016/j.compositesb.2016.09.028.

Budiansky, B. and Fleck, N. A. (1993). Compressive failure of fibre composites. *Journal of the Mechanics and Physics of Solids* 41(1), 183–211. ISSN: 0022-5096. DOI: 10.1016/0022-5096(93)90068-Q.

Bulut, M., Erkliğ, A. and Yeter, E. (2016). Hybridization effects on quasi-static penetration resistance in fiber reinforced hybrid composite laminates. *Composites Part B: Engineering* 98(Supplement C), 9–22. ISSN: 13598368. DOI: 10.1016/j.compositesb.2016.05.025.

Byrne, E. (2018). Subset, Step Size and Strain Filter Selection: correlated SOLUTIONS: Knowledgebase: Application Notes. Ed. by Correlated SOLUTIONS. URL: `http://www.correlatedsolutions.com/support/index.php?/Knowledgebase/Article/View/10/1/subset-step-size-and-strain-filter-selection` (Accessed: 06 June 2018).

Cabrera-Ríos, M. and Castro, J. M. (2006). An economical way of using carbon fibers in sheet molding compound compression molding for automotive applications. *Polymer Composites* 27(6), 718–722. ISSN: 02728397. DOI: 10.1002/pc.20257.

Caprino, G., Langella, A. and Lopresto, V. (2003). Indentation and penetration of carbon fibre reinforced plastic laminates. *Composites Part B: Engineering* 34(4), 319–325. ISSN: 13598368. DOI: 10.1016/S1359-8368(03)00002-7.

Cardarelli, F. (2008). Materials Handbook: A Concise Desktop Reference. Springer-Verlag: London. ISBN: 978-1-84628-669-8. DOI: 10.1007/978-1-84628-669-8.

Castañeda, P. P. and Suquet, P. (1997). Nonlinear Composites. In: *Advances in Applied Mechanics*. Ed. by E. van der Giessen and T. Y. Wu. Vol. 34. Elsevier, 171–302. ISBN: 0065-2156. DOI: 10.1016/S0065-2156(08)70321-1.

Castro, J. M. and Griffith, R. M. (1989). Sheet molding compound compression-molding flow. *Polymer Engineering & Science* 29(10), 632–638. ISSN: 1548-2634. DOI: 10.1002/pen.760291004.

Castro, J. M. and Lee, C. C. (1987). Thermal and cure analysis in sheet molding compound compression molds. *Polymer Engineering & Science* 27(3), 218–224. ISSN: 1548-2634. DOI: 10.1002/pen.760270307.

CES EduPack (2017). Cambrigde, UK: Granta Design Limited.

Chaturvedi, S. K. and Sierakowski, R. L. (1983). Residual strength assessment of SMC composites subjected to dynamic impact. *Composite Structures* 1(2), 137–161. ISSN: 0263-8223. DOI: 10.1016/0263-8223(83)90009-0.

Chaturvedi, S. K. and Sierakowski, R. L. (1985). Effects of impactor size on impact damage-growth and residual properties in an SMC-R50 composite. *Journal of Composite Materials* 19(2), 100–113. ISSN: 0021-9983. DOI: 10.1177/002199838501900201.

Chaturvedi, S. K., Sun C. T. and Sierakowski R. L. (1983). Mechanical characterization of sheet molding compound composites. *Polymer Composites* 4(3), 167–171. ISSN: 02728397. DOI: 10.1002/pc.750040306.

Chen, C. Y. and Tucker, C. L. (1984). Mechanical property predictions for short fiber/brittle matrix composites. *Journal of Reinforced Plastics and Composites* 3(2), 120–129. DOI: 10.1177/073168448400300202.

Chen, Z., Huang, T., Shao, Y., Li, Y., Xu, H., Avery, K., Zeng, D., Chen, W. and Su, X. (2018). Multiscale finite element modeling of sheet molding compound (SMC) composite structure based on stochastic mesostructure reconstruction. *Composite Structures* 188, 25–38. ISSN: 0263-8223. DOI: 10.1016/j.compstruct.2017.12.039.

Chen, Z. et al. (2017). "A Comparative Study of Two RVE Modelling Methods for Chopped Carbon Fiber SMC". In: *WCX™ 17: SAE World Congress Experience*. SAE International. DOI: 10.4271/2017-01-0224. URL: https://doi.org/10.4271/2017-01-0224.

Cheresh, C. M. and McMichael, S. (1986). Instrumented impact test data interpretation. In: *Instrumented impact testing of plastics and composite materials,* ed. by S. Kessler. West Conshohocken, PA: ASTM International, 9–23.

Corbridge, D. M., Harper, L. T., Focatiis, D. de and Warrior, N. A. (2017). Compression moulding of composites with hybrid fibre architectures. *Composites Part A: Applied Science and Manufacturing* 95, 87–99. ISSN: 1359-835X. DOI: 10.1016/j.compositesa.2016.12.018.

Czél, G., Jalalvand, M. and Wisnom, M. R. (2015). Demonstration of pseudo-ductility in unidirectional hybrid composites made of discontinuous carbon/epoxy and continuous glass/epoxy plies. *Composites Part A: Applied Science and Manufacturing* 72, 75–84. ISSN: 1359-835X. DOI: 10.1016/j.compositesa.2015.01.019.

Czél, G. and Wisnom, M. R. (2013). Demonstration of pseudo-ductility in high performance glass/epoxy composites by hybridisation with thin-ply carbon prepreg. *Composites Part A: Applied Science and Manufacturing* 52, 23–30. ISSN: 1359-835X. DOI: 10.1016/j.compositesa.2013.04.006.

Dano, M. L., Gendron, G., Maillette, F. and Bissonnette, B. (2006). Experimental characterization of damage in random short glass fiber reinforced composites. *Journal of Thermoplastic Composite Materials* 19(1), 79–96. DOI: 10.1177/0892705706055447.

Dear, J. P. and Brown, S. A. (2003). Impact damage processes in reinforced polymeric materials. *Composites Part A: Applied Science and Manufacturing* 34(5), 411–420. ISSN: 1359-835X. DOI: 10.1016/S1359-835X(03)00082-4.

Derrien, K., Fitoussi, J., Guo, G. and Baptiste, D. (2000). Prediction of the effective damage properties and failure properties of nonlinear anisotropic discontinuous reinforced composites. *Computer Methods in Applied Mechanics and Engineering* 185(2), 93–107. ISSN: 00457825. DOI: 10.1016/S0045-7825(99)00253-4.

Desrumaux, F., Meraghni, F. and Benzeggagh, M. L. (2001). Generalised Mori-Tanaka scheme to model anisotropic damage using numerical Eshelby Tensor. *Journal of Composite Materials* 35(7), 603–624. ISSN: 0021-9983. DOI: 10.1177/002199801772662091.

DIN EN ISO 14125 (1998). Fibre reinforced plastic composites - Determination of flexural properties (ISO 14125:1998 + Cor.1:2001 + Amd.1:2011): Deutsches Institut für Normung e.V.. Berlin: Beuth Verlag GmbH.

DIN EN ISO 14126 (1999). Fibre reinforced plastic composites - Determination of compressive properties in the in-plane direction (ISO 14126:1999): Deutsches Institut für Normung e.V.. Berlin: Beuth Verlag GmbH.

DIN EN ISO 179 (2010). Plastics – Determination of Charpy impact properties – Part 1: Non-instrumented impact test (ISO 179-1:2010): Deutsches Institut für Normung e.V.. Berlin: Beuth Verlag GmbH.

DIN EN ISO 527-1 (2012). Plastics - Determination of tensile properties - Part 1: General principles (ISO 527-1:2012): Deutsches Institut für Normung e.V.. Berlin: Beuth Verlag GmbH.

DIN EN ISO 527-4 (1997). Plastics - Determination of tensile properties - Part 4: Test conditions for isotropic and orthotropic fibre-reinforced plastic composites (ISO 527-4 : 1997): Deutsches Institut für Normung e.V.. Berlin: Beuth Verlag GmbH.

DIN EN ISO 527-5 (2009). Plastics - Determination of tensile properties - Part 5: Test conditions for unidirectional fibre-reinforced plastic composites (ISO 527-5 : 2009): Deutsches Institut für Normung e.V.. Berlin: Beuth Verlag GmbH.

Dong, C. and Davies, I. J. (2012). Flexural properties of glass and carbon fiber reinforced epoxy hybrid composites. *Proceedings of the IMechE* 227(4), 308–317. ISSN: 1464-4207. DOI: 10.1177/1464420712459396.

DSM Daron 41/B1 (2012). Product Data Sheet : Daron 41/B1.

Dumont, P., Orgéas, L., Favier, D., Pizette, P. and Venet, C. (2007). Compression moulding of SMC: In situ experiments, modelling and simulation. *Composites Part A: Applied Science and Manufacturing* 38(2), 353–368. ISSN: 1359-835X. DOI: 10.1016/j.compositesa.2006.03.010.

EN ISO 6603-2 (2000). English version of DIN EN ISO 6603-2, Plastics: Determination of puncture impact behaviour of rigid plastics, Part 2: Instrumented puncture test. Deutsches Institut für Normung e.V.. Berlin: Beuth Verlag GmbH.

Eshelby, J. D. (1957). The determination of the elastic field of an ellipsoidal inclusion, and related problems. *Proceedings of the Royal Society of London. Series A. Mathematical and Physical Sciences* 241(1226), 376. DOI: 10.1098/rspa.1957.0133.

Eshelby, J. D. (1959). The elastic field outside an ellipsoidal inclusion. *Proceedings of the Royal Society of London. Series A. Mathematical and Physical Sciences* 252(1271), 561. DOI: 10.1098/rspa.1959.0173.

European Commission (2016). Communication from the Commission to the European Parliament, the Council, the European Economic and Social Committee and the Committee of the Regions: A European Strategy for Low-Emission Mobility. URL: `https://ec.europa.eu/clima/policies/transport/vehicles/cars_en` (Accessed: 15 July 2019).

European Union (2009). Regulation [EC] No 443 of the European Parliament and of the Council of 23 April 2019 setting emission performance standards for new passenger cars as part of the Community's integrated approach to reduce CO2 emissions from light-duty verhicles. URL: `https://ec.europa.eu/clima/policies/transport/vehicles/cars_en` (Accessed: 15 July 2019).

Eyer, G., Montagnier, O., Charles, J.-P., Hochard, C. and Mazerolle, F. (2016). Influence de l'alignement des fibres sur la rupture des composites en compression sens fibre. *Matériaux & Techniques* 104(404).

Feld, N., Maeyens, C., Delattre, B. and Grandmaison, N. (2017). Modelling the effect of process-induced anisotropy on the constitutive behavior of chopped fiber composites. *Composites Part A: Applied Science and Manufacturing* 101, 334–343. ISSN: 1359-835X. DOI: 10.1016/j.compositesa.2017.06.012.

Fengler, B., Kärger, L., Henning, F. and Hrymak, A. (2018). Multi-Objective Patch Optimization with Integrated Kinematic Draping Simulation for Continuous–Discontinuous Fiber-Reinforced Composite Structures. *Journal of Composites Science* 2(2). DOI: 10.3390/jcs2020022.

Feraboli, P., Peitso, E., Cleveland, T. and Stickler, P. B. (2009). Modulus Measurement for Prepreg-based Discontinuous Carbon Fiber/Epoxy Systems. *Journal of Composite Materials* 43(19), 1947–1965. ISSN: 0021-9983. DOI: 10.1177/0021998309343028.

Fette, M., Hentschel, M., Köhler, F., Wulfsberg, J. and Herrmann, A. (2016). Automated and cost-efficient production of hybrid sheet moulding compound aircraft components. *16th Machining Innovations Conference for Aerospace Industry - MIC 2016* 6(Supplement C), 132–139. ISSN: 2351-9789. DOI: 10.1016/j.promfg.2016.11.017.

Fette, M., Hentschel, M., Santafe, J. G., Wille, T., Büttemeyer, H. and Schiebel, P. (2017). New Methods for Computing and Developing Hybrid Sheet Molding Compound Structures for Aviation Industry. *1st CIRP Conference on Composite Materials Parts Manufacturing (CIRP CCMPM 2017)* 66(Supplement C), 45–50. ISSN: 2212-8271. DOI: 10.1016/j.procir.2017.03.289.

Feuillade, V., Bergeret, A., Quantin, J.-C. and Crespy, A. (2006). Relationships between the glass fibre sizing composition and the surface quality of sheet moulding compounds (SMC) body panels. *Composites Science and Technology* 66(1), 115–127. ISSN: 0266-3538. DOI: 10.1016/j.compscitech.2005.05.009.

Fisk, C. (1953). Process for increasing viscosity of uncured alkyd copolymer resinous mixtures and product: US-Patent 2, 268, 209.

Fitoussi, J., Guo, G. and Baptiste, D. (1998). A statistical micromechanical model of anisotropic damage for S.M.C. composites. *Composites Science and Technology* 58(5), 759–763. ISSN: 0266-3538. DOI: 10.1016/S0266-3538(97)00163-2.

Förster, R. and Knappe, W. (1971). Experimentelle und theoretische Untersuchungen zur Rißbildungsgrenze an zweischichtigen Wickelrohren aus Glasfaser/Kunststoff unter Innendruck. *Kunststoffe* 61(8), 583–588.

Friedrich, K. (1989). Fractographic analysis of polymer composites. In: *Application of Fracture Mechanics to Composite Materials*. Ed. by K. Friedrich, 425–487.

Fu, S. Y., Lauke, B., Mäder, E., Yue, C. Y. and Hu, X. (2000). Tensile properties of short-glass-fiber- and short-carbon-fiber-reinforced polypropylene composites. *Composites Part A: Applied Science and Manufacturing* 31(10), 1117–1125. ISSN: 1359-835X. DOI: 10.1016/S1359-835X(00)00068-3.

Fu, S. Y., Lauke, B., Mäder, E., Yue, C. Y., Hu, X. and Mai, Y. W. (2001). Hybrid effects on tensile properties of hybrid short-glass-fiber-and short-carbon-fiber-reinforced polypropylene composites. *Journal of Materials Science* 36(5), 1243–1251. ISSN: 1573-4803. DOI: 10.1023/A:1004802530253.

Fu, S. Y., Xu, G. and Mai, Y. W. (2002). On the elastic modulus of hybrid particle/short-fiber/polymer composites. *Composites Part B: Engineering* 33(4), 291–299. ISSN: 13598368. DOI: 10.1016/S1359-8368(02)00013-6.

Fu, S., Lauke, B. and Mai, Y. (2009). Science and Engineering of Short Fibre Reinforced Polymer Composites. Cambridge, UK: Woodhead Publishing Limited.

Gardiner, G. (2016). Is the BMW 7 Series the future of autocomposites?. URL: `http://www.compositesworld.com/articles/is-the-bmw-7-series-the-future-of-autocomposites` (Accessed: 24 Jan. 2018).

Garmendia, J., Olaizola, M., Etxeberria, I., Franco, J. C. and Mondragon, I. (1995). Influence of processing and testing conditions on the mechanical behaviour of sheet-moulding compound laminates. *Journal of Materials Science* 30(20), 5287–5294. ISSN: 1573-4803. DOI: 10.1007/BF00356083.

Gibson, R. F. (2007). Principles of Composite Material Mechanics. 2nd ed. Boca Raton, FL: CRC Press - Taylor & Francis Group.

GOM (2018). ARAMIS Benutzerhandbuch - Software. Gesellschaft für Optische Messtechnik.

Gortner, F., Medina, L. and Mitschang, P. (2015a). "Advanced SMC-Processing in Combination with Textile Reinforcements". In: ed. by 20th International Conference on Composite Materials. 20th International Conference on Composite Materials, 19-24 July. Copenhagen.

Gortner, F., Medina, L. and Mitschang, P. (2015b). Influence of textile reinforcement on bending properties and impact strength of SMC-components. *International Journal of Applied Science and Technology* 8(4), 259–269. DOI: 10.14416/j.ijast.2015.07.005.

Griffith, A. A. (1921). VI. The phenomena of rupture and flow in solids. *Philosophical Transactions of the Royal Society of London. Series A, Containing Papers of a Mathematical or Physical Character* 221(582-593), 163. DOI: 10.1098/rsta.1921.0006.

Gross, D. and Seelig, T. (2011). Bruchmechanik: Mit einer Einführung in die Mikromechanik. 5th ed. Berlin Heidelberg: Springer-Verlag.

Hahn, H. and Williams, J. (1986). Compression failure mechanisms in unidirectional composites. In: *Composite Materials: Testing and Design (Seventh Conference)*, ed. by Whitney, J., Ed. West Conshohocken, PA: ASTM International, 115–139.

Hahn, H. T. and Tsai, S. W. (1980). Introduction to Composite Materials. Lancaster, PA: Technomic Publishing Company, Inc. ISBN: 9780877622888.

Halpin, J. C. (1969). Stiffness and Expansion Estimates for Oriented Short Fiber Composites. *Journal of Composite Materials* 3(4), 732–734. ISSN: 0021-9983. DOI: 10.1177/002199836900300419.

Halpin, J. C. and Pagano, N. J. (1969). The laminate approximation for randomly oriented fibrous composites. *Journal of Composite Materials* 3(4), 720–724. ISSN: 0021-9983. DOI: 10.1177/002199836900300416.

Hamada, H., Oya, N., Yamashita, K. and Maekawa, Z.-I. (1997). Tensile strength and its scatter of unidirectional carbon fibre reinforced composites. *Journal of Reinforced Plastics and Composites* 16(2), 119–130. DOI: 10.1177/073168449701600202.

Hardaker, K. M. and Richardson, M. O. W. (1980). Trends in hybrid composite technology. *Polymer-Plastics Technology and Engineering* 15(2), 169–182. ISSN: 0360-2559. DOI: 10.1080/03602558008070011.

Hashin, Z. and Shtrikman, S. (1962). A variational approach to the theory of the elastic behaviour of polycrystals. *Journal of the Mechanics and Physics of Solids* 10(4), 343–352. ISSN: 0022-5096. DOI: 10.1016/0022-5096(62)90005-4.

Hassan, A., Salleh, N. M., Yahya, R. and Sheikh, M. (2011). Fiber length, thermal, mechanical, and dynamic mechanical properties of injection-molded glass-fiber/polyamide 6,6: Plasticization effect. *Journal of Reinforced Plastics and Composites* 30(6), 488–498. DOI: 10.1177/0731684410397898.

Hayashi, T. (1972). On the improvement of mechanical properties of composites by hybrid composition. *Proc 8th Intl Reinforced Plastics Conference*, 149–152.

Henning, F., Drechsler, K. and Chatzigeorgiou, L. (2011). Faserverstärkte Kunststoffe. In: *Handbuch Leichtbau - Methoden, Werkstoffe, Fertigung*. Ed. by F. Henning and E. Moeller. München, Wien: Carl Hanser Verlag, 341–392.

Henry, J. and Pimenta, S. (2017a). Modelling hybrid effects on the stiffness of aligned discontinuous composites with hybrid fibre-types. *Composites Science and Technology* 152, 275–289. ISSN: 0266-3538. DOI: 10.1016/j.compscitech.2017.08.017.

Henry, J. and Pimenta, S. (2017b). Semi-analytical simulation of aligned discontinuous composites. *Composites Science and Technology* 144, 230–244. ISSN: 0266-3538. DOI: 10.1016/j.compscitech.2017.01.027.

Hild, F. and Roux, S. (2006). Digital Image Correlation: from Displacement Measurement to Identification of Elastic Properties – a Review. *Strain* 42(2), 69–80. ISSN: 1475-1305. DOI: 10.1111/j.1475-1305.2006.00258.x.

Hill, R. (1963). Elastic properties of reinforced solids: Some theoretical principles. *Journal of the Mechanics and Physics of Solids* 11(5), 357–372. ISSN: 0022-5096. DOI: 10.1016/0022-5096(63)90036-X.

Hill, R. (1965). A self-consistent mechanics of composite materials. *Journal of the Mechanics and Physics of Solids* 13(4), 213–222. ISSN: 0022-5096. DOI: 10.1016/0022-5096(65)90010-4.

Hillig, W. B. (1994). Effect of fibre misalignment on the fracture behaviour of fibre-reinforced composites. *Journal of Materials Science* 29(2), 419–423. ISSN: 1573-4803. DOI: 10.1007/BF01162501.

Hohberg, M., Kärger, L., Henning, F. and Hrymak, A. (2017). Rheological measurements and rheological shell model considering the compressible behavior of long fiber reinforced sheet molding compound (SMC). *Composites Part A: Applied Science and Manufacturing* 95, 110–117. ISSN: 1359-835X. DOI: 10.1016/j.compositesa.2017.01.006.

Hour, K. Y. and Sehitoglu, H. (1993). Damage development in a short fiber reinforced composite. *Journal of Composite Materials* 27(8), 782–805. ISSN: 0021-9983. DOI: 10.1177/002199839302700803.

Hull, D. and Clyne, T. W. (1996). An Introduction to Composite Materials. 2nd ed. Cambridge Solid State Science Series. Cambridge: Cambridge University Press. ISBN: 9780521381901. DOI: 10.1017/CBO9781139170130.

Ikbal, M. H., Azzam, A., Qingtao, W., Shuai, Z. and Wei, L. (2016). Hybrid composites made of unidirectional T600S carbon and E-glass fabrics under quasi-static loading. *Journal of Industrial Textiles* 46(7), 1511–1535. ISSN: 1528-0837. DOI: 10.1177/1528083715624259.

Jendli, Z., Fitoussi, J., Meraghni, F. and Baptiste, D. (2005). Anisotropic strain rate effects on the fibre–matrix interface decohesion in sheet moulding compound composites. *JNC13-AMAC-Strasbourg* 65(3), 387–393. ISSN: 0266-3538. DOI: 10.1016/j.compscitech.2004.09.027.

Jendli, Z., Meraghni, F., Fitoussi, J. and Baptiste, D. (2009). Multi-scales modelling of dynamic behaviour for discontinuous fibre SMC composites. *Mechanical Response of Fibre Reinforced Composites* 69(1), 97–103. ISSN: 0266-3538. DOI: 10.1016/j.compscitech.2007.10.047.

Johanson, K., Harper, L. T., Johnson, M. S. and Warrior, N. A. (2015). Heterogeneity of discontinuous carbon fibre composites: Damage initiation captured by Digital Image Correlation. *Composites Part A: Applied Science and Manufacturing* 68, 304–312. ISSN: 1359-835X. DOI: 10.1016/j.compositesa.2014.10.014.

Johns Manville (2018). Product description : MultiStar 272. URL: https://www.jm.com/content/dam/jm/global/en/engineered-products/EP-documents/Product_Data_Sheets/Fibers/Assembled_Rovings/Europe/MultiStar%20272.pdf (Accessed: 28 July 2018).

Jones, R. M. (1999). Mechanics of Composite Materials. 2nd ed. Boca Raton, FL: CRC Press - Taylor & Francis Group. ISBN: 9781315272986. DOI: 10.1201/9781498711067.

Ju, J. W. and Chen, T. M. (1994). Micromechanics and effective moduli of elastic composites containing randomly dispersed ellipsoidal inhomogeneities. *Acta Mechanica* 103(1), 103–121. ISSN: 1619-6937. DOI: 10.1007/BF01180221.

Kanatani, K. (1984). Distribution of directional data and fabric tensors. *International Journal of Engineering Science* 22(2), 149–164. ISSN: 0020-7225. DOI: 10.1016/0020-7225(84)90090-9.

Kanouté, P., Boso, D. P., Chaboche, J. L. and Schrefler, B. A. (2009). Multiscale Methods for Composites: A Review. *Archives of Computational Methods in Engineering* 16(1), 31–75. ISSN: 1886-1784. DOI: 10.1007/s11831-008-9028-8.

Karcher, M. (2016). Beitrag zur Umsetzung, Charakterisierung und Evaluierung eines Direktverfahrens zur Herstellung von strukturellen Bauteilkomponenten aus kohlenstofffaserverstärktem Kunststoff (InlinePrepreg). Dissertation. Karlsruhe: Karlsruhe Institute of Technology.

Karcher, M., Gerlitziki, M. and Thoma, B., Henning, F. (2015). Evaluation of a New Inlineprepreg Process Approach to Established Processes For the Manufacturing of Stuctural Components Out Of Carbon Fibre Reinforced Plastics. Novi, MI.

Kau, H. T. (1990). A study of the impact behavior of chopped fiber reinforced composite. *Polymer Composites* 11(5), 253–264. ISSN: 1548-0569. DOI: 10.1002/pc.750110502.

Kaw, A. K. (2005). Mechanics of Composite Materials. 2nd ed. Boca Raton, FL: CRC Press Taylor & Francis Group. ISBN: 9781420058291.

Kehrer, L., Wicht, D., Wood, J. T. and Böhlke, T. (2018). Dynamic mechanical analysis of pure and fiber–reinforced thermoset– and thermoplastic–based polymers and free volume–based viscoelastic modeling. *GAMM–Mitteilungen* 41(1). ISSN: 0936-7195. DOI: 10.1002/gamm.201800007.

Kelly, A. and Davies, G. J. (1965). The principles of the fibre reinforcement of metals. *Metallurgical Reviews* 10(1), 1–77. ISSN: 0076-6690. DOI: 10.1179/mtlr.1965.10.1.1.

Khetan, R. P. and Chang, D. C. (1983). Surface damage of sheet molding compound panels subject to a point impact loading. *Journal of Composite Materials* 17(2), 182–194. ISSN: 0021-9983. DOI: 10.1177/002199838301700206.

Kia, H. G. (1993). Sheet Molding Compounds: Science and Technology. München: Carl Hanser Verlag. ISBN: 9781569901540.

Kim, J., Shiau, Y. C., Lee, L. J. and Im, Y. T. (1992). Compression molding simulation of chopped fiber reinforced polymeric composites in plate–rib type geometry. *Polymer Composites* 13(2), 97–107. ISSN: 02728397. DOI: 10.1002/pc.750130205.

Kim, K. T. and Im, Y. T. (1996). Experimental study on physical properties of compression molded SMC parts under plane strain condition. *Composite Structures* 35(2), 131–141. ISSN: 0263-8223. DOI: 10.1016/0263-8223(95)00158-1.

Knakal, C. and Ireland, D. (1986). Instrumented Dart Impact Evaluation of Some Automotive Plastics and Composites. In: *Instrumented impact testing of plastics and composite materials*, ed. by S. Kessler. West Conshohocken, PA: ASTM International, 44–57.

Krajcinovic, D. (1998). Selection of damage parameter – Art or science?. *Mechanics of Materials* 28(1), 165–179. ISSN: 0167-6636. DOI: 10.1016/S0167-6636(97)00057-4.

Krajcinovic, D. and Mastilovic, S. (1995). Some fundamental issues of damage mechanics. *Mechanics of Materials* 21(3), 217–230. ISSN: 0167-6636. DOI: 10.1016/0167-6636(95)00010-0.

Kretsis, G. (1987). A review of the tensile, compressive, flexural and shear properties of hybrid fibre-reinforced plastics. *Composites* 18(1), 13–23. ISSN: 0010-4361. DOI: 10.1016/0010-4361(87)90003-6.

Lamanna, G. and Ceprano, A. (2014). Mechanical characterization of sheet moulding composites for the automotive industry. *The Open Materials Science Journal* 8(1), 108–113. ISSN: 1874-088X. DOI: 10.2174/1874088X01408010108.

Larbi, A. B. C., Sidhom, H., Sai, K. and Baptiste, D. (2006). Constitutive model of micromechanical damage to predict reduction in stiffness of a fatigued SMC composite. *Journal of Materials Engineering and Performance* 15(5), 575–580. ISSN: 1544-1024. DOI: 10.1361/105994906X124569.

Lauke, B., Schultrich, B. and Pompe, W. (1990). Theoretical considerations to toughness of short-fibre reinforced thermoplastics. *Polymer-Plastics Technology and Engineering* 29(7-8), 607–806. ISSN: 0360-2559. DOI: 10.1080/03602559008050638.

Laurin, F., Charrier, J.-S., Lévêque, D., Maire, J.-F., Mavel, A. and Nuñez, P. (2012). Determination of the properties of composite materials thanks to digital image correlation measurements. *Procedia IUTAM* 4, 106–115. ISSN: 22109838. DOI: 10.1016/j.piutam.2012.05.012.

Lavengood, R. E. and Goettler, L. A. (1971). Stiffness of Non-Aligned Fiber Reinforced Composites. Defense Technical Information Center - Monsato Reserach Corp St. Louis, MO.

Le, T.-H., Dumont, P., Orgéas, L., Favier, D., Salvo, L. and Boller, E. (2008). X-ray phase contrast microtomography for the analysis of the fibrous microstructure of SMC composites. *Composites Part A: Applied Science and Manufacturing* 39(1), 91–103. ISSN: 1359-835X. DOI: 10.1016/j.compositesa.2007.08.027.

Lee, C. C. and Tucker, C. L. (1987). Flow and heat transfer in compression mold filling. *Journal of Non-Newtonian Fluid Mechanics* 24(3), 245–264. ISSN: 0377-0257. DOI: 10.1016/0377-0257(87)80040-X.

Lee, L. J., Marker, L. F. and Griffith, R. M. (1981). The rheology and mold flow of polyester sheet molding compound. *Polymer Composites* 2(4), 209–218. ISSN: 1548-0569. DOI: 10.1002/pc.750020412.

Lee, S. M. (1995). Dictionary of composite materials technology. CRC Press, Taylor and Francis Group, Boca Raton, FL. ISBN: 0877626006.

Lee, S. M., Cheon, J. S. and Im, Y. T. (1999). Experimental and numerical study of the impact behavior of SMC plates. *Tenth International Conference on Composite Structures* 47(1–4), 551–561. ISSN: 0263-8223. DOI: 10.1016/S0263-8223(00)00021-0.

Lei, H. F., Zhang, Z. Q. and Liu, B. (2012). Effect of fiber arrangement on mechanical properties of short fiber reinforced composites. *Composites Science and Technology* 72(4), 506–514. ISSN: 0266-3538. DOI: 10.1016/j.compscitech.2011.12.011.

Lengsfeld, H., Wolff-Fabris, F., Krämer, J., Lacalle, J. and Altstädt, V. (2014). Faserverbundwerkstoffe: Prepregs und ihre Verarbeitung. München: Carl Hanser Verlag GmbH & Co. KG. ISBN: 978-3-446-43300-7. DOI: 10.3139/9783446440807.

Li, C., Hu, N., Cheng, J., Fukunaga, H. and Sekine, H. (2002). Low-velocity impact-induced damage of continuous fiber-reinforced composite laminates. Part II. Verification and numerical investigation. *Composites Part A: Applied Science and Manufacturing* 33(8), 1063–1072. ISSN: 1359-835X. DOI: 10.1016/S1359-835X(02)00078-7.

Lin, C. and Weng, C. (1999). Simulation of compression molding for sheet molding compound considering the anisotropic effect. *Polymer Composites* 20(1), 98–113. ISSN: 1548-0569. DOI: 10.1002/pc.10338.

Malanti, P. (2015). Prepreg compression molding makes its commercial debut. URL: https://www.compositesworld.com/articles/prepreg-compression-molding-makes-its-commercial-debut (Accessed: 24 Apr. 2018).

Malik, M., Choudhary, V. and VARMA, I. K. (2000). Current Status of Unsaturated Polyester Resins. *Journal of Macromolecular Science, Part C* 40(2-3), 139–165. ISSN: 1532-1797. DOI: 10.1081/MC-100100582.

Mallick, P. (1986). Effect of fiber misorientation on the tensile strength of compression molded continuous fiber composites. *Polymer Composites* 7, 14–18. ISSN: 1548-0569. DOI: 10.1002/pc.750070104.

Mallick, P. K. (2007). Fiber Reinforced Composites: Materials, Manufacturing and Design. 3rd ed. Boca Raton, FL: CRC Press - Taylor & Francis Group. ISBN: 9780849342059.

Mallick, P. K. and Raghupathi, N. (1979). Effect of cure cycle on mechanical properties of thick section fiber–reinforced poly/thermoset moldings. *Polymer Engineering & Science* 19(11), 774–778. ISSN: 1548-2634. DOI: 10.1002/pen.760191103.

Manders, P. W. and Bader, M. G. (1981). The strength of hybrid glass/carbon fibre composites. *Journal of Materials Science* 16(8), 2233–2245. ISSN: 1573-4803. DOI: 10.1007/BF00542386.

Mansor, M. R., Sapuan, S. M., Zainudin, E. S., Nuraini, A. A. and Hambali, A. (2013). Stiffness prediction of hybrid kenaf/glass fiber reinforced polypropylene composites using rule of mixtures (ROM) and rule of hybrid mixtures (RoHM). *Journal of Polymer Materials* 30(3), 321–334.

Marissen, R. and Linsen, J. (1999). Variability of the flexural strength of sheet moulding compounds. *Composites Science and Technology* 59(14), 2093–2100. ISSN: 0266-3538. DOI: 10.1016/S0266-3538(99)00068-8.

Marom, G. (1989). Environmental effects on fracture mechanical properties of polymer composites. In: *Application of Fracture Mechanics to Composite Materials*. Ed. by K. Friedrich, 397–424. DOI: 10.1016/B978-0-444-87286-9.50014-0.

Marom, G., Fischer, S., Tuler, F. R. and Wagner, H. D. (1978). Hybrid effects in composites: Conditions for positive or negative effects versus rule-of-mixtures behaviour. *Journal of Materials Science* 13(7), 1419–1426. ISSN: 1573-4803. DOI: 10.1007/BF00553194.

McConnell, V. P. (2007). SMC has plenty of road to run in automotive applications. *Reinforced Plastics* 51(1), 20–25. ISSN: 0034-3617. DOI: 10.1016/S0034-3617(07)70027-9.

McConnell, V. P. (2008). New recipes for SMC innovation. *Reinforced Plastics* 52(8), 34–39. ISSN: 0034-3617. DOI: 10.1016/S0034-3617(08)70309-6.

Mei, T. and Piggott, M. R. (2004). Mesostructure development during molding of sheet molding compounds. *Polymer Composites* 17(4), 548–555. ISSN: 02728397. DOI: 10.1002/pc.10645.

Meraghni, F. and Benzeggagh, M. L. (1995). Micromechanical modelling of matrix degradation in randomly oriented discontinuous-fibre composites. *Composites Science and Technology* 55(2), 171–186. ISSN: 0266-3538. DOI: 10.1016/0266-3538(95)00096-8.

Meraghni, F., Blakeman, C. J. and Benzeggagh, M. L. (1996). Effect of interfacial decohesion on stiffness reduction in a random discontinuous-fibre composite containing matrix microcracks. *Composites Science and Technology* 56(5), 541–555. ISSN: 0266-3538. DOI: 10.1016/0266-3538(96)00039-5.

Mészáros, L. (2018). Editorial corner – a personal view Polymer matrix hybrid composites: The efficient way of improved performance. *eXPRESS Polymer Letters* 8(11), 790. DOI: 10.3144/expresspolymlett.2014.81.

Mildred, R. J., Sourour, J. A. and Schultz, J. M. (2004). Fatigue behavior of thermosetting–polyester–matrix sheet–molding compounds. *Polymer Composites* 3(1), 18–28. ISSN: 02728397. DOI: 10.1002/pc.750030105.

Mittelstedt, C. and Becker, W. (2017). Strukturmechanik ebener Laminate: Kapitel 7 - Klassische Laminattheorie. 1st ed. Technische Universität Darmstadt FB Mechanik, Bibliothek. ISBN: 978-3-935868-99-0.

Mori, T. and Tanaka, K. (1973). Average stress in matrix and average elastic energy of materials with misfitting inclusions. *Acta Metallurgica* 21(5), 571–574. ISSN: 0001-6160. DOI: 10.1016/0001-6160(73)90064-3.

Motaghi, A. and Hrymak, A. N. (2017). Microstructure characterization in direct sheet molding compound. *Polymer Composites*. ISSN: 02728397. DOI: 10.1002/pc.24495.

Mrkonjic, M., Rayling, U., Weidenmann, K. A., Kärger, L. and Henning, F. (2015). "Phenomenological characterization and macromechnical modeling of anisotropic, non-linear behavior of sheet molding compounds (SMC)". In: *12th International Conference on the Mechanical Behavior of Materials*. Karlsruhe.

Mrse, A. M. and Piggott, M. R. (1993). Compressive properties of unidirectional carbon fibre laminates: II. The effects of unintentional and intentional fibre misalignments. *Composites Science and Technology* 46(3), 219–227. ISSN: 0266-3538. DOI: 10.1016/0266-3538(93)90156-B.

Naik, N. K. and Kumar, R. S. (1999). Compressive strength of unidirectional composites: Evaluation and comparison of prediction models. *Composite Structures* 46(3), 299–308. ISSN: 0263-8223. DOI: 10.1016/S0263-8223(99)00098-7.

Neitzel, M., Mitschang, P. and Breuer, U. (2014). Handbuch Verbundwerkstoffe: Werkstoffe, Verarbeitung, Anwendung. 2., aktual. und erw. Aufl. München: Carl Hanser Verlag. ISBN: 978-3-446-43697-8.

Nestler, D. (2012). Beitrag zum Thema VERBUNDWERKSTOFFE - WERKSTOFFVERBUNDE: Status quo und Forschungsansätze. Habilitation. Chemnitz: TU Chemnitz. URL: http://nbn-resolving.de/urn:nbn:de:bsz:ch1-qucosa-134459 (Accessed: 14 July 2018).

Newman, S. and Fesko, D. G. (1984). Recent developments in sheet molding compound technology. *Polymer Composites* 5(1), 88–96. ISSN: 02728397. DOI: 10.1002/pc.750050114.

O'Brien, T. K., Chawan, A. D., Demarco, K. and Paris, I. (2001). Influence of specimen preparation and specimen size on composite transverse tensile strength and scatter. *NASA Langley Technical Report Server*.

Odenberger, P. T., Andersson, H. M. and Lundström, T. S. (2004). Experimental flow-front visualisation in compression moulding of SMC. *Composites Part A: Applied Science and Manufacturing* 35(10), 1125–1134. ISSN: 1359-835X. DOI: 10.1016/j.compositesa.2004.03.019.

Okoli, O. I. (2001). The effects of strain rate and failure modes on the failure energy of fibre reinforced composites. *Third International Conference on Composite Science and Technology* 54(2–3), 299–303. ISSN: 0263-8223. DOI: 10.1016/S0263-8223(01)00101-5.

Oldenbo, M. (2004). Anisotropy and non-linear effects in SMC composites: From material data to FE-simulation of structures. PhD thesis. Luleå University of Technology.

Oldenbo, M., Fernberg, S. P. and Berglund, L. A. (2003). Mechanical behaviour of SMC composites with toughening and low density additives. *Composites Part A: Applied Science and Manufacturing* 34(9), 875–885. ISSN: 1359-835X. DOI: 10.1016/S1359-835X(03)00155-6.

Oldenbo, M., Mattsson, D., Varna, J. and Berglund, L. A. (2004). Global stiffness of a SMC panel considering process induced fiber orientation. *Journal of Reinforced Plastics and Composites* 23(1), 37–49. DOI: 10.1177/0731684404028700.

Orgéas, L., Dumont, P. J. J. and Nicolais, L. (2011). Sheet molding compounds. In: *Wiley Encyclopedia of Composites*. Ed. by L. Nicolais and A. Borzacchiello. Hoboken, NJ, USA: John Wiley & Sons, Inc. ISBN: 9781118097298. DOI: 10.1002/9781118097298.weoc222.

Osswald, T. A. and Menges, G. (2012). Material science of polymers for engineers. In: *Materials Science of Polymers for Engineers*. Carl Hanser Verlag GmbH & Co. KG, I–XIX. ISBN: 978-1-56990-514-2. DOI: 10.3139/9781569905241.fm.

Palmer, J., Savage, L., Ghita, O. R. and Evans, K. E. (2010). Sheet moulding compound (SMC) from carbon fibre recyclate. *Composites Part A: Applied Science and Manufacturing* 41(9), 1232–1237. ISSN: 1359-835X. DOI: 10.1016/j.compositesa.2010.05.005.

Pandya, K. S., Veerraju, C. and Naik, N. K. (2011). Hybrid composites made of carbon and glass woven fabrics under quasi-static loading. *Materials & Design* 32(7), 4094–4099. ISSN: 02613069. DOI: 10.1016/j.matdes.2011.03.003.

Phillips, L. N. (1976). The hybrid effect — does it exist?. *Composites* 7(1), 7–8. ISSN: 0010-4361. DOI: 10.1016/0010-4361(76)90273-1.

Piggott, M. R. (1980). Load Bearing Fibre Composites. 1st ed. Pergamon Press. ISBN: 9780080242309.

Piggott, M. R. and Harris, B. (1981). Compression strength of hybrid fibre-reinforced plastics. *Journal of Materials Science* 16(3), 687–693. ISSN: 1573-4803. DOI: 10.1007/BF02402786.

Reddy, J. N. (2003). Mechanics of laminated composite plates and shells: Theory and analysis. 2nd ed. CRC Press. ISBN: 9780849315923.

Reuss, A. (1929). Berechnung der Fließgrenze von Mischkristallen auf Grund der Plastizitätsbedingung für Einkristalle. *Journal of Applied Mathematics and Mechanics* 9(1), 49–58. DOI: 10.1002/zamm.19290090104.

Riegner, D. A. and Sanders, B. A. (1979). A characterization study of automotive continuous and random glass fiber composites: Society of Plastics Engineers. *Proceedings of the National Technical Conference*.

Roche, J. L. and Kakarala, S. N. (1986). Methodology for selecting impact tests of composite materials in automotive applications. In: *Instrumented impact testing of plastics and composite materials*, ed. by S. Kessler. West Conshohocken, PA: ASTM International, 24–43.

Rosen, B. W. (1965). Mechanics of composite strengthening: Fibre composite materials. *American Society of Metals, Chapter 3*.

Rösler, J., Harders, H. and Bäker, M. (2012). Mechanisches Verhalten der Werkstoffe. 4th ed. Springer Fachmedien Wiesbaden: Springer Vieweg. ISBN: 978-3-8348-2241-3. DOI: 10.1007/978-3-8348-2241-3.

Rösner, A. (2015). Beschreibung des viskoelastischen und viskoplastischen Deformationsverhaltens von kontinuierlich faserverstärktem Polyamid-6. Doctoral Dissertation. Karlsruhe: Karlsruhe Institute of Technology.

Roux, S., Réthoré, J. and Hild, F. (2008). Recent progress in digital image correlation: From measurement to mechanical identification. *Journal of Physics: Conference Series* 135, 12002. ISSN: 1742-6596. DOI: 10.1088/1742-6596/135/1/012002.

Sadasivam, B. and Mallick, P. K. (2002). Impact damage resistance of random fiber reinforced automotive composites. *Journal of Thermoplastic Composite Materials* 15(3), 181–191. DOI: 10.1177/0892705702015003438.

SAE J211-1 (1995). Instrumentation for Impact Test - Part 1 - Electronic Instrumentation. SEA International -The Engineering Society for Advancing Mobility Land Sea Air and Space.

Saint-Venant, B. (1855). Memoire sur la torsion des prismes: avec des considérations sur leur fléxion ainsi que sur l'équilibre intérieur des solides élastiques en général, et des formules pratiques pour le calcul de leur résistance à divers efforts s'exerçant simultanément. *Mémoires présentés par divers savants à l'Académie des Sciences de l'Institut Impérial de France* 14, 233–560.

Sathishkumar, T. P., Naveen, J. and Satheeshkumar, S. (2014). Hybrid fiber reinforced polymer composites – a review. *Journal of Reinforced Plastics and Composites* 33(5), 454–471. DOI: 10.1177/0731684413516393.

Sause, M., Gribov, A., Unwin, A. R. and Horn, S. (2012). Pattern recognition approach to identify natural clusters of acoustic emission signals. *Pattern Recognition Letters* 33(1), 17–23. ISSN: 0167-8655. DOI: 10.1016/j.patrec.2011.09.018.

Schoßig, M. (2011). Schädigungsmechanismen in faserverstärkten Kunststoffen: Quasistatische und dynamische Untersuchungen. 1st ed. Fachmedien Wiesbaden GmbH, Wiesbaden: Vieweg+Teubner Verlag, Springer. ISBN: 978-3-8348-1483-8. DOI: 10.1007/978-3-8348-9924-8.

Schürmann, H. (2007). Konstruieren mit Faser-Kunststoff-Verbunden. 2nd ed. Springer-Verlag Berlin Heidelberg 2007. ISBN: 978-3-540-72189-5. DOI: 10.1007/978-3-540-72190-1.

Selezneva, M. and Lessard, L. (2015). Characterization of mechanical properties of randomly oriented strand thermoplastic composites. *Journal of Composite Materials* 50(20), 2833–2851. ISSN: 0021-9983. DOI: 10.1177/0021998315613129.

Selmy, A. I. (2018). Mechanical properties of inter-ply hybrid composites reinforced with glass and polyamide fibers. *Journal of Thermoplastic Composite Materials*, 0892705717751022. DOI: 10.1177/0892705717751022.

Selmy, A. I., Elsesi, A. R., Azab, N. A. and Abd El-baky, M. A. (2011). Monotonic properties of unidirectional glass fiber (U)/random glass fiber (R)/epoxy hybrid composites. *Materials & Design* 32(2), 743–749. ISSN: 02613069. DOI: 10.1016/j.matdes.2010.07.031.

Selmy, A. I., Elsesi, A. R., Azab, N. A. and Abd El-baky, M. A. (2012). In-plane shear properties of unidirectional glass fiber (U)/random glass fiber (R)/epoxy hybrid and non-hybrid composites. *Composites Part B: Engineering* 43(2), 431–438. ISSN: 13598368. DOI: 10.1016/j.compositesb.2011.06.001.

Serna Moreno, M. C., Romero Gutiérrez, A. and Martínez Vicente, J. L. (2016). Different response under tension and compression of unidirectional carbon fibre laminates in a three-point bending test. *Composite Structures* 136(Supplement C), 706–711. ISSN: 0263-8223. DOI: 10.1016/j.compstruct.2015.06.017.

SGL Group (2011). Composite Materials: Carbon Fiber Fabrics and Prepregs for the Marine Industry.
URL: http://www.rimast.com/pdf/SGL_Group_Marine_e.pdf
(Accessed: 19 June 2018).

Shirinbayan, M., Fitoussi, J., Abbasnezhad, N., Meraghni, F., Surowiec, B. and Tcharkhtchi, A. (2017). Mechanical characterization of a Low Density Sheet Molding Compound (LD-SMC): Multi-scale damage analysis and strain rate effect. *Composites Part B: Engineering* 131, 8–20. ISSN: 13598368. DOI: 10.1016/j.compositesb.2017.08.004.

Shirinbayan, M., Fitoussi, J., Meraghni, F., Surowiec, B., Bocquet, M. and Tcharkhtchi, A. (2015). High strain rate visco-damageable behavior of Advanced Sheet Molding Compound (A-SMC) under tension. *Composites Part B: Engineering* 82, 30–41. ISSN: 13598368. DOI: 10.1016/j.compositesb.2015.07.010.

Shirrell, C. D. (1983). Variability in static strengths of sheet molding compounds (SMC). *Polymer Composites* 4(3), 172–179. ISSN: 02728397. DOI: 10.1002/pc.750040307.

Shirrell, C. D. (1985). The influence of microstructural variability upon the scatter in mechanical properties of R25 sheet molding compound. In: *High modulus fiber composites in ground transportation and high volume applications*. Ed. by D. W. Wilson. ASTM International- STP873-EB. West Conshohocken, PA, 3–22.

Shirrell, C. D. and Onachuk, M. (1986). Influence of mold coverage upon the notch strength of R25 sheet molding compounds. In: *Composite Materials: Fatigue and Fracture*. Ed. by T. H. Hahn. ASTM International-STP 907. West Conshohocken, PA, 32–50.

Song, Y., Gandhi, U., Pérez, C., Osswald, T., Vallury, S. and Yang, A. (2017). Method to account for the fiber orientation of the initial charge on the fiber orientation of finished part in compression molding simulation. *Composites Part A: Applied Science and Manufacturing* 100(Supplement C), 244–254. ISSN: 1359-835X. DOI: 10.1016/j.compositesa.2017.05.021.

Soni, S. R. and Pagano, N. J. (1983). Elastic response of composites laminates. In: *Mechanics of Composite Materials*. Ed. by Z. Hashin and C. T. Herakovich. Pergamon, 227–242.
ISBN: 978-0-08-029384-4.
DOI: 10.1016/B978-0-08-029384-4.50022-5.

Soutis, C. (1997). Compressive Strength of Unidirectional Composites: Measurement and Prediction. In: *Compressive Strength of Unidirectional Composites: Measurement and Prediction*.

Sridharan, N. S. (1982). Elastic and strength properties of continuous/chopped glass fiber hybrid sheet molding compounds. In: *Short Fiber Reinforced Composite Materials*. Ed. by B. A. Sanders. American Society for Testing and Materials: ASTM International STP 772, 167–182.

Stachel, P. (2012). Serienfertigung mit Verbundwerkstoffen - AVK e.V. - Pressemitteilung.
URL: `http://www.pressebox.de/inaktiv/avk-ev/Serienfertigung-mit-Verbundwerkstoffen/boxid/535921` (Accessed: 03 Aug. 2018).

Summerscales, J. and Short, D. (1978). Carbon fibre and glass fibre hybrid reinforced plastics. *Composites* 9(3), 157–166.
ISSN: 0010-4361. DOI: 10.1016/0010-4361(78)90341-5.

Sutherland, L. S., Shenoi, R. A. and Lewis, S. M. (1999). Size and scale effects in composites: I. Literature review. *Composites Science and Technology* 59(2), 209–220. ISSN: 0266-3538.

Sutherland, L. S. and Soares, C. G. (2005). Contact indentation of marine composites. *Composite Structures* 70(3), 287–294. ISSN: 0263-8223. DOI: 10.1016/j.compstruct.2004.08.035.

Swolfs, Y., Gorbatikh, L. and Verpoest, I. (2014). Fibre hybridisation in polymer composites: A review. *Composites Part A: Applied Science and Manufacturing* 67(Supplement C), 181–200. ISSN: 1359-835X. DOI: 10.1016/j.compositesa.2014.08.027.

Taggart, D. G., Pipes, R. B., Blake, R. A., Gillespie JR., J. W., Prabhakaran, R. and Whitney, J. (1979). Properties of SMC Composites. University of Delaware: Center for Composite Materials.

The European Alliance for SMC/BMC (2013). Life cycle assessment (LCA): SMC/BMC Light composite materials at their best. URL: `https://smcbmc-europe.org/publications.php` (Accessed: 03 Aug. 2018).

The European Alliance for SMC/BMC (2016). Design for success: A design & technology manual for SMC/BMC. URL: `https://smcbmc-europe.org/publications.php` (Accessed: 03 Aug. 2018).

Thomason, J. L. and Vlug, M. A. (1996). Influence of fibre length and concentration on the properties of glass fibre-reinforced polypropylene: 1. Tensile and flexural modulus. *Composites Part A: Applied Science and Manufacturing* 27(6), 477–484. ISSN: 1359-835X. DOI: 10.1016/1359-835X(95)00065-A.

Thomason, J. L. and Vlug, M. A. (1997). Influence of fibre length and concentration on the properties of glass fibre-reinforced polypropylene: 4. Impact properties. *Composites Part A: Applied Science and Manufacturing* 28(3), 277–288. ISSN: 1359-835X. DOI: 10.1016/S1359-835X(96)00127-3.

Thomason, J. L., Vlug, M. A., Schipper, G. and Krikor, H. (1996). Influence of fibre length and concentration on the properties of glass fibre-reinforced polypropylene: Part 3. Strength and strain at failure. *Composites Part A: Applied Science and Manufacturing* 27(11), 1075–1084. ISSN: 1359-835X. DOI: 10.1016/1359-835X(96)00066-8.

Trauth, A., Bondy, M., Weidenmann, K. A. and Altenhof, W. (2018). Mechanical properties and damage evolution of a structural sheet molding compound based on a novel two step curing resin system. *Materials & Design* 143, 224–237. ISSN: 02613069. DOI: 10.1016/j.matdes.2018.02.002.

Trauth, A., Bücheler, D. and Weidenmann, K. A. (2016). Mechanical properties of unidirectional continuous carbon fiber reinforced SMC. In: *Proceeding of the 17th European Conference on Composite Materials; Munich; Germany;* Aachen: European Society for Composite Materials (ESCM).

Trauth, A., Pinter, P. and Weidenmann, K. A. (2017a). Investigation of quasi-static and dynamic material properties of a structural sheet molding compound combined with acoustic emission damage analysis. *Journal of Composites Science* 1(2). DOI: 10.3390/jcs1020018.

Trauth, A. and Weidenmann, K. A. (2016). Mechanical properties of continuously-discontinuously hybrid sheet molding compounds. In: *Proceedings of the 2nd Internationale Konferenz Euro Hybrid Materials and Structures*. Kaiserslautern.

Trauth, A., Pinter, P. and Weidenmann, K. A. (2017b). Acoustic Emission Analysis during Bending Tests of Continuous and Discontinuous Fiber Reinforced Polymers to Be Used in Hybrid Sheet Molding Compounds. *Key Engineering Materials* 742, 644–651. ISSN: 1662-9795. DOI: 10.4028/www.scientific.net/KEM.742.644.

Trauth, A. and Weidenmann, K. A. (2018). Continuous-discontinuous sheet moulding compounds – Effect of hybridisation on mechanical material properties. *Composite Structures* 202, 1087–1098. ISSN: 0263-8223. DOI: 10.1016/j.compstruct.2018.05.048.

Tucker, C. L. and Liang, E. (1999). Stiffness predictions for unidirectional short-fiber composites. *Composites Science and Technology* 59(5), 655–671. ISSN: 0266-3538. DOI: 10.1016/S0266-3538(98)00120-1.

Varna, J., Berglund, L. A. and Ericson, M. L. (1992). Specimen size effects on modulus of GMT and other inhomogeneous composites. *Jnl of Thermoplastic Composite Materials* 5(2), 105–114. ISSN: 0892-7057. DOI: 10.1177/089270579200500202.

Voigt, W. (1887). Über die Beziehung zwischen den beiden Elastizitätskonstantenisotroper Körper. *Annalen der Physik* 38, 573–587. DOI: 10.1002/andp.18892741206.

Walpole, L. J. (1969). On the overall elastic moduli of composite materials. *Journal of the Mechanics and Physics of Solids* 17(4), 235–251. ISSN: 0022-5096. DOI: 10.1016/0022-5096(69)90014-3.

Walrath, D. E., Adams, D. F., Riegner, D. A. and Sanders, B. A. (1982). Mechanical behavior of three sheet molding compounds. In: *Short Fiber Reinforced Composite Materials*. Ed. by B. A. Sanders. American Society for Testing and Materials: ASTM International STP 772, 113–132.

Wang, R. M., Zheng, S. R. and Zheng, Y. G. (2011). Polymer Matrix Composites and Technology. 1st ed. Sawston, Cambridge: Woodhead Publishing. ISBN: 9780857092229.

Wang, S. S. and Chim, E.-M. (1983). Fatigue damage and degradation in random short-fiber SMC composite. *Journal of Composite Materials* 17(2), 114–134. ISSN: 0021-9983. DOI: 10.1177/002199838301700203.

Wang, S. S., Chim, E.-M. and Zahlan, N. M. (1983). Fatigue crack propagation in random short-diber SMC composite. *Journal of Composite Materials* 17(3), 250–266. ISSN: 0021-9983. DOI: 10.1177/002199838301700306.

Watanabe, T. and Yasuda, M. (1982). Fracture behaviour of sheet moulding compounds. Part 1. Under tensile load. *Composites* 13(1), 54–58. ISSN: 0010-4361. DOI: 10.1016/0010-4361(82)90171-9.

Wisnom, M. R. (1990). The effect of fibre misalignment on the compressive strength of unidirectional carbon fibre/epoxy. *Composites* 21(5), 403–407. ISSN: 0010-4361. DOI: 10.1016/0010-4361(90)90438-3.

Wisnom, M. R. (1991). The effect of specimen size on the bending strength of unidirectional carbon fibre-epoxy. *Composite Structures* 18(1), 47–63. ISSN: 0263-8223. DOI: 10.1016/0263-8223(91)90013-O.

Wisnom, M. R. (1999). Size effects in the testing of fibre-composite materials. *Composites Science and Technology* 59(13), 1937–1957. ISSN: 0266-3538. DOI: 10.1016/S0266-3538(99)00053-6.

Witten, E., Kraus, T. and Kühnle, M. (2016). Composites Market Report - Market developments, trends, outlook and challenges.

Wulfsberg, J., Herrmann, A., Ziegmann, G., Lonsdorfer, G., Stöß, N. and Fette, M. (2014). Combination of carbon fibre sheet moulding compound and prepreg compression moulding in aerospace industry. *Procedia Engineering* 81, 1601–1607. ISSN: 18777058. DOI: 10.1016/j.proeng.2014.10.197.

Yahaya, R., Sapuan, S. M., Jawaid, M., Leman, Z. and Zainudin, E. S. (2014). Quasi-static penetration and ballistic properties of kenaf–aramid hybrid composites. *Materials & Design* 63, 775–782. ISSN: 02613069. DOI: 10.1016/j.matdes.2014.07.010.

Yu, H. N., Longana, M. L., Jalalvand, M. Wisnom, M. R. and Potter, K. D. (2015). Pseudo-ductility in intermingled carbon/glass hybrid composites with highly aligned discontinuous fibres. *Composites Part A: Applied Science and Manufacturing* 73, 35–44. ISSN: 1359-835X. DOI: 10.1016/j.compositesa.2015.02.014.

Yu, H. N., Longana, M. L., Jalalvand, M. Wisnom, M. R. and Potter, K. D. (2018). Hierarchical pseudo-ductile hybrid composites combining continuous and highly aligned discontinuous fibres. *Composites Part A: Applied Science and Manufacturing* 105, 40–56. ISSN: 1359-835X. DOI: 10.1016/j.compositesa.2017.11.005.

Zaoui, A. (2002). Continuum Micromechanics : Survey. *Journal of Engineering Mechanics* 128(8), 808–816. DOI: 10.1061/(ASCE)0733-9399(2002)128:8(808).

Zhang, J., Chaisombat, K., He, S. and Wang, C. H. (2012). Hybrid composite laminates reinforced with glass/carbon woven fabrics for lightweight load bearing structures. *Materials & Design* 36, 75–80. ISSN: 02613069. DOI: 10.1016/j.matdes.2011.11.006.

Zhou, Y., Wang, Y., Xia, Y. and Jeelani, S. (2010). Tensile behavior of carbon fiber bundles at different strain rates. *Materials Letters* 64(3), 246–248. ISSN: 0167-577X. DOI: 10.1016/j.matlet.2009.10.045.

Zoltek (2015). Certificate of Analysis: Cert.No:4093.

Zoltek (2018a). Technical Datasheet: PANEX35 Commercial Carbon Fiber. URL: `http://zoltek.com/products/px35/` (Accessed: 30 July 2018).

Zoltek (2018b). Technical Datasheet: PANEX35 PrepregTapes. URL: `http://zoltek.com/products/px35/` (Accessed: 30 July 2018).

Zoltek (2018c). Technical Datasheet: PANEX35, Stitch-bonded uni-directional carbon fabric.
URL: http://zoltek.com/wp-content/uploads/2018/06/TDS_PX35_Uni-Directional_Fabric.pdf (Accessed: 06 Aug. 2018).

Zoltek (2018d). Technical Datasheet: PX35 Uni-Directional Fabrics.
URL: http://zoltek.com/products/px35/uni-directional-fabric/ (Accessed: 22 July 2018).

Zweben, C. (1977). Tensile strength of hybrid composites. *Journal of Materials Science* 12(7), 1325–1337. ISSN: 1573-4803.
DOI: 10.1007/BF00540846.

Zweben, C., Smith, W. and Wardle, M. (1978). Test methods for fiber tensile strength, composite flexural modulus, and properties of fabric-reinforced laminates. In: *Composite Materials: Testing and Design: STP 674*. Ed. by S. W. Tsai, 228–262.
DOI: 10.1520/STP36912S.

A Appendix

A.1 Influence of subset size and step size

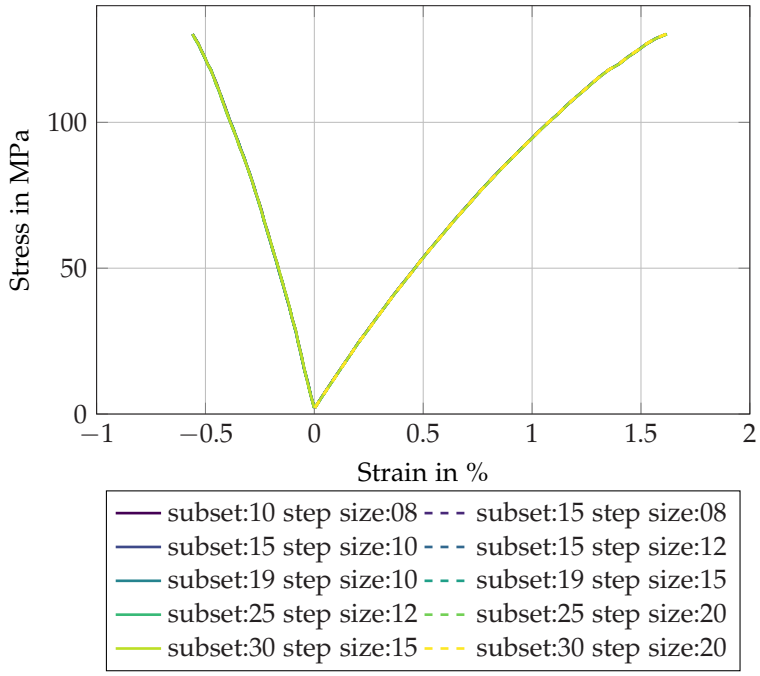


Figure A.1: Influence of subset size and step size on evaluated strains and tensile modulus of elasticity and failure strain (1/2).

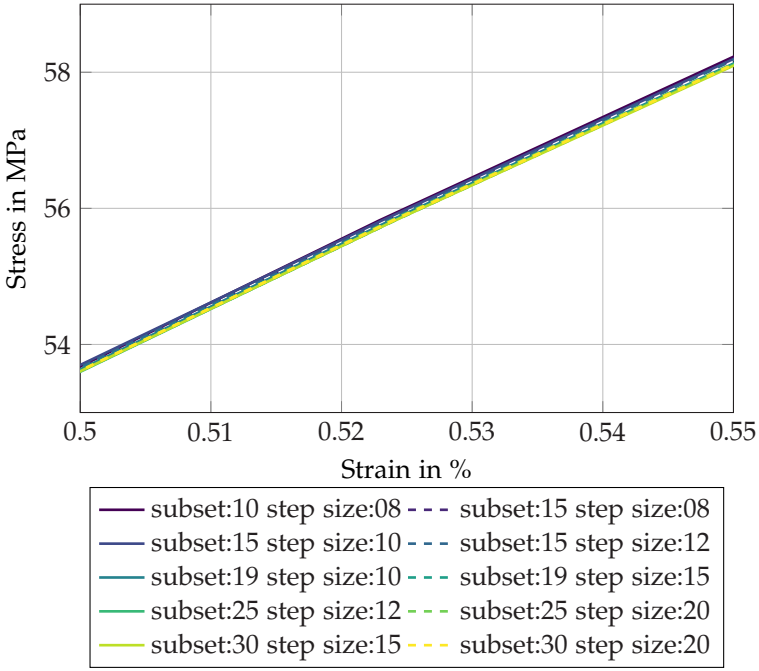


Figure A.2: Influence of subset size and step size on evaluated strains and tensile modulus of elasticity and failure strain (2/2).

A.2 Influence of edge preparation

No edge preparation

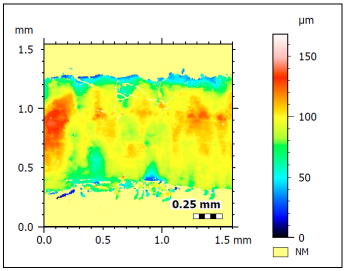


Figure A.3: Surface quality of continuous carbon fibre SMC in fibre direction (0°) before edge preparation.

Edge preparation

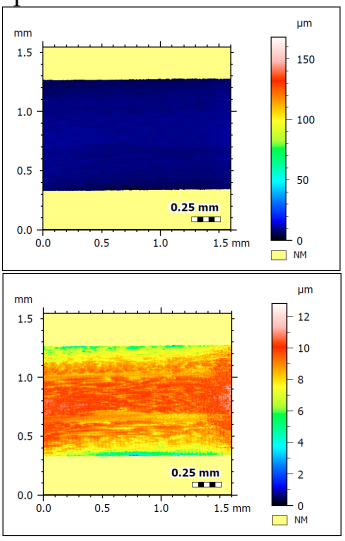


Figure A.4: Surface quality of continuous carbon fibre SMC in fibre direction (0°) after edge preparation.

A.3 Tensile properties of discontinuous glass fibre SMC (2D)

Table A.1: Tensile properties of discontinuous glass fibre SMC (2D) with tensile modulus of elasticity (E_t), tensile strength (R_t) and failure strain ($\varepsilon_{max,t}$) corresponding to a decrease of sustained load to 0.8· preceding F_{max}. Variable n indicates number of evaluated specimens.

		Charge region 0°	Flow region 0°	Charge region 90°	Flow region 90°
E_t		(n=10)	(n=10)	(n=11)	(n=10)
$\bar{x}$	in GPa	11.3	12.4	11.0	11.5
μ	in GPa	0.5	1.4	0.6	1.0
CV	in %	4.8	11.6	5.2	8.4
R_t		(n=10)	(n=10)	(n=11)	(n=10)
$\bar{x}$	in MPa	145	169	146	156
μ	in MPa	15	20	11	18
CV	in %	10.6	11.5	7.5	11.7
$\varepsilon_{max,t}$		(n=8)	(n=8)	(n=8)	(n=8)
$\bar{x}$	in %	1.7	1.7	1.7	1.7
μ	in %	0.2	0.1	0.1	0.1
CV	in %	11.4	6.6	6.2	5.8

A.4 Tensile properties of discontinuous glass fibre SMC (1D)

Table A.2: Tensile properties of discontinuous glass fibre SMC (1D flow with approximately 33% initial mould coverage), with tensile modulus of elasticity (E_t), Poisson's ratio (ν_t), tensile strength (R_t), elongation at tensile strength ($\varepsilon_{R,t}$) and failure strain ($\varepsilon_{max,t}$) corresponding to a decrease of sustained load to 0.8· preceding F_{max}. Variable n indicates number of evaluated specimens.

		Charge region 0°	Flow region 0°	Charge region 90°	Flow region 90°
E_t		(n=9)	(n=15)	(n=17)	(n=10)
$\bar{x}$	in GPa	13.0	13.2	9.3	9.9
μ	in GPa	1.1	0.8	0.7	1.4
CV	in %	8.3	6.0	7.7	13.9
ν_t		(n=9)	(n=15)	(n=17)	(n=10)
$\bar{x}$	-	0.38	0.37	0.27	0.30
μ	-	0.02	0.02	0.03	0.04
CV	in %	5.5	5.5	12.4	12.8
R_t		(n=9)	(n=15)	(n=17)	(n=10)
$\bar{x}$	in MPa	167	183	84	101
μ	in MPa	30	30	17	30
CV	in%	17.7	16.6	20.3	29.9
$\varepsilon_{R,t}$		(n=7)	(n=8)	(n=7)	(n=7)
$\bar{x}$	in %	1.5	1.6	1.2	1.2
μ	in %	0.3	0.3	0.3	0.3
CV	in %	19.5	17.6	23.2	27.4
$\varepsilon_{max,t}$		(n=7)	(n=8)	(n=7)	(n=7)
$\bar{x}$	in %	1.5	1.7	1.2	1.2
μ	in %	0.3	0.3	0.3	0.3
CV	in %	19.5	17.8	27.7	22.1

A.5 Compressive properties of discontinuous glass fibre SMC

Table A.3: Compressive properties of discontinuous glass fibre SMC (1D flow with approximately 33% initial mould coverage), with compressive modulus of elasticity (E_c), compressive strength (R_c) elongation at compressive strength ($\varepsilon_{R,c}$) and failure strain ($\varepsilon_{max,c}$) corresponding to a decrease of sustained load to 0.8· preceding F_{max}. Variable n indicates number of evaluated specimens.

		Charge region 0°	Flow region 0°	Charge region 90°	Flow region 90°
E_c		(n=7)	(n=8)	(n=7)	(n=8)
$\bar{x}$	in GPa	12.7	12.5	9.1	9.3
μ	in GPa	1.1	0.7	0.9	1.7
CV	in %	8.4	5.7	9.7	18.6
R_c		(n=7)	(n=8)	(n=7)	(n=8)
$\bar{x}$	in MPa	290	305	228	221
μ	in MPa	46	15	15	32
CV	in %	16.0	4.8	6.6	14.6
$\varepsilon_{R,c}$		(n=7)	(n=8)	(n=7)	(n=8)
$\bar{x}$	in %	2.7	2.9	3.4	3.1
μ	in %	0.2	0.2	0.5	0.3
CV	in %	7.5	7.6	14.5	10.4
$\varepsilon_{max,c}$		(n=7)	(n=8)	(n=7)	(n=8)
$\bar{x}$	in %	2.7	2.9	3.4	3.2
μ	in %	0.2	0.2	0.5	0.3
CV	in %	7.4	7.2	14.9	9.7

A.6 Tensile and compressive properties of continuous carbon fibre SMC

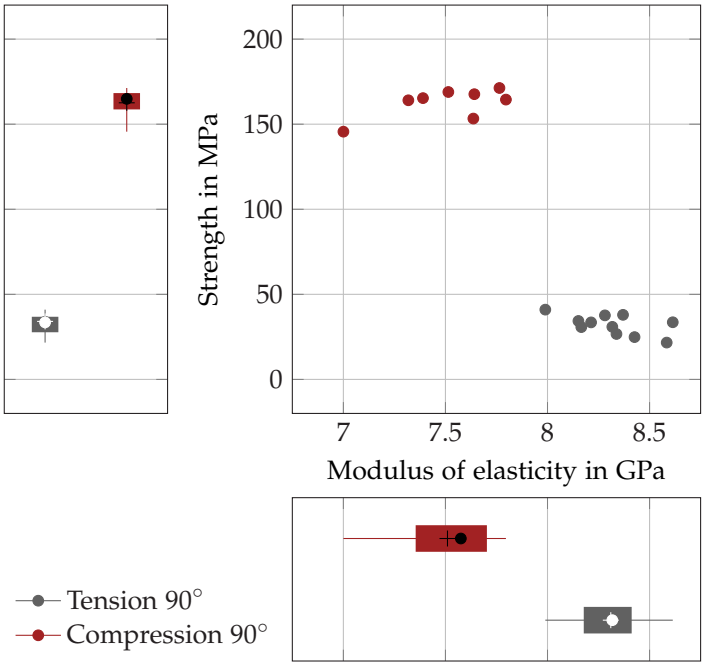


Figure A.5: Tensile and compressive moduli of elasticity and tensile and compressive strength of continuous carbon fibre SMC perpendicular to fibre direction (• = median, + = mean, box = 25^{th} to 75^{th} percentile, lines indicate minimum and maximum or 1.5 interquartile range, respectively, ○ = outlier).

A.7 Flexural properties of continuous carbon fibre SMC

Table A.4: Three-point bending properties of continuous carbon fibre SMC in fibre direction for a span to thickness ratio of 40:1, with flexural modulus of elasticity (E_f), flexural strength (R_f), elongation at flexural strength (ε_{R_f}) and failure strain ($\varepsilon_{max,f}$) corresponding to a decrease of sustained load to 0.8· preceding F_{max}. Variable n indicates number of evaluated specimens.

E_f		(n=6)	R_f		(n=6)
$\bar{x}$	in GPa	105.9	$\bar{x}$	in MPa	946
μ	in GPa	5.7	μ	in MPa	85
CV	in %	5.4	CV	in %	9.0

$\varepsilon_{R,f}$		(n=6)	$\varepsilon_{max,f}$		(n=6)
$\bar{x}$	in %	0.9	$\bar{x}$	in %	0.9
μ	in %	0.1	μ	in %	0.1
CV	in %	6.6	CV	in%	7.2

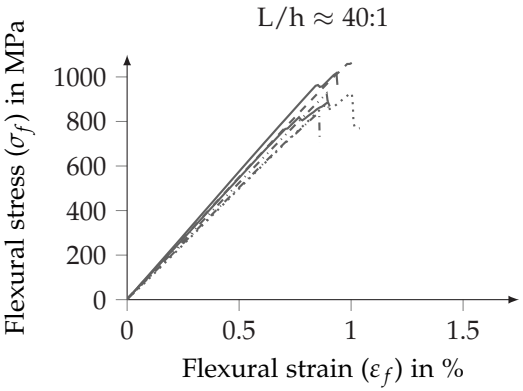


Figure A.6: Stress-strain curves resulting from three-point bending of continuous carbon fibre SMC in fibre direction (0°) for a span to thickness ratio of 40:1.

A.8 Flexural properties of continuous-discontinuous glass/carbon fibre SMC

Table A.5: Three-point bending properties of continuous-discontinuous glass carbon fibre SMC in fibre direction for a span to thickness ratio of 40:1, with flexural modulus of elasticity (E_f), flexural strength (R_f), elongation at flexural strength ($\varepsilon_{R,f}$) and failure strain ($\varepsilon_{max,f}$) corresponding to a decrease of sustained load to 0.8· preceding F_{max}. Variable n indicates number of evaluated specimens.

E_f		(n=6)	R_f		(n=6)
$\bar{x}$	in GPa	57.7	$\bar{x}$	in MPa	608
μ	in GPa	3.0	μ	in MPa	141
CV	in %	5.2	CV	in %	23.1

$\varepsilon_{R,f}$		(n=6)	$\varepsilon_{max,f}$		(n=6)
$\bar{x}$	in %	1.1	$\bar{x}$	in %	1.1
μ	in %	0.3	μ	in %	0.3
CV	in %	24.4	CV	in %	24.0

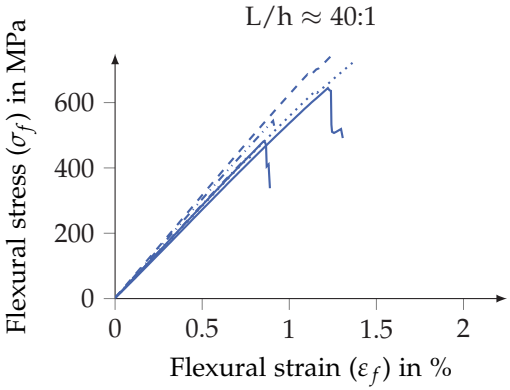


Figure A.7: Stress-strain curves resulting from three-point bending of continuous-discontinuous glass/carbon fibre SMC for a span to thickness ratio of 40:1.

A.9 Classical laminate theory: calculations

Q_{11}, Q_{12}, Q_{22} and Q_{66} of the discontinuous glass and continuous carbon fibre read

$$Q_{11} = \frac{E_{11}}{1 - \nu_{12}^2 \cdot \frac{E_{22}}{E_{11}}}, \tag{A.1}$$

$$Q_{12} = \frac{\nu_{12} E_{22}}{1 - \nu_{12}^2 \cdot \frac{E_{22}}{E_{11}}}, \tag{A.2}$$

$$Q_{22} = \frac{E_{22}}{1 - \nu_{12}^2 \cdot \frac{E_{22}}{E_{11}}}, \tag{A.3}$$

$$Q_{66} = G_{12}. \tag{A.4}$$

Schriftenreihe des Instituts für Angewandte Materialien

ISSN 2192-9963

Band 1 Prachai Norajitra
Divertor Development for a Future Fusion Power Plant. 2011
ISBN 978-3-86644-738-7

Band 2 Jürgen Prokop
Entwicklung von Spritzgießsonderverfahren zur Herstellung von Mikrobauteilen durch galvanische Replikation. 2011
ISBN 978-3-86644-755-4

Band 3 Theo Fett
New contributions to R-curves and bridging stresses – Applications of weight functions. 2012
ISBN 978-3-86644-836-0

Band 4 Jérôme Acker
Einfluss des Alkali/Niob-Verhältnisses und der Kupferdotierung auf das Sinterverhalten, die Strukturbildung und die Mikrostruktur von bleifreier Piezokeramik $(K_{0,5}Na_{0,5})NbO_3$. 2012
ISBN 978-3-86644-867-4

Band 5 Holger Schwaab
Nichtlineare Modellierung von Ferroelektrika unter Berücksichtigung der elektrischen Leitfähigkeit. 2012
ISBN 978-3-86644-869-8

Band 6 Christian Dethloff
Modeling of Helium Bubble Nucleation and Growth in Neutron Irradiated RAFM Steels. 2012
ISBN 978-3-86644-901-5

Band 7 Jens Reiser
Duktilisierung von Wolfram. Synthese, Analyse und Charakterisierung von Wolframlaminaten aus Wolframfolie. 2012
ISBN 978-3-86644-902-2

Band 8 Andreas Sedlmayr
Experimental Investigations of Deformation Pathways in Nanowires. 2012
ISBN 978-3-86644-905-3

Die Bände sind unter www.ksp.kit.edu als PDF frei verfügbar oder als Druckausgabe bestellbar.

Band 9 Matthias Friedrich Funk
Microstructural stability of nanostructured fcc metals during cyclic deformation and fatigue. 2012
ISBN 978-3-86644-918-3

Band 10 Maximilian Schwenk
Entwicklung und Validierung eines numerischen Simulationsmodells zur Beschreibung der induktiven Ein- und Zweifrequenzrandschichthärtung am Beispiel von vergütetem 42CrMo4. 2012
ISBN 978-3-86644-929-9

Band 11 Matthias Merzkirch
Verformungs- und Schädigungsverhalten der verbundstranggepressten, federstahldrahtverstärkten Aluminiumlegierung EN AW-6082. 2012
ISBN 978-3-86644-933-6

Band 12 Thilo Hammers
Wärmebehandlung und Recken von verbundstranggepressten Luftfahrtprofilen. 2013
ISBN 978-3-86644-947-3

Band 13 Jochen Lohmiller
Investigation of deformation mechanisms in nanocrystalline metals and alloys by in situ synchrotron X-ray diffraction. 2013
ISBN 978-3-86644-962-6

Band 14 Simone Schreijäg
Microstructure and Mechanical Behavior of Deep Drawing DC04 Steel at Different Length Scales. 2013
ISBN 978-3-86644-967-1

Band 15 Zhiming Chen
Modelling the plastic deformation of iron. 2013
ISBN 978-3-86644-968-8

Band 16 Abdullah Fatih Çetinel
Oberflächendefektausheilung und Festigkeitssteigerung von niederdruckspritzgegossenen Mikrobiegebalken aus Zirkoniumdioxid. 2013
ISBN 978-3-86644-976-3

Band 17 Thomas Weber
Entwicklung und Optimierung von gradierten Wolfram/EUROFER97-Verbindungen für Divertorkomponenten. 2013
ISBN 978-3-86644-993-0

Die Bände sind unter www.ksp.kit.edu als PDF frei verfügbar oder als Druckausgabe bestellbar.

Band 18 Melanie Senn
Optimale Prozessführung mit merkmalsbasierter Zustandsverfolgung. 2013
ISBN 978-3-7315-0004-9

Band 19 Christian Mennerich
Phase-field modeling of multi-domain evolution in ferromagnetic shape memory alloys and of polycrystalline thin film growth. 2013
ISBN 978-3-7315-0009-4

Band 20 Spyridon Korres
On-Line Topographic Measurements of Lubricated Metallic Sliding Surfaces. 2013
ISBN 978-3-7315-0017-9

Band 21 Abhik Narayan Choudhury
Quantitative phase-field model for phase transformations in multi-component alloys. 2013
ISBN 978-3-7315-0020-9

Band 22 Oliver Ulrich
Isothermes und thermisch-mechanisches Ermüdungsverhalten von Verbundwerkstoffen mit Durchdringungsgefüge (Preform-MMCs). 2013
ISBN 978-3-7315-0024-7

Band 23 Sofie Burger
High Cycle Fatigue of Al and Cu Thin Films by a Novel High-Throughput Method. 2013
ISBN 978-3-7315-0025-4

Band 24 Michael Teutsch
Entwicklung von elektrochemisch abgeschiedenem LIGA-Ni-Al für Hochtemperatur-MEMS-Anwendungen. 2013
ISBN 978-3-7315-0026-1

Band 25 Wolfgang Rheinheimer
Zur Grenzflächenanisotropie von $SrTiO_3$. 2013
ISBN 978-3-7315-0027-8

Band 26 Ying Chen
Deformation Behavior of Thin Metallic Wires under Tensile and Torsional Loadings. 2013
ISBN 978-3-7315-0049-0

Band 27 Sascha Haller
Gestaltfindung: Untersuchungen zur Kraftkegelmethode. 2013
ISBN 978-3-7315-0050-6

Band 28 Nicht erschienen

Band 29 Gunnar Picht
Einfluss der Korngröße auf ferroelektrische Eigenschaften dotierter $Pb(Zr_{1-x}Ti_x)O_3$ Materialien. 2013
ISBN 978-3-7315-0106-0

Band 30 Esther Held
Eigenspannungsanalyse an Schichtverbunden mittels inkrementeller Bohrlochmethode. 2013
ISBN 978-3-7315-0127-5

Band 31 Pei He
On the structure-property correlation and the evolution of Nanofeatures in 12-13.5% Cr oxide dispersion strengthened ferritic steels. 2014
ISBN 978-3-7315-0141-1

Band 32 Jan Hoffmann
Ferritische ODS-Stähle – Herstellung, Umformung und Strukturanalyse. 2014
ISBN 978-3-7315-0157-2

Band 33 Wiebke Sittel
Entwicklung und Optimierung des Diffusionsschweißens von ODS Legierungen. 2014
ISBN 978-3-7315-0182-4

Band 34 Osama Khalil
Isothermes Kurzzeitermüdungsverhalten der hoch-warmfesten Aluminium-Knetlegierung 2618A (AlCu2Mg1,5Ni). 2014
ISBN 978-3-7315-0208-1

Band 35 Nicht erschienen

Band 36 Christoph Hage
Grundlegende Aspekte des 2K-Metallpulverspritzgießens. 2014
ISBN 978-3-7315-0217-3

Band 37 Bartłomiej Albiński
Instrumentierte Eindringprüfung bei Hochtemperatur für die Charakterisierung bestrahlter Materialien. 2014
ISBN 978-3-7315-0221-0

Die Bände sind unter www.ksp.kit.edu als PDF frei verfügbar oder als Druckausgabe bestellbar.

Band 38 Tim Feser
Untersuchungen zum Einlaufverhalten binärer alpha-Messinglegierungen unter Ölschmierung in Abhängigkeit des Zinkgehaltes. 2014
ISBN 978-3-7315-0224-1

Band 39 Jörg Ettrich
Fluid Flow and Heat Transfer in Cellular Solids. 2014
ISBN 978-3-7315-0241-8

Band 40 Melanie Syha
Microstructure evolution in strontium titanate Investigated by means of grain growth simulations and x-ray diffraction contrast tomography experiments. 2014
ISBN 978-3-7315-0242-5

Band 41 Thomas Haas
Mechanische Zuverlässigkeit von gedruckten und gasförmig abgeschiedenen Schichten auf flexiblem Substrat. 2014
ISBN 978-3-7315-0250-0

Band 42 Aron Kneer
Numerische Untersuchung des Wärmeübertragungsverhaltens in unterschiedlichen porösen Medien. 2014
ISBN 978-3-7315-0252-4

Band 43 Manuel Feuchter
Investigations on Joule heating applications by multiphysical continuum simulations in nanoscale systems. 2014
ISBN 978-3-7315-0261-6

Band 44 Alexander Vondrous
Grain growth behavior and efficient large scale simulations of recrystallization with the phase-field method. 2014
ISBN 978-3-7315-0280-7

Band 45 Tobias Kennerknecht
Fatigue of Micro Molded Materials – Aluminum Bronze and Yttria Stabilized Zirconia. 2014
ISBN 978-3-7315-0293-7

Band 46 Christopher Scherr
Elektrochemisches Verhalten von Lithium-Schwefel-Zellen mit unterschiedlicher Kathodenstruktur. 2015
ISBN 978-3-7315-0296-8

Band 47 Konstantin Frölich
Der Decal-Prozess zur Herstellung katalysatorbeschichteter Membranen für PEM-Brennstoffzellen. 2015
ISBN 978-3-7315-0334-7

Band 48 Benedikt Haspel
Werkstoffanalytische Betrachtung der Eigenschaften von mittels neuartiger RTM-Fertigungsprozesse hergestellten glasfaserverstärkten Polymerverbunden. 2015
ISBN 978-3-7315-0337-8

Band 49 Marco Berghoff
Skalenübergreifende Modellierung und Optimierung vom atomistischen kristallinen Phasenfeldmodell bis zur mesoskopischen Phasenfeldmethode. 2015
ISBN 978-3-7315-0416-0

Band 50 Michael Selzer
Mechanische und Strömungsmechanische Topologie-optimierung mit der Phasenfeldmethode. 2016
ISBN 978-3-7315-0431-3

Band 51 Michael Mahler
Entwicklung einer Auswertemethode für bruchmechanische Versuche an kleinen Proben auf der Basis eines Kohäsivzonenmodells. 2016
ISBN 978-3-7315-0441-2

Band 52 Christoph Bohnert
Numerische Untersuchung des Verformungs- und Bruchverhaltens von einkristallinem Wolfram auf mikroskopischer Ebene. 2016
ISBN 978-3-7315-0444-3

Band 53 Stefan Guth
Schädigung und Lebensdauer von Nickelbasislegierungen unter thermisch-mechanischer Ermüdungsbeanspruchung bei verschiedenen Phasenlagen. 2016
ISBN 978-3-7315-0445-0

Band 54 Markus Klinsmann
The Effects of Internal Stress and Lithium Transport on Fracture in Storage Materials in Lithium-Ion Batteries. 2016
ISBN 978-3-7315-0455-9

Band 55 Thomas Straub
Experimental Investigation of Crack Initiation in Face-Centered Cubic Materials in the High and Very High Cycle Fatigue Regime. 2016
ISBN 978-3-7315-0471-9

Band 56 Maren Lepple
Kupfer- und Eisenoxide als Konversions-Elektrodenmaterialien für Lithium-Ionen-Batterien: Thermodynamische und Elektrochemische Untersuchungen. 2016
ISBN 978-3-7315-0482-5

Band 57 Stefan Andreas Slaby
Charakterisierung und Bewertung der Zug- und Ermüdungseigenschaften von Mikrobauteilen aus 17-4PH Edelstahl. Ein Vergleich von mikropulverspritzgegossenem und konventionell hergestelltem Material. 2017
ISBN 978-3-7315-0484-9

Band 58 Kumar Ankit
Phase-field modeling of microstructural pattern formation in alloys and geological veins. 2016
ISBN 978-3-7315-0491-7

Band 59 Kuo Zhang
Characterization and Modeling of the Ratcheting Behavior of the Ferritic-Martensitic Steel P91. 2017
ISBN 978-3-7315-0503-7

Band 60 Nicht erschienen

Band 61 Fabian Lemke
Untersuchung des Sinterverhaltens von $SrTiO_3$ unter Berücksichtigung der Defektchemie. 2016
ISBN 978-3-7315-0510-5

Band 62 Johannes Kümmel
Detaillierte Analyse der Aufbauschneidenbildung bei der Trockenzerspanung von Stahl C45E mit Berücksichtigung des Werkzeugverschleißes. 2016
ISBN 978-3-7315-0518-1

Band 63 László Hagymási
Modellierung der Stoffübertragung beim Niederdruckcarbonitrieren mit Ammoniak und Acetylen. 2016
ISBN 978-3-7315-0568-6

Band 64 Reza Eslami
A novel micro-mechanical model for prediction of multiaxial high cycle fatigue at small scales. 2017
ISBN 978-3-7315-0583-9

Band 65 Sebastian Schulz
Phase-field simulations of multi-component solidification and coarsening based on thermodynamic datasets. 2017
ISBN 978-3-7315-0618-8

Band 66 Markus Stricker
Die Übertragung von mikrostrukturellen Eigenschaften aus der diskreten Versetzungsdynamik in Kontinuumsbeschreibungen. 2017
ISBN 978-3-7315-0658-4

Band 67 Luis Straßberger
Untersuchung und Modellierung des viskoplastischen Verformungsverhaltens oxidpartikelverstärkter Stähle. 2018
ISBN 978-3-7315-0674-4

Band 68 Mark Wobrock
Microplasticity of idealized single crystalline Ag cantilevers characterized with methods of high resolution. 2017
ISBN 978-3-7315-0682-9

Band 69 Amritesh Kumar
Micromechanical study on the deformation behaviour of directionally solidified NiAl-Cr eutectic composites. 2017
ISBN 978-3-7315-0694-2

Band 70 Johannes Hötzer
Massiv-parallele und großskalige Phasenfeldsimulationen zur Untersuchung der Mikrostrukturentwicklung. 2017
ISBN 978-3-7315-0693-5

Band 71 Thomas Hupfer
Herstellung von LATP für den Einsatz als Festkörperelektrolyt und dessen Eigenschaften. 2017
ISBN 978-3-7315-0702-4

Band 72 Florentin Pottmeyer
Schädigungsverhalten von in CFK-Laminaten eingebetteten Inserts unter bauteilnahen Beanspruchungen. 2017
ISBN 978-3-7315-0719-2

Band 73 Andres Höweling
Untersuchung der Hochvoltstabilität und Tiefentladung von dotierten $LiNi_{0,5}Mn_{1,5}O_4$-Hochvoltspinellen. 2018
ISBN 978-3-7315-0728-4

Band 74 Tabea Gisela Schwark
Deformation and Fracture Properties of the Soft Magnetic Composite Somaloy 700 3P on Different Length Scales. 2018
ISBN 978-3-7315-0759-8

Band 75 Klaudia Lichtenberg
Metallmatrixverbunde mit Verstärkungselementen aus metallischem Glas $Ni_{60}Nb_{20}Ta_{20}$ – Herstellung und Charakterisierung. 2018
ISBN 978-3-7315-0782-6

Band 76 Claudio Findeisen
Charakterisierung und Modellierung von instabilen Metamaterialien. 2019
ISBN 978-3-7315-0869-4

Band 77 Nilesha Mishra
Influence of strain on the functionality of ink-jet printed thin films and devices on flexible substrates. 2019
ISBN 978-3-7315-0853-3

Band 78 Simon Werner Bonk
Plastische Verformungsmechanismen in hochgradig kaltgewalzten, ultrafeinkörnigen Wolframblechen. 2019
ISBN 978-3-7315-0878-6

Band 79 Tim Gräning
Herstellung, Charakterisierung und Optimierung von austenitischen ODS Stählen. 2019
ISBN 978-3-7315-0732-1

Band 80 Peter Rupp
Herstellung, Prüfung und Modellierung neuartiger hybrider Aluminiumschaum-CFK-Sandwichverbunde. 2019
ISBN 978-3-7315-0880-9

Band 81 Benjamin Sebastian Ehreiser
Einfluss mechanischer Lasten auf die Herstellung von Stahl-Glaskeramik-Verbunden. 2019
ISBN 978-3-7315-0954-7

Band 82 Hans Giel
Weiterentwicklung experimenteller Methoden zur Ermittlung thermodynamischer Werkstoffdaten von Lithium-Ionen-Batterien. 2019
ISBN 978-3-7315-0981-3

Band 83 Anna Trauth
Characterisation and Modelling of Continuous-Discontinuous Sheet Moulding Compound Composites for Structural Applications. 2020
ISBN 978-3-7315-0950-9

KARLSRUHER INSTITUT FÜR TECHNOLOGIE (KIT)
SCHRIFTENREIHE DES INSTITUTS FÜR ANGEWANDTE MATERIALIEN

A novel approach in hybridisation of composites focusses on the combination of a discontinuous glass fibre reinforced sheet moulding compound (SMC) with continuous carbon fibre SMC, manufactured in an adapted SMC process. In general, a hybrid continuous-discontinuous SMC composite is an interesting hybrid material to allow for tailorable material properties of structural components by local reinforcements. It thereby achieves a property profile superior to the sum of the properties of the individual materials.

The main objective of this work is to significantly deepen the understanding of the material and the structural behaviour of continuous-discontinuous SMC composites, following a holistic approach to investigate microscopic aspects, macroscopic mechanical behaviour as well as failure evolution at the coupon, structure and component level. In addition, criteria to evaluate the effect of hybridisation are introduced and modelling approaches are presented and discussed.

ISSN 2192-9963
ISBN 978-3-7315-0950-9

ISBN 978-3-7315-0950-9

Gedruckt auf FSC-zertifiziertem Papier